DRAFT

LAWRENCE LIVERMORE LABORATORY
EARTH SCIENCES (K) DIVISION
T-1406, L-224

EG 78-10

cc J.W.S. we need a site description like this, could you or RMIEE do it

M E M O R A N D U M - February 14, 1978

TO: Doug Stephens

FROM: Harold Ganow

SUBJECT: Preliminary Results of the Geotechnical Instrumentation Program for Subsidence Monitoring - UCG Experiment II

INTRODUCTION

We have installed several types of geotechnical instrument systems at our Hoe Creek, Wyoming *in situ* coal gasification site to measure both surface and subsurface deformations resulting from gasification cavity creation. The subsurface instruments include two six-position borehole extensometers (MPBX) in borings EX-1 and EX-2, two electrical shear strips in borings SS-1 and SS-2, a piezometer borehole PZ-1 containing four hydraulically isolated pore pressure transducers, and six boreholes SI-1, SI-2, SI-3, H-2, H-3, and H-4, completed so as to allow the use of a wire-line inclinometer device. The plan-view locations of these boreholes in relation to the main process wells A, B, and C are shown in Figure 1. A brief description of the function of these instruments can be found in the April-June Quarterly Progress Report. The surface instrument system consists of 33 isolation bench marks arrayed in four lines radiating outward from an origin bench mark located near process Well A.

Preliminary data are now available from the extensometers, shear strips, and piezometers. Although much work remains to be done, a relatively clear picture of overburden deformation and roof collapse in response to gasification cavity growth is beginning to appear. The deflectometer data will require several additional weeks of computational effort for reduction, and inclement weather conditions at Hoe Creek have prevented post-experiment surface monument remeasurement.

Hoe Creek Site II Geology

The general geology of the Hoe Creek 80 acre UCG Site has been discussed by Qualheim (1977) and will not be repeated here. However, knowledge of certain geologic details pertaining to the origin of the Felix coals and their enclosing sedimentary rock is essential for a more complete understanding of the data that will be presented.

The Felix coals are two of several limnic coals contained within the Eocene age Wasatch Formation. This formation consists principally of sands, silts, and clays that have been transported and deposited in freshwater fluvial and lacustrine environments. These sediments have been subjected to considerable overburden loads in the geologic past that have led to their consolidation but, for the most part, cementation has not occurred. At Hoe Creek, the coarse-grained units are mostly dense sands and not sandstones, and the finer grained units vary from dense silts and clays to very weak siltstones and claystones.

We certainly leave the loop

Figure 2 is a folded geologic cross section of Gasification Site II at Hoe Creek. It has been constructed from natural gamma logs taken in boreholes I-12, H-5, I-4, and C with plan-view locations shown in Figure 3. The top of the 25-foot thick Felix No. 2 Coal is located at a depth of from 125 to 129 feet below the ground surface, while the base of overlying ten-foot thick Felix No 1 Coal is at a depth of from 93 to 109 feet. The intervening clastic wedge thins markedly from 32 (Well C) to 20 (I-12) feet in a horizontal distance of 80 feet. This wedge, which is composed of one or two distinct uniform clean fine-grained sands, and silts and clays is interpreted to be a crevasse splay deposit which forms when a natural levee bordering a delta distributary channel is breached during times of flooding. The apex of this splay is probably located to the northeast of Site II and may be only a few tens of feet away from process Well C.

The Felix No. 1 Coal is immediately overlain by a thin lensose uniform sand ranging from one to three feet in thickness followed by a thinly interbedded sequence of sands and silts ranging from three to six feet thick, and a sequence of thick extraordinary uniformly graded coarse sand. The last unit ranges from 30 to 35 feet thick and contains discontinuous clayey silt lenses and small pods of calcium carbonate cemented sandstones. Its probable origin is that of a major stream channel. This channel sand is, in turn, overlain by a transition sequence of sand to clayey siltstones and lastly by silty sands that extend to the ground surface.

Several features of the geologic section at Site II are worthy of additional emphasis. First, these sediments and weak sedimentary rocks are generally quite coarse grained and permeable to the flow of fluids. Second, most impermeable strata are located in a six-foot thick zone immediately overlying the Felix No. 2 Coal, and a 10 to 20-foot thick zone overlying the channel sand located high in the geologic section. Third, the sediment split between the two Felix coals is thicker in the immediate vacinity of Site II than at any other known location at Hoe Creek.

Multiple Position Borehole Extensometers (MPBX)

Six wire-line extensometer systems were installed in boreholes EX-1 and EX-2. Their purpose was to measure overburden relaxation and collapse that results from creation of the gasification cavity. Construction overview and detail drawings indicating anchor positions are shown in Figures 4A and 4B, and Figures 5A and 5B for boreholes EX-1 and EX-2, respectively. During the design phase of Experiment II, concern was expressed that semi-open extensometer boreholes might allow the escape of product gases into the Felix No. 1 Coal or other stratigraphically higher and permeable units causing their contamination, and that the presence of gasification cavity pressures on roof strata might detrimentally affect their physical strength and behavior. Thus, it was decided to case these boreholes through the Felix No. 1 Coal and into the sediments between the Felix coals. Following anchor installation, and to further mitigate these problems, the borings

were plugged with a neat cement grout that extended six to ten feet into the casings. This last measure involved some risk of locking extensometers in place should unwanted grout intrusion occur between the extensometer sensing wire and its sheath.

Figures 6A and 6B are slightly smoothed compound drawings showing the time-deflection history curves for the various extensometers in boreholes EX-1 and EX-2, respectively. These curves were originally constructed from discrete digital data (voltage analogs of displacement) acquired by the Vidar/HP-21 computer data logging system and outputted using the linear-line graphics code PLOT2. Salient features of these figures and other pertinent data are summarized in Tables 1 and 2 for EX-1 and EX-2, respectively. A crucial assumption is that the anchors remain affixed to the rock material to which they were originally attached while the rock strata are deforming. Recalling the low strength nature of these sediments, it is clear this assumption may not always be true, but inspection of the curves in Figure 6 suggests that the hydraulic anchors performed remarkably well.

The forward combustion portion of Experiment II began on Julian Day 301.4 and lasted until Julian Day 359.9. Cavity formation in the Felix No. 2 Coal proceeded circumferentially outward from Injection Well A and funneled toward Production Wells B and C; thus, extensometers in EX-2 were the first to respond (Figure 6B). The lowermost anchor (No. 1) in EX-2 slipped during a post-installation pull test, and it was suspected that this extenso-

meter would be locked in place by the cement grout. The data acquired and presented in Figure 6B confirm this suspicion. Therefore, during construction, Anchor No. 2 was positioned essentially on top of Anchor No. 1 to act as a back-up.

Extensometer No. 2 documented what is interpreted to be sudden roof collapse on day 308.12. All of its motion occurred between successive data scans that were being taken at one-half hour intervals. Extensometer No. 3 shows rapid motion beginning on day 308.52 followed by collapse on day 309.02. The electrical shear strip in boring SS-1 also failed in tension at 123.5±1 foot on day 308.67± 0.08. This event is followed by a five-day hiatus before first motions were registered by Extensometer Nos. 4, 5, and 6 on day 314. These data suggest that a significant change, following the motions observed by extensometer No. 3, occurred in the manner and position of cavity formation. Operations records confirm that a radical change of injection air-flow geometry was made on day 311.38.

Extensometer Nos. 1 and 2 in EX-1 (Figure 6A) sensed motion beginning on day 310.68 that appears to be time-linear and elastic until about days 314.1 and 315.0, respectively. This suggests progressive roof relaxation over a nearby cavity of rather limited lateral extent. Ultimately, these motions accelerated until collapse occurred on day 316.22 and 316.98 for extensometer Nos. 1 and 2, respectively. Extensometer No. 3 in EX-1, which was not fully inflated because of a premature inflation line burst, showed no motion.

Extensometer Nos. 4, 5, and 6 in EX-2 tended to move together as a unit as measurable strain quickly progressed upward through the splay deposit at this location. These motions accelerated on days 318 and 319, and reached the extension limit of the MPBX head assembly on day 320. Unfortunately, the head could not be reset before overburden collapse occurred on day 321. It is likely that a cavity of large areal extent caused these motions. The dashed-line curves shown in Figure 6B show the approximate extent of this plastic deformation before collapse. It is suggested these data recorded on day 321 do represent a collapse event because only about 0.5% of wire strain could reasonably have occurred between time the head extension limit was reached and subsequent anchor release. This is well within the elastic range of the invar extensometer wire.

In EX-1 data from Extensometers 4, 5, and 6 indicate a slower rate of gasification cavity induced roof deformation. First motions were registered on days 315.72, 317.56, and 318.30, respectively; and are characterized by long periods of elastic quasi-plastic motion. A distinct acceleration of motion indicating major roof stress readjustments was registered by Extensometer No. 4 on day 321 about the same time as the previously discussed roof collapse occurred in the vicinity of the top three extensometer anchors in EX-2. Roof materials in the vicinity of anchors 5 and 6 do not appear to have been affected by this event. The downward motion detected by Extensometer No. 5 in EX-1 accelerated on day 324 and gaps totaling five inches of thickness were closed to about one inch when sudden renewed motion was

induced in the strata containing Anchor No. 4 on day 325. A sudden downward deflection occurred in strata containing Anchor No. 6 at the same time as convergence of the lower roof occurred. Taken together, these movements probably resulted from roof stress readjustment following roof collapse elsewhere in the cavity.

On day 326.34, the sensing elements in the EX-1 head assembly for Extensometer Nos. 4 and 5 were successfully reset which resulted in their yielding several additional days of deformation history. The deflections recorded by Extensometers Nos. 4, 5, and 6 were at first quite slow, followed by accelerating and then decelerating motions, and ultimately by collapse or anchor release on days 333.88, 334.19, and 334.32, respectively. It is not known with certainty whether collapse occurred at these times or whether deformation and/or thermally induced deterioration of the roof strata allowed these anchors to be released.

Other indirect evidence of continued roof collapse has also been obtained from the extensometer boreholes. On day 333, the extensometer head assembly of EX-2 began to leak product gases, and on day 342, the same event occurred at EX-1. It seems likely that roof collapse had proceeded to the extent that the lower ends of casings were exposed to the gasification cavity environment. It is also likely that the Felix No. 1 Coal had began to combust by this time. The action of these product gases, or thermal expansion of the casings, or both had either caused the release of the neat cement plugs or burn-off of the casings thereby allowing the escape of product gases.

Electrical Shear Strips

The performance of commercially available electrical shear strips was also evaluated as a part of the geotechnical subsidence program. One of the 60 ft. long shear strips having a two-foot resistor spacing was installed in borehole SS-1 as shown in Figure 7. In this location, it was expected that shear strip failure would occur in tension as the cavity roof sags and ultimately collapses; rather than in a shearing mode The first event detected by this unit occurred on day 308.67± 0.08 at a depth of 123.5± 1 feet and its significance has been discussed in the preceeding section. However, following this break saline groundwater intruded under the polyvinyl chloride paint water barrier shunting the copper foil conductors and causing a continuous decline in the strip's apparent resistance. Occasional resistance measurements, obtained by using an ohmmeter, were not sufficient to delineate the continuous resistance change that resulted. Although subsequent higher breaks undoubtedly occurred, they could not be detected.

The second shear strip was installed in boring SS-2 as shown in Figure 7. Its purpose was to detect shearing deformation such as may take place along an inclined surface known as the angle-of-break. This device was broken on day 331.34 at a depth of 111± 1 feet, or about two feet below the base of the Felix No. 1 Coal. Calculations of the distance to this single break by using both top and bottom apparent resistance values yielded the same result. Because of the break's position and the corroborative calculations, it seems unlikely that combustion at the base of the Felix No. 1 Coal burned through

this shear strip. Ground-water incursion did not occur in this instance possibly because little free water existed at this location. Although the presence of an angle-of-break shear is not definitely established by this single event, this particular mode of subsidence deformation is cearly a possibility that demands further investigation.

Piezometers

Four electrical pore-fluid pressure transducers or piezometers were installed in a single borehole designated PZ-1 as shown in Figure 8. Their purpose was to monitor changes in ground-water pressure over the expanding cavity. This borehole was advanced without the aid of drilling muds to avoid plugging the permeable rock units which required piezometer installation to be done through the drill rods to prevent hole collapse. The sensing elements were placed in the center of at least four-foot long sand filter sections that are hydraulically isolated from each other by bentonite pellet plugs. The piezometer electrical leads were attached to the scanning vidar/HP-21 computer data acquisition system. Piezometer No. 1 was placed in sand at the bottom of the borehole approximately 2.5 feet above the top of the Felix No. 2 Coal at a depth of 124.5 feet. The enclosing sediments are dense slightly silty clays of probable lacustrine origin that form the cap-rock of the No. 2 coal. The second piezometer was placed at a depth of 116.5 feet in a four foot thick fine-grained sand whose base is located about ten feet above the top of the Felix No. 2. The third and fourth piezometers were

placed at depths of 103 and 85 feet near the bases of the Felix No. 1 Coal and previously discussed channel sand, respectively.

Stone and Snoeberger (1976) have studied the native hydrology of the Hoe Creek in situ coal gasification site. Although they were concerned principally within the Felix coals, the hydraulic characteristics of the enclosing strata were also studied. They concluded from well tests that the various major geologic units constitute a multiple leaky aquifer system. The Felix Nos. 1 and 2 Coals and the coarse channel sand deposit are classed as the principal aquifers. While the extremely fine-grained underclay of Felix No. 2 Coal confines the base of this aquifer, the degree of confinement provided by the overlying crevasse splay deposits varies from modest to non-existent depending on which of various experimental sub-sites is being considered. Therefore, this coal is classed as a leaky to very leaky confined aquifer. A single well test of the Felix No. 1 Coal indicated that vertical leakage is more severe than was observed for the deeper No. 2 coal leading to its classification as a very leaky to unconfined aquifer.

Stone and Snoeberger (1976) also noted a progressive decline in the piezometric head potential in wells completed in successively deeper lithic units. They interpreted this resulting head loss to be caused by a vertically downward component of ground-water flow such as occurs in recharge regions. The steady state piezometric heads measured over a 20-day time period by the four transducers before air-flow tests gave the same result as shown in column

four of Table 3. It is interesting to note that minimal head loss occurs between piezometer Nos. 4 and 3 (about 0.45 foot-of-water), and Nos. 3 and 2 (about 0.24 foot-of-water). An average head loss of 4.25 feet-of-water occurs between piezometers Nos. 2 and 1 suggesting that the most impermeable strata are located in the region immediately overlying the Felix No. 2 Coal.

Figure 9 is a plot of the raw piezometer data in psis obtained during their useful life, and the A-well head air injectin pressure in psia. A six-hour plotting interval has been used to somewhat reduce the data variation. The proximity of borehole PZ-1 to injection Well A suggests that injection pressure rather than cavity back-pressure provides a more meaningful basis for comparison.

The digital data acquisition became active on Julian day 284.7 during the pre-ignition air flow tests portion of the experiment (Figure 9). A-well pressure varied rapidly over a wide range as different injection/production well and pressure configurations were tested. Ignition near the base of the No. 2 Coal occurred on day 287.4, and the B-well to C-well and B-well to A-well reverse combustion links were completed on days 289.5 and 301.0, respectively. The forward combustion portion of the experiment began shortly following completion of the well B to well A link and continued until day 359.9.

Figure 9 clearly shows that ground-water pressures sensed by the four piezometers are highly correlated with the A-well injection pressure. The

mean pre-test piezometric pressures (Table 3, column 3), shown along the left margin of Figure 9, provide a basis of comparison for the subsequent data. During the reverse combustion linking of wells B and A, a relatively high ambient air injection pressure of about 84 psia was required until a dramatic reduction in flow impedance occurred on day 298. Piezometers Nos. 1 and 2 visibly respond to this pressure while piezometers Nos. 3 and 4 were only affected to a minor extent. The observed pressure differentials (Table 3, column 5) were 28, 32, 54, and 60 psi for piezometers 1, 2, 3, and 4, respectively. It is evident that the overburden seal was leaking slightly during the high pressure linking operation, but is still intact.

Very soon after forward combustion mode began on day 301, the air injection pressure was reduced to a relatively low 20 to 30 psia. The piezometric heads measured at that time by transducers 1 and 2 were less than the static ground-water heads measured prior to the experiment indicating that significant de-watering of the lower portion of the solay deposit occurred during the linking operation. The original two psi pressure differential between piezometers 1 and 2 was reduced to less than one psi and the net ground-water flow was toward the expanding cavity.

On day 302.7, the output from piezometer No. 1 is judged to have become unreliable, for it no longer responds in a logical manner to changes in air injection pressure. It is suggested that this condition, termed incipient failure, was caused by excessive tranducer temperature and in turn suggests

that combustion was occurring in the upper part of the Felix No. 2 Coal in the immediate vicinity of well A. This piezometer continued to operate marginally until day 307.3 when its millivolt level output signal began to fluctuate wildly, suggesting physical separation of the sensing element from its electrical cable by roof collapse.

A distinct change in the response characteristics of piezometer No. 2 is observed to begin on about day 306. The pressure differential between A-well air injection pressure and the unit No. 2 piezometric pressure steadily declined indicating progressive deterioration of the gasification cavity roof seal. Incipient failure occurred on day 309.6 about 1-1/2 days after piezometer No. 2 had indicated exposure to full injection air pressure and was probably caused by excessive temperature. Marginal operation continued until day 319.8 when catastropic failure, possibly indicating sensor detachment by a roof collapse mechanism, was observed.

The response characteristics of piezmeters Nos. 3 and 4 also changed on about day 306. Before this time, these units had indicated only slight pressure changes in response to gross changes in air injection pressure. Now, the sensed pressure fluctuations became more pronounced, and the air injection pressure to fluid head pressures differentials began to decline--again indicating cavity seal deterioration. Between days 311 and 313, the piezometric head measured by unit No. 3 exceeded the head measured by unit No. 4 and corresponds roughly with excessive product gas loss detected by monitors at the ground surface. This phenomenon may possibly have been caused by strain induced pore-water pressure changes.

Beginning on about day 323, and shortly following the roof collapse event documented by extensometer Nos. 4, 5, and 6 in EX-2, piezometer No. 3 observed a rapid increase in pressure (decline in pressure differential) until incipient failure occurred on day 324.5. Catastrophic failure followed shortly on day 327.3 and is judged to represent sensor thermal destruction. The Felix No. 1 Coal may well have began to participate in the gasification process about this time.

Piezometer No. 4 responded in a very similar manner with a rapid pressure increase beginning on about day 330 followed by incipient failure on day 336.4. Ultimate transducer failure occurred seven days later. At about this time, chemical mass-balance calculations indicated that unacceptable amounts of product gas were being lost to the overburden and the gasification cavity back-pressure would have to be reduced. Also, large amounts of steam were observed in the flare plume. It is clear that a combination of roof collapse and thermal induced effects such as rock shrinkage and fissure formation with drying had essentially breached the rock units forming the gasification cavity seal.

Summary Comments

In general, the extensometers installed in EX-1 and EX-2 successfully documented progressively higher cavity roof strain and collapse. At first the roof strains were quite rapid and were followed quickly by collapse events. Subsequent strains were slower, more sporadic in nature, and apparently, were

followed by periods of stress readjustment around the growing cavity. Ultimately, roof collapse extended into the Felix No. 1 Coal which then almost certainly participated in the gasification reaction. Simplified two-dimensional finite element code calculations by Greenlaw, et al, (1977) suggested that roof collapse might extend about half way through the crevasse splay deposit. Although this model represents a distinct improvement in the state-of-the-art, other factors such as gasification induced pore-water pressure phenomenon, thermal induced strains, and roof strata buckling need to be included.

Shear strip performance was adequate but clearly can be improved through better apparatus design and an improved data aquisition system. More suitable water barrier coatings such as epoxies or a segmented strip design may be successful in preventing ground-water intrusion. An automatic resistance measuring system would aid in more precisely defining the time and distance to shear strip breaks, or monitoring ground-water intrusion, should it occur.

The four electrical piezometers in borehole PZ-1 did an excellent job of measuring the effect of the A-well injection pressure with time on the piezometric heads at their locations. They successfully documented the effect of progressively higher roof collapse and heat induced deterioration of the roof strata that provided the gasification reaction zone seal. Indirectly, they gave indications of excessive temperatures and probably

of roof collapse in the case of units Nos. 1 and 2. However, these data pertain to only one particular plan-view location (i.e., at PZ-1) and a three-dimensional picture will require several boreholes of this type.

In conclusion, given the inherently difficult nature of this problem which is one of measuring rock deformation and attendant phenomenon over an in situ coal gasifier producing a hot, toxic, and flammable gaseous product, these instrument systems performed exceptionally well during this first geotechnical experiment.

HCG:ky
Attachments

cc: Don Davis, L-156
Dick Hill, L-367
Bob Langland, L-90
Warren Mead, L-212
Bob Schock/Larry Schwartz, L-203
John Tewhey, L-224

DRAFT

FIGURE CAPTIONS

Figure 1	Plan-view of Experiment II showing extensometer EX boreholes, shear strip SS boreholes, piezometer PZ borehole, and deflectometer SI and H boreholes; and their relationship to process wells A, B, and C. Solid symbols represent instrument systems discussed in this report
Figure 2	Simplified folded geologic cross-section of Hoe Creek UCG Site II
Figure 3	Plan-view locations of boreholes used to construct geologic cross section shown in Figure 2
Figure 4A	Borehole EX-1 construction overview
Figure 4B	Borehole EX-1 anchor placement detail
Figure 5A	Borehole EX-2 construction overview
Figure 5B	Borehole EX-2 anchor placement detail
Figure 6A	MPBX borehole EX-1 time vs. deflection history
Figure 6B	MPBX borehole EX-2 time vs. deflection history
Figure 7	Electrical shear strip boreholes SS-1 AND SS-2.
Figure 8	Multiple piezometer borehole PZ-1
Figure 9	Injection pressure and piezometric tranducer pressures time history

DRAFT

REFERENCES CITED

R. C. Greenlaw, H. C. Ganow, and R. T. Langland, Subsidence and Stability Studies for Underground Coal Gasification, Lawrence Livermore Laboratory, Rept. UCID-17674

LLL In Situ Coal Gasification Program Quarterly Progress Report, April through June, 1977, Lawrence Livermore Laboratory, Rept. UCRL-50026-77-2

B. J. Qualheim, Geological Exploration of Potential Underground Coal Gasification Sites in the Powder River Basin of Wyoming and Montana, Lawrence Livermore Laboratory, Rept. UCRL-52237

Randolph Stone and David F. Snoeberger, Evaluation of the Native Hydraulic Characteristics of the Felix Coal (Eocene, Wasatch Formation) and Associated Strata, Hoe Creek Site, Campbell County, Wyoming, Lawrence Livermore Laboratory, Rept. UCRL-51992

DRAFT

TABLE 1

MPBX DEFLECTION HISTORY EX-1

Anchor No.	Depth to Anchor (ft.)	Height Above No. 2 Coal (ft.) [1/]	Julian Day of - First Motion	Julian Day of - Collapse	Total Deflection (inches)	Comments
1	125.25	1.25	310.68	316.22	8.8	Shortest time histor in this borehole
2	121.75	4.75	310.68	316.98	3.7	Anchor slippage may have occurred
3	118.25	8.25	--	--	--	Locked in position
4	114.0	12.5	315.72	333.88	14.9	Longest time history and largest measured deflection of all extensometers
5	110.75	15.75	317.56	334.19	13.7	Motion here caused renewed motion on Anchor 4, some wire-drag interference
6	107.75	18.75	318.30	334.32	5.6	Extremely long quasi-elastic motion history

Note: [1/] Estimated depth to the top of the Felix No. 2 Coal is 126.5 feet

DRAFT

TABLE 2

MPBX DEFLECTION HISTORY EX-2

Anchor No.	Depth to Anchor (ft.)	Height Above No. 2 Coal (ft.) [1/]	Julian Day of - First Motion	Julian Day of - Collapse	Total Deflection (inches)	Comments
1	124.0	2.0	--	--	--	Locked in position
2	123.25	2.75	308.12	308.12	-1.0	Collapse signature only
3	120.25	5.75	308.52	309.02	7.2	Extremely rapid deflection
4	117.25	8.75	314.04	321.43	~18	Anchors 4, 5, & 6 in materials that tended to deform as a unit. MPBX head assembly could not be reset on day 321
5	114.25	11.75	314.65	321.50	~18	
6	109.5	16.5	314.82	321.50	~18	

Note: [1/] Measured depth to the top of the Felix No. 2 Coal is 126 feet

TABLE 3

PIEZOMETERS RESPONSE HISTORY SUMMARY

Piezometer Unit Number	Depth (ft.)	Pre-test[1] Fluid Pressure (psig)	Depth to Equivalent Water table (ft.)	ΔP[2] During Reverse Linking (psi)	Incipient Failure ΔP[2] (psi)	Incipient Failure Time(days)	Time of Catastrophic Failure days	Comments
1	124.5	25.05 ±0.60	66.65	28	<0	302.7	307.3	Sensor may have been physically detached by roof collapse
2	116.5	22.84 ±0.36	62.40	32	∿0	309.6	319.8	Sensor may have been physically detached by roof collapse
3	103.0	17.69 ±0.12	62.16	54	∿4	324.5	327.3	Sensor may have been physically burned
4	85.0	10.09 ±0.09	61.71	60	∿3	336.4	343.4	Sensor probably suffered thermal degradation

Notes: [1] The average ±3 standard deviations of 14 measurements taken over a 20 day pre-test time interval.

[2] Absolute pressure differential between the A-well injection pressure and the respective piezometer pressures using an average 12.3 psi atmosphere pressure.

DRAFT

PROCESS WELL AND SUBSURFACE GEOTECHNICAL BOREHOLE PLAN VIEW

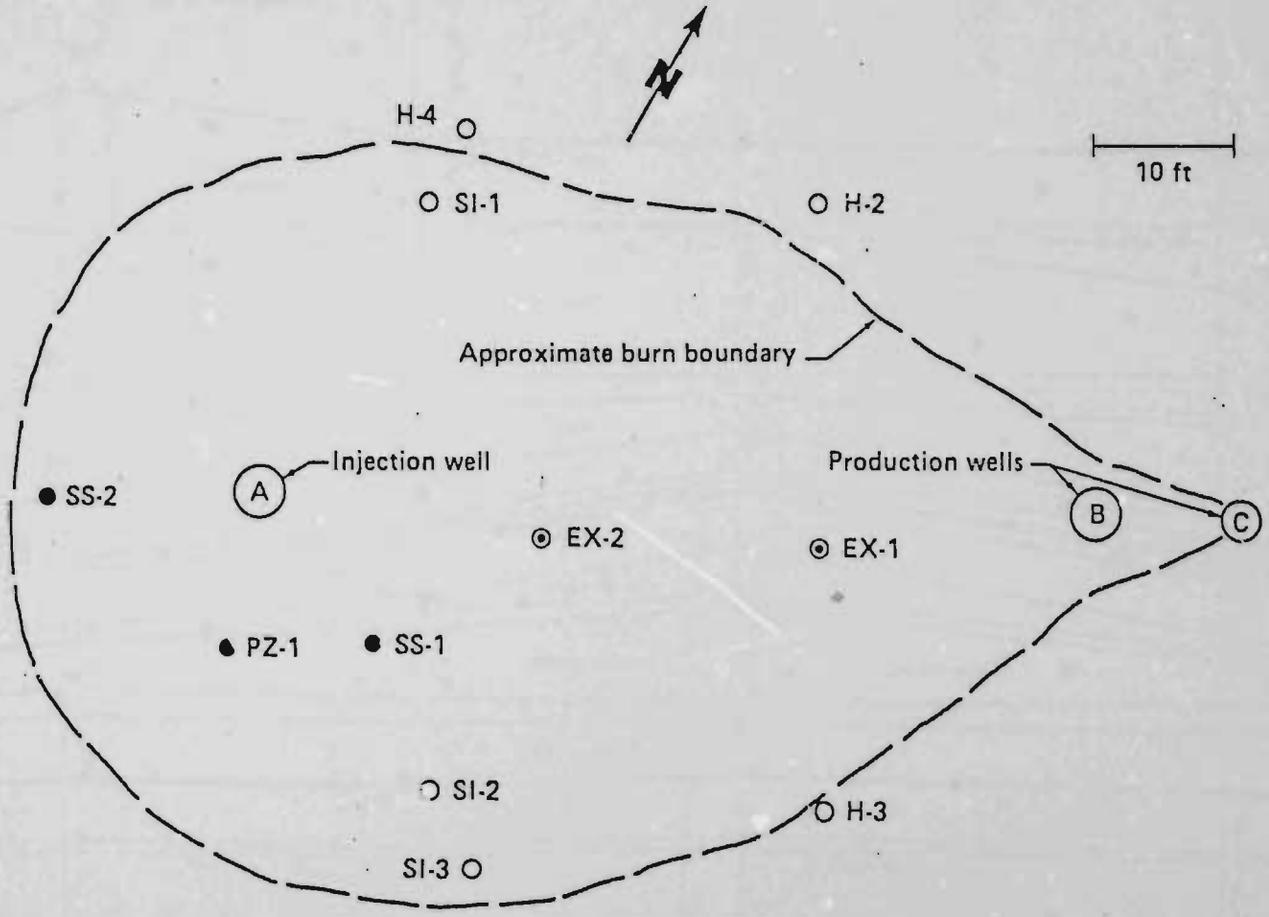

FIGURE 1

DRAFT

HOE CREEK U.C.G. SITE II

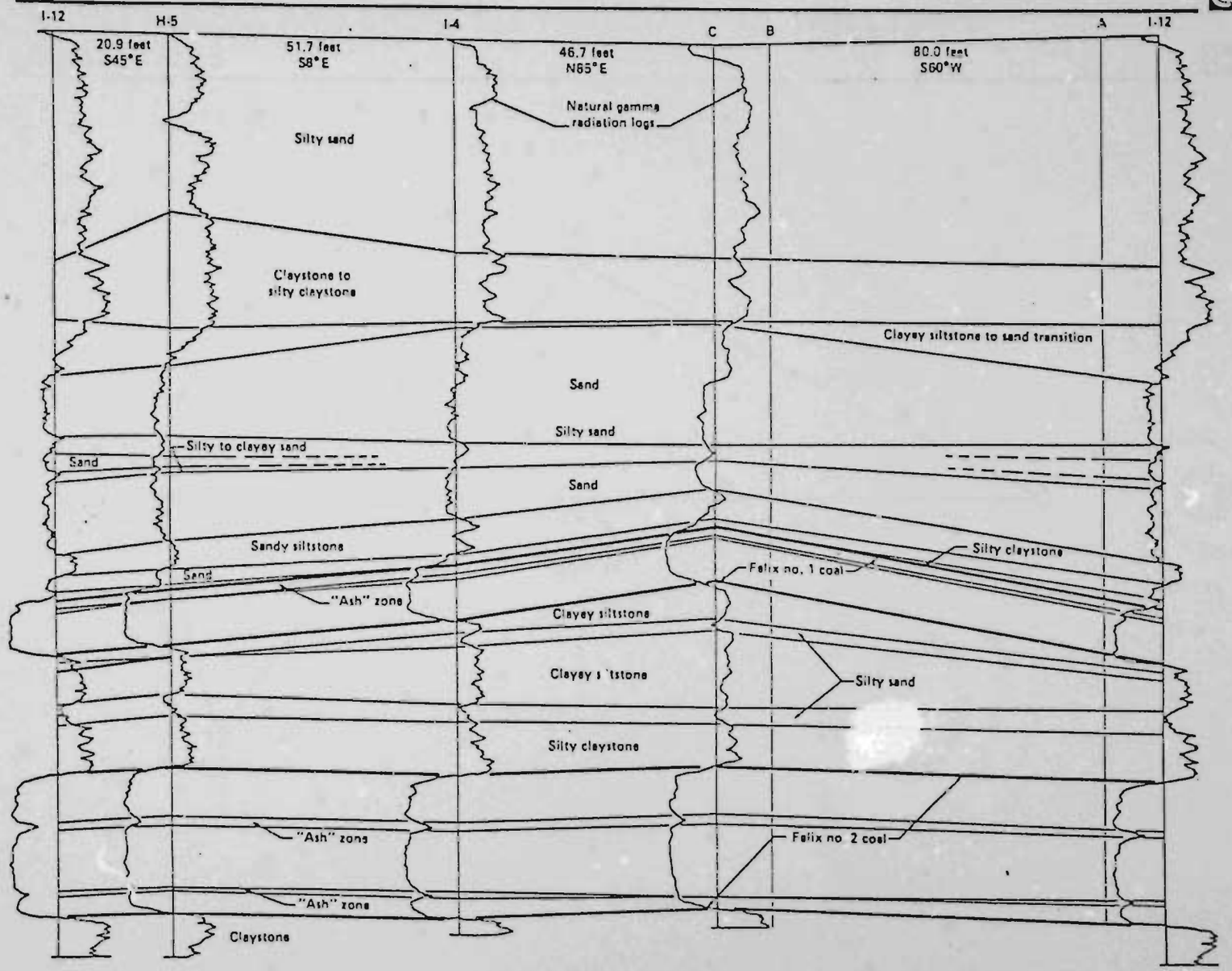

FIGURE 2

MAIN PROCESS AND CROSS SECTION CONTROL WELLS AND BOREHOLES

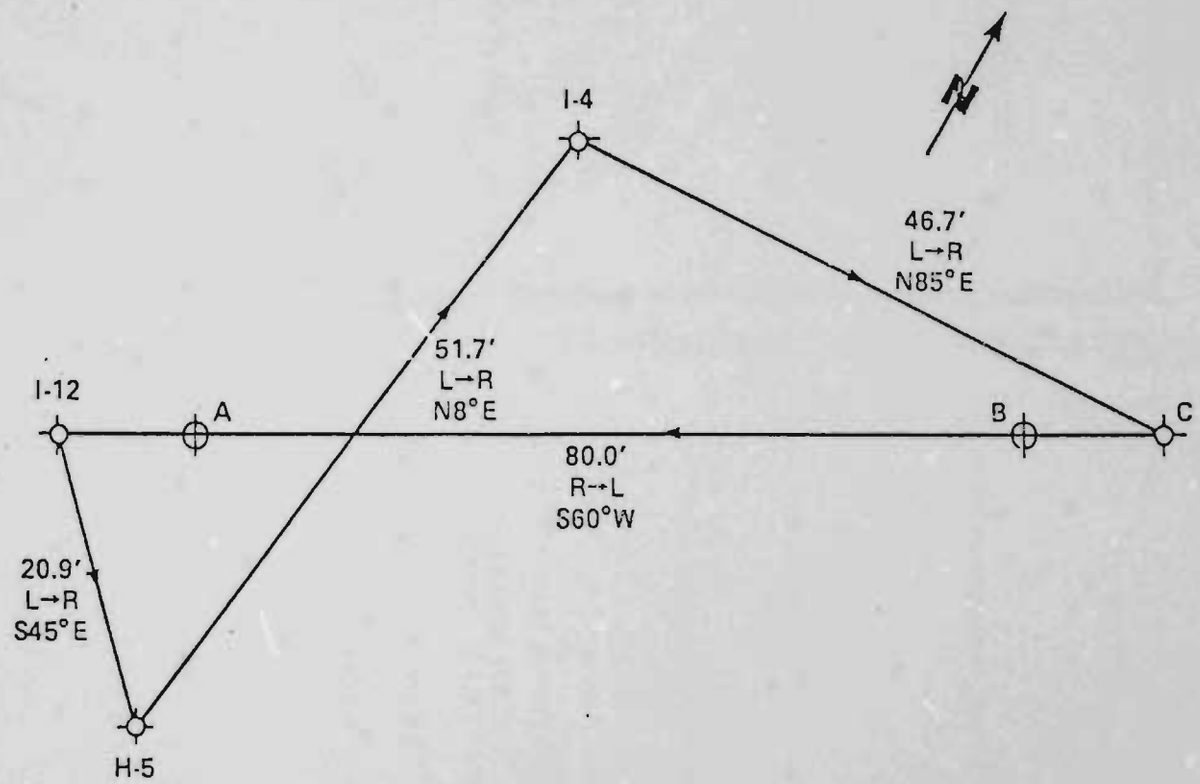

FIGURE 3

DRAFT

EX-1 AS-BUILT OVER-VIEW

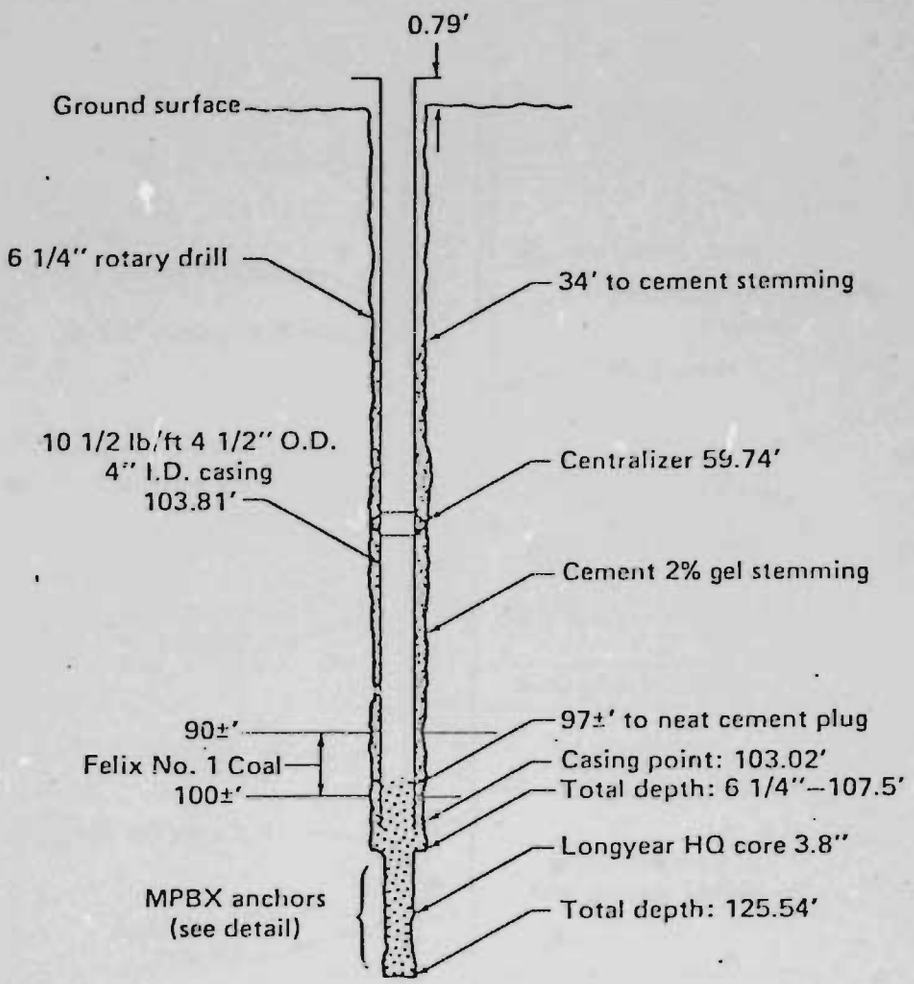

FIGURE 4 A

DRAFT

EX-1 AS-BUILT DETAIL

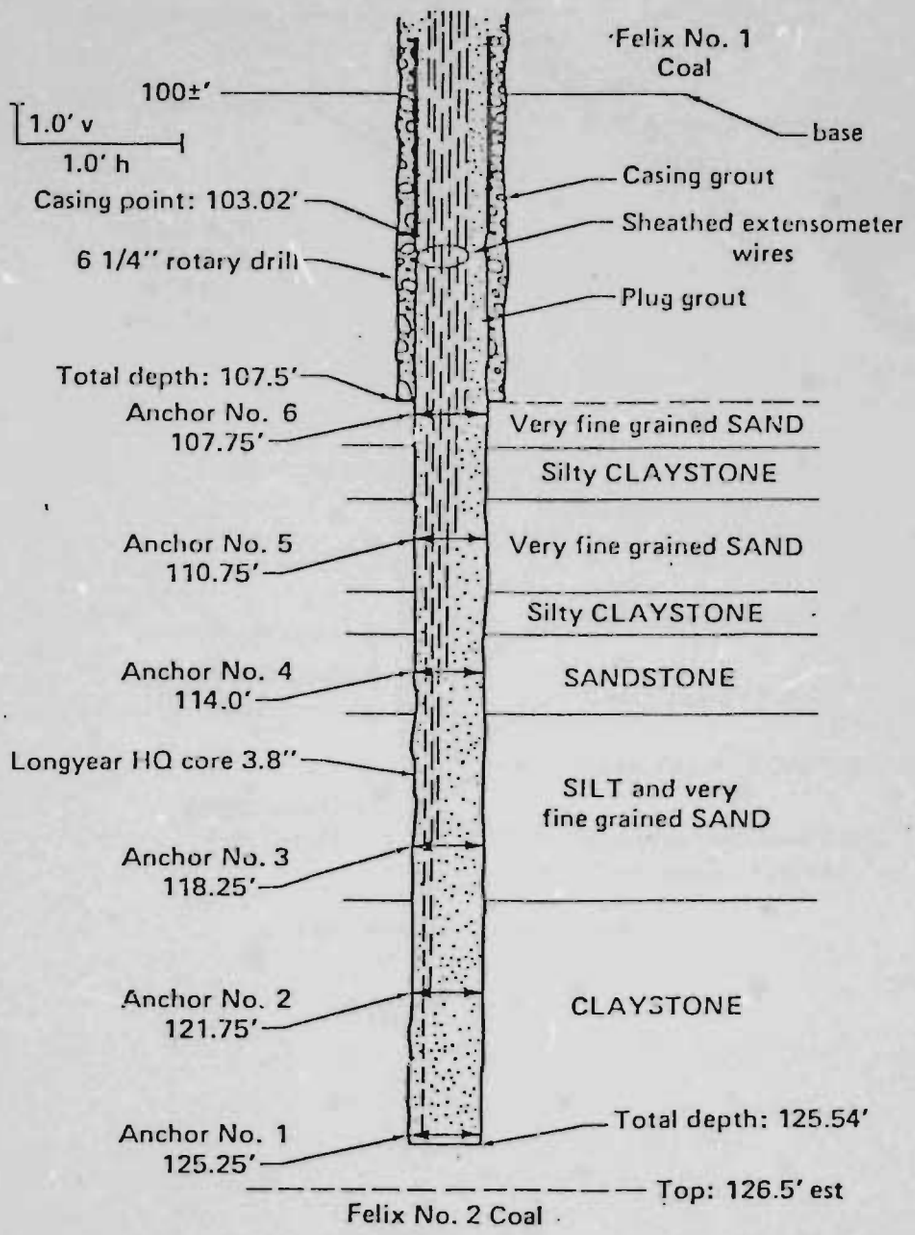

FIGURE 4 B

DRAFT

EX-2 AS-BUILT OVER-VIEW

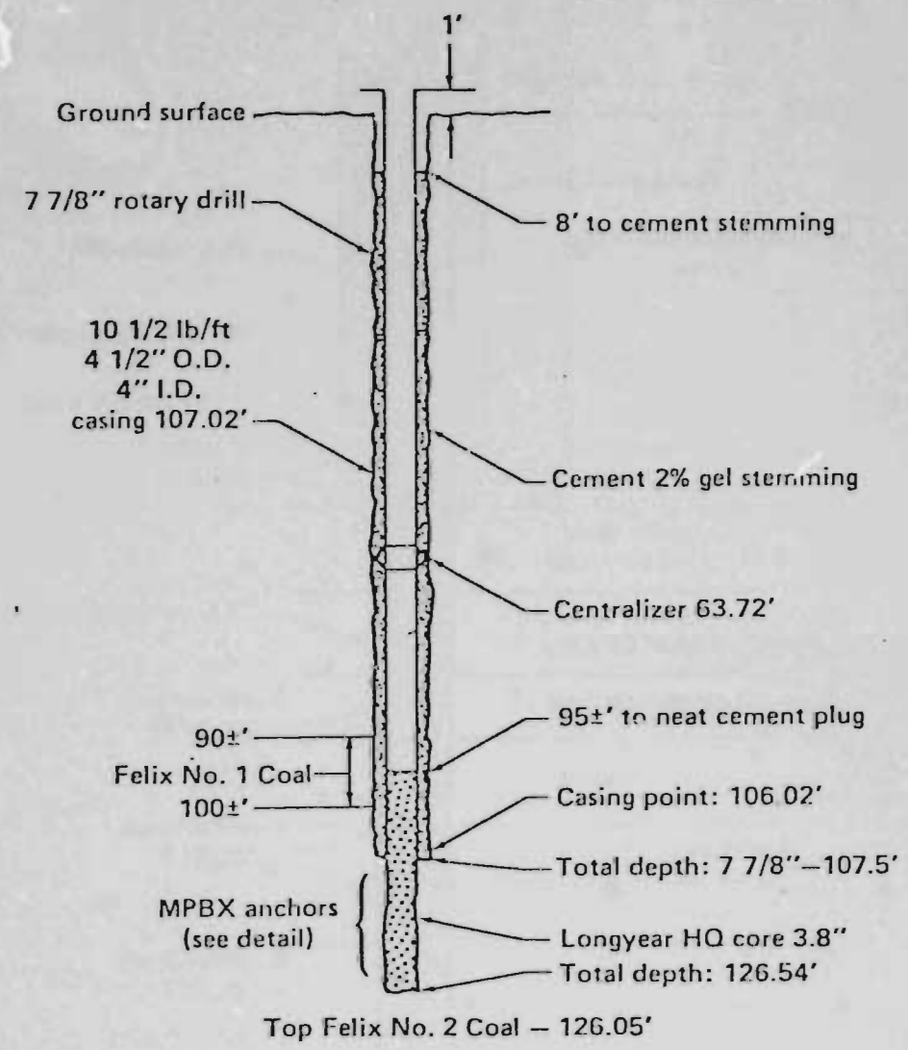

FIGURE 5 A

DRAFT

EX-2 AS-BUILT DETAIL

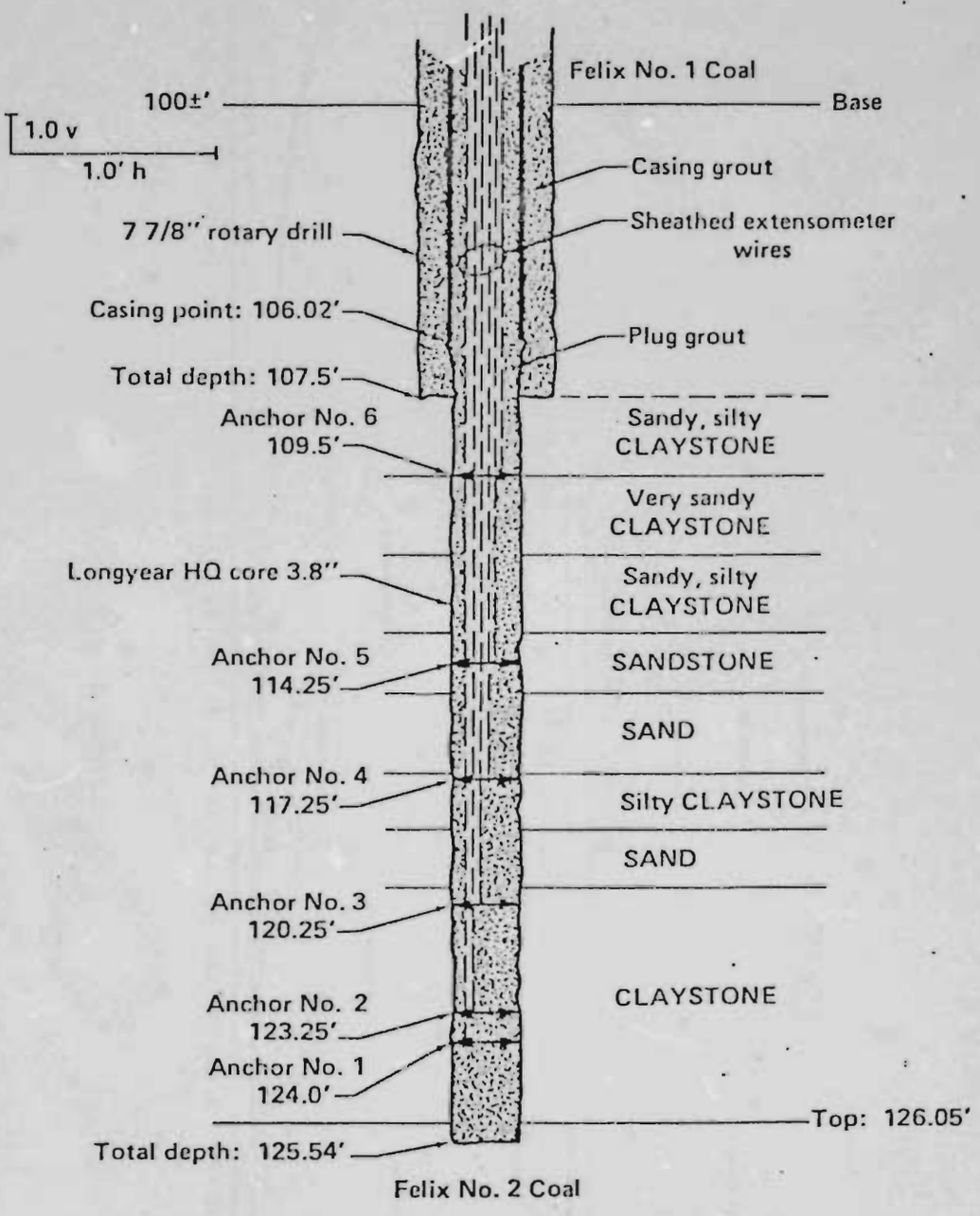

FIGURE 5 B

DRAFT

MPBX TIME / DEFLECTION HISTORY

FIGURE 6 A

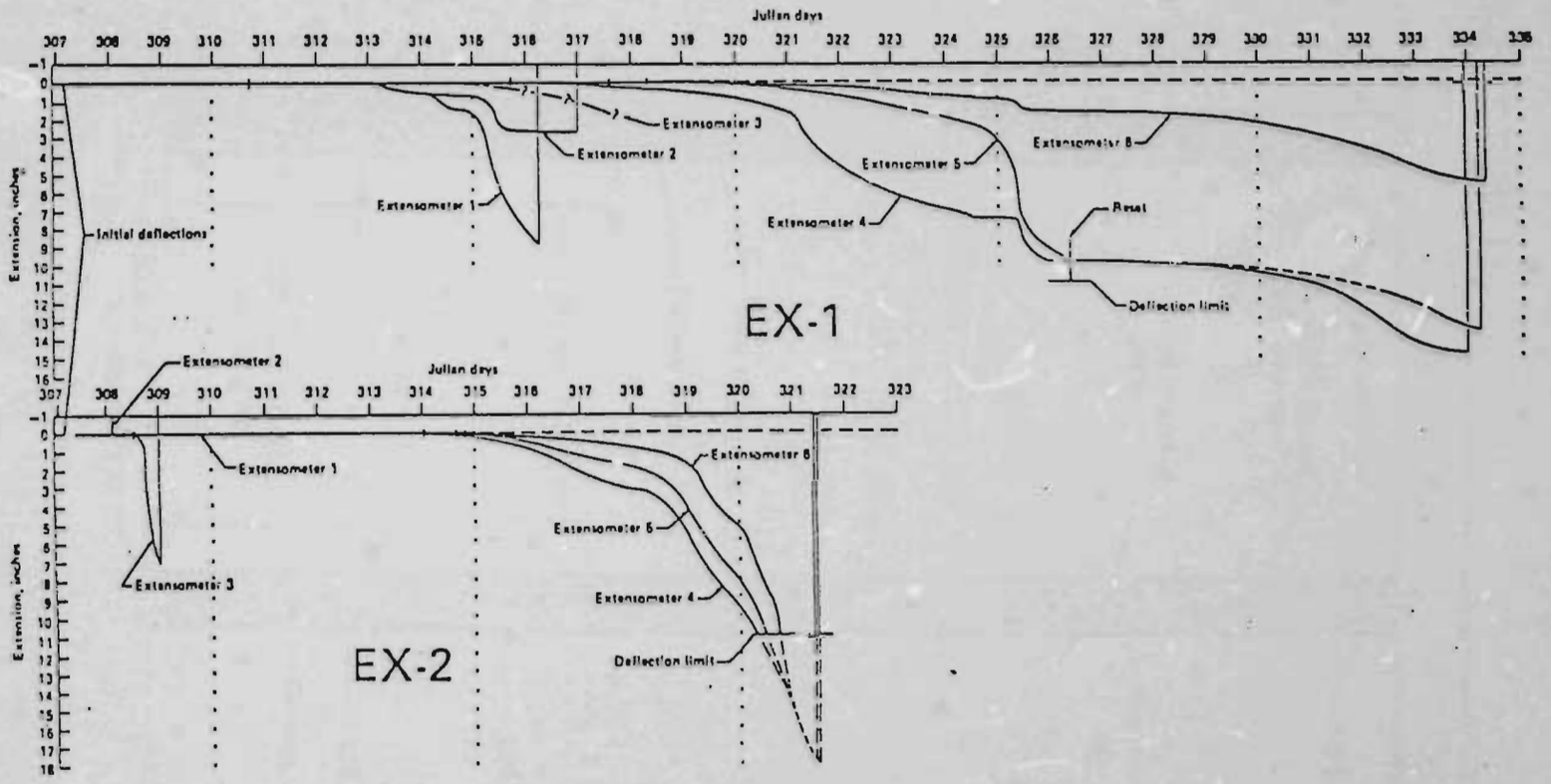

FIGURE 6 B

DRAFT

SS-1 AND SS-2 AS-BUILTS

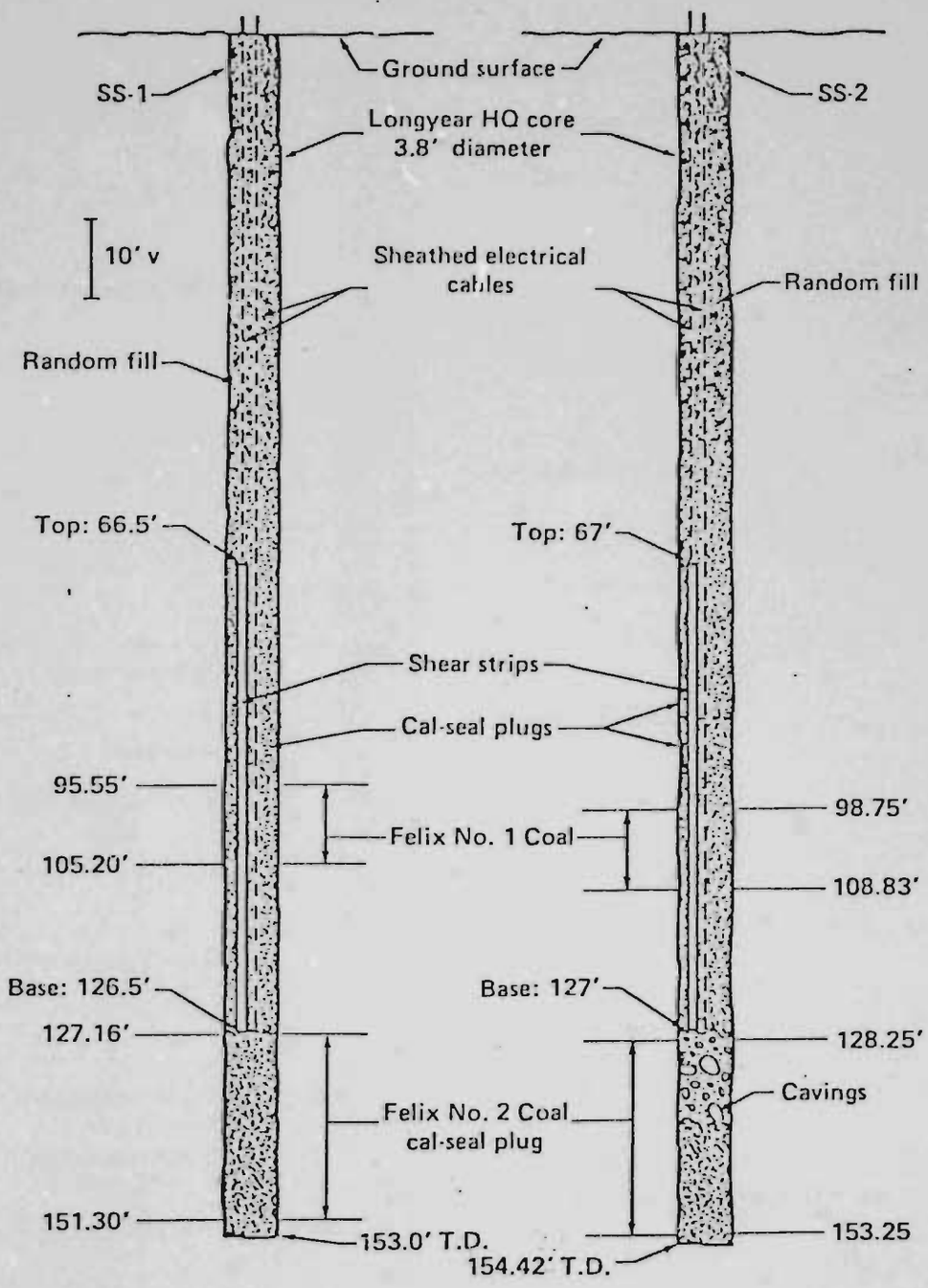

FIGURE 7

DRAFT

PZ-1 AS-BUILT

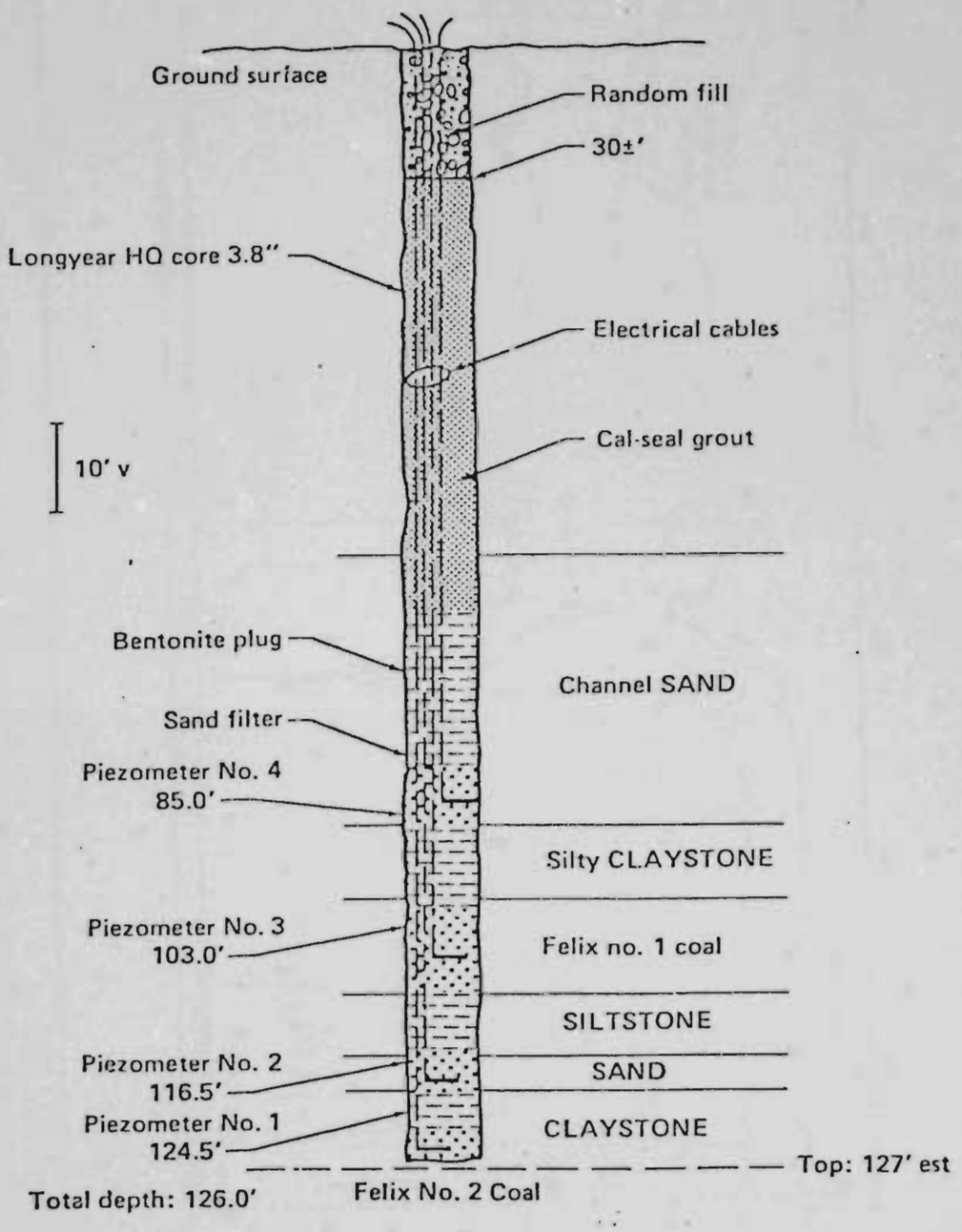

FIGURE 8

INJECTION PRESSURE AND PIEZOMETRIC TRANSDUCER PRESSURES TIME HISTORY

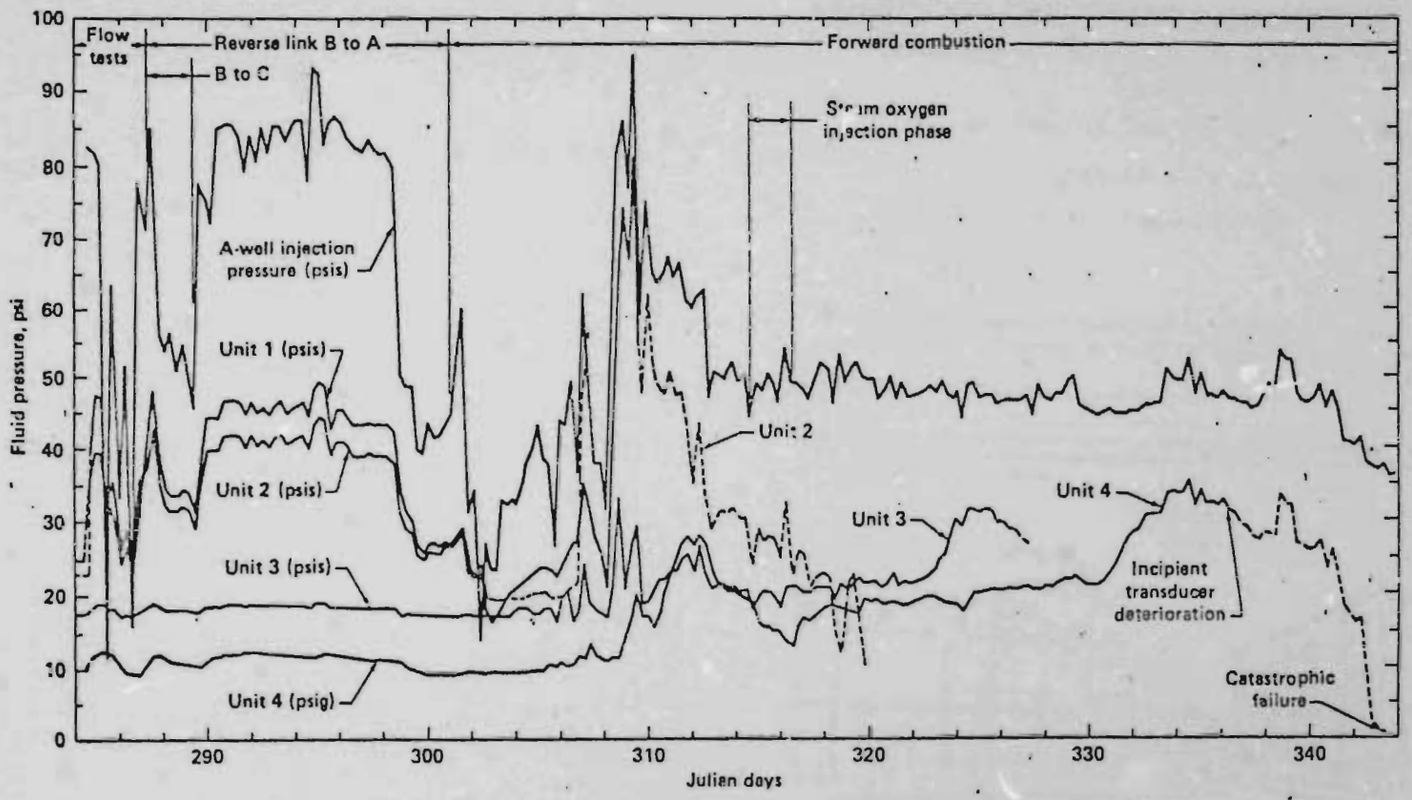

FIGURE 9

Samson
FYI
and distribute
as needed

PREPRINT UCRL- 60592

Lawrence Livermore Laboratory

THE HOE CREEK II FIELD EXPERIMENT ON UNDERGROUND COAL GASIFICATION, PRELIMINARY RESULTS

W.R. Aiman, C.B. Thorsness, R.W. Hill, R.B. Rozsa

R. Cena, D.W. Gregg, D.R. Stephens

February 27, 1978

This paper was prepared for submission to the Combustion Institute/Western States Section 1978 Spring Meeting, April 17-18, 1978, Boulder, Colorado

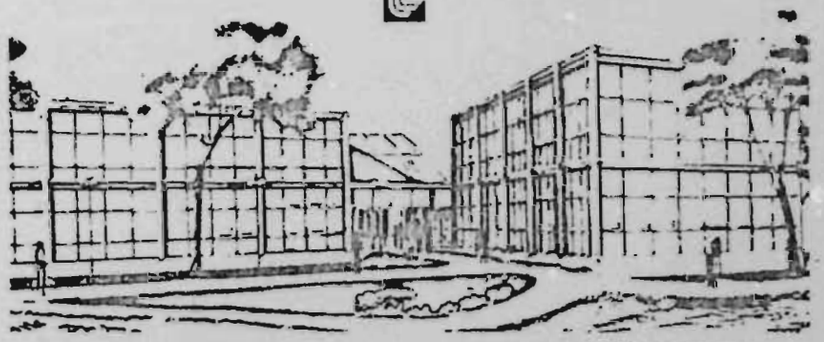

THE HOE CREEK II FIELD EXPERIMENT ON UNDERGROUND COAL GASIFICATION

PRELIMINARY RESULTS*

W.R. Aimsn, C.B. Thorsness, R. W. Hill,, R.B. Rozsa

R. Cena, D.W. Gregg and D.R. Stephens

ABSTRACT

A second in-situ coal gasification experiment was performed by Lawrence Livermore Laboratory at Hoe Creek in Wyoming. The Linked Vertical Wells scheme for in-situ coal gasification was used. The experiment took 100 days for air flow testing, reverse combustion linking, forward combustion gasification, and post-burn steam flow. Air was used for gasification except for a 2 day test with oxygen and steam.

Reverse combustion linking took 14 days at 1.5 m/day. Air requirements for linking were 0.398 Mgmol per meter of link assuming a single direct link. The coal pyrolysed during linking was 17 m^3, which corresponds to a single link 1.0 m in diameter. There was, however, strong evidence of at least two linkage paths. The detected links stayed below the 3 m level in the 7.6 coal seam; however, the product flow from the forward-burn gasification probably followed the coal-overburden interface not the reverse burn channels at the 3 m level.

A total of 232 Mgmols (194 Mscf) of gas was produced with heating value above 125 kJ/mol (140 Btu/scf) for significant time periods and an average of 96 kJ/mol (108 Btu/scf). During the oxygen-steam test the heating value was above 270 kJ/gmol (300 Btu/scf) twice and averaged 235 kJ/gmol (265 Btu/scf).

* "Work performed under the auspices of the U.S. Department of Energy by the Lawrence Livermore Laboratory under contract number W-7405-ENG-48."

The coal recovery was 1310 m^3 (1950 ton). Gasification was terminated because of decreasing product quality not because of burn through. The product quality decreased because of increasing underground heat loss.

Introduction

In-situ coal gasification is an old idea which has become more attractive as the alternatives have become less attractive. The basic concept involves partial oxidation of a coal deposit underground and subsequent recovery of a combustible gas at the surface. Practical means for in-situ coal gasification were developed in the USSR in the 1930's, but discovery of large oil and natural gas resources caused a decline in the use of in-situ gasification by the USSR. Development of these techniques also started in the United States in the 1950's, but low cost oil and natural gas precluded our use of in-situ coal gasification at that time.

The progressive depletion of oil and natural gas resources has made use of coal resources much more attractive. However, large increases in coal production using conventional methods are difficult because of new emphasis on human health and well being in the case of deep mining and because of environmental impact concerns in the case of strip mining.

In-situ coal gasification obtains energy from coal deposits without the underground labor associated with deep mining and without the massive surface disruption associated with strip mining. The economic and resource recovery factors are also attractive (1, 2, 3, 4).

The basic coal gasification process is simple in concept, consisting of three steps: 1) the coal is heated which drives off water and then volatiles to form char (as in destructive distillation), 2) the char reacts with hot steam to form CO + H_2, and 3) finally the remaining char reacts with O_2. The char/O_2 reaction provides the heat to drive all the other reactions, which are endothermic. The char/H_2O reaction produces CO and H_2. The pyrolysis reaction also produces CO and H_2 as well as a wide range of hydrocarbon products.

For maximum product heating value a particular amount of water must enter the reactions. Since the bound-water content of the coal at Hoe Creek is higher than the optimum amount, influx of ground water causes decreases in product heating value.

The overall scheme of in-situ gasification used in the Hoe Creek II experiment is called the Linked Vertical Wells process, which was first used in the USSR more than 30 yrs. ago.(4) The Linked Vertical Wells process is also being developed by the Laramie Energy Research Center (LERC) at Hanna, Wyoming in their in-situ gasification experiments.(5) All gasification schemes involve the three basic steps, but the methods of promoting contact between coal and oxygen differ.

A fundamental problem in in-situ coal gasification is that the permeability of undisturbed (or "solid") coal is too low (< 1 darcy) to allow sufficient gas flow through the coal for practical gasification. Before gasification can proceed, the permeability of the coal must be increased.* In the Linked Vertical Well process, the permeability can be increased by a "reverse" combustion process. This process provides a "link" or high permeability path between the injection and production well.

"Reverse" and "forward" combustion are the two possible processes which can occur when an oxidizer flows through a permeable solid fuel. "Reverse" combustion is occurring when the combustion fronts move upstream against the flow of oxidizer. In a fuel bed ignited at the center, reverse combustion can occur if the oxidizer flow is sufficiently low so that the heat transfer can successively ignite the fuel ahead of the combustion front. Forward

*In the Hoe Creek I experiment the coal seam was fractured with chemical explosives. The permeability enhancement was not as great as had been expected. (6, 7, 8)

combustion occurs if the oxidizer flow rate is too high. Forward combustion also occurs when the burn zone reaches the oxidizer source, because there is no more fuel upstream.

Reverse combustion tends to concentrate into a small zone leaving a high permeability channel behind, through which the combustion products flow.[4] This channel is not empty but is filled with char since reverse combustion consumes only the volatile material in the coal.[4]

Reverse combustion has another important property. During the combustion, the products flow through a channel in which the permeability has been increased. The products from a forward combustion must flow through cold, unreacted coal. The water and tars produced by the combustion processes can condense and block the porosity of the coal. Thus, forward combustion can be self-inhibiting.

The procedure of applying the Linked Vertical Well method is quite straightforward: 1) Drill two wells (A and B) into the coal and case them to near the bottom of the seam. 2) Link the wells at the bottom by reverse combustion; i.e., inject a low flow of air at high pressure into A Well and ignite coal in B Well so that reverse combustion proceeds from B Well to A Well. 3) When the link is completed to A Well (which dramatically decreases the flow resistance), increase the air flow into A Well and gasify the coal seam with forward combustion.

There are three major questions about this Linked Vertical Well method: 1) How can the reverse combustion process be controlled to provide a single link at the bottom of the coal seam while linking at the maximum possible rate? 2) How wide will the final combustion zone be? That is, how much coal will be reacted? 3) What will the product quality be through the burn?

In the Linked Vertical Wells scheme for in-situ gasification, it appears to be important that the link between the wells is at the bottom of the seam (4, 9). It is postulated that caving of coal into the growing cavity spreads the gasification zone and enhances contact between air and coal.

The injection and production wells were cased to within 0.3 m of the bottom of the 7.6 m coal seam so the starting and finishing points of the link were at the bottom of the seam. One of the factors to be determined in the experiment was how high the link might rise during the reverse combustion process.

The path of the reverse combustion link between the injection and exhaust points in the coal seam is probably governed by three factors: 1) random wandering, 2) water in the lower portion of the seam, and 3) bouyancy effects. Random wandering of the path is caused by the non-uniformly distributed fracture patterns in the cleat structure of the coal seam. The reverse combustion will, of course, not penetrate a significant amount of water at the bottom of the seam. The buoyancy of the burned products may cause a tendency of the link to rise in the seam as it proceeds through the coal.

The product quality from gasification of a given coal depends primarily on how much CO_2 and N_2 dilutes the product, since the other major species, H_2 and CO, have nearly identical heating values. The amount of CO_2 depends on how much water enters the reaction and on how much heat is lost from the process. Use of O_2 rather than air can eliminate the N_2 dilution.

The long-term goal of the In-Situ Gasification Program is to develop a process which yields medium heating value gas (200 - 300 Btu/scf). To produce this product O_2 must be used rather than air to eliminate the N_2 diluent in the product gas. In previous experiments air has been used for reasons of simplicity and economy. However, the dynamics of the in-situ process may be

significantly different with O_2 rather than air as the oxidizer. Our next field experiment, Hoe Creek III, will be a full O_2-steam gasification. A short period of O_2-steam gasification was incorporated into the Hoe Creek II experiment to gain some experience and to provide preliminary data.

The above considerations led to the following maj objectives for the Hoe Creek II experiment:

1) Investigate reverse combustion process in rm, wet, hydrologically active coal seam.
2) Determine forward gasification parameters with injected air flows of 40-80 gmol/s (2000-4000 scfm).
3) Conduct a short oxygen-steam burn within the Hoe Creek II air burn.
4) Evaluate diagnostic instrumentation.
5) Evaluate operational parameters.
6) Evaluate environmental concerns.

The Coal Seam and the Experimental Equipment

The Felix #2 coal seam, which we gasified, is a wet, hydrologically active seam with a nearly zero dip, which underlies the thinner Felix #1 coal seam (Fig 1). The Felix # 2 coal has low ash (4.05%), but high water (30.11%) content. (Table I shows an analysis.) The ash-free coal can be represented by a pseudo coal molecule of $CH_{0.91}O_{0.19}N_{0.018}S_{0.027}$ (+0.41 H_2O) with a molecular weight of 16.3 (23.7) and a higher heating value of 481 kJ/gmol. (The actual molecular weights of coal molecules are greater than 1000.) The seam is 7.6 m thick and the bottom of the seam is nominally 45.7 m deep.

A preliminary estimate of 1000 m^3 was made of the coal volume which would be gasified in a 7.6 m seam between wells 18.3 m apart. The model used in making the estimate treats coal as a permeable medium (10). The estimated gasification zone width was 12 m.

The process wells (0.340 m diam) were cased to within 0.3 m of the bottom of the coal to control the location of the reverse combustion link. C Well (0.197 m diam) was intended to be an auxiliary dewatering well and was linked to the bottom of the production well by reverse combustion.

These three wells were each equipped with both air injection and production piping, but Well A was intended as the injection well, Well B as the production well (18.47 m from A), and Well C as a dewatering well (3.31 m from B). Wells A and B served as intended, but Well C was also used as an auxiliary production well. Details of the process wells are shown in Fig. 2. The surface plant provided for compression and injection of the air and for flaring of the product gas. The injection and production flows were measured via orifice plates in the lines.

There were 12 instrument wells emplaced in a pattern designed to monitor the burn zone as it developed. (See Fig. 3). Each instrument well carried seven thermocouples (or more - the levels* are shown in Table II) and a stainless steel tube with an open bottom at the 2.1 m level, which was used for pressure measurements and for gas sampling (except for I-10). Three of these wells, I-1, I-5, and I-10, also had inconel tubes (closed at the bottom) for a traveling thermocouple. The traveling thermocouple consisted of a thermocouple which was lowered down the tube on an I Well by a winch mechanism. The winch mechanism was programmed to stop at various levels while the thermocouple responded to the temperature at that point. The process wells also carried fixed thermocouples at the levels shown in Table II.

The wells designated H-1 through H-6 and SI-1, SI-2, and SI-3 were used for high frequency electromagnetic (HFEM) transmission measurements[11] with a

*The term "level" will be used to indicate distances above the bottom of the coal seam.

transmitting antenna in one well and a receiving antenna in another. Pyrolysis of the coal to form hot char increases the absorption of the HFEM beam, so the HFEM probe can locate the burn zone underground. Wells EX-1, EX-2, SS-1, and SS-2 contained instrumentation to monitor subsurface ground motion. The well PZ-1 contained four piezometer gauges to measure local pressure changes in the layers above the coal. Wells WS-1 through WS-9 were designed for water sampling, primarily post burn, for environmental monitoring. All down hole instrumentation was operating properly at the time of ignition.

The product gas was sampled and analyzed continuously by a set of three chromatographs and by a dew point hygrometer. In addition, water and tar were condensed out of a sample stream for measurement and analysis. Concentrations of H_2O, N_2, O_2, CO, CO_2, H_2, CH_4, C_2H_4, C_2H_6, C_3H_6, C_3H_8, "Higher HC" (nominally C_5H_{12} obtained by backflushing the HC column), and "Tar" were recorded which allowed the computer to calculate heating values and energy recovery rates.

A Hewlett Packard 21 MX-E* computer system recorded, processed, and displayed the data from the gas analyzers, the pressure transducers, and the thermocouples. In excess of 1/2 million data points were recorded and processed. Numerous plotting and tabulating programs allowed access to the raw data and to processed data. The ability to monitor and process much of the data in real time proved valuable in operating the experiment. Computer storage of the data also greatly simplified post-experiment data reduction.

The data reduction codes were based on heat and material balances as previously reported (12). Further details concerning the preparations for the experiment are available (13, 14, 15).

*"Reference to a company or product name does not imply approval or recommendation of the product by the University of California or the U.S. Department of Energy to the exclusion of others that may be suitable."

Conduct of the Experiment

Site Preparation, Hydrogical Testing, and Air Flow Testing

Site preparation started on April 17, 1977. The 37 wells to be used in the experiment were drilled in the pattern shown in Fig. 3. Water pump-down tests showed that B Well, the intended production well, was much "tighter" than A Well or B Well. This low permeability at B Well was reflected in the results of the air flow tests.

Air flow testing started when the surface piping was completed on 10/4/77 (day 277 of 1977). Air flow testing was continued over the next 10 days, while the process systems were completed and checked. During the air flow testing (and reverse combustion) any water which accumulated in the process wells was periodically blown out through special "dewatering" lines by opening a valve and increasing the system's back pressure. These lines, which extended into sumps at the bottom of the wells, were made of 2" stainless steel pipe so that they could survive the combustion processes. The dewatering line in C Well also had a pump to aid in dewatering during the reverse combustion process. However, this pump was burned out early in the reverse combustion process. Fortunately no difficulty was encountered in removing water from B Well through its dewatering line.

The average flow conductance between the wells was:

Well Combination	C 10^{-12} gmol/s Pa^2	C 10^{-3} scfm/$psia^2$
A to B	1.65	3.9
C to B	2.26	5.1
A to C	1.69	4.0

where:

$$C = \frac{Q_{prod}}{P_{inj}^2 - P_{prod}^2}$$

This conductance did not appear to increase significantly after the first few days of the air flow tests nor did it seem to be a function of the system pres-

sures. System pressure did affect water influx, as expected. Flow rates out of the production well of 0.3-0.4 gmol/s (15-20 scfm) were produced with a back pressure of 310 kPa (45 psia) and with a reasonable injection pressure of 552 kPa (80 psia). This flow rate was considered to be high enough to support an adequate reverse combustion link.

Ignition and Reverse Combustion Linking

The coal was ignited (day 287.392) at the bottom of B Well with air injection into both C Well and A Well. (A helium tracer test showed that about 60% of the air arriving at B well had been injected into C well. This fraction increased to above 80% just after ignition.) The flow out of B Well was to be controlled at about 2.0 gmol/s (100 scfm)* throughout the reverse combustion and the pressure was to be controlled at about 345 kPa (50 psia). To ignite the coal bed, loose coal was placed in the bottom several feet of B Well, an electrical ignitor was placed on top of the loose coal, and several feet of wax coated charcoal was placed on the ignitor.**

Within one hour after the ignitor was turned on, a sample of the product gas contained combustion products with essentially zero O_2; however, 7 hours were were required before the thermocouple at the bottom of the B Well casing fully reflected the onset of combustion (T > 200 C.).

The reverse combustion linkage was completed to C Well at 289.542. Completion of the link was signaled by an increase in the temperature at the C well. C Well is 3.31 m from B Well so, assuming a direct path, the linkage rate was 1.5 m/day

*In the text, flow rates are on a wet basis. Table III lists dry basis flow rates.
**Waterproof ignition materials are essential because water can reinvade the bottom of the well during the charcoal loading process because the system pressure is low. Our first ignition attempt failed because the charcoal disintegrated when it got wet and fell away from the ignitor into the sump (Fig. 2).

(18 μm/s). During the B to C linkage process, the average injection and production well head pressures were 419 kPa (61 psia) and 308 kPa (45 psia). The average production flow rate was 2.43 gmol/s (122 scfm).

The reverse combustion linkage was completed to A Well at 301.046. A Well is 18.47 m from B Well so the linkage rate was 1.6 m/day (19 m/s), assuming negligible progress toward A Well during the B to C linkage process. During the B to A linkage process, the average injection and production well head pressures were 517 kPa (75 psia) and 316 kPa (46 psia). The average production flow rate was 1.86 gmol/s (93 scfm).

Because the B - C link and the B - A link were burning at the same time, these processes can not be completely separated in analyzing the product flow data. Thus, two links were lumped together for calculating the air requirements for linking.

A carbon balance, using the composition and flow rate of the product gases, showed that 8.76 m^3 of coal was completely consumed leaving an empty channel or that 17 m^3 of coal was pyrolysed leaving a char filled channel. For a total link distance of at least 21.78 m (B to C plus B to A, assuming direct paths), this means a single, direct reverse combustion channel would have a diameter of less than 1 m if char filled (0.7 m if empty). The air injected was 8.67 Mgmol or 0.398 Mgmol per meter of link.

The linkage rate calculations assumed that the link took the shortest path between the wells. However, the permeability of the coal formation was very non-uniform and the linkage paths were not direct from well to well. The thermocouples on the instrument wells responded to the reverse combustion as shown in Figure 4.

From this thermocouple response data we can conclude that the reverse combustion was not a single channel (nor were the channels straight). At least

two paths were involved and perhaps more. None of the wells attained a temperature above the steam plateau (100°C) at any level above 3 m. The HFEM probing located a link at 2.5 - 3 m but saw no evidence of reverse combustion above 3 m during the reverse combustion phase. The observed data indicated that all links were at or below the 3 m level and that the reverse combustion process had been satisfactory. However, the product flow from the forward combustion gasification left these channels soon after the start of forward combustion.

Gasification in Forward Combustion

As the reverse combustion link approached the A Well, the flow conductance increased gradually, as the link was completed, to 1.1 x 10^{-10} gmol/s Pa^2 (0.25 scfm/$psia^2$) (Figure 5). With this low flow resistance, high flow rates were possible at reasonable injection pressures. The flow was increased in three steps, from the 2.0 gmol/s (100 scfm) flow used in reverse combustion up to 2 gmol/s (1050 scfm) by the end of day 301. The product gas had a good heating value of about 125 kJ/gmol (140 Btu/scf) but large amounts of particulate matter were also blown out of the production well. Analysis of the particulate matter showed that it was not ash but either char or dried coal. The responses of thermocouples on A Well and I-10 indicated that the burn pattern development was upward as much as horizontal during this period.

When the flow was increased (301.365) at the start of forward combustion, the thermocouples in all of the reverse combustion channels responded, indicating flow in these channels. The initial flow was along an A Well to I-6 Well to I-1 Well to B Well channel, but thermal responses were seen at all of the other thermocouples in the reverse combustion channels indicating flow in several reverse combustion channels.

At 301.70 all of the thermocouples which had been indicating flow in the

reverse combustion channels simultaneously started to cool again which indicated that the flow in these channels had stopped. No further indication of hot gas flow was observed in any of the links which had been detected during reverse combustion.

There was a large increase in the conductance between A Well and B Well at 301.7 which closely corresponded to the flow stoppage in the original reverse burn channels. The opening up of a previously undetected channel would explain these observations. The channel may have been along the coal-overburden interface but there were no thermocouple junctions located there. However, later in the experiment, numerous thermocouples were burned off between the 7.16 and 8.53 m levels, which bracketed the coal-overburdened interface. In addition, the movement of the burn zone to the top of the coal seam was confirmed by the HFEM measurements and by the traveling thermocouple data.

This burning off of thermocouples was a continuing problem during the experiment. A burned-off thermocouple was easily detected by a simple resistance check between the leads and the sheath since they were originally isolated electrically. At many of the wells the thermocouple bundle would burn off just as the temperature response started during forward burn. The traveling thermocouple tubes in I-1, I-5, and I-10 survived much longer to provide critically needed information. The traveling thermocouple probe was lost on day 315 when the tube in I-5 burned off with the probe down hole.

Although the burn apparently moved quite quickly to the top of the seam, five days of good gas production followed the increase in flow rate at 301.4. During this time, H_2 and CO concentrations decreased slightly but increases in the hydrocarbon concentrations caused the product heating value to remain near 125 kJ/gmol (140 Btu/scf) (Fig. 6). Although good gas was produced, the particulate problem continued.

On day 304 a hole was eroded through the case of the automatic back pressure control valve because of the particulate matter in the product gas. Back pressure control was shifted to a manual valve but other leaks developed in bellows expansion joints in the production line. On day 305 the flow was cut in half and the back pressure was increased, but the particulate production continued and more leaks developed. On day 306 the production flow was bypassed through a 3" line while repairs were made to the production line. The injection flow was reduced to 17 gmol/s (850 scfm) at a back pressure (B Well) of 310 kPa (45 psia). Repairs took 7 hours.

The product's heating value began to decline just before the repair period. Over the next five days the heating value fell from the 125 kJ/gmol (140 Btu/scf) level to essentially zero (Fig. 7). During the decline, production from C Well rather than from B Well was tried. No effect was found on the product heating value, but the particulate production was reduced. Production from C Well became the standard mode of operation for the remainder of the experiment. At this point in the experiment it was postulated that the injection well casing had broken or that a hole had been burned through the casing at the top of the coal seam allowing air to bypass the preferred reaction zone at the bottom of the coal seam. It was further postulated that a bypass channel existed along the top of the seam over to the production well.

These postulates implied that the reaction zone was located at the top of the seam which would cause two problems. A long term problem was that a large part of the coal seam could be bypassed if the burn proceeded over the top. The immediate problem was heat loss to the overburden. The heating value of the product is strongly dependent on the extent of the steam-char reaction which is endothermic and of the pyrolysis reaction which requires heating of the coal.

These processes are driven by the heat released by the oxidation reaction. If the heat released by the oxidation reaction is lost from the system then the product will be mostly CO_2 and N_2.

The heat may have been lost because the coal gasification reaction occurred in the coal just under the overburden or there may have been dual air injection points. One injection point may have been in the coal seam, where coal was gasified. The other injection point may have been in the overburden, perhaps where the well casing was broken. If the gasification products were burned in the overburden by the air from the secondary air injection, then the heat released would be lost to the inert overburden.

The broken casing and bypass channel postulates were not definitely confirmed, but on day 311 they led us to switch the injection flow from the A Well casing to the 2" stainless steel dewatering line which extended to the bottom of A Well. (See Fig. 2). This 2" line was protected by the outer casing from the combustion gases and from relative movements of the overburden and the coal seam.

When the air injection was switched to the dewatering pipe in A Well the heating value quickly increased to the 110 kJ/gmol (120 Btu/scf) level (Fig. 8). The success of the dewatering pipe mode of operation tends to confirm the bypass postulates.

The product heating value remained at the 110 kJ/gmol (120 Btu/scf) level for the next 3 days. Then, in preparation for the O_2-steam mini-experiment, the air injection was returned to the outer casing of A Well on day 314 and the heating value dropped again.

At this point the anticipated results for the O_2-steam mini-experiment were very poor, because the O_2 entered the coal formation at about the same level as the air injected in the outer casing. (See Fig. 2.) It was expected

that heat loss would again prevent the reactions which produce the fuel gases.

After O_2-steam injection started, the heating value initially decreased. But then a rapid increase commenced, which carried the heating value to above 270 kJ/gmol (300 Btu/scf) (Fig. 9). The rise in heating value was curtailed by a failure of the O_2 supply system. The flow of O_2 was near zero for an hour and periodic decreases of flow plagued the experiment for the entire O_2 phase.

The O_2-steam gasification phase was terminated at 316.4 when oxygen breakthrough into the product gases occurred. The total duration of the O_2-steam phase was 2.2 days. Neglecting the transient periods, the produced gas had a 235 kJ/gmol (264 Btu/scf) average heating value. This corresponds to 663 kJ per gmol of injected O_2.

The success of the O_2 phase of the experiment must have been due to the high temperature of O_2-coal combustion. The heat loss to the overburden must have been overwhelmed by the amount of energy available.

After the O_2-steam phase it was decided to check air gasification using the same injection point by injecting air with the O_2 lance. The product had poor heating value and O_2 breakthrough occurred in 2 hours.

Air injection was then returned to the dewatering line which extended to the bottom of the coal seam. The heating value rose rapidly to the 125 kJ/gmol (140 Btu/scf) level (Fig. 10). Apparently there was still a reaction zone available at the bottom of the coal seam where the endothermic reactions were not prevented by heat loss.

Gasification continued with injection in the dewatering line for another 43.1 days. During this time period the product's heating value decreased more-or-less linearly with time (Fig. 10). This decline in heating value apparently was due to increases in heat loss to inert materials underground. The product's higher heating value correlates fairly well with the calculated

underground heat loss, considering the imprecision in this calculated term (Fig. 11). Changes in water influx did not match the decline in heating value.

Gasification was terminated by shutting off the compressors on Christmas Day (359.8) when the heating value was 59 kJ/gmol (67 Btu/scf). Burn through had not occurred and ungasified coal remained near the production wells.

After the compressors were shut off and combustion stopped, large quantities of steam continued to flow out of the production wells as the ground water filled the hot burn zone. A small amount of pyrolysis gas was also produced in the early part of the steam flow period. Flow ceased on day 377 (Jan. 12, 1978) when the production wells cooled to below the steam temperature and a liquid seal formed.

SUMMARY

The experiment took 100 days from the first air injection to the final steam production. Table III provides an overall data summary. The injection flow and the heating value of the product gas are shown in Fig. 12 which is also marked along the timeline with the major events of the experiment. The variations in product gas composition are shown in Fig. 13. System pressure, net water influx, and gas recovery (N_2 balance) are shown in Fig. 14.

The total energy production (gas + tar) was 2.4×10^{13} J (2.3×10^{10} Btu) from the gasification of 1310 m^3 (1952 ton) of coal. The average gas quality was quite good at 96 kJ/gmol (108 Btu/scf) for air injection and 235 kJ/gmol (264 Btu/scf) for O_2 injection. A total of 2.11×10^8 gmol of air was injected and the average system pressure was 324 kPa (47 psia). Of the N_2 contained in the injected air, 19.9% was not recovered in the product over the course of the experiment. The gas which was lost probably reacted with the coal before flowing out into the formation. Thus another 325 m^3 of coal probably gasified but the products were lost. The fate of these gases is not entirely known but

no large quantity of gas was observed leaving the ground in any localized area near the gasification site.

During the entire gasification period excess water influx occurred. The product quality decreased when the system pressure fell below the hydrostatic pressure, especially during the early part of the experiment. Gas losses limited the use of high pressure to control water intrusion.

Ignition and reverse burn linking seemed to go very well. Ignition occurred with the second try on day 287.4. Linking to C Well occurred on 299.5 and to A Well on 301.0 for a linkage rate of 1.6 m/day. At least two and perhaps three linkage paths were inferred from the responses of the downhole thermocouples. All of these links were below the 3 m level in the 7.6 m seam. Later events lead us to postulate another flow path across the top of the seam.

Forward combustion gasification started out well on day 301 and good gas was produced (135 kJ/gmol - 140 Btu/scf) for the first five days, however heavy particulate production occured which damaged the production lines. During this period the burn pattern development was upward as much as horizontal. The initially detected flow in the reverse burn channels at the 3 m level stopped at 301.7. The flow was probably then along the coal-overburden interface. Production of reasonably good gas continued until 306.4 at which time some not-fully-identified change in the formation caused the onset of a decline in the heating value of the production gas. A leak in the injection well casing may have resulted in the reaction zone moving to the top of the coal seam, where heat was lost to the overburden. Shifting injection flow to an auxiliary line which extended to the bottom of the coal seam inside the A Well casing, caused the product's heating value to return to the 125 kJ/gmol (140 Btu/scf) level.

The oxygen-steam mini experiment (314.889 to 316.513) went quite well.

The product's heating value exceeded 270 kJ/gmol (300 Btu/scf) twice and averaged 235 kJ/gmol (264 Btu/scf). Following the oxygen-steam experiment, air was again injected into the auxiliary line and gasification continued for another 43 days (316.7 to 359.84). The heating value started again at the 125 kJ/gmol (140 Btu/scf) level but steadily declined to 59 kJ/gmol (66 Btu/scf) at shut down.

After the injection flow was shut off, steam continue to flow for 17 more days (359-367) as inflowing water contacted hot rubble in the burn zone. The energy produced during the steam flow period was 81.9% of the integral heat loss from the preceeding periods of the experiment. The overall net heat loss underground was 2.6% of the energy contained in the coal gasified. The size of this loss term is comparable with the experimental errors involved.

The combustion zone never burned through to B or C well during the later stages of operation. Gasification was terminated because of the decreasing product quality. During the final phase, there was a direct trade off between quality and quantity (Fig. 15).

The final burn zone was very large in area. All of the wells in Fig. 3 showed evidence of contact with the burn zone, except for H-1, H-2, WS-4 and WS-5. Thus the burn zone was at least 16 m wide. A portion of the coal, near the production wells was probably not consumed. A coring test is planned to better define the burn zone.

Discussion

Despite the many difficulties encountered the final results were quite good. Problems were encountered with a gradual heating value decline in the latter part of the experiment, with control of the burn pattern, with particulate production, with water influx, and with high well head temperatures.

The gas quality was good but it varied widely, partly because of the problem of controlling the burn pattern. The gasification was terminated

because increasing heat loss to inert materials underground had caused the product's heating value to decline. A sizable amount of coal near the production well was not gasified, but the total coal recovery was quite good anyway because the gasification zone was wider than expected.

The forward combustion process apparently did not follow the reverse combustion channels at the 3 m level in the 7.6 m seam. Shortly after forward combustion started, the flow in these channels stopped, then the product flow was probably at the coal, overburden interface. Caving of the inert overburden materials directly into the burn zone may have caused the high underground heat loss which was responsible for the decline in the product's heating value.

Particulate production was a problem particularly during the early part of the gasification. These particulates eroded holes in the backpressure control valve and in several expansion bellows in the production line.

Water influx into the burn zone was a problem, particularly in the early parts of the experiment, whenever the system pressure was below the hydrostatic head at the bottom of the coal seam.

Excessive production well head temperatures were experienced during the latter parts of the experiment. Water injection into the production well was used to keep the well head below the metal softening temperature (~430 C).

The water sampling portion of the experiment is only just underway. This project is concerned with the quantity and the fate of water pollutants such as phenol and CN^- formed during the combustion processes. Water sampling will continue over the next 24 months in order to determine how much and what kind of pollutants were formed and how they move through the coal seam. Fortunately, the coal seam acts like an adsorption column to slow the movement of pollutants away from the burn zone. During the slow desorption process, the ground water flow may dilute the pollutants to below acceptable limits.

Surface subsidence is the other environmental impact concern which we addressed in this experiment. A detailed survey of the monuments placed on the surface above the burn zone has not been done, but as of this date no substantial subsidence has occured. These monuments will be monitored over the next 18 months in order to detect any future subsidence.

CONCLUSIONS

1. Good quality gas was produced. 94 kJ/gmol (106 Btu/scf) and 235 kJ/gmol (264 Btu/scf) average for air and for O_2 gasification respectively.
2. Gasification was terminated because of decreasing product quality-59 kJ/gmol (66 Btu/scf) at termination.
3. The amount of coal gasified was 1310 m^3 (1952 ton).
4. The total energy recovery at the surface was 97% with 63% in the form of combustible gas.
5. Gas loss underground was 19.9% (N_2 balance).
6. Reverse combustion appeared to proceed as desired with linking at the 3 m level in the 7.6 m seam and no clear indication of links at higher levels. The linkage rate was 1.6 m/day (B Well to A Well).
7. Despite the apparent linking only at the 3 m level, the main flow path shifted on the first day of forward gasification to a level near the top of the coal seam, perhaps at the overburden interface.
8. In the later stages of the gasification it was essential to inject the air into the coal seam through a dewatering line which extended to the bottom of the seam. Injection into the main well casing produced low quality gas, probably because of a broken well casing.
9. The gasification zone was exceptionally wide, which accounts for the high coal recovery even though the coal near the production wells was not consumed.

PLANS

1. Exploratory wells will be drilled to locate the burn zone boundaries.
2. The subsidence and water quality monitoring programs will continue in order to determine the environmental impacts of the process.
3. Further data analysis and modeling will be done in order to more fully understand the reverse and forward combustion processes which occured during this experiment.

ACKNOWLEDGEMENT

We would like to thank the rest of the LLL In Situ Coal Gasification team, who all had a part in making this experiment a success. They fought the weather at the test site (-34 F once and several blizzards), several unanticipated events, and a tight schedule to get the job done.

REFERENCES

1. Buder, M. K., Fisher, R. A., McCone, A. I., Terichov, O. N., and Wong, M. J., "Factors Influencing the Economics of Large-Scale In Situ Coal Gasification Operations", Second Annual Underground Coal Gasification Symposium, Morgantown, August 10-13, 1976, (NTIC #MERC/SP-7613), p. 145.

2. Garon, A. M., "On Economic Evaluation of Underground Coal Gasification", Second Annual Underground Coal Gasification Symposium, Morgantown, August 10-13, 1976, (NTIC #MERC/SP-7613), p. 155.

3. Kreinin, E., and Revva, M., Underground Gasification of Coal, Podzemnaya Gazifikatsiya Uslei, Kemerous, Kocknizhnoe Izdatel'stvo (1966), (UCRL Trans. - 10810)

4. Skafa, P. U., Underground Gasification of Coal, Gosudarstvennoe Nauchno-Tekhnicheskoe Izdatel'stno Literaratury Po Gornomu Delu, Moscow (1960) (UCRL Trans. - 10860)

5. Brandenburg, C. F., Reed, R. P., Boyd, R. M., Northrop, D. A., and Jennings, J. W., "Interpretation of Chemical and Physical Measurements from an In Situ Coal Gasification Experiment", 50th Annual Fall Meeting of the Society of Petroleum Engineers of AIME, Dallas, Sept. 28 - Oct. 1, 1975.

6. Hill, R. W., Stephens, D. R., and Thorsness, C. B., "The LLL In-Situ Coal Gasification Project", Proceedings of the Third Annual Underground Coal Conversion Symposium, Fallen Leaf Lake, California, Jun 6-9, 1977, (NTIC # Conf. - 770652) p. 29.

7. Thorsness, C. B., Hill, R. W., and Stephens, D. R., "Preliminary Results from an In-Situ Coal Gasification Experiment Using Explosive Fracturing", Division of Fuel Chemistry, Am. Chem. Soc., Montreal, May, 1977.

8. Hill, R. W., and Thorsness, C. B., Results from an In Situ Coal Gasification Experiment Involving Explosive Fracturing: Hoe Creek Experiment No. 1., Lawrence Livermore Laboratory Rept., UCRL - 52229, February 15, 1977.

9. Arinenkou, D. M. and Markman, L. M., Underground Gasification of Coal, Knizhnoe Izdatel'stvoStalino-Donbass, 1960, (UCRL Trans. 11007).

10. Thorsness, C. B., Rozas, R. B. and Wong, R., "Two-Dimensional Modeling of In-Situ Coal Gasification", Third Annual Underground Coal Conversation Symposium, Fallen Leaf Lake, California, June 6-9, 1977.

11. Davis, D. T., and Lytle, R. J., In Situ Coal Gasification Burnfront Mapping by Monitoring Reflected High Frequency Electromagnetic Waves, UCRL - 52325, Sept. 8, 1977.

12. Hill, R. W. and Thorsness, C. B., Results from an In Situ Coal Gasification Experiment Involving Explosive Fracturing: Hoe Creek Experiment No. 1, UCRL - 52229, Feb. 15, 1977.

REFERENCES (Con't.)

13. Thompson, D. S. and Madsen, S. K., LLL In Situ Coal Gasification Program Quarterly Progress Report, Jan- Mar 1977, UCRL - 50026-77-1, June 1, 1977.

14. Adelmann, C. R., and Minkel, K. J., LLL In Situ Coal Gasification Program Quarterly Progress Report, April-June 1977, UCRL - 50025-77-2, Oct. 1, 1977.

15. Olness, D. U. and Madsen, S. K., LLL In Situ Coal Gasification Program Quarterly Progress Report, July-Sept. 1977, UCRL - 50026-77-3, Nov. 1, 1977.

TABLE 1. Analysis of Coal.

	Proximate analysis, % As received	Dry Basis		Ultimate analysis, % As received	Dry Basis
Moisture	30.11	-	Moisture	30.11	-
Ash	4.05	5.80	Carbon	48.38	69.23
Volatile	32.12	45.96	Hydrogen	3.66	5.24
Fixed Carbon	33.72	48.24	Nitrogen	1.01	1.45
	100.00	100.00	Chlorine	0.00	0.00
			Sulfur	0.34	0.49
Heating Value Btu/#	8,359	11,960	Ash	4.05	5.80
kJ/g	19.4	27.8	Oxygen (diff)	12.45	17.79
				100.00	100.00

TABLE II.* Down-Hole Thermocouple Levels

Level* m	I-1	I-2	I-3	I-4	I-5	I-6	I-7	I-8	I-9	I-10	I-11	I-12	A	B	C
13.4													x		
12.2		x			x					x			x		
11.0													x		
9.8													x		
8.5	x	x	x	x	x	x	x	x	x	x	x	x	x	x	x
7.2	x	x	x	x	x	x	x	x	x	x	x	x	x	x	x
5.8	x	x	x	x	x	x	x	x	x	x	x	x	x	x	x
4.4	x	x	x	x	x	x	x	x	x	x	x	x	x	x	x
3.0	x	x	x	x	x	x	x	x	x	x	x	x			x
1.7	x	x	x	x	x	x	x	x	x	x	x	x	x	x	x
.3	x	x	x	x	x	x	x	x	x	x	x	x			x

* "Level" is used to indicate distances above the bottom of the coal seam.

TABLE III. Summary of Data

Time Period,* day of 1977	Energy Flow Rate (Gas & Tar) MW	Injection Flow Rate, gmol/s	Injection Flow Rate, scfm	Production (Dry Basis) Flow Rate, gmol/s	Production (Dry Basis) Flow Rate, scfm	System Pressure kPa	System Pressure psia	Total Produced Dry Gas, Mgmol	Total Produced Dry Gas, Mscf	Total Energy Produced (Gas & Tar). 10^{12} J	Total Energy Produced (Gas & Tar). 10^{9} Btu	Coal Gasified. m^3	Coal Gasified. Ton
287.400-				Reverse Combustion Period									
301.395	0.13	7.2	361	1.51	75.8	407	59.1	1.83	1.5	0.16	0.15	8.8	13.1
301.395-				Initial Gasification Period									
306.492	6.24	27.9	1401	45.4	2279	238	34.5	20.0	16.72	2.75	2.61	122	181.8
306.830-				Decline Period									
311.378	3.47	38.4	1928	40.9	2053	480	69.5	16.08	13.44	1.36	1.29	84.6	126.1
311.400-				Dewatering Pipe Injection Period									
314.549	2.93	30.6	1536	25.3	1320	357	51.8	7.16	5.99	.80	0.76	42.0	62.6
314.950-				O_2 - Steam Injection Period									
316.497	6.60	11.3	567	24.6	1235	314	45.6	3.24	2.75	.88	0.83	41.3	61.5
316.700-				Terminal Period									
359.788	4.88	46.1	2314	49.6	2490	288	41.8	184.7	154.43	18.17	17.22	1020	1519.8
359.788-				Steam Flow Period									
377	(2.77)**	0.0	0	(53.3)**	2676	85	12.4	(79)**	66.05	(4.1)**	(3.89)**	-	-
301.400-				Total Forward Burn Gasification									
359.734	4.78	41.9	2103	46.1	2314	324	47.0	232.2	194.15	24.08	22.82	1310	1951.9

* These time periods, used in the integral averages, exclude transition periods.
** Steam equivalent.

TABLE III cont.

Time Period,	Product Composition, mol frac N_2	H_2	CH_4	CO	CO_2	Higher Heating Value, kJ/gmol	Higher Heating Value, Btu/scf	Reactant Stoichiometry O_2/C	Reactant Stoichiometry H_2O/C
287.400-			Reverse Combustion Period						
301.395	0.619	0.119	0.024	0.043	0.175	87	98	0.53	0.21
301.395-			Initial Gasification Period						
306.492	0.515	0.175	0.024	0.122	0.147	127	143	0.506	0.153
306.830-			Decline Period						
311.378	0.665	0.078	0.013	0.051	0.170	63	71	0.60	0.00
311.400-			Dewatering Pipe Injection Period						
314.549	0.539	0.155	0.020	0.098	0.176	100	112	0.507	0.170
314.950-			O_2-Steam Injection Period						
316.497	0.001	0.365	0.056	0.228	0.337	235	264	0.423	0.254
316.700-			Terminal Period						
359.788	0.568	0.137	0.024	0.071	0.185	93	105	0.534	0.180
359.788-			Steam Flow Period						
377	-	-	-	-	-	-	-	-	-
301.400-			Total Forward-Burn Gasification						
359.734	0.564	0.140	0.023	0.077	0.183	96	108	0.522	0.171

TABLE III cont.

Time Period	Energy Distribution, %					Gas Loss, %	Energy per O_2, kJ/gmol	Net Water Influx Rate, gmol/s
	Combustible Gas	Combustible Tar	Steam	Sensible Heat	Underground Heat Loss			
287.400-			Reverse Combustion Period					
301.395	67.3	-	9.67	0.81	22.23	83.25	87	-
301.395-			Initial Gasification Period					
306.492	77.4	6.42	12.08	6.04	Nil	Nil	1060	14.3
306.830-			Decline Period					
311.378	44.5	15.79	13.45	7.77	18.4	11.0	431	11.8
311.400-			Dewatering Pipe Injection Period					
314.549	63.3	7.26	7.98	4.17	17.3	32.1	453	5.5
314.950-			O_2 - Steam Injection Period					
316.497	69.9	9.43	9.55	1.69	9.46	26.2	663	12.1
316.700-			Terminal Period					
359.788	63.2	3.59	9.93	7.31	15.96	21.9	501	10.9
359.788-			Steam Flow Period					
377	-	-	-	-	-	-	-	53.3
301.400-			Total Forward Burn Gasification					
359.734	63.4	5.03	22.03	6.94	2.6*	19.9	530	11.0

*The Energy recovery during the Steam Flow Period was subtracted from the previous Heat Loss term and added to the Steam term.

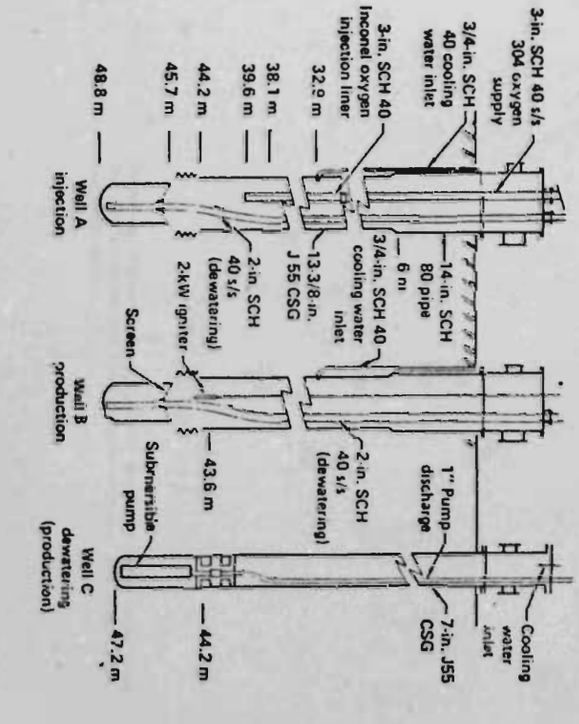

Figure 2. Process well details. The top and bottom of the Felix #2 coal seam are at 38.1 m and 45.7 m respectively.

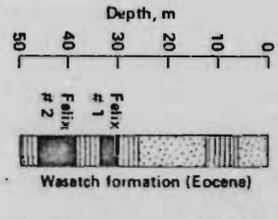

Figure 1. Site stratigraphy obtained from cored wells.

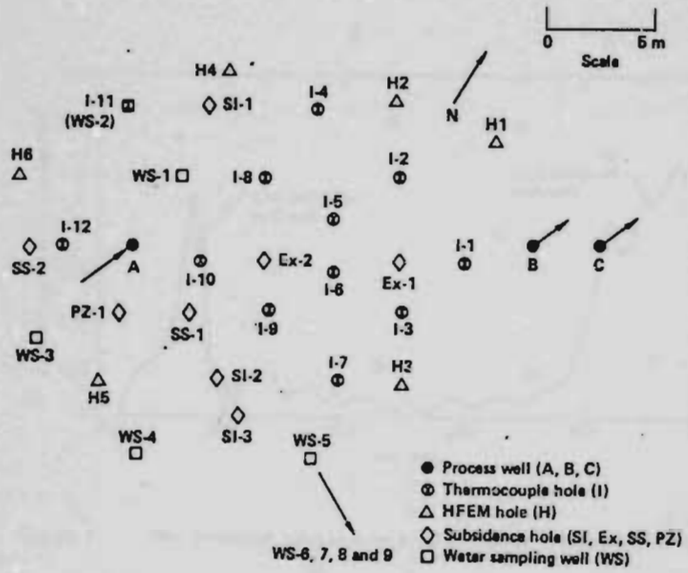

Figure 3. Well layout for the Hoe Creek II In Situ Coal Gasification Experiment.

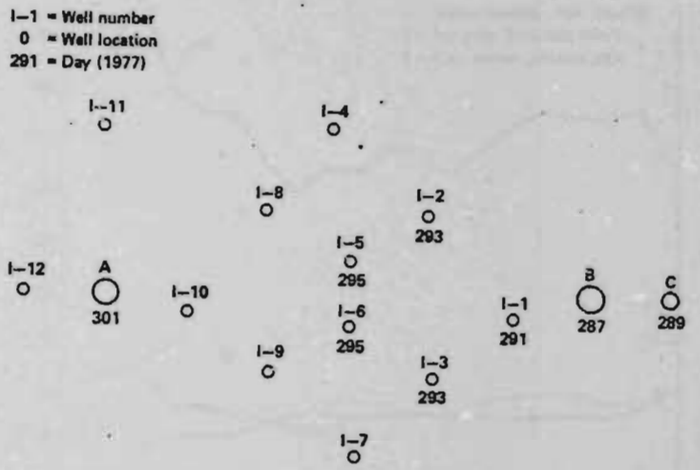

Figure 4. Downhole thermocouple responses during reverse combustion. The day on which the temperature exceeded 100°C is shown for each well.

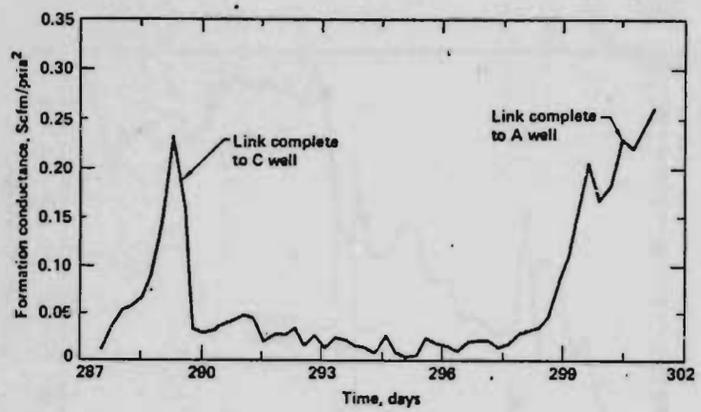

Figure 5. The formation conductance during reverse combustion linking.

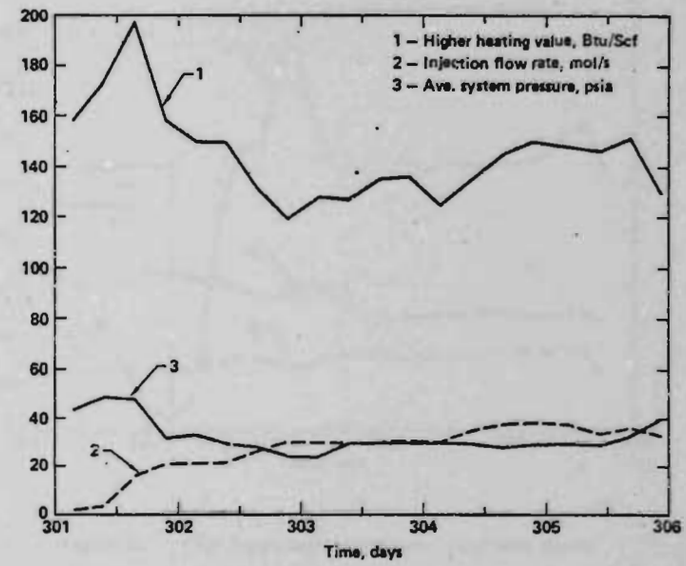

Figure 6 The initial forward combustion phase.

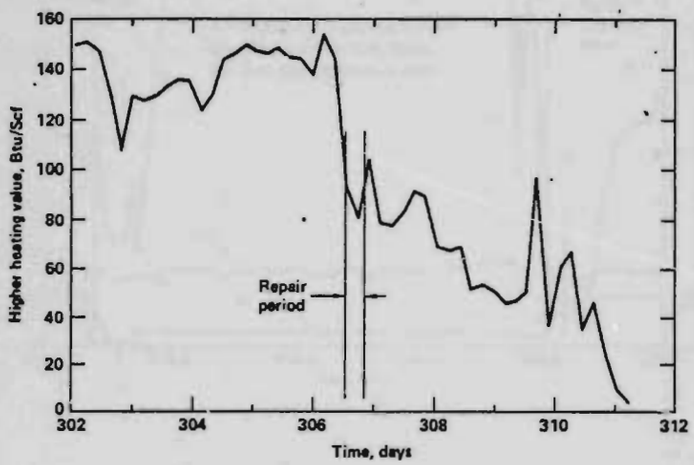

Figure 7. The product quality decline phase.

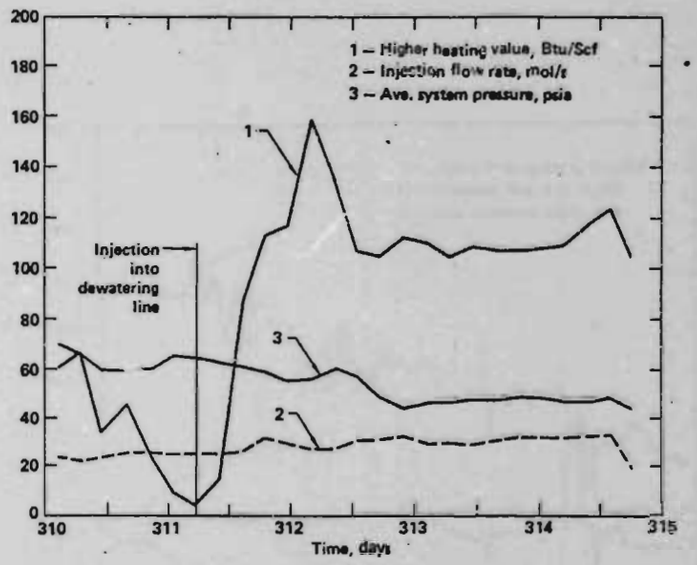

Figure 8. The injection-in-the-dewatering-line phase.

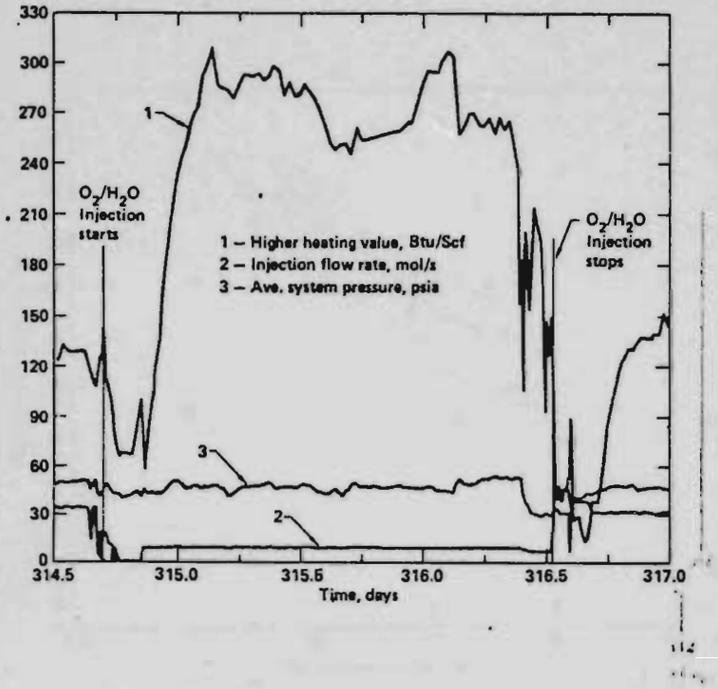

Figure 9. The oxygen-steam gasification phase.

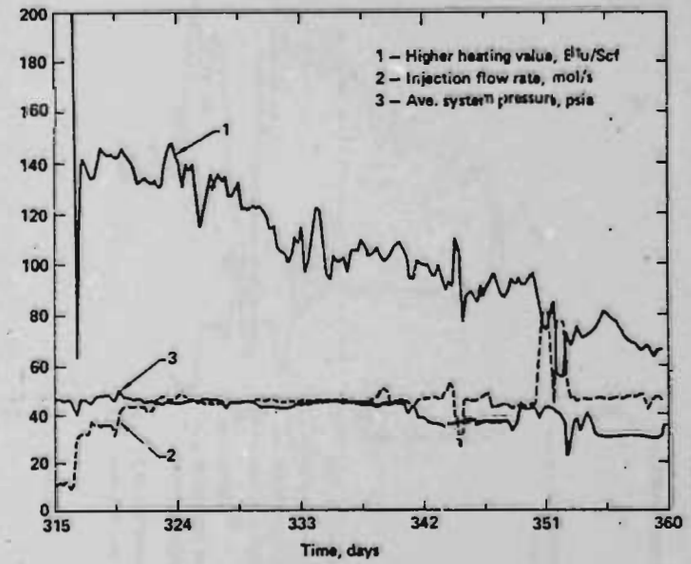

Figure 10. The terminal phase.

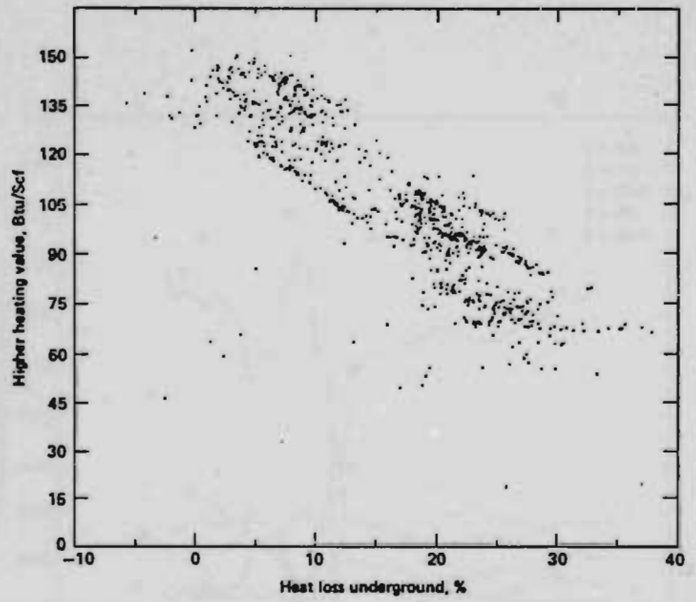

Figure 11. Correlation between heating value and heat loss underground during the terminal phase.

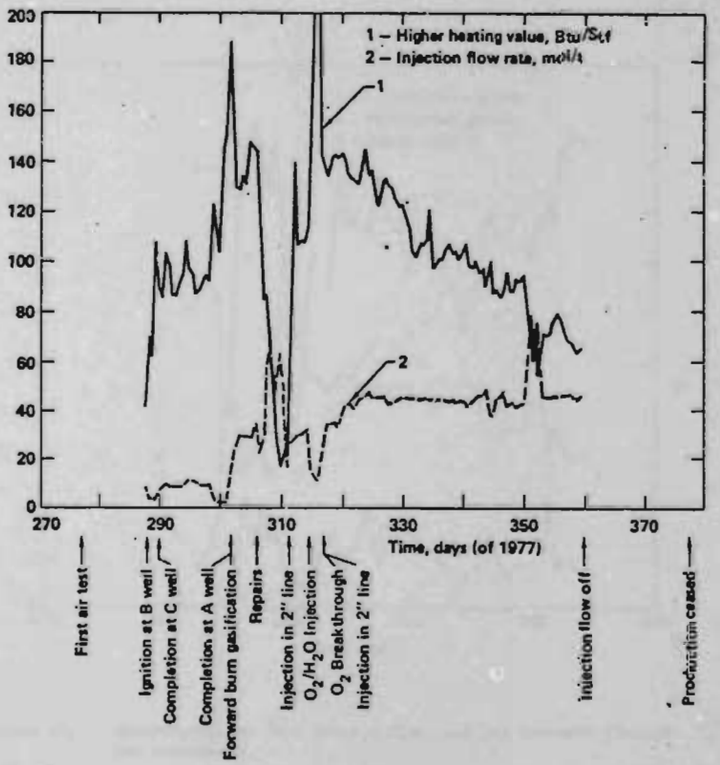

Figure 12. Product heating value and injection flow rate through the experiment.

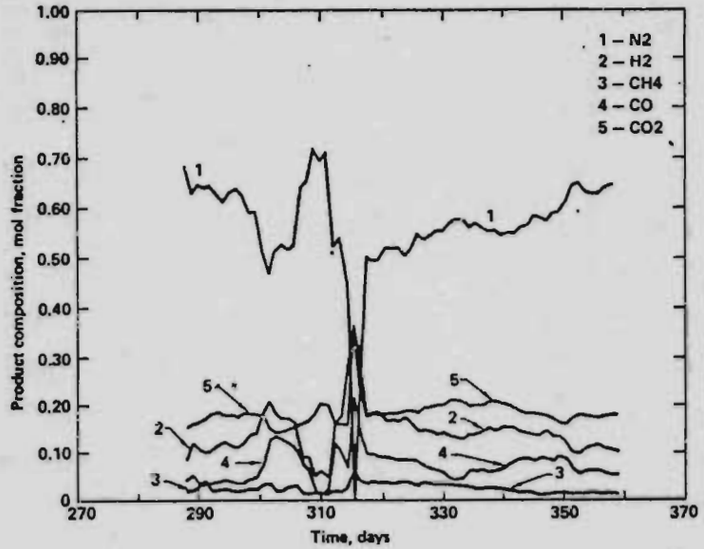

Figure 13. Product composition through the experiment.

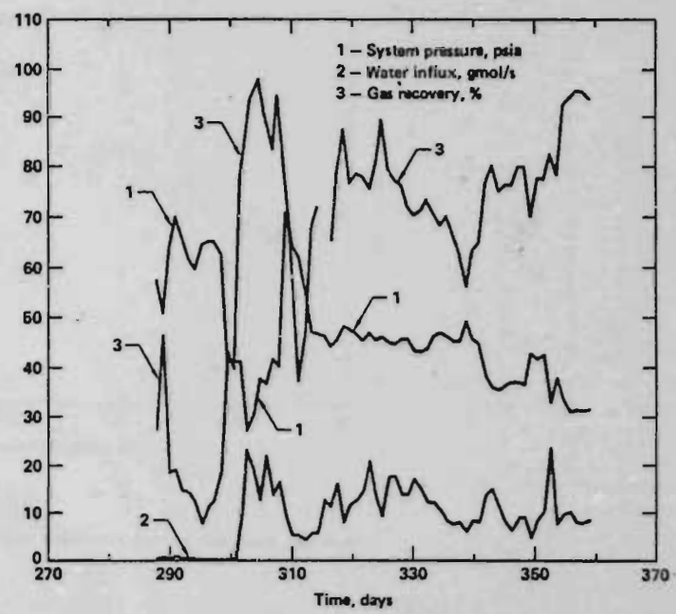

Figure 14. System pressure, net water influx, and gas recovery through the experiment.

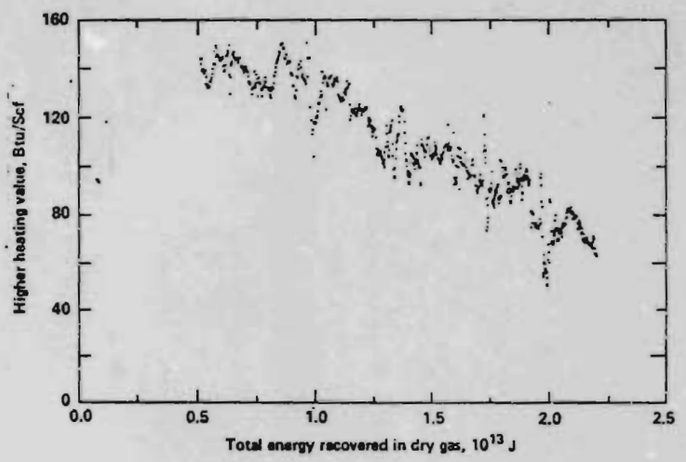

Figure 15. Product quality vs quantity trade off during the terminal phase.

UCRL-52438

INTERPRETATIONS OF FIELD HYDRAULIC TESTS IN EXPLOSION-FRACTURED COAL: HOE CREEK, SITE CHARACTERIZATION TO EXPERIMENT NO. 1

M. M. Moody

March 15, 1978

Work performed under the auspices of the U.S. Department of Energy by the UCLLL under contract number W-7405-ENG-48.

LAWRENCE LIVERMORE LABORATORY
University of California/Livermore

Distribution Category
UC-90c

LAWRENCE LIVERMORE LABORATORY
University of California / Livermore, California / 94550

UCRL-52438

INTERPRETATIONS OF FIELD HYDRAULIC TESTS IN EXPLOSION-FRACTURED COAL: HOE CREEK, SITE CHARACTERIZATION TO EXPERIMENT NO. 1

M. M. Moody

MS. date: March 15, 1978

CONTENTS

LIST OF SYMBOLS

a	half the spacing between dual wells, one injecting and the other pumping at the same flowrate
A	cross sectional area
b	coal seam thickness
h	hydraulic head
H	residual water level in casing during slug test
H_0	initial water level in casing during slug test
i	hydraulic gradient
k	intrinsic permeability
$\overline{k}$	equivalent isotropic permeability (intrinsic)
m	coordinate transformation that eliminates areal anisotropy
Q	steady flow rate from pumped well
r_c	radius of well casing
R	lumped parameter wel' resistance
s	drawdown of hydraulic head
s_0	dimensionless drawdown constant
S	storage coefficient
t	pumping time
T	horizontal transmissivity
u	Theis model dimensionless parameter
x	distance from a draining fracture
ϵ_f	total deviatoric strain
$\bar{T}$	dimensionless time constant
σ	porosity
π_f	tensile fracture porosity
v	voltage difference on Vidar tape from drawdown of hydraulic head

INTERPRETATIONS OF FIELD HYDRAULIC TESTS IN EXPLOSION-FRACTURED COAL: HOE CREEK, SITE CHARACTERIZATION TO EXPERIMENT NO. 1

ABSTRACT

In connection with the LLL program for *in situ* coal gasification, we have performed several phases of hydraulic testing at Hoe Creek. This report contains a synopsis of the hydraulic program and summaries of all hydraulic tests. These data are interpreted and relative test methods are evaluated. The particular aspects of hydraulic testing in modestly permeable coal seams that produce analytical difficulties are the effects of (1) installing several casings close together, which causes changes in the storage coefficient and perturbations of the flow regime; (2) using large well-casings relative to the low formation transmissivity, which causes prolonged well-bore storage effects; and (3) anisotropy due to fractures and explosive fracturing.

The most successful methods of testing *in situ* coal permeability to date have been long-time, drawdown tests and dual-well tests. Single-well slug tests provide a rapid measure of the vertical variation in hydraulic conductivity for a local region. The least successful method of testing has been short-term drawdown tests.

Hydraulic tests show three major permeability regions surrounding the two explosion centers of Experiment No. 1: an inner core out to 10 feet with an average equivalent isotropic permeability of 10 darcys (D), an enhanced region of 10-50 ft with an average equivalent isotropic permeability of 1.5 D, a transition zone of 50-100 ft with an average equivalent isotropic permeability of 0.3 D. There is an areal anisotropy with maximum permeability in the E-W direction and minimum permeability in the N-S direction. An unpredicted low permeability ridge separated the two explosion centers.

Results also suggest that the radial distribution of permeability enhancement vs distance from the shot area follows an inverse distance ($1/r$) power law, from the enhanced region through the transition zone in the eastern-quadrant shot interaction area, containing four of the five environmental monitoring wells. The reduction of permeability along the axis of minimum permeability appears to follow a $(1/r)^4$ decrease.

INTRODUCTION

The Lawrence Livermore Laboratory program for *in situ* coal gasification requires that the region around the underground reaction zone be characterized as completely as possible. One of the more versatile geophysical methods of underground characterization is ground water hydraulics. Hydraulic tests made both before and after fracturing and gasification can yield valuable information concerning the underground changes that occur during these processes.

The field program being conducted near Hoe Creek in the Powder River Basin of northeastern Wyoming includes several types of hydraulic tests. This report summarizes the test data and analyses of

Hoe Creek hydraulic data from site characterization through Experiment No. 1, and evaluates the effectiveness of the different types of tests in providing information relative to the design of *in situ* experiments.

Hydraulic evaluation techniques for aquifers have evolved in two directions. Multiple aquifer systems have been modeled and type curves prepared demonstrating characteristic observation-well response for ground-water systems with high permeabilities. In addition, evaluation techniques for production-well data interpretation and fractured reservoir evaluation have been developed for oil producing systems with low permeabilities. The complete characterization of explosively fractured coal seams required a synthesis of these two separate developments. The data interpretations in this paper draw from both fields.

SITE CHARACTERIZATION

The Hoe Creek site is located in Campbell County, 24 km south of Gillette, Wyoming, between country road 50 and state highway 59. The site covers 0.3 km^2 and the topography is shown in Fig. 1. The first gasification experiment was conducted at subsite 1.

Stratigraphy

Cores from the three subsites show that the subbituminous Felix coal, contained in the Eocene Wasatch Formation, lies 30-50 m below the surface at subsite 1.[1] Figure 2 illustrates the site stratigraphy. The Felix coal lies nearly horizontal beneath the site; it is divided into two seams by a siltstone-claystone layer ~5 m thick. The upper Felix No. 1 is 3 m thick and the lower Felix No. 2 is 7.6 m thick. We conducted the first gasification experiment in the lower Felix No. 2.

The Felix No. 2 coal seam contains two orthogonal sets of naturally occurring fractures.[2] The better developed set of fractures, the face cleat, has an average orientation of about N 70° W. The lesser developed set of fractures, the butt cleat, has an average orientation of N 29° W. The maximum hydraulic conductivity follows the face cleat.

Geohydrology

Stone and Snoeberger[2] evaluated the native hydraulic characteristics of both Felix coal seams. Drawdown tests and slug tests were conducted at the three subsites, with the testing at subsite 1 occurring slightly northwest of the gasification site. Standard analytic techniques discussed in Appendix A were used to obtain aquifer and aquitard characteristics. The results of this work appear in Table 1. The values of horizontal permeability for Felix No. 2 were 0.4 D along the direction of maximum permeability N 59°E and 0.2 D along the

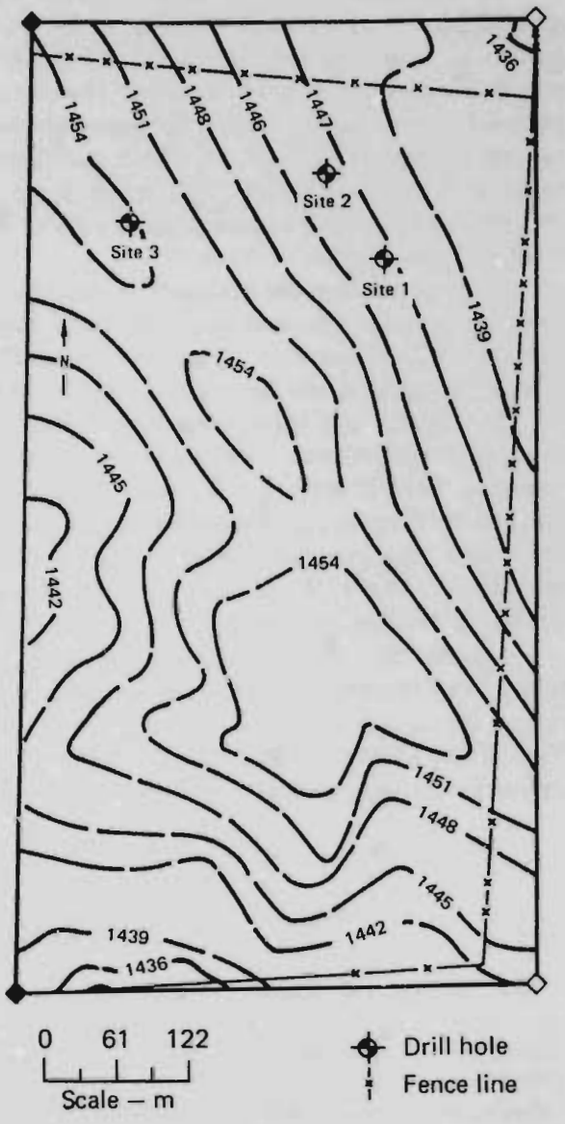

Fig. 1. Hoe Creek site in Campbell County, Wyoming (W1/2, SW1/4 Sec. 7, T47N R72W). The contour interval is 3 m.

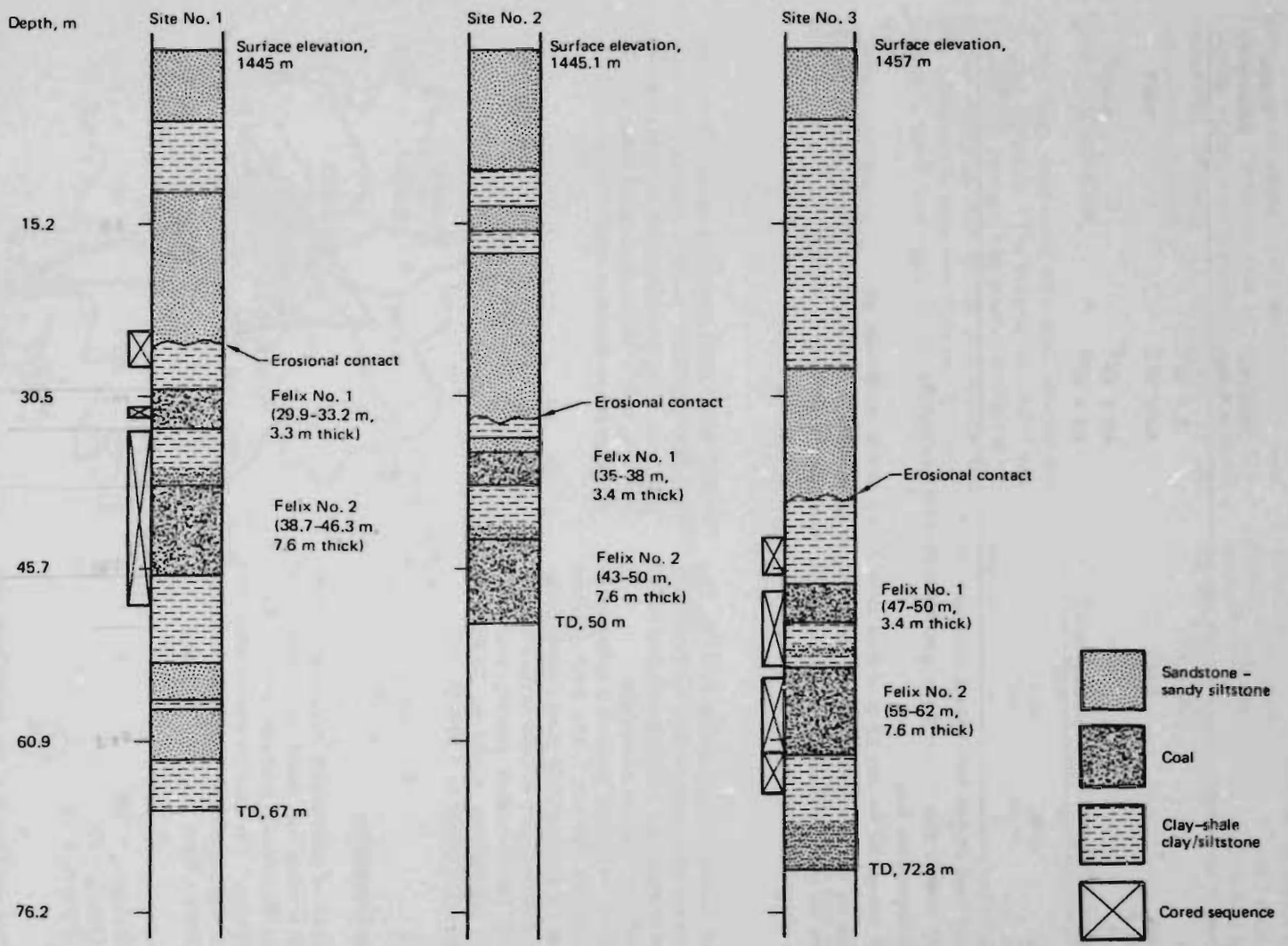

Fig. 2. Comparison of lithologic logs of Hoe Creek subsites 1, 2, and 3.

Table 1. Hydraulic characteristics of Felix coal and associated strata, Hoe Creek subsite 1, preshot.[a]

Stratum	Horizontal permeability, D	Coefficient of storage	Vertical permeability, D
Felix No. 1	0.48[b]-1.42[c]	2×10^{-2}	–
Strata between Felix No. 1 and No. 2	0.12[c]	2.2×10^{-3}	0.022
		4.9×10^{-4}[d]	0.0015[d]
Felix No. 2	0.41[e] 0.23[f]	1.2×10^{-3}	–
Strata below Felix No. 2	–	–	<0.0015[g]

[a]This table is based on data from Stone & Snoeberger, Ref. 2.

[b]A range of values is given for two different-type, single-well tests in the same well.

[c]Results of slug-injection tests.

[d]Values are averages for the first 8.9 ft of strata above the top of Felix No. 2 coals.

[e]Value along the axis of maximum hydraulic conductivity, which trends N 59° E.

[f]Value along the axis of minimum hydraulic conductivity, which trends N 31° W.

[g]Refers to average values for first 2.1 m of strata below bottom of Felix No. 2 coal.

direction of minimum permeability N 31°W. The values of storage were relatively high for an artesian aquifer; the estimates for leakage parameters varied with the different methods of analysis.

The regional water level gradient is estimated to be 0.007 towards the east.[3] The local gradient measured at the site was 0.002 in an easterly direction. The regional velocity of water in the Felix coal for a 1-10% interconnected porosity and 0.3 D native coal permeability would be 20-200 ft/yr, while at the site it would be 5-50 ft/yr.

Explosion Fracturing

A prediction of permeability enhancement from explosion fracturing was based on hydraulic test results from explosively fractured coal at Kemmerer, Wyoming.[4] The intrinsic permeabilities expected to be associated with total, failure-induced deviatoric strain ϵ_f were:

$k \geq 100$ D for $\epsilon_f \geq 10\%$
$k = 2$ D for $\epsilon_f = 2\%$
$k = 1/2$ D for $\epsilon_f = 1\%$

A two-shot configuration for Hoe Creek was designed. Figure 3 illustrates the plan view of calculated permeability enhancement which extends ~40 ft from either explosion center. During the two-shot explosion, surface displacements were measured.[5] The isodisplacement configuration was elliptical, with a major axis aligned along an ESE direction perpendicular to the axis of the two shots.

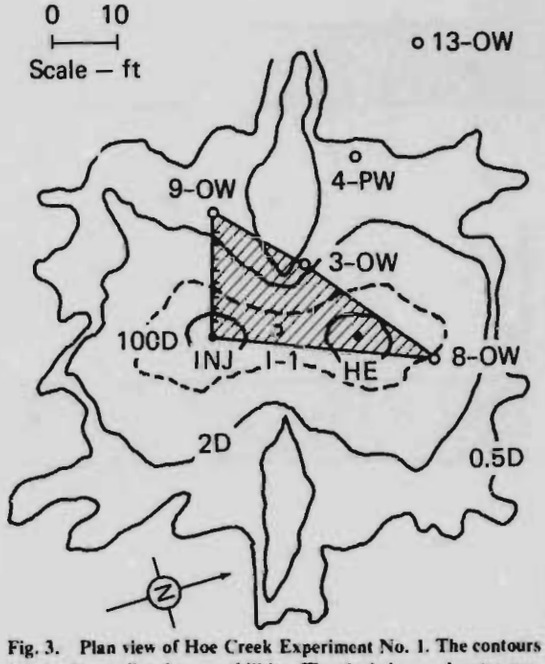

Fig. 3. Plan view of Hoe Creek Experiment No. 1. The contours denote the predicted permeabilities. The shaded area denotes permeabilities of 1.5-4 D, as measured in hydrological tests.

The total area showing greater than 0.05 ft displacement covers an ellipse ~160 ft long by 100 ft wide. This pattern correlated with the enhanced permeability region, with the direction of maximum permeability following the major axis of the isodisplacement ellipse.

Well Configuration

Only those wells cased with steel survived the two-shot explosion.[5] The preshot wells 4-PW and I-0 were not damaged significantly during the explosive fracturing, but all the polyvinylchloride (PVC) observation wells were damaged. As a result, preshot hydraulic tests could not be repeated post shot.

Additional dewatering wells, instrument wells, core borings, and production wells were drilled post shot. Figure 4 is a schematic of the hole bottom locations. In addition, five monitor wells were installed around the perimeter of the subsite from the northeast towards the south. Figure 5 indicates the locations of these wells. Completion data concerning the pumped wells are shown in Table 2.

Table 2. Pumped-well completion data.

Well No.	Casing diam, in.	Casing depth, ft	Screen interval, ft
I-0	19-3/4	127	(127-152)[a]
P-1	9-5/8	147	147-152
DW1-6	7	168	147-152

[a]Casing to top of HF hole that is open from 127-152 ft.

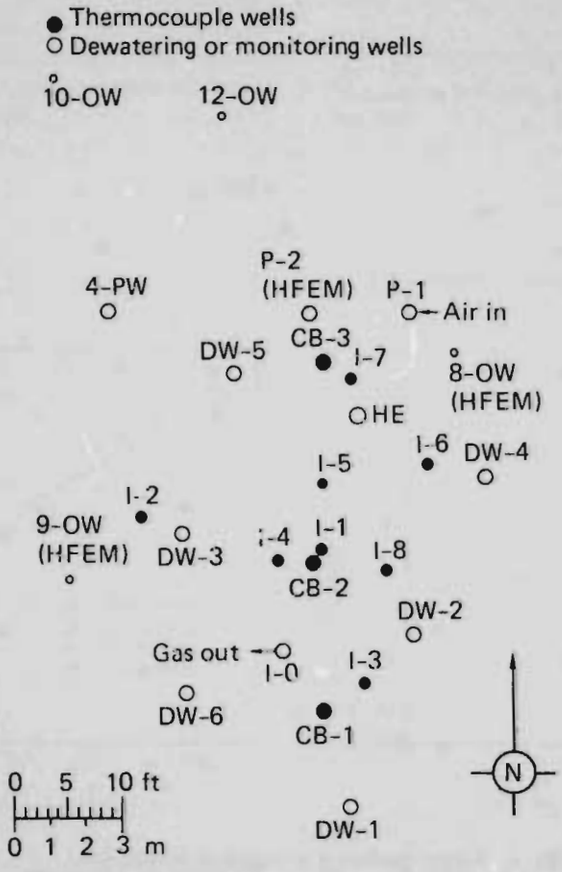

Fig. 4. Hole bottom locations.

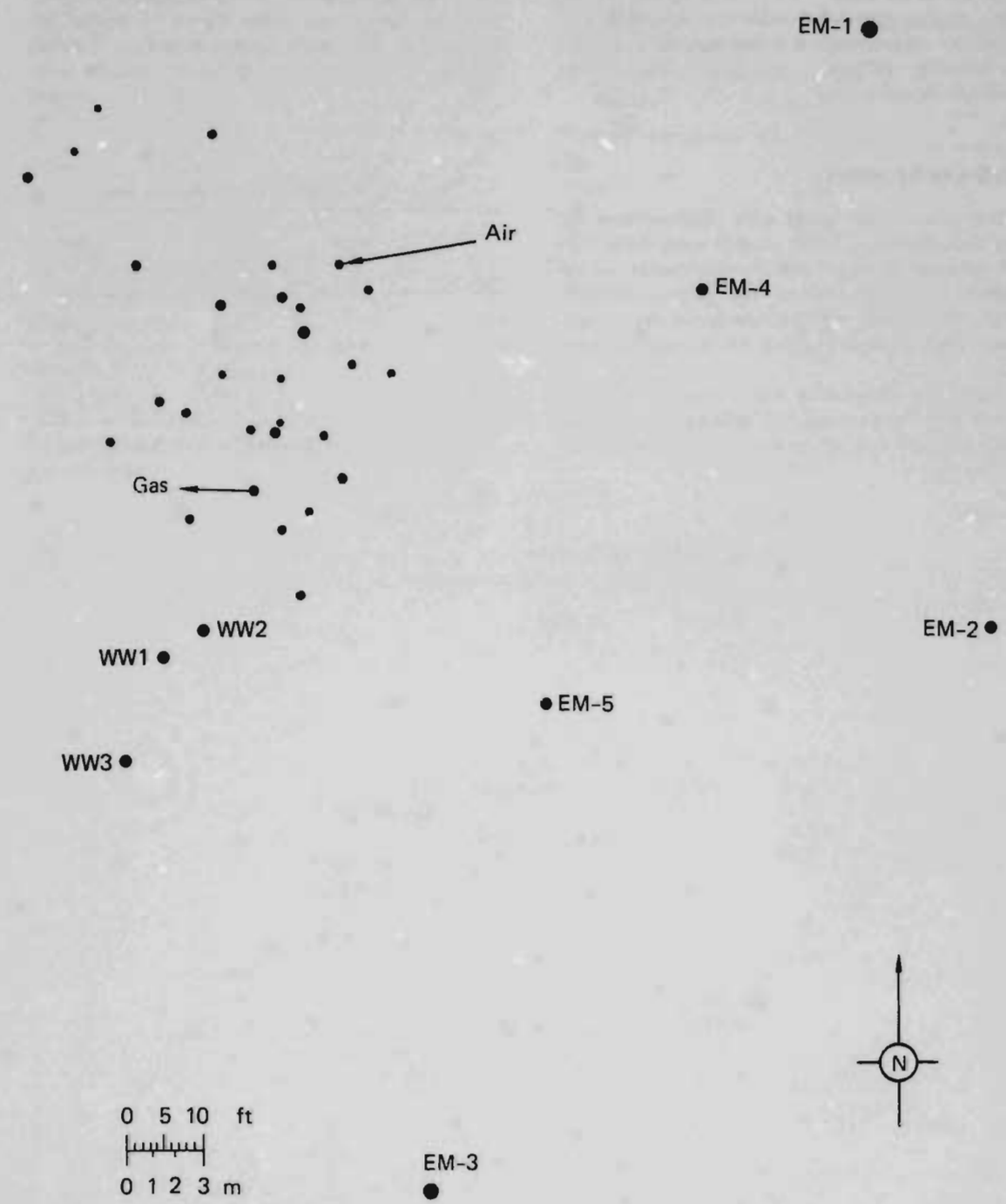

Fig. 5. Relative locations of environmental monitor wells.

INITIAL POST-SHOT HYDRAULIC TESTS

Initial post-shot permeability calculations, based on field work performed in the fall of 1975, indicated that the permeability enhancement of the coal was not as extensive as predicted by rock mechanic calculations and correlations between permeability and failure shear strain observed at Kemmerer. In particular, a high inner-core permeability of k > 100 D was not observed.[5] Table 3 lists the most reliable permeability calculations obtained from the data. The maximum permeabilities measured are ~4 D at 3-OW and 3 D at 9-OW. Additional dewatering tests indicated that leakage from the Felix No. 1 to the Felix No. 2 was not extensive, because the well in Felix No. 1 did not respond to the dewatering of Felix No. 2.

During the test on November 11, 1975, the water levels in 9-OW and I-1 followed those of the pumped well I-0 very closely, indicating a direct connection. Both exhibited well-bore storage for 15 min followed by a fracture flow for the duration of the test (i.e., 150 min). 8-OW and 3-OW did not appear to be connected directly to I-0, although these two responded as though they were near a draining fracture. Figures 6 and 7 are plots of drawdown vs time for these wells.

Table 3. Results of initial post-fracturing permeability tests. November and December 1975.[a]

Pumped well	Observed well	Permeability, D
9-OW	3-OW	3.0
(Nov)	8-OW	1.8-2.6
9-OW (2 min pulse)[b]	3-OW	2.3
(Nov)	8-OW	2.3
I-0	I-1	1.5
(Nov)	3-OW	1.7
	9-OW	3.3
	HE	1.6
	8-OW	1.7
	4-PW	0.7
I-0	I-2	3.3
(Dec)	3-OW	4.2
	HE	2.7
	8-OW	3.4
8-OW	3-OW	0.5
(Nov)	9-OW	0.5
	HE	0.4

[a]The data in this table is taken from UCRL-50026-75-4, Ref. 6.

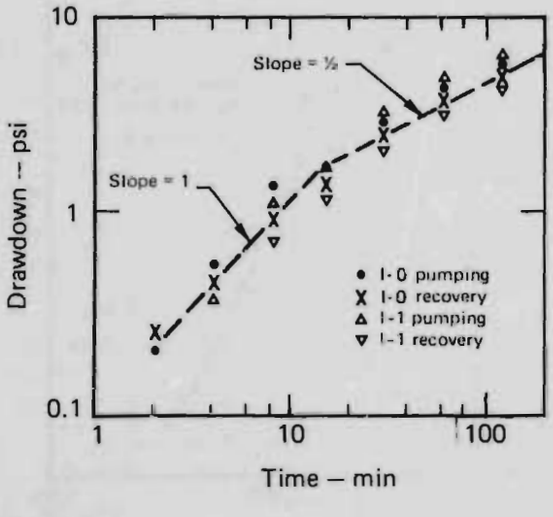

Fig. 6. Drawdown and recovery in wells I-0 and I-1 by pumping I-0 for post-shot test (Nov. 14, 1975).

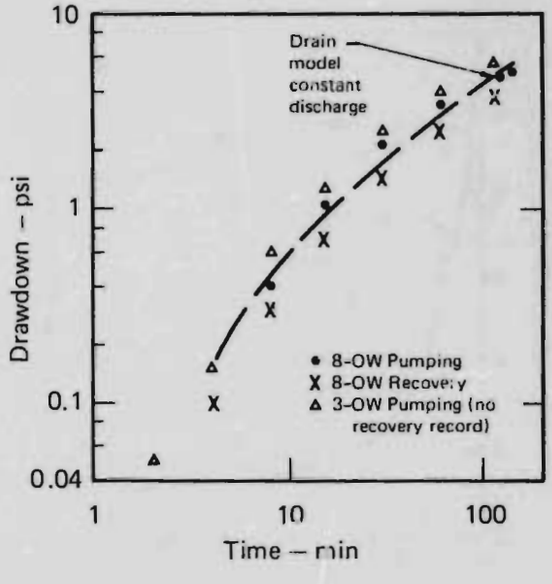

Fig. 7. Drawdown and recovery in wells 8-OW and 3-OW by pumping I-0 for post-shot test (Nov. 14, 1975).

PREGASIFICATION HYDRAULIC TESTS

A testing program was designed and implemented to measure permeability distribution (especially for the purpose of improving the upper bound estimate of inner-core permeability), to locate fractures, and to measure interconnected porosity. Several types of tests were run to compare the effectiveness of each type in providing this *in situ* information.

Slug Tests

Slug tests were designed to empty known amounts of water from a large storage tank into a well casing. The amount of released water loaded the casing with a 25-ft column of water. Generally, 45 gal of water were injected in less than half a minute. We recorded the declining water level position in the casing on strip charts and in the data acquisition system as a function of time. Since the bubblers could not always follow the rapid rise in water level, preset sounding probes were required to measure the peak water level in the casing. We also recorded observation well responses. We designated the maximum water level recorded during the test "H_0" and the subsequent data "H". Values of H/H_0 were plotted vs log time for comparison with the type curves for the slug test model. The slug tests indicated well constriction, interwell fractures, and intercasing flow.

Tests 1, 2, 3, 8, and 13 were slug tests of wells DW-6, DW-6 repeat, DW-2, DW-1, and DW-6 repeat, respectively. The water-level response in DW-6 during Test 1 showed an irregular response. We repeated Test 2 to verify that the behavior was reproducible. The response had two phases. Phase 1 showed a rapid loss in head while adjacent casings were filling with water. Further examination of the data indicated that the initial height of water in the casing was only about half the anticipated rise, so half the water flowed into the system in the 1/2 min required to fill the casing. Phase 2 showed a more gradual loss in head while all interior casings lost their water to the coal seam. Figure 8 is a plot of head vs time for Test 2, demonstrating the different phases of flow. Using an exponential model, we obtained time constants of 1 min for phase 1 and 2.5 min for phase 2.

The water level in DW-2 during Test 3 demonstrated the anticipated rise and exponential decay with a time constant of 12.3 min as shown in Fig. 9. The water level in DW-1 during Test 8 did

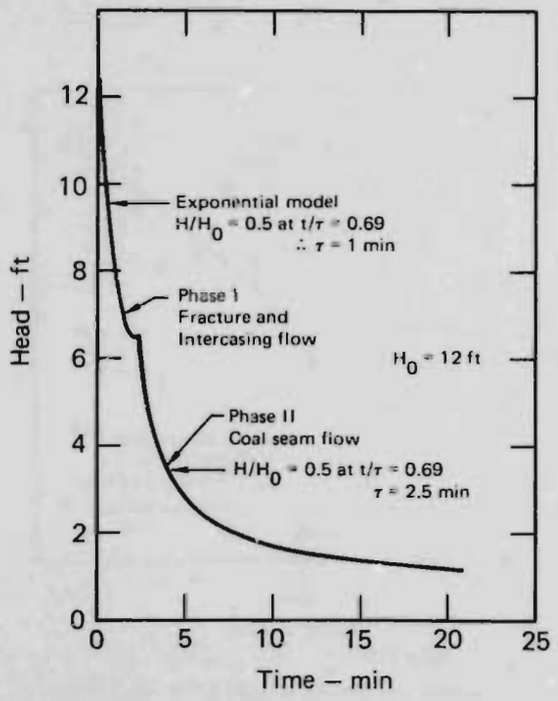

Fig. 8. Test 2: Water level in DW-6 after loading with 45 gal of water.

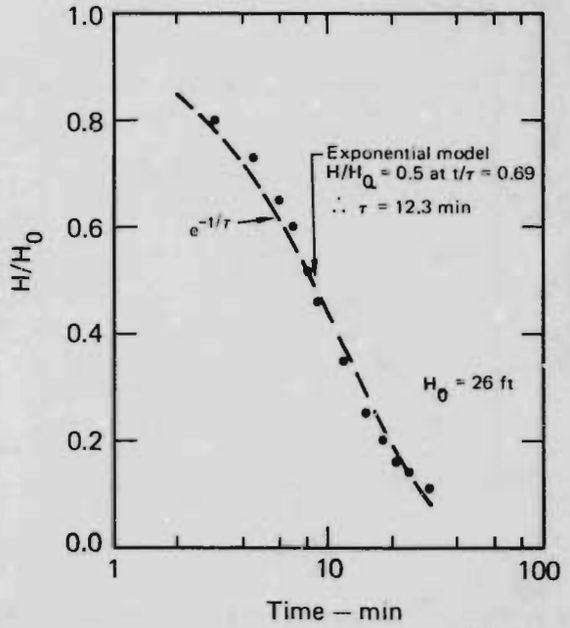

Fig. 9. Test 3: Water level recovery in DW-2 after loading with 45 gal of water.

not rise as high as we anticipated; the time constant was 2.2 min as shown in Fig. 10.

DW-6 was tested again with 144 gal of water. The initial head rise was 45 ft and the decay was exponential with a time constant of 2.2 min as shown in Fig. 11.

The time constants obtained in the exponential model relate to interwell resistance. An equivalent permeability could be obtained if the dimensions of the connecting region were known. If the resistance were distributed into an equivalent homogeneous infinite aquifer, permeabilities of 0.5-4 D would be obtained, with the lower permeabilities being associated with the longer time constants.

Observation-well responses to slug tests resulted in very low values of inner-core permeability. Pumped-well skin friction and observation-well flow perturbations prevented the measurement of the higher inner-core permeabilities with slug tests.

The slug-test response in observation wells resulted in permeabilities of the same order of magnitude as the single-well calculations. The large flow required to change the water levels in the observation wells results in reduced and delayed maximums.

Drawdown and Injection Tests

Drawdown and injection tests were designed to withdraw or inject water at a constant rate, Q. We recorded the discharge rate throughout the tests, and occasionally adjusted flow rates to account for pump characteristics. We performed injection tests by pumping a preset value of flow from a holding tank through a flow meter and into the well.

All the wells were open to the surface. We used subsurface bubbler tubes, differential strain-gage transducers, and sounding lines with a fluid conductivity probe to establish water elevations in the wells. Data from the bubbler tubes and the transducers were recorded as a function of time on strip charts and on both paper and magnetic tape in a Vidar 5403 data aquisition system. We recorded some sounding data manually and generally limited these data to environmental monitor-well responses and slug tests.

Tests ran 5-8 h. We plotted changes in water level vs time on logarithmic paper for comparison with the type curves for the various hydraulic models. The most significant result from drawdown tests was the radial variation of K we obtained from late-time Jacob analysis.

Test 4

We pumped DW-4 at an average flow rate of 1.8 gpm for 300 min. The pumped-well response is initially exponential but fails to be followed by a Theis* response (see Fig. 12). The exponential response occurs because DW-4 is a highly resistant well requiring a large drawdown to produce water.

*A Theis response is one in which all the pressure vs time plots follow a single Theis-type curve. See Appendix A for further explanation.

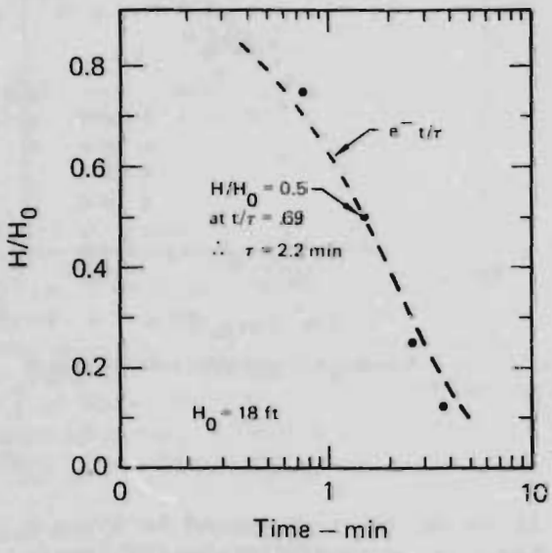

Fig. 10. Test 8: Water level recovery in DW-1 after loading with 50 gal of water.

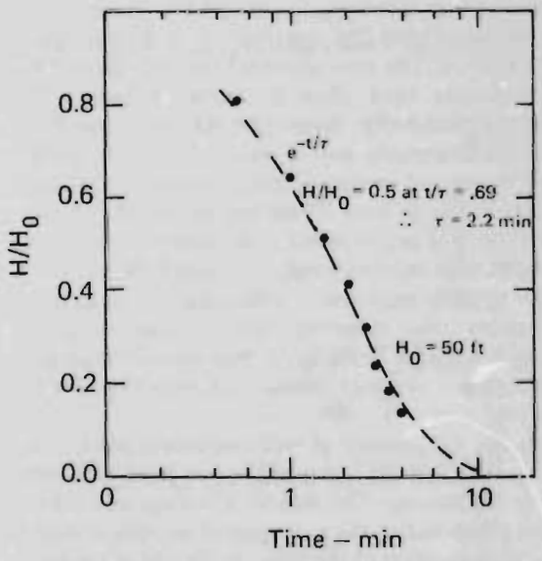

Fig. 11. Test 13: Water level recovery in DW-6 after loading with 144 gal of water.

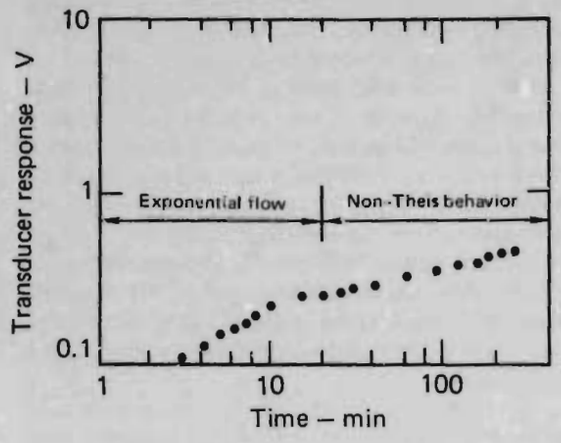

Fig. 12. Test 4: Response in pumped well DW-4 for 2 gpm.

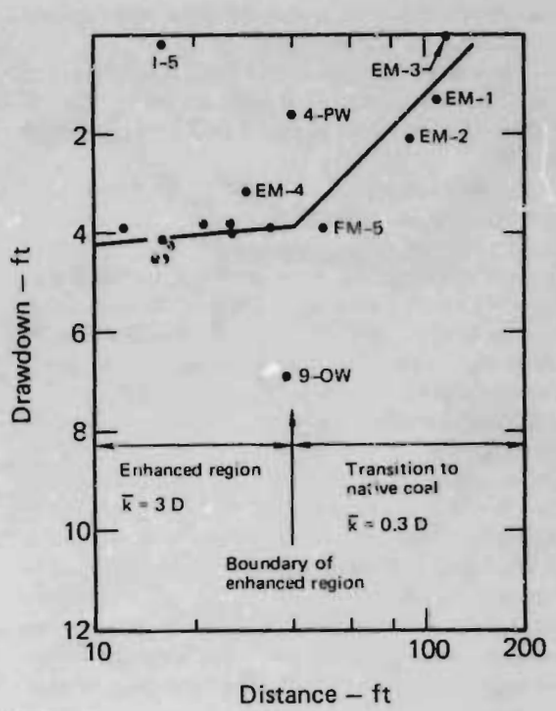

Fig. 13. Test 4: Observation-well drawdowns at 300 min for 2 gpm in pumped well DW-4.

In the second phase, pressure increased approximately as the fourth root of time. This indicates that the cone of depression is encountering more resistive material as it expands or that more flow is coming from the coal as intercasing flow decreases. In either case, the water level continued to decline excessively in the pumped well. Results of matching techniques for this test would be suspect because of the changing characteristics.

Even though we did not observe Theis behavior at the pumped well by the end of the test, late-time approximate (Jacob) analysis for data at t = 300 min shows the distribution of permeability (see Fig. 13). The environmental wells are located in a transition zone from noticeably enhanced to native permeability. Well EM-3 did not respond to the 300-min pump test of well DW-4. Well 4-PW had a reduced response, indicating that it is in a native region of coal. These two responses indicate that the N-S axis is along a direction of minimum permeability enhancement. All the dewatering wells had similar responses, indicating a noticeably enhanced region extending 50 ft in an easterly direction. Well 9-OW had a larger than normal response, indicating a fracture located between DW-4 and 9-OW.

In the environmental well responses, plotted as t/r^2 in Fig. 14, the width of the data band indicates some anisotropy. The well-bore storage and intercasing flow during the early part of the tests obscure the interpretation of the data. At the end of the test, leakage factors were not discernable within the range of measured accuracy.

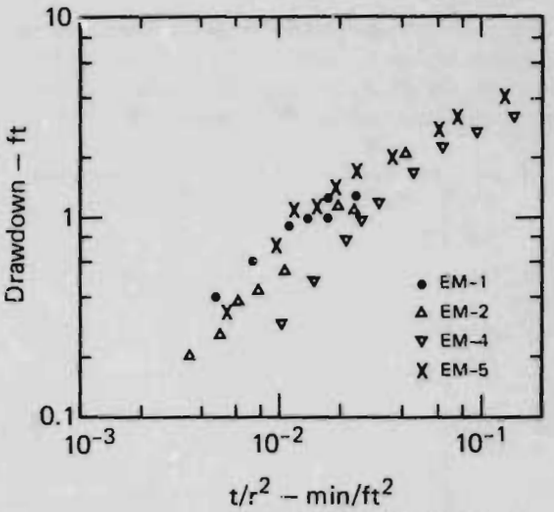

Fig. 14. Test 4: Responses in environmental wells for 2 gpm in pumped well DW-4.

Test 5

In this test, DW-2 was pumped for 80 min at 4.9 gpm. We terminated the test when DW-2 was essentially dewatered. During that time, the pumped well showed well-bore storage effects for 15 min,

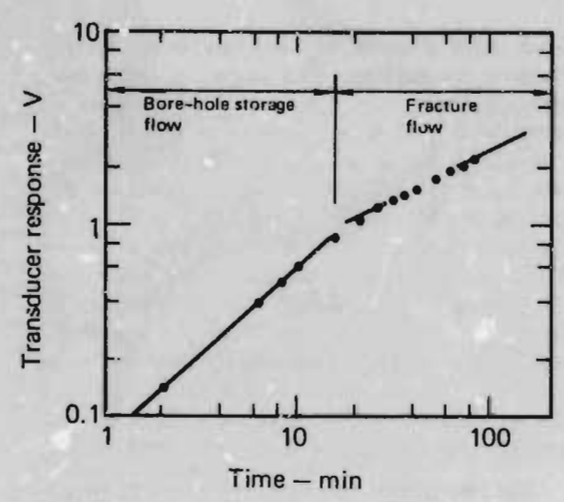

Fig. 15. Test 5: Responses in pumped well DW-2 for 4.9 gpm.

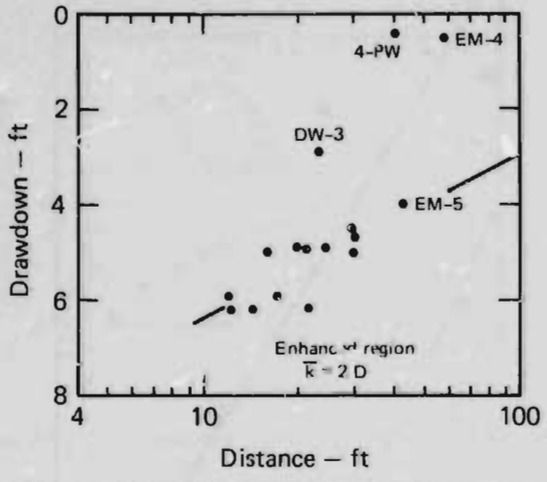

Fig. 16. Test 5: Observation-well drawdowns at 80 min for 4.9 gpm in pumped well DW-2.

followed by fracture flow for the rest of the test (see Fig. 15). Theis behavior was not observed during the test. Even though Theis behavior was not observed, a late-time approximate analysis of observation-well data gave an enhanced region permeability of 2 D extending 50 ft, as shown in Fig. 16. Wells 4-PW, EM-4, and DW-3 did not respond significantly to the pumping of DW-2; and EM 1, 2, and 3 did not respond at all during the test.

Test 6

In this test, we pumped DW-3 at 3.8 gpm for 40 min. During that time, DW-3 dewatered and the observation wells did not respond.

Test 7

The well I-0 was pumped at 3.0 gpm for 500 min. The pumped well-bore storage response appeared to be modified by the presence of the high explosives (HE) cavity (see Fig. 17). Towards the end of the test, Theis behavior began to be observable at the pumped well and a late-time analysis of the data at t = 500 min resulted in an inner-core permeability of 20 D, an enhanced region of 1 D, and a transition to native region of 0.3 D (see Fig. 18). The environmental monitor-well data followed different Theis-type curves as shown in Figs. 19 and 20. A scale factor of five exists between EM-3 and the other monitor wells, indicating areal anisotropy. Monitor wells EM-1 and EM-2 follow lower Theis curves than EM-4 and EM-5 because of the radial decrease in permeability. The radial anisotropy between the close and far monitor wells makes the drawdown

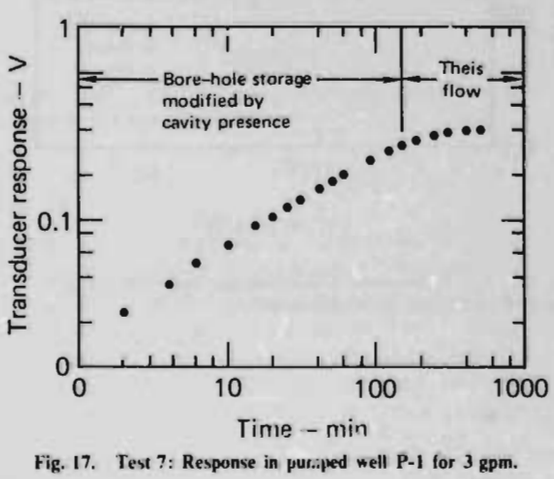

Fig. 17. Test 7: Response in pumped well P-1 for 3 gpm.

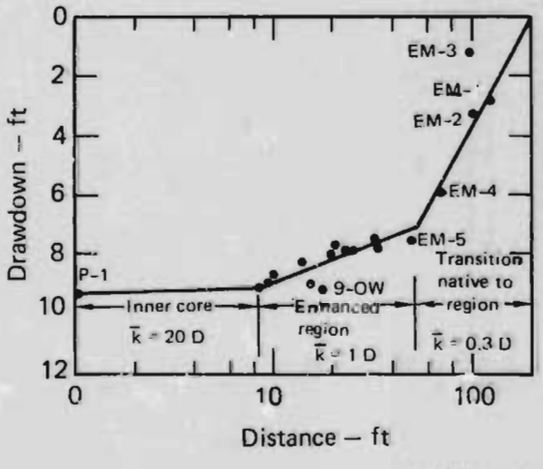

Fig. 18. Test 7: Observation-well drawdowns at 500 min for 3 gpm in pumped well P-1.

versus t/r^2 appear to fit a leaky model, but the hydraulic parameters are inconsistent with the permeabilities obtained from the Jacob analysis and realistic values of S. Therefore, we believe that the radial variation in K, well-bore storage, and inter-casing flow perturbations have altered the environmental-well response, making matching techniques of transient data suspect.

The method of drawdown difference, discussed by Sherwood et al.,[6] for interpretation of Hoe Creek data appears to eliminate many of the problems encountered with matching techniques, especially those created by the radial variation in permeability and bore-hole storage effects. Well-bore storage during Test 7 affects the environmental data for about 300 min, yet when drawdown differences of EM-1 to EM-4 and EM-5 to EM-2 are plotted vs reciprocal time, a straight line, as shown in Fig. 21, is obtained throughout the entire test. The permeability calculations for the transition to native coal region, obtained from the intercepts, were 0.3 and 0.4 D, and the storage coefficient was 3×10^{-4}. This technique is dependent on radial flow assumptions, and pumped wells that are in the inner-core area should be used for the best results.

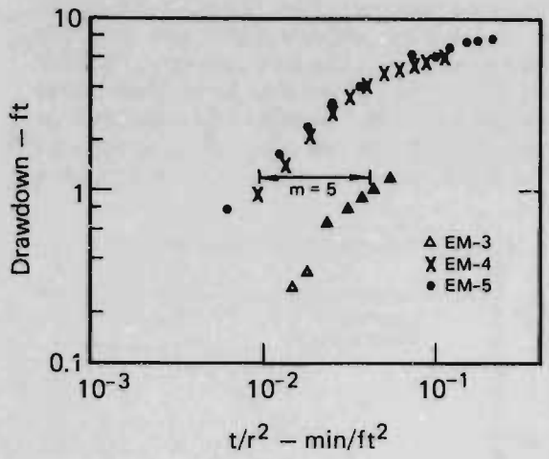

Fig. 19. Test 7: Responses in environmental wells EM-3, EM-4, and EM-5 for 3 gpm in pumped well P-1.

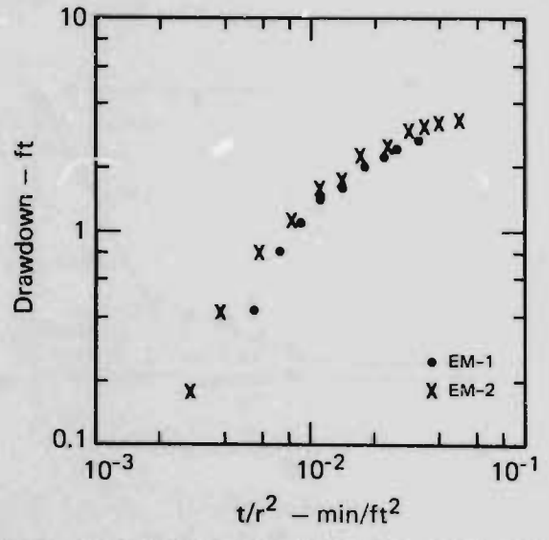

Fig. 20. Test 7: Responses in environmental wells EM-1 and 2 for 3 gpm in pumped well P-1.

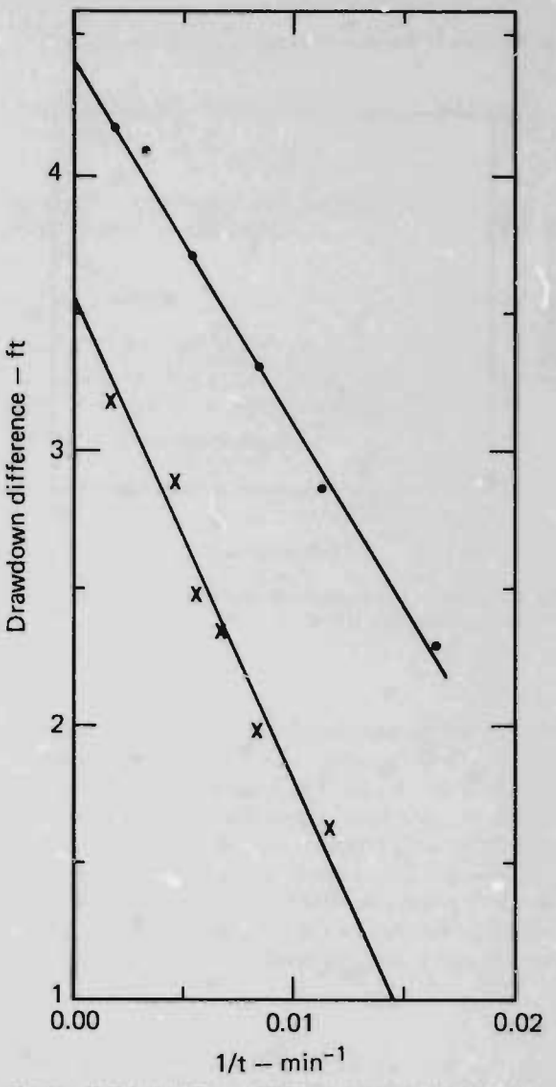

Fig. 21. Test 7: Drawdown difference between pairs EM-1/EM-4 and EM-2/EM-5 for 3 gpm in pumped well P-1.

Test 9

Well DW-1 was injected at the rate of 2.9 gpm for 145 min. The pumped-well response was a straight line on logarithmic paper with a slope of 1/2.5, as shown in Fig. 22. The recovery response was exponential for 10 min, then followed a cube root of time, as shown in Fig. 23. The interpretation of this test is predicated on the non-Theis behavior of the pumped-well responses. The lack of Theis behavior implies that the flow is gradually restricted as the cone of pressure buildup expands from the inner core into less permeable regions. During the test, flow stabilized in the enhanced region, but not in the transition to native coal region. A late-time analysis of the enhanced region yields a permeability of 2 D, as shown in Fig. 24. Both I-5 and DW-3 responded sluggishly to the pumping of DW-1.

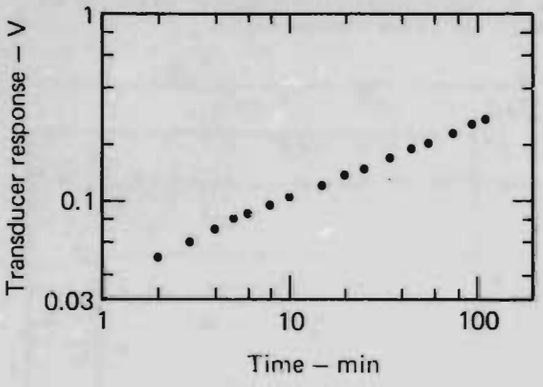

Fig. 22. Test 9: Response in injection well DW-1 for 2.9 gpm.

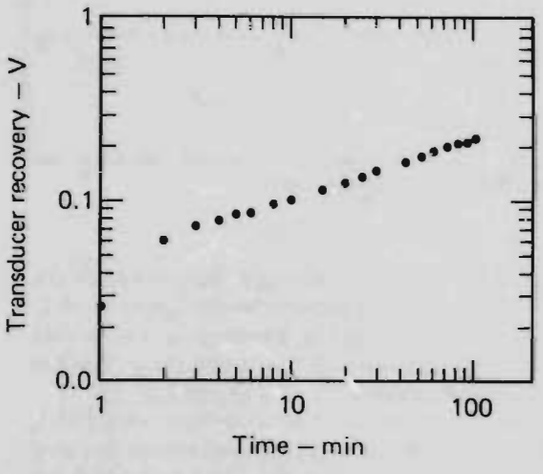

Fig. 23. Test 9: Water-level recovery in injection well DW-1 after 2.9 gpm flow ceased.

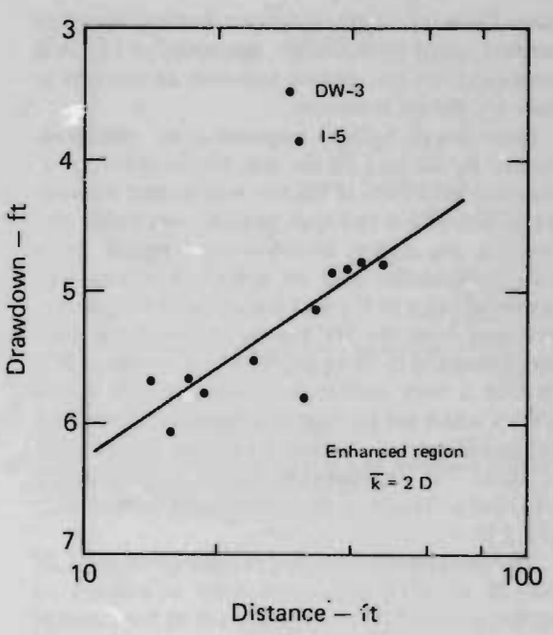

Fig. 24. Test 9: Observation-well drawdowns at 100 min for 2.9 gpm in injection well DW-1.

Test 11

Well P-1 was pumped at 3.2 gpm for 400 min. This well is screened in the bottom 5 ft of the coal seam. The pumped-well response, shown in Fig. 25, is very similar to that of I-0 during Test 7, except that it did not clearly demonstrate a Theis response during this late time. The pumped-well response demonstrated two phases: one in which pressure follows the square root of time, followed by a second in which pressure follows the cube root of

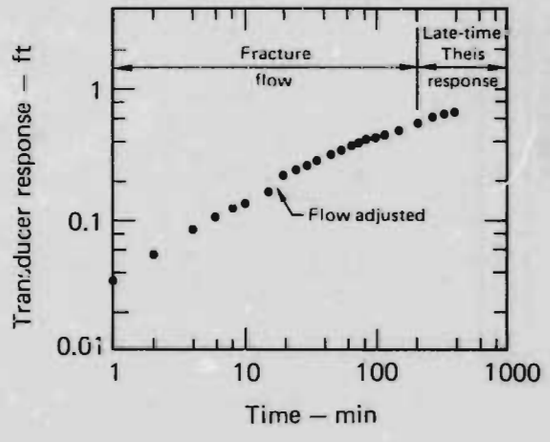

Fig. 25. Test 11: Response in pumped well I-0 for 3.2 gpm.

time. These two phases indicate fracture flow and reduced radial permeability, respectively. The shift separating the two phases indicates an increase in flow during the transition.

Even though a Theis response is not clearly indicated by the end of the test, the drawdown distribution at the end of the test was plotted on semi-log paper, and a late-time analysis was performed (see Fig. 26). Again, we observed a region native with permeability and an enhanced region. The restricted entry at P-1 and the offset of the production well from the HE region obscured the inner core permeability. Well 8-OW, which is close to P-1, showed a very similar drawdown to DW-4 and DW-5, which are four times as far away. These data points indicate an average inner-core permeability of about 7 D, an enhanced region permeability of 2 D, and a transition to native-region permeability of 0.3 D.

The environmental-well data shown in Figs. 27 and 28 demonstrated some areal anisotropy to pumping from P-1, but not as much as from pumping I-0.

Test 12

Well DW-1 was pumped at 3.7 gpm for 440 min. The pumped-well data followed a straight line of slope 0.4 for 100 min, then changed to a late-time Theis curve towards the end of the test, as shown in

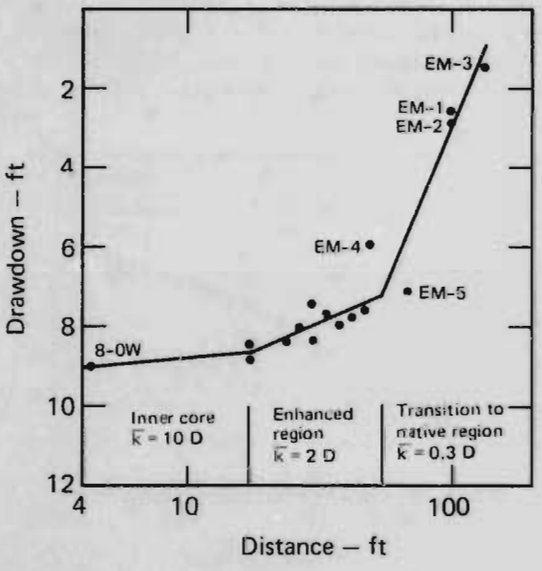

Fig. 26. Test 11: Observation-well drawdowns at 400 min for 3.2 gpm in pumped well I-0.

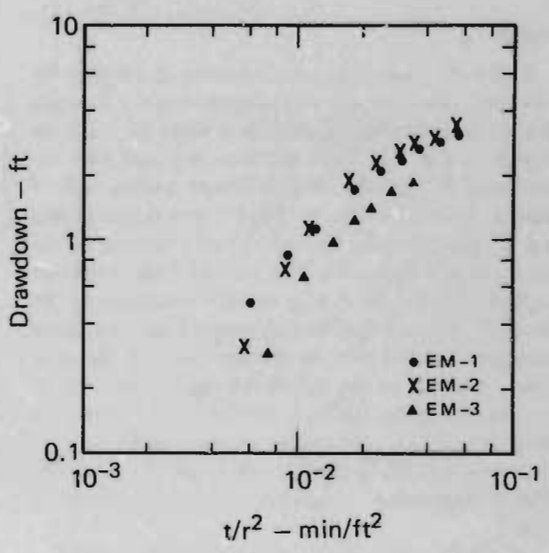

Fig. 27. Test 11: Response in environmental wells EM-1, EM-2, and EM-3 for 3.2 gpm in pumped well I-0.

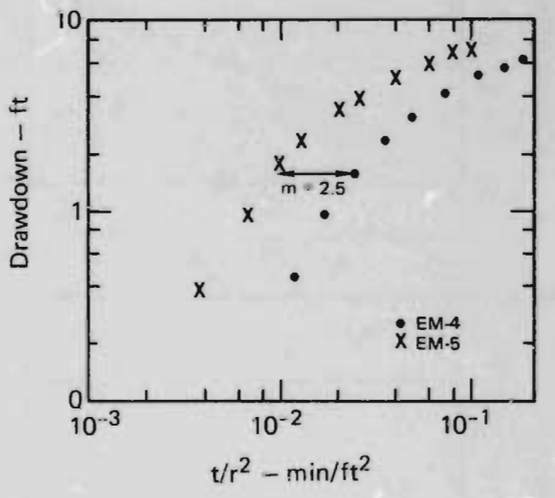

Fig. 28. Test 11: Responses in environmental wells EM-4, and EM-5 for 3.2 gpm in pumped well I-0.

Fig. 29. A semi-log plot of the drawdowns at the end of the test and a late-time analysis shows EM-1, 2, 3, and 4 to be in the transition to native coal region, but EM-5 is in the enhanced region that has an average permeability of 2 D (see Fig. 30).

The data for environmental-monitor wells EM-1, EM-2, and EM-3 show an areal anisotropy factor of five in Fig. 31. The data for EM-4 and EM-5 are shown in Fig. 32.

Test 15

Well DW-5 was pumped for 50 min. During the first 6 min the flow was 6.8 gpm; thereafter it was reduced to 4.9 gpm. Although the pumped-well response did not demonstrate Theis behavior (see Fig. 33), a late-time analysis of the closer observation wells at 50 min yielded an enhanced permeability of 1 D, as shown in Fig. 34. The environmental-monitor wells did not respond significantly during this pump test.

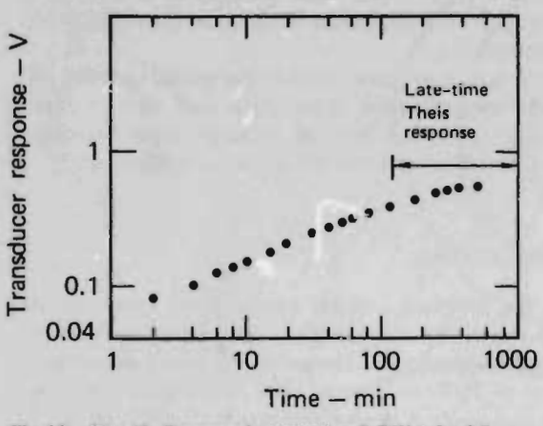

Fig. 29. Test 12: Response in pumped well DW-1 for 3.7 gpm.

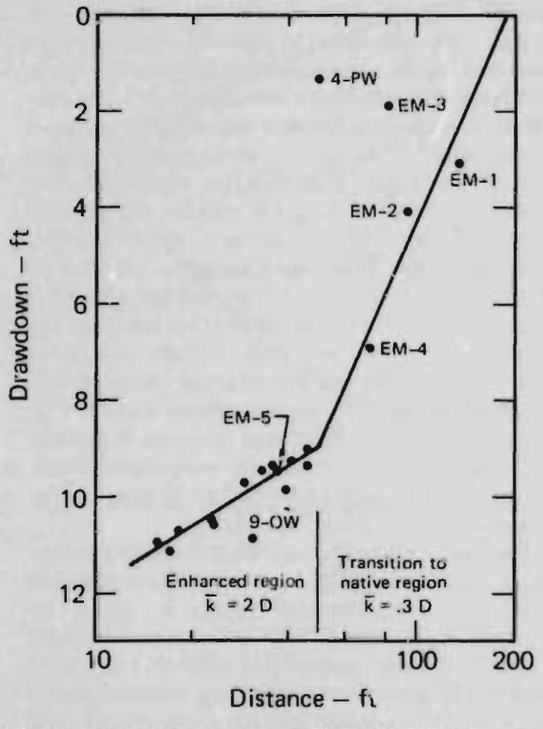

Fig. 30. Test 12: Observation-well drawdowns at 440 min for 3.7 gpm in pumped well DW-1.

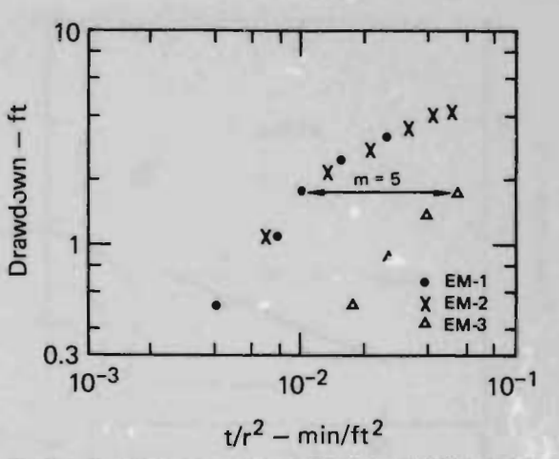

Fig. 31. Test 12: Responses in environmental wells EM-1, EM-2, and EM-3 for 3.7 gpm in pumped well DW-1.

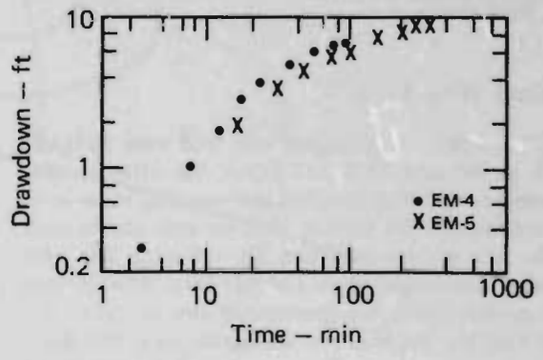

Fig. 32. Test 12: Responses in environmental wells EM-4 and EM-5 for 3.7 gpm in pumped well DW-1.

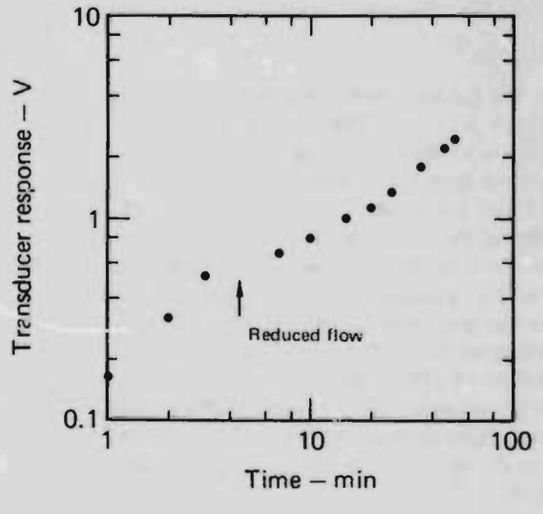

Fig. 33. Test 15: Response in pumped well DW-5 for 5 gpm.

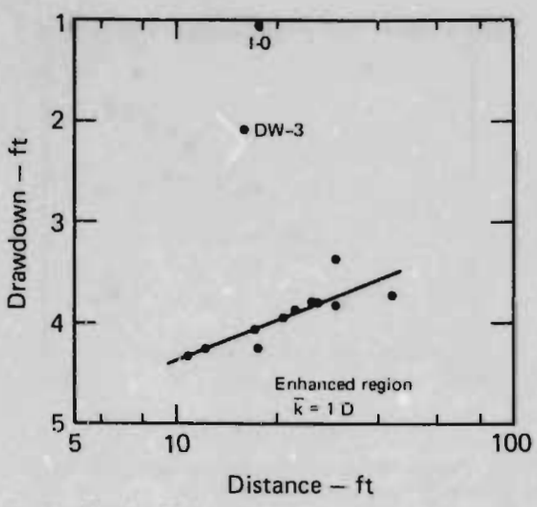

Fig. 34. Test 15: Observation-well drawdowns at 50 min for 5 gpm in pumped well DW-5.

Dual Well Tests

Dual injection-pumped well tests were designed to pump one well and inject the effluent into another well. We observed and recorded water-level responses in the various wells on strip charts until the flow pattern stabilized (in ~30 min). The tests were terminated when a steady-state flow pattern was established. We constructed flow nets from the drawdown patterns and calculated local hydraulic conductivity from the constructed flow channel width and gradients.* These tests permitted higher flows and lower total drawdown, thereby increasing the sensitivity of K calculations in the inner-core area. We also noted permeability irregularities.

Test 9A

We pumped well 1-0 at 15 gpm and put the effluent into P-1. The flow stabilized in ~30 min. Figure 35 shows the pattern of equipotentials and stream lines we obtained during the test. The inner core of the northern HE area appears smaller than that of the southern HE area. Permeability contrast between the southern and northern area is evident, but the symmetry of the flow pattern, with respect to the permeability distribution, and the partial penetration of P-1, combined with the sluggish nature of DW-3 and 4-PW, precluded a definitive interpretation of the apparent asymmetry. The calculated permeability of the 1-0 inner core is 16 D, the P-1 inner core is 6 D, and the enhanced region is 4 D.

*See Flow Net section in Appendix A.

Tests 16, 17, 18, and 19

For Tests 16, 17, 18, and 19, we pumped water respectively from DW-4 to DW-5 at 7 gpm until the flow stabilized, to DW-6 at 7.2 gpm until the flow stabilized, to 9-OW at 7.4 gpm until the flow stabilized, and to DW-2 at 7.1 gpm until the flow stabilized. In each test, the flow stabilized in ~30 min. The flow net in Fig. 36 shows the permeability irregularities obtained during Test 17. In particular, the areal extent of the low permeability ridge between the shot centers is illustrated. Figure 37 is a composite of the areal distribution of permeability.

Although average values of permeability could be calculated for each observation well, these values would not reflect the real variation in permeability that is obtained from a flow-net construction.

Tracer Tests

We designed a tracer test to inject a stream of known NaBr concentration into a stabilized, dual injection-pump well operation. As native concentration of NaBr in the coal seam had been established at $\sim 2\ \mu g/\ell$, a feed-water concentration of 10^{-3} moles/litre of Br^- was established by mixing 2 lb of NaBr into 40 gal of water, which was injected at a rate of 10 gal/h into the mainstream flow of 10 gpm. We sampled the effluent regularly and measured the Br^- concentration electrically with a calibrated electrode that is sensitive to Br^-. We performed a second test the next day and increased the concentration of Br to 10^{-2} moles/litre by mixing 45 lb of NaBr into 55 gal of water, which was then injected at a rate of 10 gal/h into the mainstream flow of 10 gpm. The test ran for a total of 7-3/4 h, including a flow stabilization period of 1 h prior to NaBr feed injection. This 1-h period was actually a second-phase continuation of the first test from the previous day at the lower level of NaBr concentration. The data from this second phase indicated that the results of the first day's test were erratic. This erratic behavior was attributed to electrode poisoning, which was eliminated by cleaning the electrode. Results of the second phase of Test 20 were consistent with the results of Test 21.

The tracer test results indicated that the interconnected porosity σ, using a porous media model,[7] in which the breakthrough time is given by $t = 4\pi\sigma a^2 b/3Q$, was 1/2%. This observed porosity is that of the low permeability ridge that separates the two HE areas. For a uniformly fractured media to yield 1/2% porosity with an average inner core permeability of 10 D, the fracture spacing would

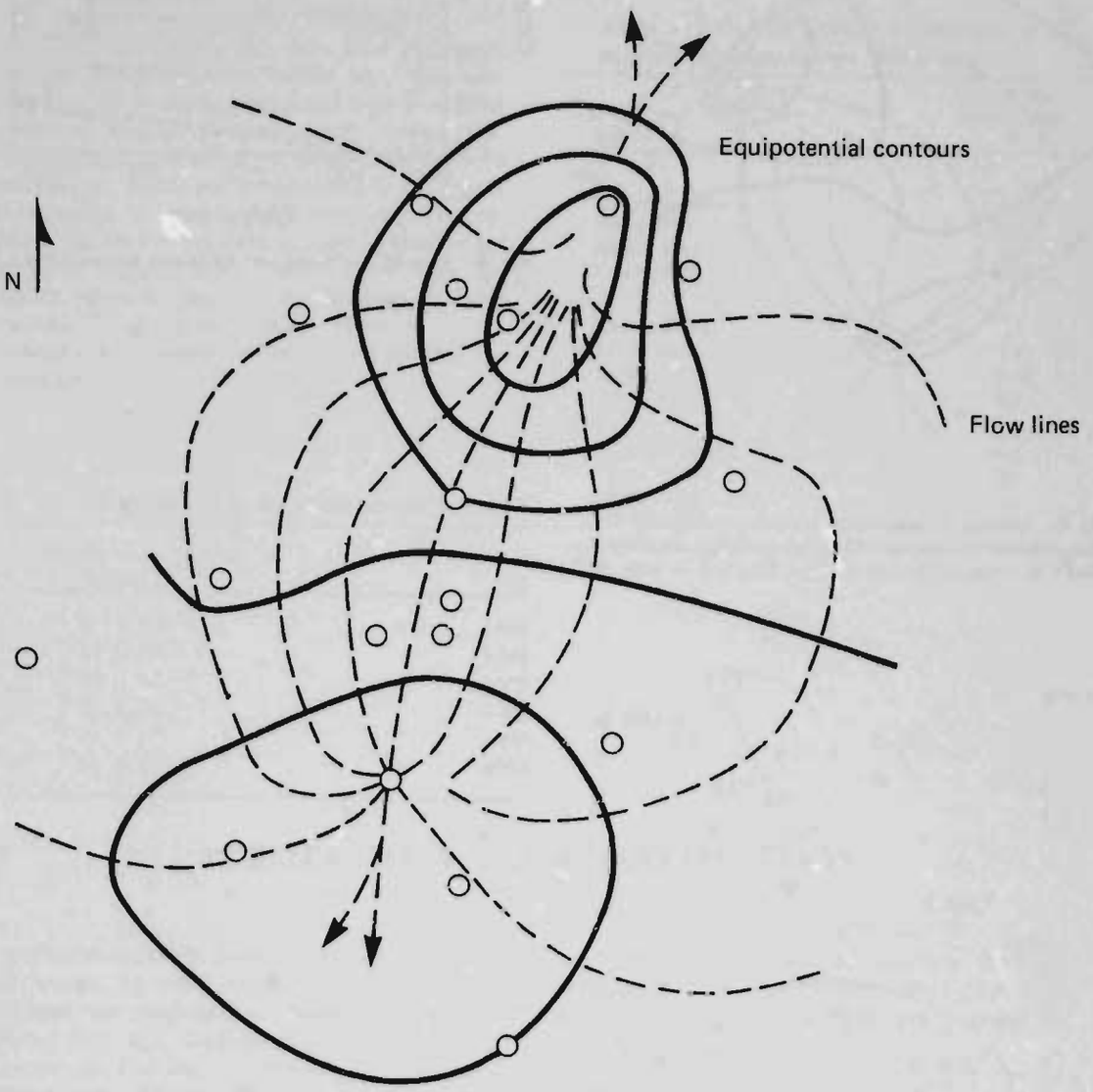

Fig. 35. Flow net. Hydraulic head (potential) contours and flow lines indicated by pumping 15 gpm from P-1 into 1-0 (Test 9A).

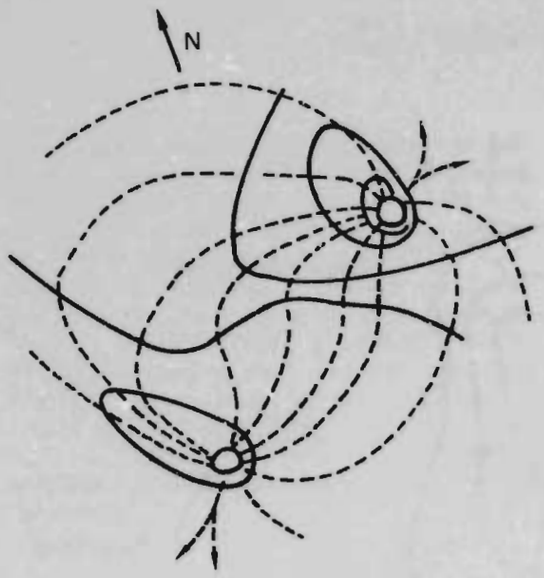

Fig. 36. Flow net. Hydraulic head (potential) contours and flow lines indicated by pumping 7.2 gpm from DW-4 into DW-6 (Test 17).

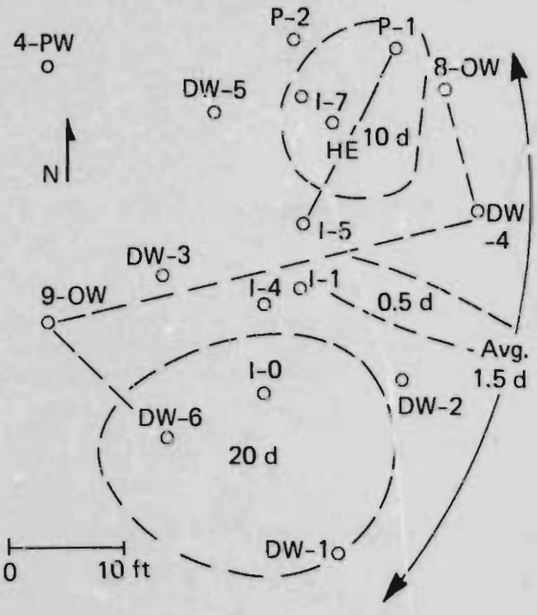

Fig. 37. Heuristic composite of channels or fractures (dashed lines), inner enhanced regions, and near native zone between the explosion centers.

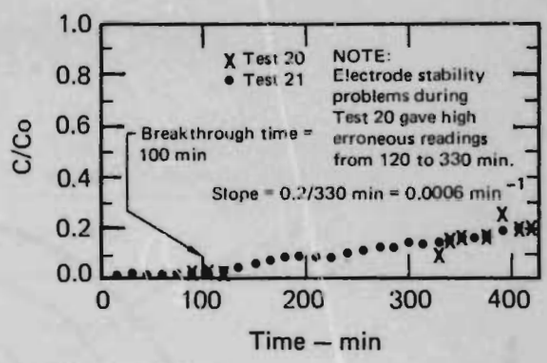

Fig. 38. Tests 20, 21: Tracer test for 10 gpm between I-0 and P-S 1.

Table 4. Final concentration of Br^- during Test 21.

Well	Br^- concentration, moles/ℓ
DW-1	4.9×10^{-3}
DW-2	3.5×10^{-3}
DW-3	1.5×10^{-5}
DW-4	1.1×10^{-3}
DW-5	7.1×10^{-4}
DW-6	3.8×10^{-3}

have to be about 10 fractures/m^2, according to McKee et al.[8] Figure 38 shows the concentration ratio of Br^- at P-1 to Br^- at I-0. The native concentration of Br^- was designated "Co" and other observed concentrations, "C." Values of C/Co were plotted vs time. Table 4 lists Br^- concentration of dewatering wells at the completion of Test 21.

POST GASIFICATION TESTS

To estimate the vertical distribution of permeability, post gasification tests were performed south of the southern HE region. Slug tests were conducted in an open, unscreened hole as drilling progressed through the coal seam. Tables of K values appear in Table 5. A 100-fold variation in permeability, which was proportional to the degree of fracturing, was obtained. [9] The highest values appeared for the bottom third of the coal seam in the enhanced region. These values agree with the highest values of permeability obtained by other methods. [10] The lowest values appeared at the periphery of the enhanced zone and are less than the native coal.

Table 5. Estimated intrinsic permeability of explosively-fractured Felix No. 2 coal.[a]

Test well and interval	Intrinsic permeability, D
WW3	
Complete seam	0.48
Upper third	0.24
Middle third	1.1
Lower third	0.15
WW1	
Complete seam	2.2
Upper third	1.3
Middle third	0.73
Lower third	4.5
WW2	
Complete seam	6.6
Upper third	1.4
Middle third	1.1
Lower third	16

[a]The data in this table is taken from Stone, Ref. 9.

PERMEABILITY MODEL VERIFICATION

Different power law distributions of permeability enhancement vs radial distance from an explosive shot have been postulated for different loading conditions. For high loading rates, a permeability enhancement that decays as the fourth power of the distance ($1/r^4$) has been postulated, and for lower loading rates, a permeability enhancement that decays as the first power of the distance ($1/r$) has been postulated. [8,11]

Data for the enhanced and transition regions from wells to the east of the explosion center obtained during pregasification tests fit a $1/r$ power law such that $\bar{k} = 30(D-m)/r(m)$. Since a $1/r$ power law variation in permeability results in a steady-state, linear gradient when late-time drawdowns are plotted as a function of r, the data have been plotted on straight graph paper to illustrate the compatibility with this law. Figures 39-41 plot drawdown vs distance on straight graph paper for

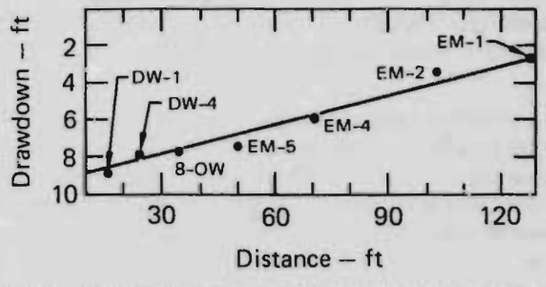

Fig. 39. Test 7: Drawdown vs distance towards the eastern quadrant for 3 gpm in I-0 at 570 min.

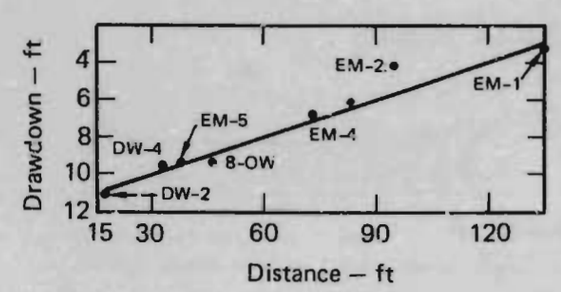

Fig. 40. Test 12: Drawdown vs distance towards the eastern quadrant for 3.7 gpm in DW-1 at 440 min.

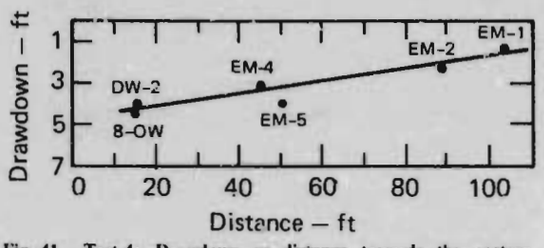

Fig. 41. Test 4: Drawdown vs distance towards the eastern quadrant for 2 gpm in DW-4 at 300 min.

Tests 7, 12, and 4, respectively. All three drawdowns fit a $1/r$ power law with a coefficient of 30 D/m. The inner-core permeability, as extrapolated from these data, indicates that the maximum inner-core permeability should have been 30 D at 1 m.

Data for the enhanced region from wells south of the explosion center obtained during post gasification tests fit a much higher power law [12]—more like $1/r^4$. The differences in power law distribution could be caused by shot interaction effects, giving rise to different types of loading in different regions. Some indeterminacy may also be the result of data scatter and system insensitivity.

Areal anisotropy was exhibited between EM-3 and EM-1, 2, 4, and 5, indicating that the maximum to minimum permeability ratio was 5. The permeability values obtained from the Jacob analysis would be the equivalent isotropic permeability k. The maximum permeability would be $\sqrt{5}\,\bar{k}$ and the minimum permeability would be $\bar{k}/\sqrt{5}$.

DATA SENSITIVITY

The pregasification testing system was not sensitive to regions of high permeability. Variations in drawdown differences of late-time data for individual well pairs indicate that the error band in drawdown data was about ±0.005 V or ±0.1 ft. Figure 42 plots drawdown difference vs time for select well pairs during Test 7. This is not within the component tolerance of the recording equipment. [13] Power supply stability may have been inadequate to maintain system reliability. The maximum value of permeability that could be measured on site with steady-state methods for the small well spacings is about 10 D. To measure high inner-core permeabilities (100 D), a sensitivity of ±0.01 ft or ±0.005 V would be required.

Drawdown differences for the environmental wells indicate that the error band in manual well soundings was ±0.2 ft. Moving the sounders from well to well decreased the accuracy that could have been obtained by leaving the sounders set for each test.

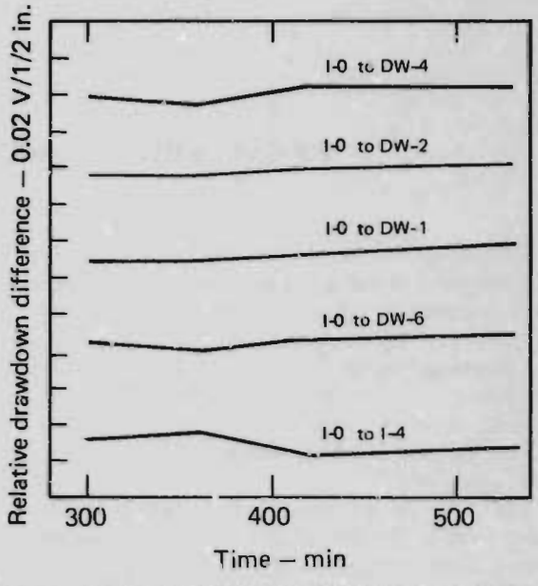

Fig. 42. Test 7: Selected drawdown differences vs late time for 3 gpm in I-0 between 300 and 570 min.

SUMMARY

The data were examined with the many methods of analysis available; the most consistent results were obtained with (1) slug tests, (2) drawdown differences and late-time approximation for drawdown injection tests, and (3) flow net construction for dual injection-withdrawal tests.

The particular aspects of hydraulic testing in coal seams that produce analytical difficulties are the effects of (1) installing several casings closely together causing changes in the storage coefficient and perturbations of the flow regime, (2) using large well-casing size relative to the low formation transmissivity causing prolonged well-bore storage effects, and (3) anisotropy due to fractures and explosive fracturing. These difficulties are best overcome using steady-state tests, particularly the dual injection-withdrawal test.

Although slug-test results are affected by inter-casing flow, slug tests can be used during drilling to measure vertical variation in permeability. They can also be used anytime afterwards to trace the performance of a well throughout time. The analytical ease of this method is generally offset by the relatively low permeability values obtained as a result of well losses.

Drawdown tests give a good measure of enhanced region permeability beyond 5 ft from the HE areas and indicate areal anisotropy. Since early-time data is distorted by well-bore storage, apparent leakage parameters obtained by matching techniques are suspect, unless a small-diameter well is pumped.

Dual injection withdrawal tests indicated permeability variations within the inner-core area. In particular, the test indicated a low k ridge separating the two HE areas that may have been responsible for the early override observed during gasification. Figure 43 shows the gasified region overlain on the hydrology composite. An advantage of this test is that a whole pattern of site permeability is obtained in 30-60 min.

The tracer tests were difficult to analyze because of the short distances involved, an irregular permeability distribution, and large void spaces at the wells. The best data relate to the breakthrough time, which yields an effective porosity calculation. Unfortunately, fracture channels can short circuit the flow, thereby giving short breakthrough times and low porosity calculations.

The permeability models postulated for explosively fractured media may apply in different regions of a dual-shot explosion. The pregasification data obtained from wells east of the shot center followed a $1/r$ variation and the post gasification data obtained from wells south of the shot center followed a $1/r^4$ variation.

The lack of sensitivity of most test methods precluded measuring high inner-core permeabilities. The data could have been more precise if larger pumps had been available for the dual injection-withdrawal tests. They would have permitted more flow between well pairs, thereby increasing the response.

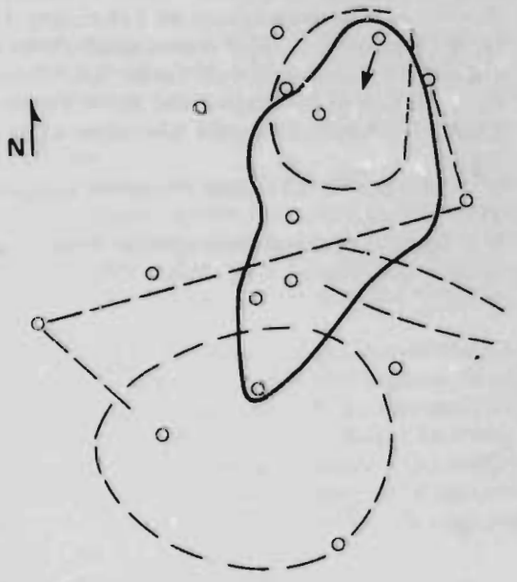

Fig. 43. Gasified region overlaid on hydrology composite.

ACKNOWLEDGMENTS

Many people who are participating in the coal program contributed to this effort. The contributions of D. F. Snoeberger, A. E. Sherwood, R. Stone, and T. Butkovich were particularly appreciated.

REFERENCES

1. B. J. Qualheim, *Geological Exploration of Potential Underground Coal Gasification Sites in the Powder River Basin of Wyoming and Montana*, Lawrence Livermore Laboratory, Livermore, Calif., Rept. UCRL-52237 (1977).
2. R. Stone and D. F. Snoeberger, *Evaluation of the Native Hydraulic Characteristics of the Felix Coal (Eocene, Wasatch Formation) and Associated Strata, Hoe Creek Site, Campbell County, Wyoming*, Lawrence Livermore Laboratory, Livermore, Calif., Rept. UCRL-51992 (1976).
3. N. J. King, "Maps Showing Occurrence of Ground Water in the Gillette Area, Campbell County, Wyoming," U.S. Geological Survey, Miscellaneous Investigations Series, Map I-848-E (1974).
4. J. R. Hearst, *Fractures Induced by a Contained Explosion in Kemmerer Coal*, Lawrence Livermore Laboratory, Livermore, Calif., Rept. UCRL-51790 (1975).
5. *LLL In Situ Coal Gasification Program, Quarterly Progress Report, October through December 1975*, Lawrence Livermore Laboratory, Livermore, Calif., Rept. UCRL-50026-75-4 (1976).
6. A. E. Sherwood, R. Quong, and D. F. Snoeberger, *Permeability of Explosive-Fractured-Coal Aquifer Modeling and Analysis of Field Hydraulic Tests*, Lawrence Livermore Laboratory, Livermore, Calif., Rept. UCRL-52250 (1977).
7. D. B. Grove, *U.S. Geological Survey Tracer Study; Amargosa Desert, Nye County, Nevada, Part II: An Analysis of the Flow Field of a Discharging-Recharging Pair of Wells*, U.S. Geological Survey, Rept. USGS-474-99 (1971).
8. C. R. McKee and M. E. Hanson, "Explosively Created Permeability from Single Charges," *Soc. Pet. Eng. J.* (Dec. 1975).
9. R. Stone, *Measurement of the Spatial Variation of Hydraulic Characteristics of an Explosion-Fractured Coal Seam*, Lawrence Livermore Laboratory, Livermore, Calif., Rept. UCRL-52298 (1977).
10. D. F. Snoeberger, *Field Hydrological Tests of Explosively Fractured Coal*, Lawrence Livermore Laboratory, Livermore, Calif., Rept. UCRL-78957 (1977).
11. C. R. McKee, M. E. Hanson, and R. W. Terhune, *Permeability from Single and Multiple Detonations of Explosive Charges*, Lawrence Livermore Laboratory, Livermore, Calif., Rept. UCRL-78207, Rev. 1 (1976).
12. T. R. Butkovich, Lawrence Livermore Laboratory, Livermore, Calif., private communication, Oct. 1977.
13. S. J. Spataro, *LLL Instrumentation for In Situ Coal Gasification*, Lawrence Livermore Laboratory, Livermore, Calif., Rept. UCRL-79551 (1977).

APPENDIX A
METHODS OF ANALYSIS

Several methods of analysis have been used for the Hoe Creek data obtained in late 1977. The different techniques yielded generally consistent results. The major uncertainties in data interpretation concern leakage parameters and inner-core permeabilities. The alternate techniques used in this effort are described below with references for more detailed discussion.

Type-Curve Analysis

When test data are converted to dimensionless form and plotted on appropriate graph paper, the flow regime can usually be determined from the unique characteristics of the data patterns. Type curves [1] can then be used to calculate hydraulic parameters using matching techniques.

The Theis-type curve is the fundamental-type curve in ground-water hydraulics. If all observation-well data taken from fully penetrating wells, plotted as drawdown vs t/r^2, fall along this curve, the aquifer is homogeneous, confined, non-leaky, and extends beyond the testing boundaries. During the late-time part of the test, the data lend themselves to an approximate method of analysis developed by Jacob, whereby a straight-line relationship is obtained between drawdown and log time or log distance.

Hantush developed type curves for leaky aquifer response in which observation well data followed different curves on a drawdown vs t/r^2 plot.

Other type curves are available for specific models including delayed storage effects, drain discharge response, and slug tests. Observation wells near fractures appear to follow a drain response when the pumped well intersects the fracture.

Deviations from type-curve response can sometimes be attributed to special effects. Well-bore storage affects pumped-well response, and drawdown vs time appears as a straight line with a slope of 1 on a logarithmic data plot. For large casings, the effect lasts far into late-time behavior. Fracture flow affects pumped-well response and appears as a straight line with a slope 1/2 on a logarithmic data plot. Frequently the two effects occur together, with fracture flow following well-bore storage flow.

Another type-curve deviation is caused by aquifer anisotropy. If the data curves are plotted as drawdown vs t/r^2 and fall on horizontally parallel Theis-type curves, the spread between the curves indicates areal aquifer anisotropy. If observation wells along the major and minor axes are plotted, their separation is the scale factor, m, required to eliminate the anisotropy. If the data curves fall on vertically parallel Theis-type curves, the spread between the curves indicates radial aquifer anisotropy, which can be confused with leaky aquifer response.

Slug tests for radial-flow geometries with distributed parameter have a family of type curves that depends on the storage coefficient. The smaller the storage coefficient the sharper the type-curve response. Some of the storage coefficients required for slug test interpretation are much lower than can be accounted for realistically. Tests requiring storage coefficients lower than 10^{-6} fit a lumped-parameter skin-friction model. This implies that there is a high local resistance at the well (skin friction) compared to resistance at the aquifer, resulting in a non-radial response at the well. The response for the skin friction is an exponential decay of water in the casing, according to the relationship $H/H_0 = e^{-(t/\pi r_c^2 R)}$ where R, the well resistance, is a lumped parameter and should not be related to a permeability value.

Type curves used in interpreting Hoe Creek data are shown in Figs. A-1 and A-2.

Flow Net Analysis

Steady-state flow regimes of similar geometry and boundary conditions have similar pressure flow distributions. Flow nets can be constructed on a plan view of pressure measurements. [1] These plots will show permeability irregularities that have distorted the flow net from that produced by a homogeneous permeability. In particular, dual injection-pump tests with the same flow values produce a symmetrical flow net in homogeneous media. Deviations from this pattern can be used to demonstrate local permeability irregularities that might otherwise be overlooked. Observation well data from a dual injection-pump test can also be used to calculate average permeabilities from the relationship $s = Q \ln (r/R) / 2\pi T$. [2]

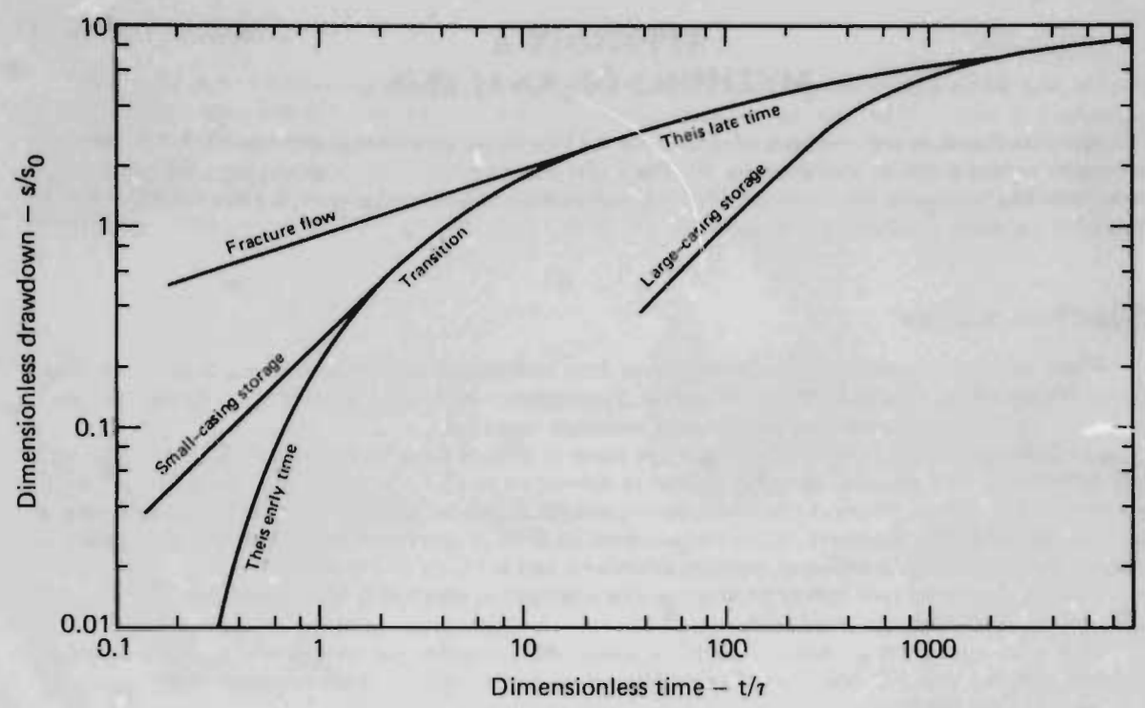

Fig. A-1. Slug test and exponential decay curves.

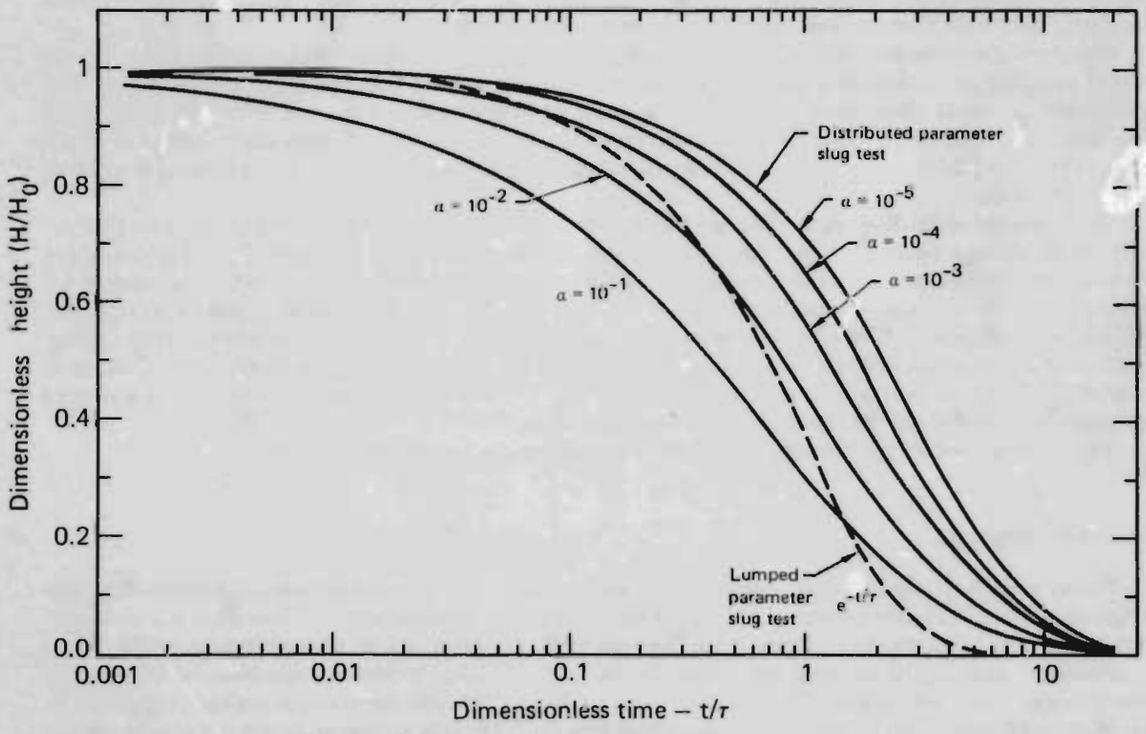

Fig. A-2. Theis, fracture flow and well-bore storage effect curves.

Numerical Analysis

Sherwood et al. [3] recommended a special analytical model for interpretation of Hoe Creek data. Drawdown differences between two observation wells were related to reciprocal time, with the resulting intercept and slope being expressed as functions of T and S/T^2 respectively. The intercept is equal to $Q\ln(r_2/r_1)/2\pi T$ and the negative slope is $QS(r_2^2 - r_1^2)/16\pi T^2 t$ $(r_2 > r_1)$. This model is particularly useful for smoothing data and providing system stability analysis. The model is also valid for concentric regions of different permeability, provided the observation wells are located in the same regions.

APPENDIX B
FACTORS AFFECTING HYDRAULIC TEST INTERPRETATION

Several complicating factors affected the interpretation of the test data. The installation of so many casings in close proximity changed the storage coefficient and perturbed the flow regime. Areal and vertical variations exist in both permeability and porosity. The fractures produce blocks of relatively impermeable coal imbedded in a more permeable flow matrix, so that most individual wells are much more resistive than the total system.

Well-Bore Storage

One of the first problems encountered in coal seams is the phenomenon of well-bore storage effect. The petroleum industry has developed analytical procedures to identify it because of the relative contrast between large casing capacity and low reservoir transmissivity. [4] The amount of fluid in the casing is appreciable compared to the immediate flow available from the reservoir. As a result, early-time flow does not leave the reservoir; rather the flow comes from fluid stored in the casing. On the other hand, the well-bore storage phenomenon is rarely a problem in ground-water evaluations because of the relative contrast between small casing capacity and high aquifer transmissivity. The amount of water stored in the casing is very small compared to the immediate flow available from the aquifer. As a result, the early-time flow comes from the reservoir after a few seconds of pumping. The low transmissivity coal seams indicates that, because of storage effects, smaller observation wells make better pump-test wells for the Hoe Creek site than the larger production and dewatering wells.

Well Friction

With well-bore storage effects, the flow across the well screen changes during early-test times. As a result, the pressure response at early times contains a component that is directly related to the change in flow across the well screen. This exponential pressure response of a well with well-bore storage is characterized at earlier times by both the cross sectional area of the casing and the well resistances. [4]

Intercasing Flow

The installation of so many open casings in close proximity to one another complicated the hydraulic testing at Hoe Creek. Two problems occurred. First, the storage coefficient of the aquifer system was increased with the installation of each new casing. Second, an appreciable percentage of the flow is required to change the water levels in the casings during pump tests, thereby causing a delayed response. Intercasing flow is a major problem in slug-test interpretation.

Fractures

Some of the naturally occurring fractures have become conduit-like in their ability to equalize pressures between observation well pairs or to cause an uneven distribution of flow from a pump well. The most important feature of fractured aquifers is that the hydraulic response of a pumped well intersecting a fracture displays a log drawdown vs log time relationship of a straight line with slope 1/2 for early time tests. [5] Observation wells that intersect the same fracture also exhibit this relationship. Observation wells close to a fracture show a drain model* response, while those further away have a distorted response that is between a drain model and a radial-flow model. Matching techniques for observation wells do not uniquely distinguish faulting patterns in a fractured aquifer. In some cases, however, observation-well responses indicate that a nearby fracture intersects the pumped well.

*The flow is unidirectional towards a drainage face.

Anisotropy

Due to the non-symmetrical orientation of the dewatering wells with respect to the inner core, tests that use dewatering wells as the pumped wells produced flow paths that were nonradial. The inner core area collimated the flow, resulting in distorted permeability calculations because the flow was not evenly distributed from all areas.

The areal and radial variations in permeability affected the pumped-well and observation responses so that available matching techniques were not applicable.

Variable Flow

Flow perturbations produce a vertical shift in data from one type curve to another. Quite often a pump will begin to produce less towards the end of the test because it is operating at a greater head and thus losing capacity. The test results then show a flattening of the data curves, reflecting the declining flow, which could be interpreted as a leakage response.

Bastie
Kerner
Lacklen

Coal Gasification

PREPRINT UCRL- 81016

Lawrence Livermore Laboratory

USE OF HIGH-FREQUENCY ELECTROMAGNETIC WAVES FOR MAPPING AN IN SITU COAL GASIFICATION BURN FRONT

D. T. Davis, R. J. Lytle, and E. F. Laine

April 7, 1978

This paper was prepared for submittal to In Situ

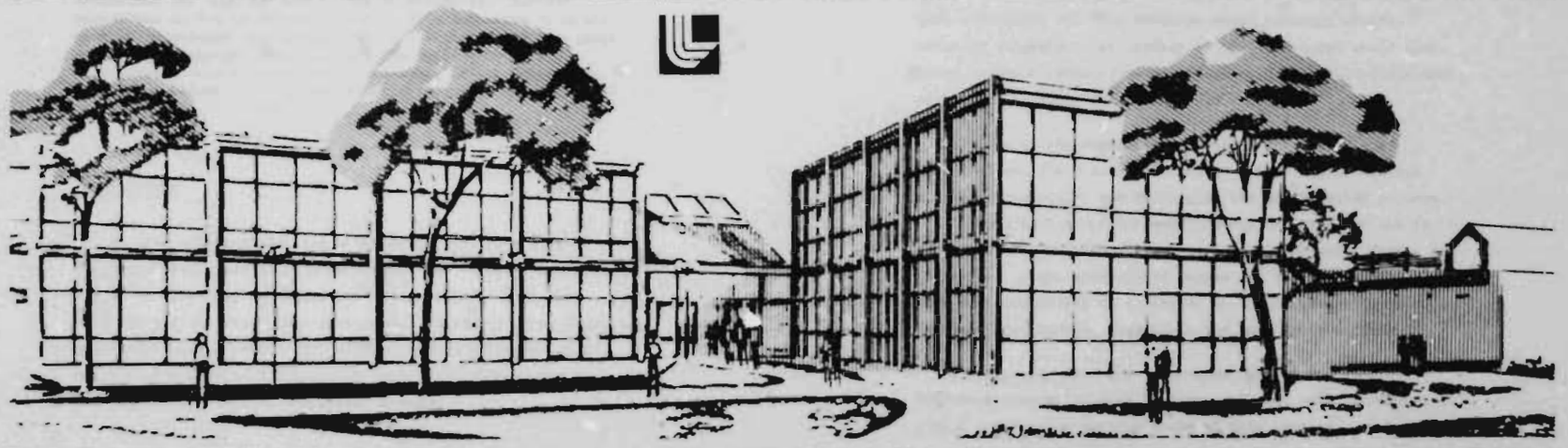

USE OF HIGH-FREQUENCY ELECTROMAGNETIC WAVES FOR MAPPING AN IN SITU COAL GASIFICATION BURN FRONT

D. T. Davis, R. J. Lytle, and E. F. Laine
Lawrence Livermore Laboratory, University of California
Livermore, California 94550

ABSTRACT

High-frequency electromagnetic waves transmitted between boreholes can be used to map the position of an underground coal gasification (UCG) burn front, as well as other geophysical anomalies. The technique uses transmitting and receiving antennas lowered down boreholes on either side of the gasified region. Results from the use of this technique in a UCG experiment show high resolution and close agreement with data from other instruments. The depth, height and lateral position of the burn front were easily determined and subsidence of overburden was also evident in the measurements. Several variations on the method were tried. This technique promises several advantages over other down-hole instrumentation: lower cost, better spatial coverage, and the ability to give measurements both during and after passage of the burn front. The UCG experiment also showed several improvements that could be made in the technique.

INTRODUCTION

In this paper we describe a technique that uses high-frequency electromagnetic waves transmitted between boreholes to map an in situ coal gasification[1-4] burn front. Both the hardware and the method are discussed. In addition, we present results from experiments with this technique performed during the Lawrence Livermore Laboratory (LLL) 1977 underground coal gasification project at Hoe Creek, Wyoming.

We at LLL have, over a period of years, advocated and advanced the use of electrical and electromagnetic probing for various geologic applications.[5-23] Some of these applications are: locating high-contrast anomalies such as voids,[15] using only one cable to monitor the detailed temperature profile within in situ energy processes,[14] determining the extent of fractures induced by high explosives emplaced within a coal seam,[17,20] monitoring three-dimensional progression of a fluid injected into a borehole,[12,18] and determining detailed maps of subsurface constitutive parameters by using cross-borehole probing.[12]

One of our colleagues first suggested the application of our high-frequency electromagnetic (HFEM) technique to monitoring an underground coal gasification (UCG) burn.[19] We were subsequently able to perform a simple experiment on LLL's first UCG project at Hoe Creek, Wyoming, in 1976.[24] Results from that experiment and from computer aided modeling studies[25] strongly suggested that certain of our techniques would work. Based on these results, we attempted our first full-scale UCG mapping experiments during LLL's 1977 project.[26]

Because of the potential importance of in situ coal gasification, the U.S. Department of Energy and others are actively researching and developing the gasification process. Coal is our most abundant fossil energy resource and can be converted to combustible gas -- an attractive energy form -- by heating in the presence of oxygen and steam. Gasifying the coal underground may be a cheaper means of recovering this resource than mining, especially for deep western coals.[24]

The LLL Fall 1977 UCG experiment had two distinctly different phases: reverse linkage, followed by a forward burn. Figure 1 shows the various steps of this process.

Our first full-scale program of experimental UCG burn-front mapping was very successful. The burn front interacted strongly with the electromagnetic waves and so was easily observable. Interpretation of the experimental data was straightforward and compared well with data from other down-hole instrumentation. Also, the spatial resolution obtained was better than expected.

In the remainder of this paper we describe our HFEM technique, present the results of our experimental program at Hoe Creek, and discuss the major accomplishments and shortcomings of our present system.

THE HFEM TECHNIQUE

In this section we describe our technique of using HFEM waves to map a UCG burn front. Both the hardware and the method are considered.

Figure 2 shows the basic setup involved in transmitting electromagnetic waves between boreholes to detect a geophysical anomaly. Watertight transmitting and receiving antennas (which are connected to the ends of coaxial cables) are lowered down individual boreholes to the depths being investigated (Fig. 3). The simple dipole transmitting antenna is driven by an oscillator and amplifier putting out 100 W at a frequency selected normally between 10 and 100 MHz. Detecting the wave transmitted through the ground is a unique receiving antenna of LLL design.

Figure 4 is a photograph of the receiver package, showing its monopole antenna, top-hat terminator and broad-band constant-sensitivity down-hole electronic amplifier. The detected signal is sent up cable to a spectrum analyzer (for amplitude measurement) or a network analyzer (for phase measurement).

For best efficiency, the length of the dipole transmitting antenna should approximately equal 1/2 the wavelength of the electromagnetic wave in the ground; that is, $L = c/2fn$, where c is the speed of light, f the frequency, and $n^2 = \epsilon$ is the relative permittivity of the ground at frequency f. For example, if f = 10 MHz and n = 3, the optimum antenna length L would be 5.0 m.

The region between the two boreholes is investigated by recording the received signal parameters (amplitude, phase, or both) as a function of depth. This is normally done by successively lowering the two antennas an incremental distance and recording the received signal. The optimum incremental distance depends on the wavelength and the desired spatial resolution, with 1 ft being typically chosen. Sometimes the two antennas are lowered with fixed offsets in their depths to give different electromagnetic views[12] of the geophysical anomaly.

The amplitude and phase of the received signal vary with depth if the path between the two antennas passes through or very near a geophysical anomaly whose conductivity and permittivity differ significantly from those of the host medium. Larger objects require less of a difference to be detectable than do smaller objects. The variation in amplitude and phase of the electromagnetic wave received is a result of reflection from, refraction through, and diffraction around the anomaly.

The signal variation with depth, referred to as the signature, yields information about the geometry of the anomaly (i.e., size, shape, and position). For many geophysical anomalies, these interpretations are easy to make. However, this is not universally true. To aid in the interpretation of

such signatures, modeling studies are often performed.[15,27] A series of computer-generated signatures (based on an appropriate model) for a range of geometrical and electrical parameter values often aid the interpretation of signatures obtained empirically.

In the case of UCG burn-front monitoring, the electrical properties of the coal and burn region vary with position in a manner that is not known in detail. Figure 5 shows roughly the expected variation of conductivity through a UCG burn front. As a result of this uncertain and complex behavior, computer-generated signatures based on simple models that describe an object of uniform properties imbedded in a homogeneous host medium have failed to match the signatures found in experiment. In spite of this handicap, however, the interpretation of our experimental results has been quite straightforward. In addition, evidence from other UCG down-hole instrumentation confirms our interpretations. Because of the complexity of accurately modeling a UCG burn, we defer that topic to a later report.

We refer to the technique described above as the transmission mode of operation (i.e., the electromagnetic wave is transmitted from one side to the other of the anomaly). One may also employ the reflection mode of operation, in which the two boreholes lie on the same side of the anomaly, as in Fig. 6. In this case, the receiving antenna responds to the sum of two waves: that directly from the transmitting antenna and that reflected off the anomaly. Because the reflected-wave phase differs from the direct-wave by an amount proportional to the path-length difference and the frequency of the wave, one can determine the path difference. The path difference is determined by noting the frequencies where minima or maxima occur in the detected signal. These extremes will occur at those frequencies for which the path difference equals an integer multiple of 1/2 wavelength (in the transmitting medium).

EXPERIMENTAL UCG BURN-FRONT MAPPING USING HFEM WAVES

In this section we describe the experiments we performed at Hoe Creek, Wyoming on LLL's second UCG project and we present burn-front mapping results obtained by interpreting our field data. The primary purpose of this first full-scale attempt at using our HFEM techniques to monitor a UCG burn front was to demonstrate their feasibility. Other important goals were mapping the progressing burn and finding areas of our technique that need further development.

We had access to a total of nine wells (boreholes) during LLL's Hoe Creek, Wyoming, UCG experiment of 1977. Figure 7 shows the plan view of the wells of interest to us. Wells A (injection) and B (production) were naturally not available to us. The nearness of SI1 to H4 and SI2 to SI3 meant that we had essentially seven locations to choose from. The wells were cased with PVC or fiberglass to permit the transmission of electromagnetic waves. These wells were drilled and cased to a depth of approximately 180 ft, 25 to 30 ft below the coal seam of interest (Felix No. 2). The Felix No. 2 coal seam (Fig. 8) is about 25 ft thick and located approximately between 127 and 153 ft deep.

We selected the location of our probe wells such that they would lie outside the expected burn region[4] and permit good mapping coverage of the region. Anticipating a lossy medium (coal of high electrical conductivity), we placed our wells just outside this region so as to minimize distances between wells and yet not lose the wells to the burn. Measurements made at the time of the UCG burn indicated that the coal was indeed quite lossy, having a conductivity of approximately 0.01 S/m. And, although we did eventually lose wells to the burn, we were very pleased with their placement and the data obtained from them.

Although, in general, any pair of wells could be used to probe the burn, we preferred certain combinations. Six paths were probed to obtain good coverage of the important region between the injection and production wells (A and B): H3 to H1, H2, and H4; SI2 to H2 and H4; and H5 to H4 (see Fig.7). In addition, SI2 and H5 to H6 probed the region to the west of Well A. Similarly, SI1 to H1, H2, and H6 were used north of Wells A and B, while H3 to SI2 and H5 served us to the south. A total of six motorized cable reels were used; three with transmitting and three with receiving antennas permanently attached to the cables with watertight connections. By locating these reels at appropriate wells, we only occasionally needed to move them to probe all the paths shown in Fig. 7.

Before the burn front started to affect the coal between a pair of wells, we measured the transmissivity as a function of depth. That is, the amplitude of the electromagnetic wave, transmitted between the pair of wells, was recorded for the antennas at 1-ft depth increments.* Figure 9 contains a typical record of such data which are referred to herein as baseline data.

Note from Fig. 9 that the signal falls off as either the underburden or overburden is approached. This is a consequence of the finite length of the transmitting antenna and the higher conductivity (greater loss) of those strata. Because the transmitting antenna was either 9 or 12 ft long, part of its

*Power into the transmitting antenna cable was fixed at 100 W. Not all of this power was radiated, however, because of the attenuation in the nearly 200 ft of cable and the impedance mismatch between the antenna and the cable. Radiated power was limited to, at most, a few watts.

length was out of the coal seam when the antenna center was within either 4.5 or 6 ft, respectively, of the coal-seam boundaries.

Some of the baseline records showed what appeared to be the effects of the two ash layers within the coal seam (see Fig. 8). This was especially true for the path H3 to H1 as shown in Fig. 10. For this path, the large dips in the transmissivity at the depths of the ash layers made data interpretation difficult. We obtained better results when we tried subtracting out the effects of these layers.

DETECTABILITY, TRACKABILITY, AND SPATIAL RESOLUTION

Changes in the signature for a given pair of wells (a given path) indicate the presence of the burn in that region. In Fig. 11 are the signatures observed on three different days for the path H5 to H4 (transmitter in H5, receiver in H4). Note from the October 29 data the sharp resolution and the large change in signal strength caused by the burn. It is apparent from the figure that the burn is centered at a depth of approximately 146 ft and is quite limited in vertical extent (a few feet). The dip at 146 ft is approximately 20 dB lower than the baseline. This very large effect makes the burn front easy to detect.

The November 1 data in Fig. 11 are also interesting. They indicate the burn has moved upward and broadened quite a bit. The burn appears to be located over the top half of the coal seam on that day. Being able to track the motion of the burn in this manner is an important feature of the HFEM technique. Note also from the figure that the November 1 signature has recovered in the region where the burn had been on October 29. We believe this results from wet coal and wet ash having nearly the same conductivity (see Fig. 6), wet ash being left behind by the burn.

Recovery of the transmissivity when the burn leaves an area greatly simplifies data interpretation and makes the burn front much easier to track.

Rather than interpret raw data such as in Fig. 11 directly, it is better to first normalize the data relative to the appropriate baseline data. Because the curves are in decibels, one need only subtract the raw data values from the baseline values to obtain normalized data. This is an important step because we are interested only in the effects of the burn and not of any preexisting features of the geology.

In Fig. 12 we present normalized curves for the path H5 to H4. Note from the figure how well the burn can be tracked. The burn is seen to move from 6 ft above the coal-seam floor on October 28 to 8 ft on October 29, 15 ft on October 31, and 19 ft (having broadened significantly) on November 1. Still later, on November 3, we see quite a difference as compared to November 1: the top 14 ft of the seam has become much more transparent. The upper 10 ft is actually more transparent on November 3 than the baseline. We interpret the data of November 3 as indicating that, by that time, a void region formed at the top of the coal seam and the burn had overridden the seam (i.e., the flow path was now in the overburden). Thermocouple data support the conclusion that an override condition existed in this region on November 3.

COMPARISON OF HFEM TO OTHER UCG INSTRUMENTATION

Our HFEM data and interpretations can be compared with those of the thermocouples and extensometers used on LLL's UCG experiment. Twelve thermocouple and two extensometer wells were employed in this experiment. Each thermocouple well had six thermocouples within the coal seam (at 1, 5.5, 10, 14.5, 19, and 23.5 ft above the coal-seam floor) and one or more in the

overburden. Each extensometer well contained six anchors located in the overburden between 1 and 20 ft above the coal-seam roof. The thermocouples sensed local temperatures, while the extensometer anchors sensed subsidence and collapsing of the overburden.

Thermocouples sense a burn parameter at a certain spatial point, but HFEM is sensitive to conditions within a volume (along and near the propagation path). In spite of this difference in sampling, we see good agreement between these two types of instrumentation. Figure 13 contains the record from a thermocouple well* and normalized HFEM data for the nearest path (S12 to H4), both for the same day. The HFEM data, which are plotted on a logarithmic scale, indicate about the same spatial extent and vertical position for the burn as the thermocouple data.

Our technique has several important advantages over thermocouples for instrumenting a UCG experiment: The HFEM technique will sense a burn anywhere along its path, whereas thermocouples must be very close or the burn can go undetected (for example, thermocouple wells often fail to sense the reverse-linkage burn). Thermocouples fail at temperatures normally encountered within the burn front (approximately 1000°C) and yield no data thereafter, whereas HFEM wells can be located outside the burn region and provide data after as well as before the burn. Also, the HFEM technique requires fewer wells to map an area and much less expense per well. (To obtain the same vertical resolution, each well would require many thermocouples.) In spite of these advantages for HFEM, we feel that thermocouples will play an important role in future UCG experiments, certainly where temperature information is desired.

---

*LLL's well No. I10.

During the first 30 days of the UCG burn, when signal attenuation was modest and our HFEM results were more easily interpreted, the extensometers recorded two overburden collapses. The extensometer anchors located 3 and 6 ft above the coal-seam roof in one extensometer well broke loose on November 4 and November 5, respectively, marking the collapse of part of the overburden (presumably into the coal seam).

Our HFEM data show a noticeable change after these events. Figure 14 contains normalized curves for November 3 and November 5 (before and after the two collapses occurred) for the path H3 to H4. Note the large signal reduction of approximately 10 dB over the upper half of the coal seam. Apparently, higher-conductivity (higher-loss) material from the overburden has fallen into the coal seam, reducing signal transmission therein.

DETECTION OF BURN-FRONT LATERAL POSITION

In addition to detecting the more important vertical position of the burn, we conducted two measurements aimed at determining its lateral position as well. One of these measurements involved using HFEM in the reflection mode of operation as described earlier and shown in Fig. 6.

The reflection-mode measurement was unsuccessful at detecting the lateral position of the burn front. With the coal having a high conductivity value of 10^{-2} S/m, the extra path difference for the reflected wave resulted in a signal strength much reduced from the direct wave and thus interference between the two was lost in the system noise. This technique migh. be successful in coal of lower conductivity, however.

The other measurement for determining the burn's lateral position was much more successful. In this HFEM technique,

recording signatures with different depth offsets between the two antennas,[15] some with the transmitter higher than the receiver and some with it lower. Located on opposite sides of the burn, the two antennas are lowered past the burn while maintaining a fixed offset in depth. Lines drawn between the two wells at the depths where the burn is seen will cross at or near the location of the burn. Figure 15 contains the results of such an experiment, showing the most likely lateral position of the burn between the well pairs H3-H1 and H3-H2 at a time during the reverse-linkage burn. Because one would expect a greater accuracy in determining the lateral position when using larger offsets, this technique should work best for UCG experiments in thicker coal seams.

DISCUSSION

Although we had previously transmitted HFEM waves between boreholes to locate and map geophysical features, LLL's 1977 UCG experiment at Hoe Creek, Wyoming, was our first full-scale attempt at mapping a burn front. The experiments we performed there were quite successful. We demonstrated that the technique works, in that significant signal-level changes resulted from passage of the burn front. We obtained better spatial resolution than expected and were able to track the motion of the burn front. Our results agreed well with those of the other UCG instrumentation (thermocouples and extensometers). Finally, the technique demonstrated certain important advantages over other down-hole instrumentation: lower cost, longer measurements, and better spatial coverage.

During these experiments, we obtained valuable insight into areas of our technique that need further development. We need a more rapid setup and data-acquisition scheme to probe each path more often. The rate of change observed in our Hoe Creek data indicates that each path should be probed at least twice daily.

We also need a more efficient coupling between the power amplifier and the ground. This could be done by designing a down-hole amplifier connected directly to the transmitting antenna. By thus increasing the radiated power from the present few watts to perhaps 100 W, we could increase the well spacings or increase the wave frequency (and spatial resolution). The increased radiated power would also better enable us to experiment with swept-frequency excitation and look for received signal resonances related to the burn-front geometry. Further, we need to develop better models and better measurements of the electrical parameters in the burn. Better models and conductivity values would permit the parameterization of the electromagnetic-wave/burn-front interaction by computer. We could then better understand and quantify the process, better plan future UCG mappings, and improve experimental techniques.

The techniques described herein for the use of HFEM waves to map UCG burn fronts might also be applied to in situ oil shale retorting. Al Duba of our laboratory first suggested this possibility. We anticipate that the electrical properties of shale and the retort region are within the range of values needed for a successful application of our technique. We are anxious to try our technique on an in situ oil shale retort in the near future.

ACKNOWLEDGMENTS

We would like to acknowledge D. R. Stephens and R. W. Hill of our laboratory for including HFEM in their in situ coal gasification instrumentation plans and for their encouragement and support throughout our experimental program. We would also

like to thank R. W. Egbert, our electronics technician, for his able services throughout, and D. L. Lager and J. T. Okada for assisting us in performing the experiments.

Work performed under the auspices of the U.S. Department of Energy by the Lawrence Livermore Laboratory under contract number W-7405-Eng-48.

REFERENCES

1. Higgins, G. H., A New Concept for In Situ Coal Gasification, Law... e Livermore Laboratory, Rept. UCRL-51217 (1972).

2. Hill R. W., and Thorsness C. B., Results from an In Situ Coal Gasification Experiment Involving Explosive Fracturing: Hoe Creek Experiment No. 1. Lawrence Livermore Laboratory, Rept. UCRL-52229 (1977).

3. Northrup, D. A., "Instrumentation-Process Control Development for In Situ Coal Gasification," Eighth Quarterly Report. Sandia Laboratories, Rept. SAND77-0251 (1977).

4. Stephens, D. R., editor, Proceedings of the Third Annual Coal Conversion Symposium, Fallen Leaf Lake, California, June 6-9, 1977. CONF-770652 (1978).

5. "Subsurface Geologic Mapping by Electrical Signals," in Energy and Technology Review. Lawrence Livermore Laboratory, Rept. UCRL-52000-76-1 (1976), p. 10.

6. Lytle, R. J., and Lager, D. L., "Using the Natural Frequency Concept in Remote Probing of the Earth," Radio Science, 11, 199 (1976).

7. Lytle, R. J., Laine, E. F., Lager, D. L., and Okada, J. T., "Determination of the In Situ High Frequency Electrical Properties of Permafrost Rock," Radio Science, 11, 245 (1976).

8. Lytle, R. J., and Lager, D. L., "The Yosemite Experiments: HF Propagation Through Rock," Radio Science, 11, 245 (1976).

9. Hearst, J. R., Butkovich, T., Laine, E., Lake, R., Leach, D., Lytle, J., Sherman, J., Snoeberger, D., and Quong, R., "Fractures Induced by a Contained Explosion in Kemmerer Coal," International Journal of Rock Mechanics and Mining Sciences, 13, 37 (1976).

10. Lytle, R. J., and Lager, D. L., "Theory Relating to Remote Electromagnetic Probing of a Non-Uniform Thickness Coal Seam," Radio Science, 11, 465 (1976).

11. Lytle, R. J., Lager, D. L., Laine, E. F., "Subsurface Probing by High Frequency Measurements of the Wave Tilt of Electromagnetic Surface Waves," IEEE Trans. Geoscience Electronics, 14, 244 (1976).

12. Lager, D. L., and Lytle, R. J., "Application of ART Algorithms for Defining a Subsurface Electrical Profile from High Frequency Measurements," Radio Science, 12, 2 (1977).

13. "Finding Anomalies in the Ground with Radio Waves," in Energy and Technology Review. Lawrence Livermore Laboratory, Rept. UCRL-52000-77-1 (1977), p.1.

14. Lytle, R. J., and Myers, G. K., Temperature Profile Determination Using Frequency Domain Reflectometry. Lawrence Livermore Laboratory, Rept. UCID-17091 (1976).

15. Davis, D. T., Lytle, R. J., Lager, D. L., and Laine, E. F., Analysis of Electromagnetic Wave Probing for Underground Voids. Lawrence Livermore Laboratory, Rept. UCRL-52214 (1977).

16. Lytle, R. J., and Laine, E. F., Design of a Miniature Directional Antenna for Geophysical Probing from Boreholes. Lawrence Livermore Laboratory, Rept. 79943 (1977), submitted to IEEE Trans. Geosci. Electr.

17. Lytle, R. J., Laine, E. F., Lager, D. L., Coal Fracture Measurements Using In Situ Electrical Method: Preliminary Results. Lawrence Livermore Laboratory, Rept. UCID-16639 (1974).

18. Lytle, R. J., Lager, D. L., Laine, E. F., Salisbury, J. D., Monitoring Fluid Flow by Using High-Frequency Electromagnetic Probing. Lawrence Livermore Laboratory, Rept. UCRL-51979 (1976).

19. Duba, A. G., The Electrical Conductivity of Coal and Coal Char. Lawrence Livermore Laboratory, Rept. UCRL-78648 (1976).

20. Lytle, R. J., Laine, E. F., and Lager, D. L., "Using Electromagnetic Remote Probing to Determine the Physical Properties of a Coal Seam," presented at the 45th Annual International Meeting of the Society of Exploration Geophysicists, Denver, Colorado, 1975.

21. Lord, D. E., and Salisbury, J. D., In Situ Instrumentation: Final Report of a Joint EE/ME Group Study. Lawrence Livermore Laboratory, Rept. UCRL-51692 (1974).

22. Lytle, R. J., Laine, E. F., Lager, D. L., Electromagnetic Monitoring of the In Situ Coal Gasification Performed at Hoe Creek, Wyoming. Lawrence Livermore Laboratory, internal memorandum (December 1976). Readers outside the laboratory who desire further information on LLL internal documents should address their inquiries to the Technical Information Department, Lawrence Livermore Laboratory, Livermore, California 94550.

23. Lytle, R. J., "Measurement of Earth Medium Electrical Characteristics: Techniques, Results, and Applications," IEEE Trans. on Geoscience Electronics, 12, (3), 81 (1974).

24. Hill, R. W., editor, LLL In Situ Coal Gasification Program, Quarterly Progress Report, October through December, 1976. Lawrence Livermore Laboratory, Rept. UCRL-50026-76-4 (1976), pp. 7-8.

25. Davis, D. T., and Lytle, R. J., In Situ Coal Gasification Burn Front Mapping by Monitoring Reflected High Frequency Electromagnetic Waves. Lawrence Livermore Laboratory, Rept. UCRL-52325 (1977).

26. Stephens, D. R., Hill, R. W., and Thorsness, C. B., "Highlights of the LLL Hoe Creek No. 2 Underground Coal Gasification Experiment, submitted to: In Situ. Also available as: Lawrence Livermore Laboratory, Rept. UCRL-80692 (1978).

27. Holmes, J. J., and Balanis, C. A., "Electromagnetic Modeling of Reflections Inside an In Situ Gasified Coal Seam," Radio Science, 12, 33 (1977).

FIGURE CAPTIONS

FIG. 1. Schematic depiction of LLL's 1977 in situ coal gasification process showing reverse-linkage and forward-burn phases.

FIG. 2. The high-frequency electromagnetic-wave probing technique.

FIG. 3. Photograph of motorized antenna-cable reel used during LLL's UCG experiment at Hoe Creek, Wyoming.

FIG. 4. Photograph of LLL-designed electromagnetic-wave detector consisting of a monopole antenna with top hat and a broad-band electronic amplifier.

FIG. 5. Electrical conductivity expected during in situ coal gasification as a function of distance from the center of the burn. Dashed lines indicate regions of large uncertainty.

FIG. 6. Reflection mode of HFEM technique. The high-conductivity burn front acts much like a mirror, reflecting part of the electromagnetic wave.

FIG. 7. Plan views of the wells we employed in LLL's 1977 UCG experiment; A is the injection well, B the production well. Part (a) shows the interwell HFEM paths used to map the region between Wells A and B. Part (b) shows the paths used to map the perimeter of the burn region. Wells used for other instrumentation are not shown.

FIG. 8. Strata around coal seams at UCG site (Hoe Creek, Wyoming), determined from core samples and well logs. The experiment took place in the Felix No. 2 seam (subbituminous). Well I12 is 10 ft west of Well A, I4 approximately half way between H2 and SI1, and Well C 10 ft east of Well B (see Fig. 7).

FIG. 9. Baseline data (October 27, 1977) for path H5 to H4 (see Fig. 7). The frequency was 19 MHz.

FIG. 10. Baseline curve (October 14, 1977) for path H3 to H1 (see Fig. 7), showing effect of ash layers on HFEM signature. The frequency was 20.5 MHz.

FIG. 11. HFEM signatures for path H5 to H4 (see Fig. 7), showing burn-front detection and tracking.

FIG. 12. Normalized HFEM signatures for the path H5 to H4. The data has been normalized with respect to the baseline data, permitting easier and more accurate interpretation.

FIG. 13. Comparison of HFEM and thermocouple data from the Hoe Creek UCG experiment.

FIG. 14. Normalized HFEM signatures before (November 3) and after (November 5) collapses in the overburden were recorded by extensometers.

FIG. 15. Locating the lateral position of the burn front from several views. Each of the lines shown results from lowering transmitter and receiver at a constant given offset. Using several offsets, or views, gives several lines, which intersect near the burn region. Shaded areas indicate region most likely to contain burn center.

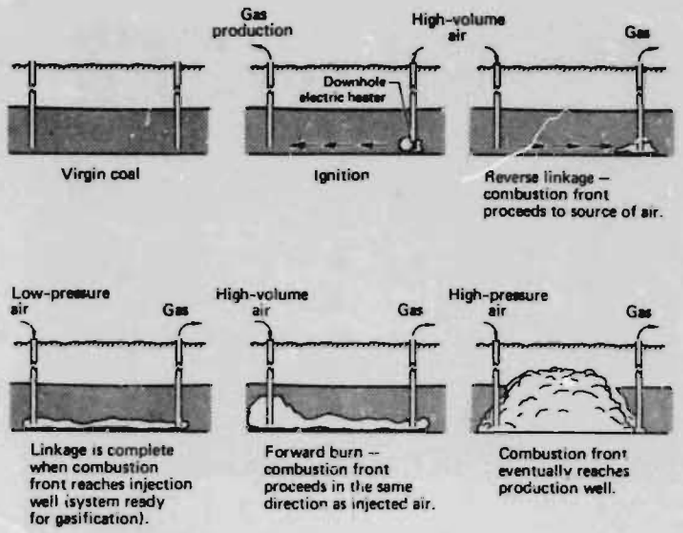

D. T. Davis - Fig. 1

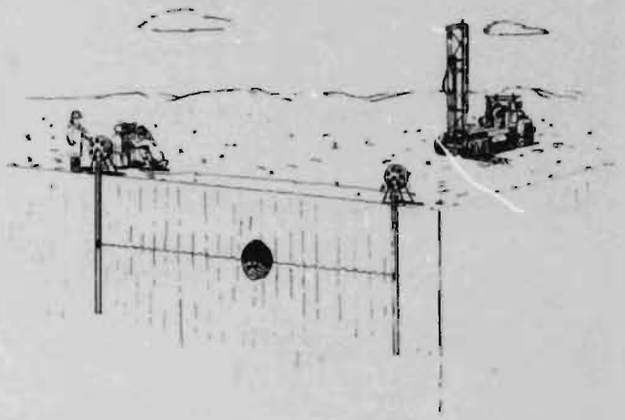

D. T. Davis - Fig. 2

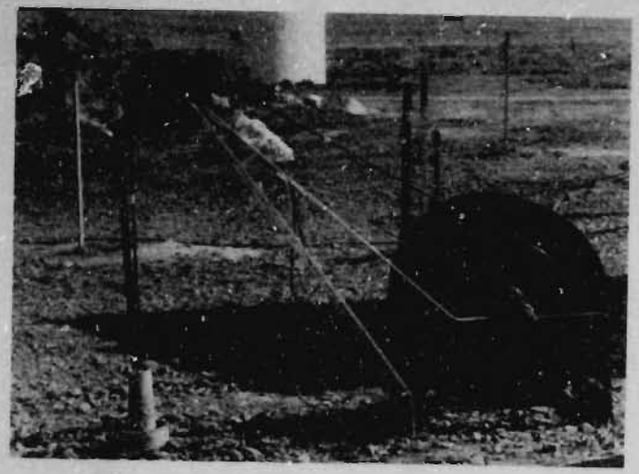

D. T. Davis - Fig. 3

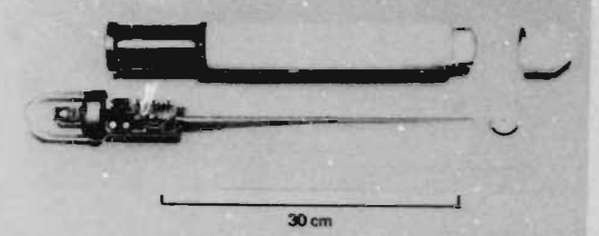

D. T. Davis - Fig. 4

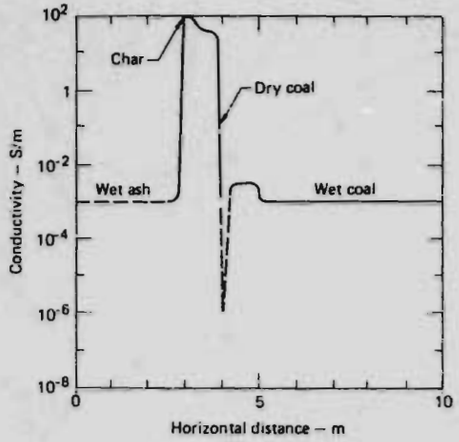

D. T. Davis - Fig. 5

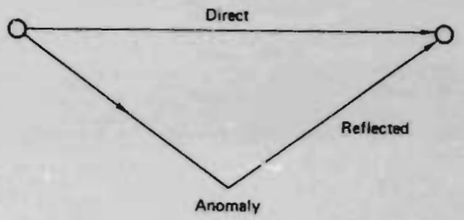

D. T. Davis - Fig. 6

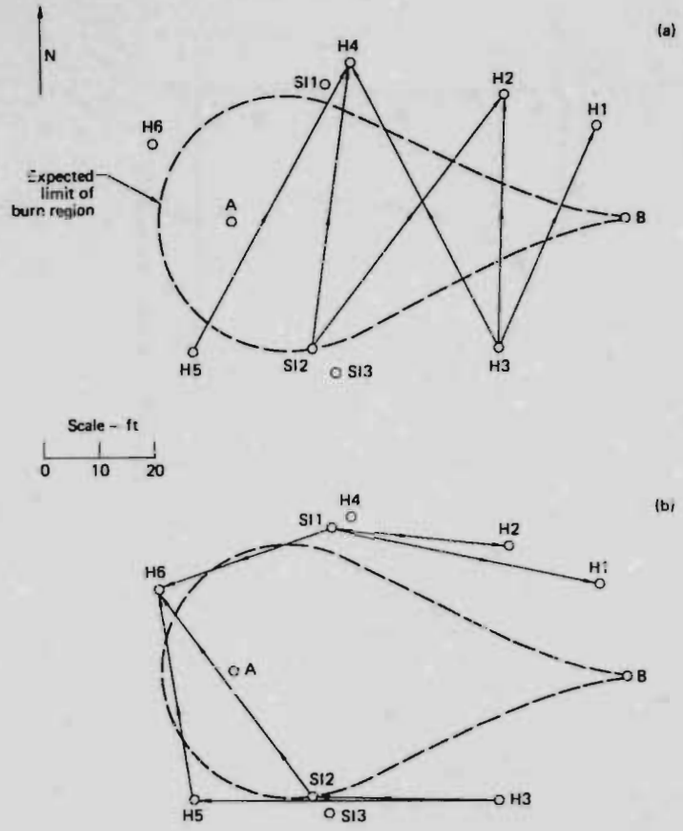

D. T. Davis - Fig. 7

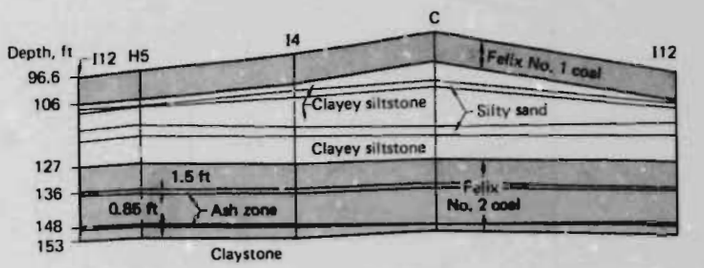

D. T. Davis - Fig. 8

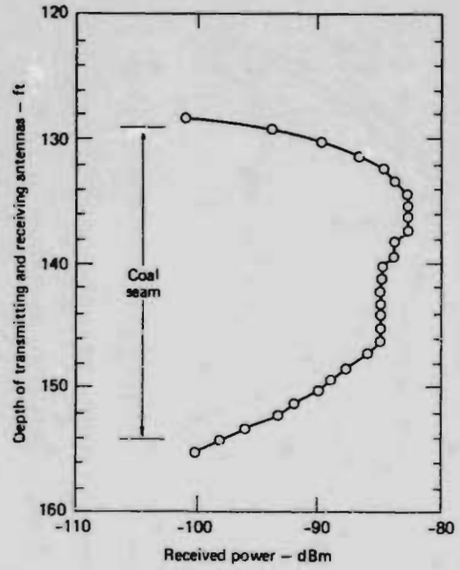

D. T. Davis - Fig. 9

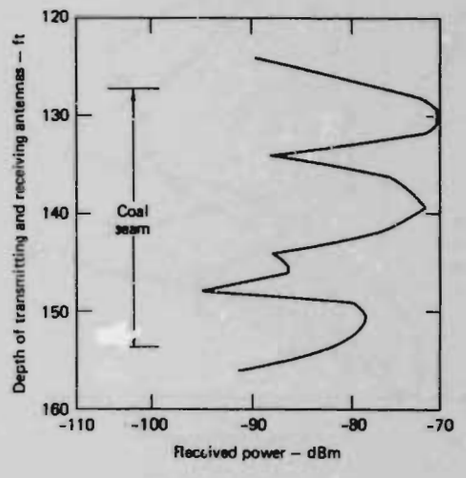

D. T. Davis - Fig. 10

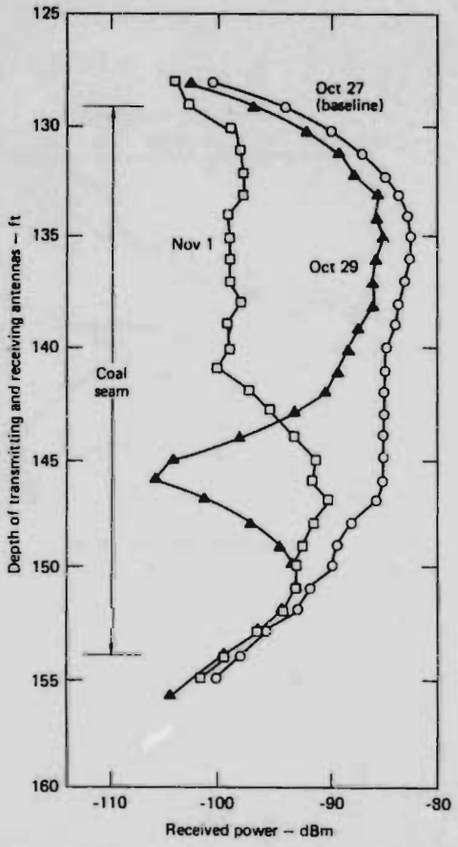

D. T. Davis - Fig. 11

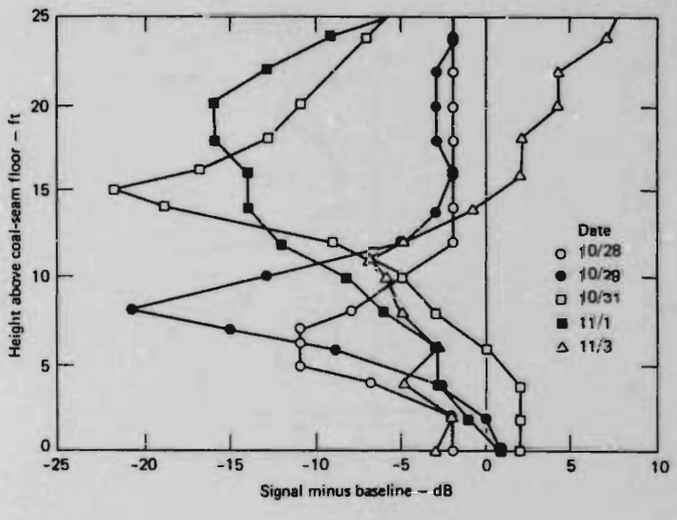

D. T. Davis - Fig. 12

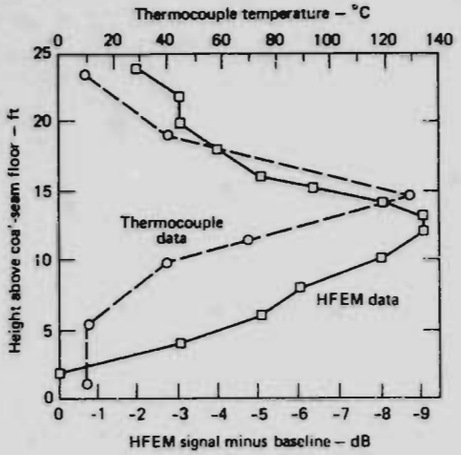

D. T. Davis - Fig. 13

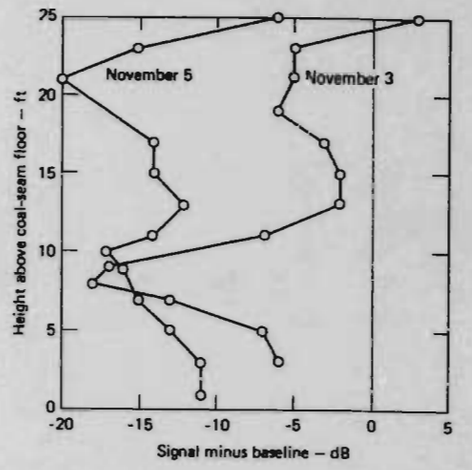

D. T. Davis - Fig. 14

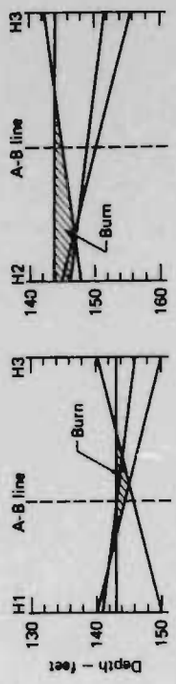

D. T. Davis - Fig. 15

Battelle

UCRL-52461

A SIMPLE MODEL FOR LOCATING THE FRONT OF A REVERSE-COMBUSTION LINK FROM THERMOCOUPLE-RESPONSE DATA

R. W. Lyczkowski
C. B. Thorsness
W. R. Aiman

April 28, 1978

Work performed under the auspices of the U.S. Department of Energy by the UCLLL under contract number W-7405-ENG-48.

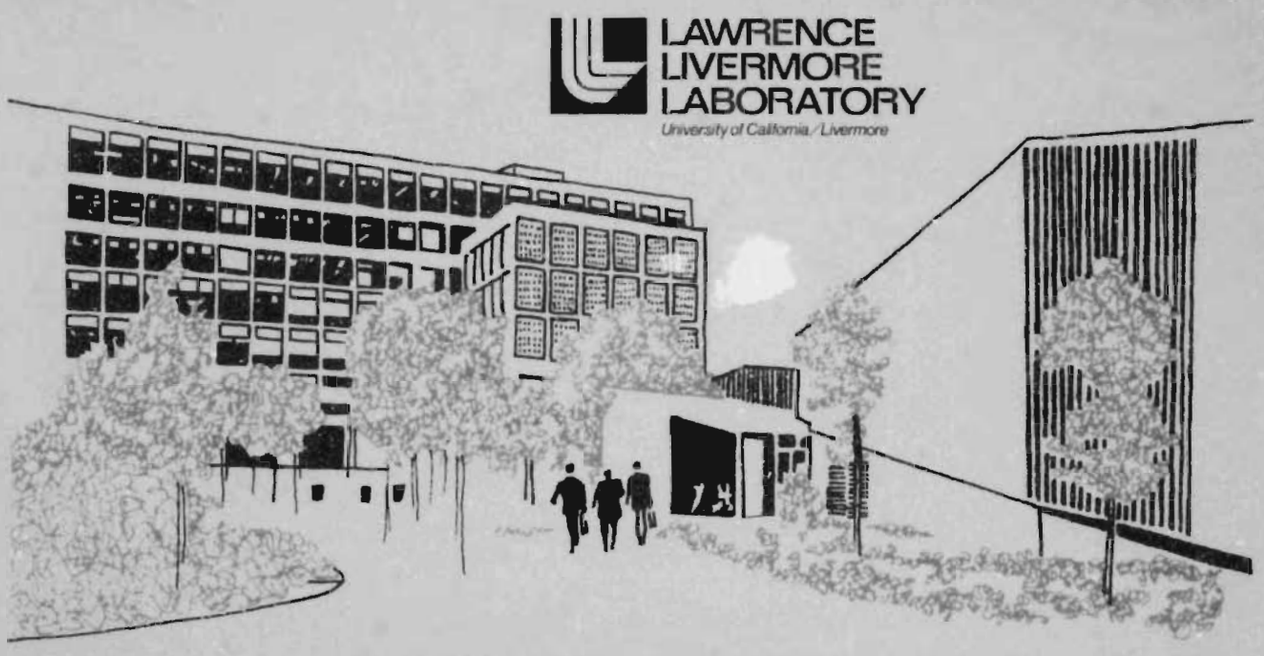

Distribution Category
UC-90c

LAWRENCE LIVERMORE LABORATORY
University of California / Livermore, California / 94550

UCRL-52461

A SIMPLE MODEL FOR LOCATING THE FRONT OF A REVERSE-COMBUSTION LINK FROM THERMOCOUPLE-RESPONSE DATA

R. W. Lyczkowski
C. B. Thorsness
W. R. Aiman

MS. date: April 28, 1978

CONTENTS

A SIMPLE MODEL FOR LOCATING THE FRONT OF A REVERSE-COMBUSTION LINK FROM THERMOCOUPLE-RESPONSE DATA

ABSTRACT

An idealized model for locating the front of a reverse-combustion link has yielded a tool that appears useful in interpreting thermocouple-response data obtained during field operation.

THE MODEL

Consider the front of a reverse-combustion link to be a point source of energy release of strength $\dot{Q}$, moving at a constant velocity of U m/s along the x axis in an infinite medium having constant physical properties. At steady state, the solution to this situation is given in Carslaw and Jaeger, [1] p. 267, as

$$\Delta T = T - T_{amb} = \frac{\dot{Q}}{4\pi k (x^2 + r^2)^{1/2}} \exp\left\{ - U \left[(x^2 + r^2)^{1/2} - x \right] / 2\alpha \right\},$$

where k is the thermal conductivity of the coal (W/°K-m) and α is the thermal diffusivity given by

$$\alpha = k/\rho Cp \ m^2/s.$$

ρ and Cp are the density (kg/m^3) and heat capacity (J/kg-°K), respectively, and ΔT is the temperature rise (°K) above ambient, T_{amb}. The task at hand is to infer the radius, r, from the axis of the point source to the thermocouples embedded in the coal field, as illustrated in Fig. 1.

This model is fundamentally different from that used by Hommert and Beard, [2] who assumed that the reverse-combustion-link formation can be represented by transient-heat conduction. The heat would be conducted into an infinite medium from a circular heat source of constant temperature arriving in the vicinity of the thermocouple at various times. In fact, their solution is an approximate one, good for only small values of the time (Ref. 1, p. 336). Our model has an exact solution. If the assumption of steady-state heat conduction in the soil is not reasonable for a given set of conditions, the analysis may be extended to include transient effects. In this case the solution becomes

$$\Delta T = \left[\frac{\dot{Q}}{2\pi^{3/2} \, k (x^2 + r^2)^{1/2}} \right] \exp(Ux/2\alpha) \int_{\left(\frac{x^2 + r^2}{4\alpha t}\right)^{1/2}}^{\infty} \exp\left\{ -\xi^2 - \left[U^2 (x^2 + r^2) / 16\alpha^2 \xi^2 \right] \right\} d\xi .$$

Data analyzed on the basis of the steady-state model will always yield estimates of r greater than those of the nonsteady-state solution. Hence, we have a conservative estimate.

METHOD OF ANALYSIS

We illustrate a preliminary method of analysis and suggest a more universal method of data reduction.

Our first idea was to infer the position of the point source by using the maximum temperature alone. This would be useful for field work, because it requires only a quick visual scan of temperature traces for peaks.

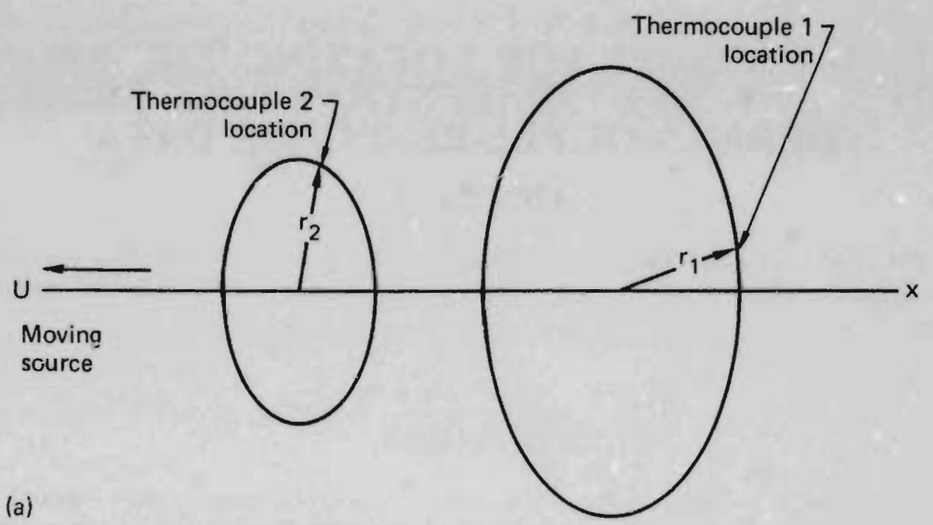

(a)

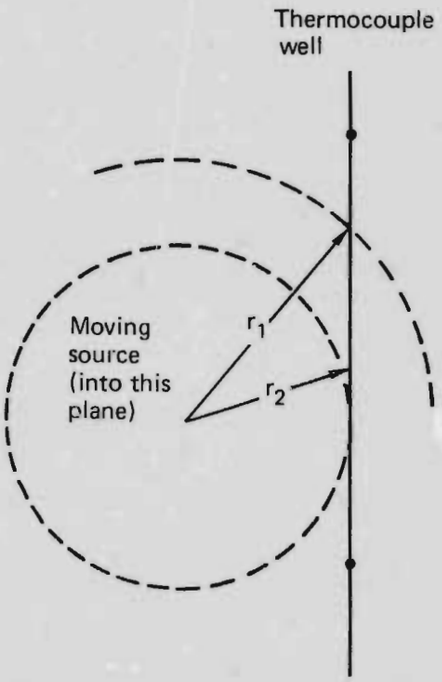

(b)

Fig. 1. Thermocouples and point sources: (a) Isometric-plan view of a point source moving through a field of thermocouples. (b) Vertical-plan view of a thermocouple well near a moving point source.

This is messy analytically, so we used a more straightforward method based on crossplots of the anaiytical solution.

Preliminary information about reverse-combustion links and average physical properties for Hoe Creek II coal are given by

$$U \simeq 1 \text{ m/day} \simeq 1.2 \times 10^{-5} \text{ m/s},^{3}$$

$$\alpha \simeq 10^{-7} \text{ m}^2/\text{s},^{4}$$

$$k \simeq 0.23 \text{ W/(°K - m)}.^{4}$$

We may estimate an upper bound for heat release, assuming complete combustion of carbon with injected oxygen in a single link, by

$$\dot{Q} \simeq (0.21) \times (2 \text{ mole/s air}) \times (10^5 \text{ cal/mole}) \times (4.186 \text{ J/cal})$$

$$\simeq 1.8 \times 10^5 \text{ W}.$$

This heat release is taken to be the strength of the point source.

Figure 2 illustrates the results of computations using the above parameters. The figure plots temperature rise as a function of distance (or, equivalently, days) with r as a parameter. All temperature responses eventually reach a maximum and then decay to zero. The model used in Ref. 2 does not yield this physically correct situation. In fact, it uses a term "to account for cooling."[2] It is quite clear that, because of the very low thermal diffusivity of wet coal, one must be quite close to the point source before an appreciable temperature

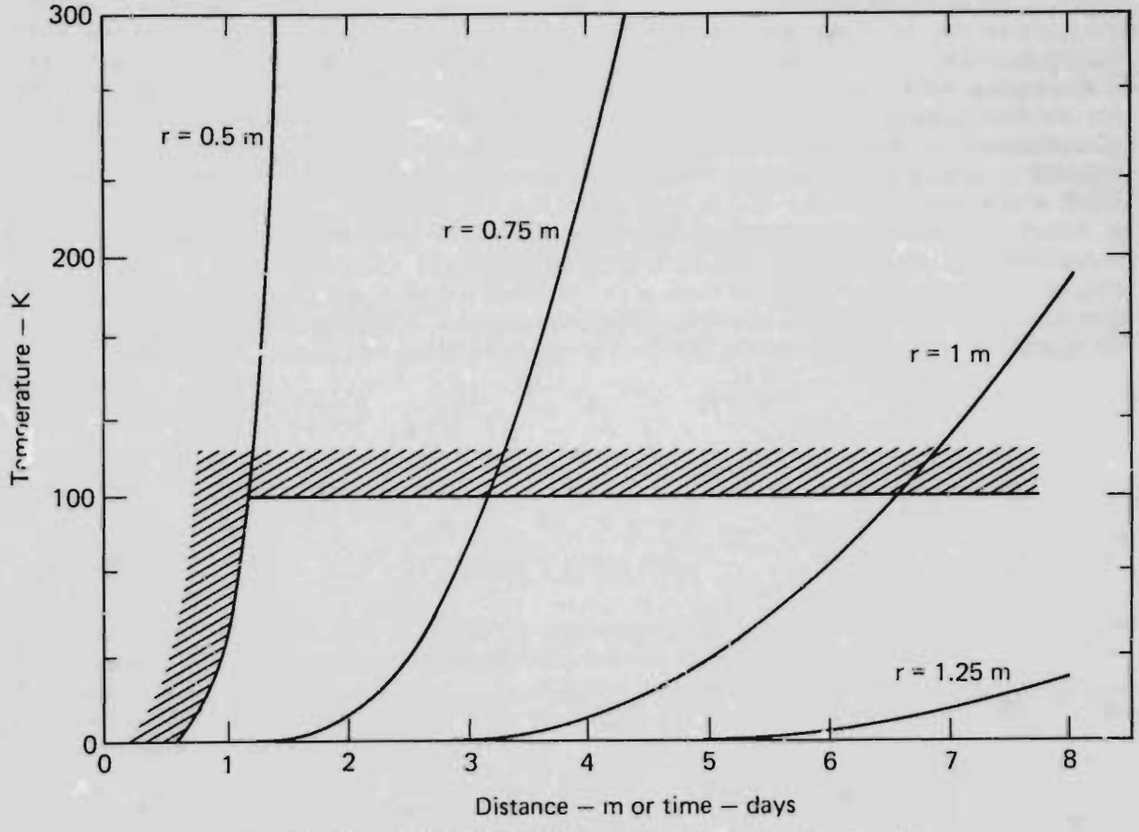

Fig. 2. Temperature rise vs distance (or time) as a function of radius to axis of the point source.

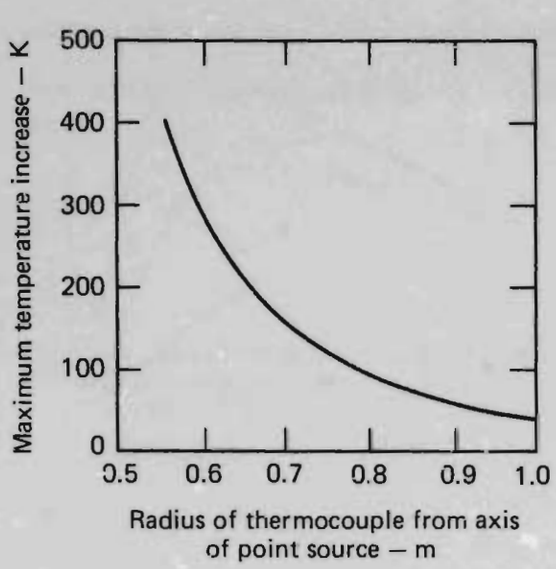

Fig. 3. Maximum temperature rise (ΔT_{max}) as a function of thermocouple radius from the axis of the point source.

response can be perceived in a reasonable amount of time. For radii greater than 1 m, the thermal response within a week is virtually nil. In addition, by the time such distant thermocouples respond, the point souce is many meters along its way, having passed by many days before.

ΔT_{max}, the maximum temperature rise above ambient, is plotted as a function of the radius of the thermocouple from the axis of the point source in Fig. 3. Quite clearly, ΔT_{max} is a very weak function of the radius, r, above about 1 m. The maximum temperature rise is much higher than the data. Significant flow in the coal seam would account for this lowering. The simple model cannot account for this convection. We think that the analysis and the curve generated are valid only for about a 100°K temperature rise, because the coal begins to dry out at this point. We further think that predicted radii much less than about 0.50 m are not admissable, because they lie within the estimated burn path. The excluded area lies outside the indicated hatched boundary in Fig. 2.

Equation (1) can be made dimensionless by introducing the following definitions for dimensionless temperature, distance, and radius:

$$T^+ = \frac{T}{\left(\frac{\dot{Q}U}{k\alpha}\right)},$$

$$X^+ = \frac{x}{\left(\frac{\alpha}{U}\right)},$$

$$r^+ = \frac{r}{\left(\frac{\alpha}{U}\right)}.$$

Here the superscript (+) denotes dimensionless quantities. Equation (2) then becomes

$$T^+ = \left[\frac{1}{4\pi(x^{+2} + r^{+2})^{1/2}}\right] \exp\left\{-\frac{1}{2}\left[(x^{+2} + r^{+2})^{1/2} - x^+\right]\right\}.$$

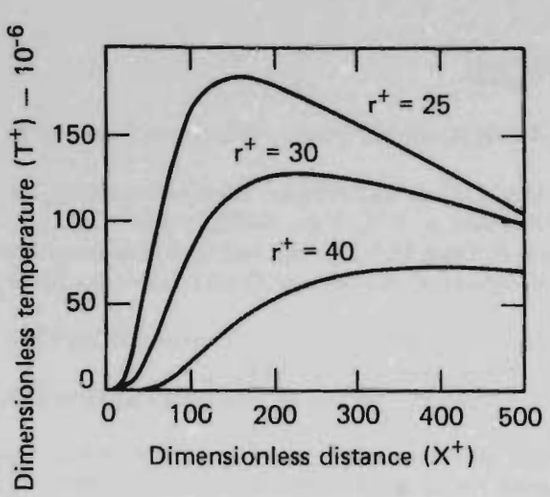

Fig. 4. Universal plot of temperature rise.

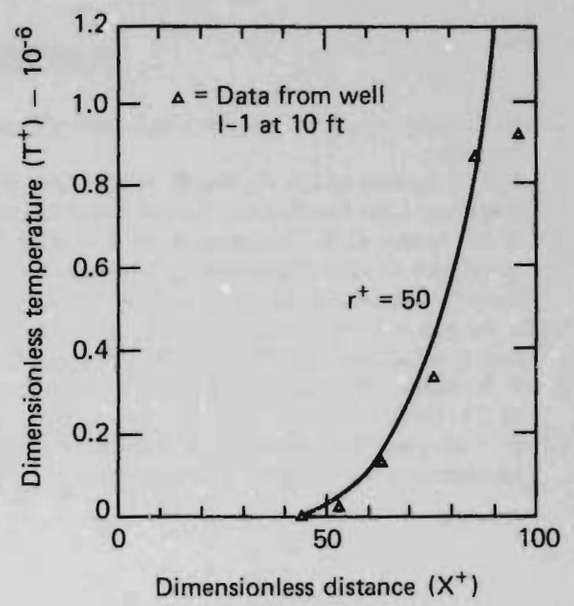

Fig. 5. Comparison of preliminary Hoe Creek II thermocouple data with model. The comparison was done in well I-1 at 10 feet.

In this dimensionless form the solution is no longer a function of system parameters. Thus, a universal family of plots, shown in Fig. 4, can be generated for use in data interpretation. The family of curves has as a parameter r^+, which is the dimensionless radius corresponding to the previously defined radius, r.

Data are interpreted by putting the temperature response in dimensionless form on the universal family of r^+ plots. The value of r is then found by determining the r^+ curve most closely corresponding to the shape of the data curve. An example of such a fit is shown in Fig. 5 for data taken from a thermocouple in the I-1 well (of the Hoe Creek II field test) [3] at 10 feet (3 m) above the bottom of the coal. The value of $r^+ = 50$ corresponds to an r value of 0.4 meters. The maximum temperature rise is much higher, quite possibly because of the convection in the coal seam, as already mentioned, or multiple link paths. Another parameter implicit in the model is the zero-time position of the point source. This parameter arises because of the quasi-steady nature of the analysis. This extra parameter allows the entire family of curves to be shifted according to the formula

$$X^+ = (t - t_0)U^2/\alpha \ .$$

CONCLUSIONS

A simple model has yielded some insight into the interpretation of thermocouple-response data taken during reverse-combustion linking. More complete models that include phenomena such as flow in the coal seam, evaporization of wet coal, and pyrolysis should exhibit the same basic trends as the simple model, which will serve as a check case for limiting conditions. Extending the model to forward combustion is possible by using moving-line or cylindrical heat sources. [5,6]

REFERENCES

1. H. S. Carslaw and J. C. Jaeger, *Conduction of Heat in Solids*, (Oxford University Press, New York, 1959), 2nd ed.
2. P. J. Hommert and S. G. Beard, *Descriptions of Reverse Linkage and Forward Gasification during Underground Coal Gasification*, Sandia Laboratories, Albuquerque, NM, Rept. SAND76-9317 (1977).
3. W. R. Aiman, C. B. Thorsness, R. W. Hill, R. B. Rozsa, R. Cena, D. W. Gregg, and D. R. Stephens, *The Hoe Creek II Field Experiment on Underground Coal Gasification, Preliminary Results*, Lawrence Livermore Laboratory, Rept. UCRL-80592 (1978).
4. S. Badzioch, D. R. Gregory, and M. A. Field, "Investigation of the Temperature Variation of the Thermal Conductivity and Thermal Diffusivity of Coal," **Fuel 43** (4), 267-280 (1964).
5. P. E. Baker, "Temperature Profiles in Underground Combustion," *Society of Petroleum Engineers* **219**, 21-27 (1962).
6. H. J. Ramey, "Transient Heat Conduction during Radial Movement of a Cylindrical Heat Source — Applications to the Thermal Recovery Process," *Petroleum Transactions, AIME* **216**, 115-122 (1959).

RW

UCRL-52456

A MECHANISTIC THEORY FOR DRYING OF POROUS MEDIA

Robert W. Lyczkowski

April 30, 1978

Work performed under the auspices of the U.S. Department of Energy by the UCLLL under contract number W-7405-ENG-48.

Distribution Category
UC-90C

LAWRENCE LIVERMORE LABORATORY
University of California / Livermore, California / 94550

UCRL-52456

A MECHANISTIC THEORY FOR DRYING OF POROUS MEDIA

Robert W. Lyczkowski

MS. date: April 30, 1978

CONTENTS

A MECHANISTIC THEORY FOR DRYING OF POROUS MEDIA

ABSTRACT

The basis of a rational phenomenological theory for drying of porous media is derived for a single equivalent drying pore by applying two-fluid, two-phase flow theory. Simplifications are made to compare with other theories and models proposed or assumed in the literature to assess their correctness. The derivation illustrates the rational way bulk motion is introduced within the porous matrix. Explicit expressions are also obtained for the evaporation rate and phase permeabilities. The extension to a global drying model is made. We outline a solution procedure for a simplified version of the model and provide an estimate of the coal semi-coking zone by solving an analytical solution for another simplified model.

SECTION 1
INTRODUCTION

Experience with Hoe Creek Experiment 2 [1] has indicated that water is important in the dynamics of underground coal gasification (UCG). Although there are plausible mechanisms to explain this, [2-4] to our knowledge, there are no mechanistic mathematical models of the process. A simple model analyzing the two-dimensional pyrolysis data [5] for wet Roland-Smith coal blocks was once begun at the Lawrence Livermore Laboratory (LLL), but is yet uncompleted. [6] Water influx and control have been cited among the major technical challenges in understanding UCG. [7]

In this paper, we develop the basis of a simple mechanistic theory that models the simultaneous drying and pyrolysis of coal. In this new theory, we use concepts from two-fluid, two-phase flow theory [8-10] and extend them to describe two-phase flow and phase change within porous media.

Two-fluid, two-phase flow theory has not been previously applied to describe coal drying. Although the model is not complete, it nevertheless embodies sufficient structure to yield much insight. The model rationally extends classical drying theory to handle rapid drying of moist solids where bulk motion of steam and water occurs within the matrix.

SECTION 2
MOTIVATION OF THE MODEL

Figure 2-1 illustrates several of the chemical processes thought to be involved in UCG. Although the processes of drying, pyrolysis, reduction, and oxidation of the coal steam are represented as primarily sequential along a single open link path, they probably occur throughout the coal seam because of the cracks, fissures, cavity formation, subsidence, and ground water movement.

The processes shown in Fig. 2-1 are idealized in Fig. 2-2. Air is injected into a (nearly) open cavity. Circulation patterns are set up possibly by jetting action, subsided coal and the link channel. An expanded portion of the wall of the burning cavity is also shown in Fig. 2-2. There, the wet virgin coal is shown to be heated

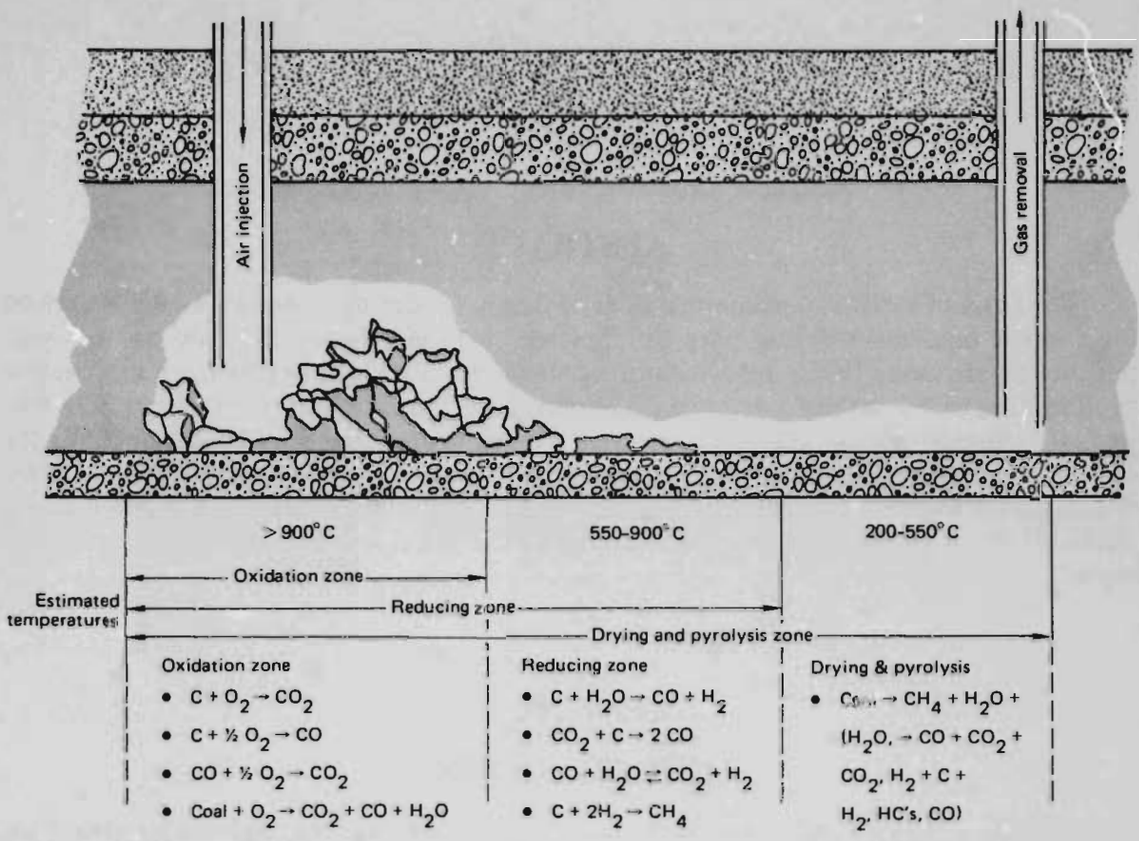

Fig. 2-1. Hypothesized processes involved in underground coal gasification.

from an ambient temperature T_o to the boiling point of water T_w. The liquid water evaporates producing steam H_2O_v, which then flows against a temperature gradient toward the hotter char. At some point, the steam begins to react with the char by the typical reactions:

$$C + H_2O \rightarrow CO + H_2 \tag{1}$$

and

$$CO + H_2O \rightarrow CO_2 + H_2. \tag{2}$$

The overall reaction with the solid in the presence of excess steam can be considered to be

$$C + 2H_2O \rightarrow CO_2 + 2H_2, \tag{3}$$

because, according to Taylor and Bowen who studied these reactions,[11] very little CO is formed: the predominant products are H_2 and CO_2. Above 805°C, the reaction is extremely rapid. In the gas phase, H_2 and O_2 react rapidly at temperature T_G providing the necessary driving force for the above reactions in the form of radiant heating of the coal face to temperature T_s. The coal face moves at velocity U_c in a direction opposite to the steam flow while it is consumed by the steam.

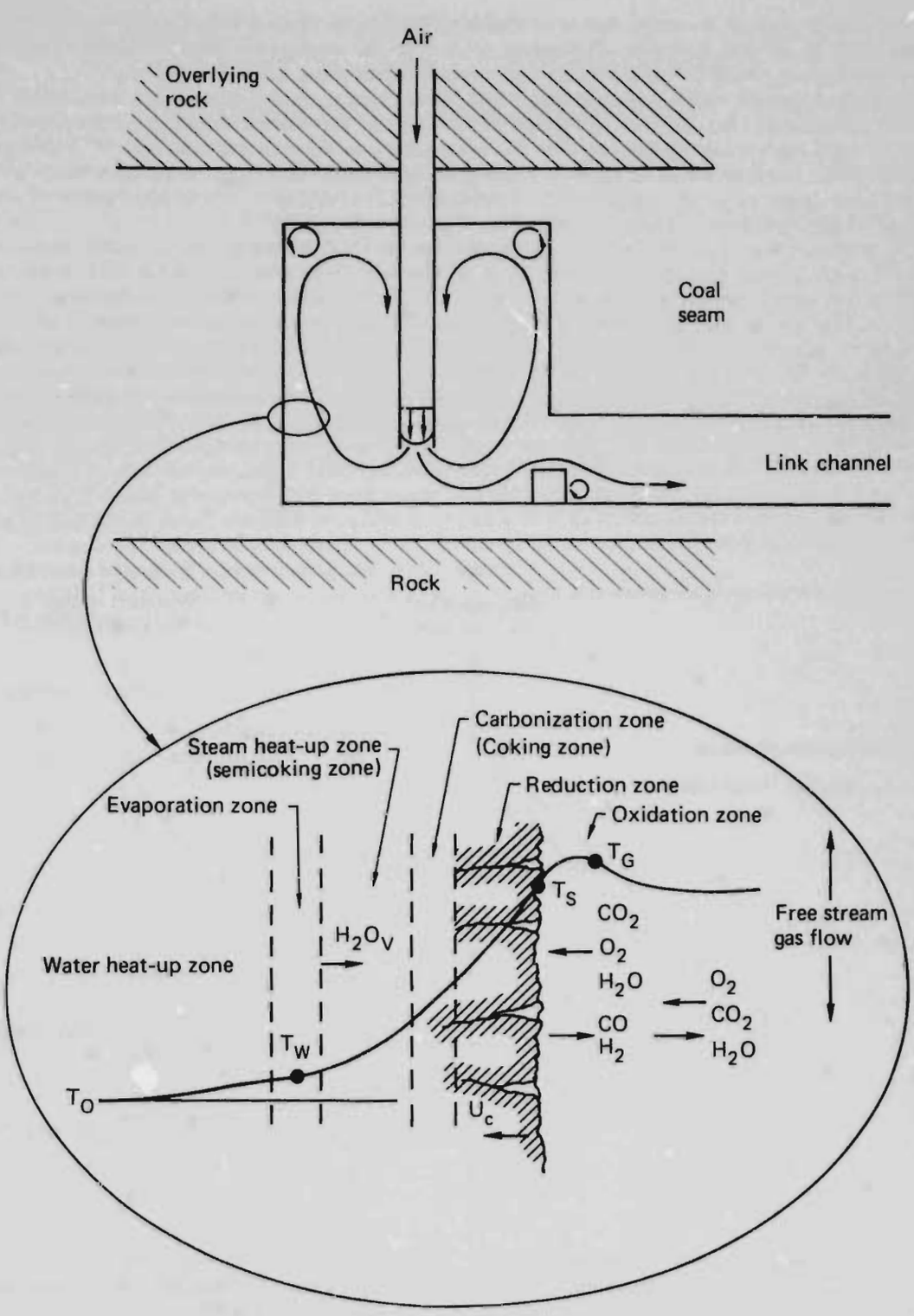

Fig. 2-2. Idealization of geometry involved in underground coal gasification and detail of a gasifying coal face.

The overall effect of the steam flow is to thermally insulate the channel walls through a transpiration cooling effect in addition to sealing off escaping gases. [12] In this respect, the physical situation resembles reverse combustion where a burn front moves opposite to the air flow.

Figure 2-3, part (a), which is adapted from Skafa [3] shows typical gas and solid surface temperatures in a direction along the coal face. Solid surface temperatures exhibiting maxima similar to Fig. 2-3 have been predicted for rapid surface-catalyzed combustion and subsequently measured experimentally. [13,14] Rapid non-catalytic surface reactions would be expected to produce similar maxima. Figure 2-3 part (b), which is also adapted from Skafa, shows the typical depth of penetration of the drying, pyrolysis, and reaction zones in response to the solid-surface temperature distribution shown in (a) of Fig. 2-3.

These processes are probably not the only ones that exist in UCG. However, we believe that these events probably occur at some point during the forward burn. The interaction of the free stream fluid mechanics is yet unknown, so the surface temperature T_s will be used in the model. Although the free stream fluid mechanics may not be entirely governed by porous media flow, [15] the drying process appears to be more amenable to such a treatment. For the reaction given by Eq. (3) to occur, much more than the initial approximately 30 wt% water is required. This water could easily be supplied by hydrostatic forces from surrounding aquifers. The delicate balance between surface temperature distribution and available water will determine the growth patterns of the walls of the combustion chamber.

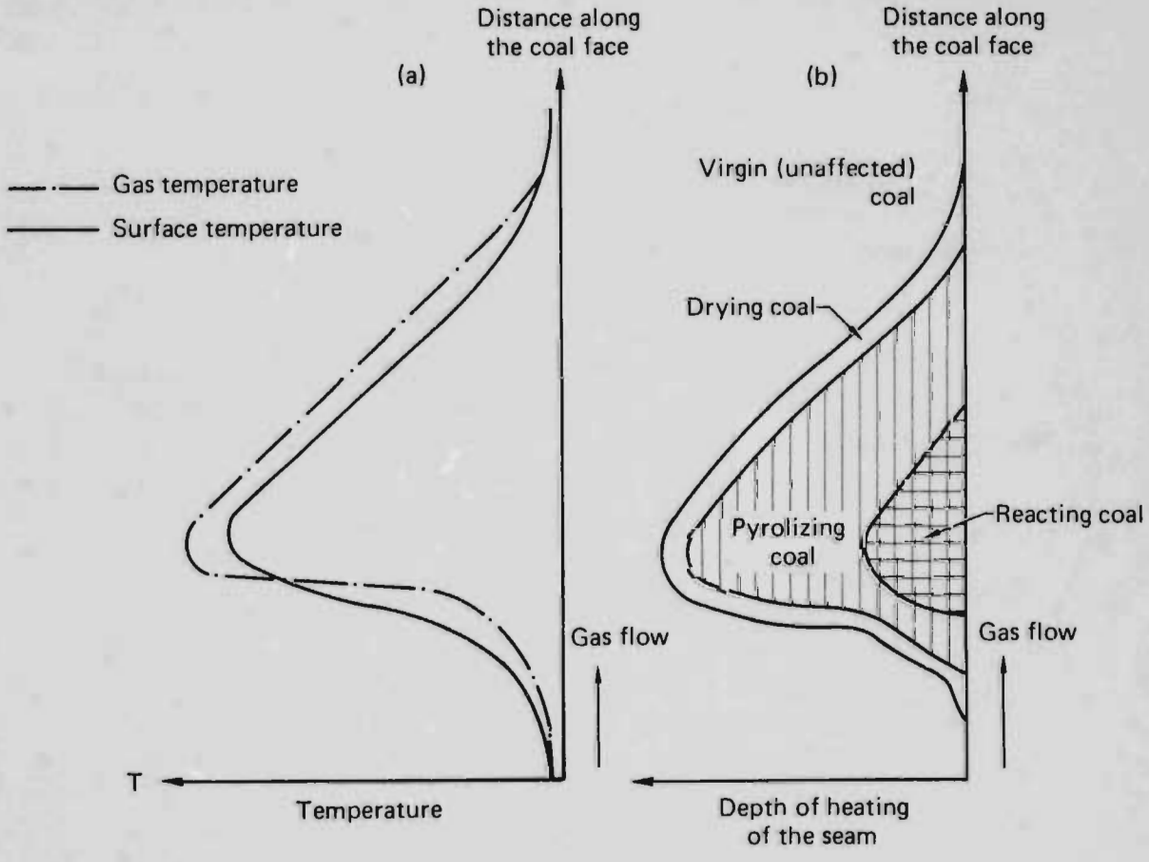

Fig. 2-3. Schematic of zonality of gasification adapted from Skafa.[3]

SECTION 3
A GENERAL THEORY OF DRYING WITHIN A SINGLE EQUIVALENT PORE

The one-dimensional area averaged equations describing a flowing nonreacting two-phase single component mixture in a single equivalent pore are developed in this section.

Figure 3–1 illustrates the drying process considered to occur. All the liquid and vaporous water are assumed to exist only within the micro and macro pores that are distributed throughout the coal. Thus, no liquid or vapor exists within the ultimate solid portions of the coal itself. This is the same approach taken by Whittaker. [16] Bound water or water of hydration is therefore not taken into account in this model. Experimental evidence indicates there is very little of this type of water in Western Coals. [17] The situation depicted in Fig. 3–1 is idealized in Fig. 3–2 where drying is considered to occur within a single equivalent pore. This single equivalent pore model naturally develops into a more general global model and serves as a useful guide in developing insight into the mechanisms involved. The model also serves as a useful heuristic base from which to construct a more general global porous media model, which includes both drying and chemical reaction.

This approach rationally and mechanistically introduces the treatment of the steam and water motion within the drying coal. In some respects the model extends a drying model developed by Whittaker. [16] Whittaker uses local volume averaging to obtain his model. The present analysis represents a straight forward but unique application of recent two-fluid two-phase flow theory [18–20] to drying. Rather than starting with the point conservation equations and averaging, we take advantage of the work already done by others using the complementary process of area averaging and shell balances.

A simplified set of one-dimensional two-fluid single component area averaged conservation equations for flow in a channel are given by [21]:

continuity equations

$$\frac{\partial}{\partial t}\left(A\alpha_g\rho_g\right) + \frac{\partial}{\partial x}\left(A\alpha_g\rho_g v^g\right) = A\dot{m} \tag{4}$$

and

$$\frac{\partial}{\partial t}\left(A\alpha_\ell\rho_\ell\right) + \frac{\partial}{\partial x}\left(A\alpha_\ell\rho_\ell v^\ell\right) = -A\dot{m} \ , \tag{5}$$

momentum equations

$$\frac{\partial}{\partial t}\left(A\alpha_g\rho_g v^g\right) + \frac{\partial}{\partial x}\left(A\alpha_g\rho_g v^g v^g\right) = -A\alpha_g\frac{\partial P}{\partial x} + A\dot{m}\,\hat{v} - A\bar{A}_{g\ell}B_{g\ell}\,(v^g - v^\ell) - A\bar{A}_{wg}B_{wg}v^g + A\alpha_g\rho_g g_x \tag{6}$$

and

$$\frac{\partial}{\partial t}\left(A\alpha_\ell\rho_\ell v^\ell\right) + \frac{\partial}{\partial x}\left(A\alpha_\ell\rho_\ell v^\ell v^\ell\right) = -A\alpha_\ell\frac{\partial P}{\partial x} - A\dot{m}\,\hat{v} - A\bar{A}_{g\ell}B_{g\ell}\,(v^\ell - v^g) - A\bar{A}_{w\ell}B_{w\ell}v^\ell + A\alpha_\ell\rho_\ell g_x \ . \tag{7}$$

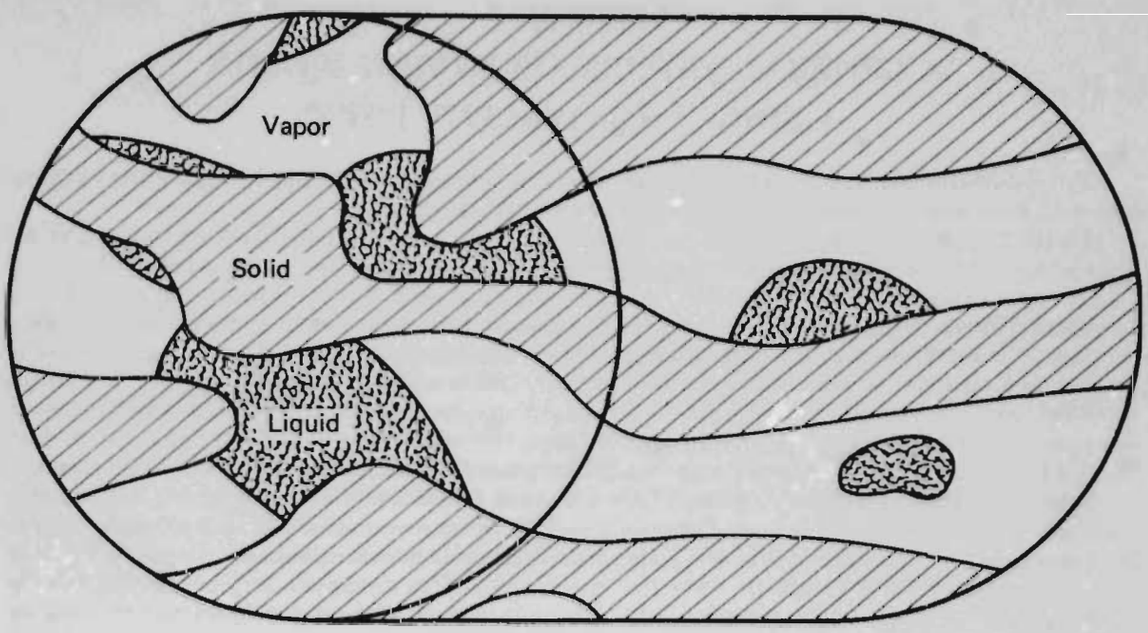

Fig. 3-1. Drying process in a porous medium.

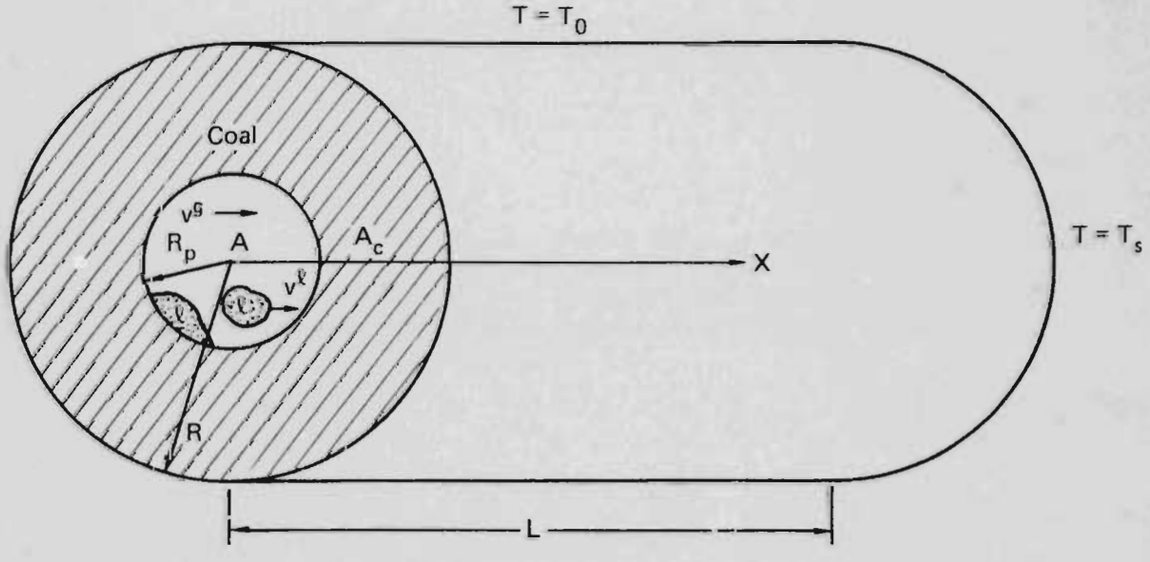

Fig. 3-2. Two-phase flow in a single equivalent drying pore.

and by energy equations

$$\frac{\partial}{\partial t}\left(A\alpha_g\rho_g h_g\right) + \frac{\partial}{\partial x}\left(A\alpha_g\rho_g v^g h_g\right) - A\alpha_g\left(\frac{\partial P}{\partial t} + v^g\frac{\partial P}{\partial x}\right) = \dot{m}h_{gs} + Aq^g \tag{8}$$

and

$$\frac{\partial}{\partial t}\left(A\alpha_\ell\rho_\ell h_\ell\right) + \frac{\partial}{\partial x}\left(A\alpha_\ell\rho_\ell v^\ell h_\ell\right) - A\alpha_\ell\left(\frac{\partial P}{\partial t} + v^\ell\frac{\partial P}{\partial t}\right) = -\dot{m}h_{\ell s} + Aq^\ell \quad . \tag{9}$$

The field equations are coupled by the interaction terms, which include the interphase friction force $\bar{A}_{ab}B_{ab}(v^a - v^b)$, the mass transfer rate $\dot{m}$, and the interphase heat transfer portions of the phase heat transfer rates q^a. The term $\dot{m}\hat{v}$ is an interphase momentum transfer term associated with phase change. Terms ρ_g and ρ_ℓ are the thermodynamic densities, A is the total pore flow area, v^g and v^ℓ are the phase velocities, P is the pressure, and h_g and h_ℓ are the specific phase enthalpies. When $\dot{m}$ is positive, evaporation occurs. Because the phase pressures have been assumed to be equal, capillary pressure forces are not present. This assumption is easily lifted as shown in the Appendix to include surface tension effects. One-dimensionality is assumed because the coal face is very thick and because a local model is desired. This local model can be used as a boundary condition coupling the open cavity space and the coal seam, as indicated in Fig. 2-2.

The enthalpy form of the energy equations was obtained from the mixed internal energy, enthalpy form derived in Ref. 21. Axial conduction, diffusion, and the stress tensor will not be considered within the individual phases because, even though the flow is slow, flow terms dominate. Equations (8) and (9) were chosen as the starting point for the analysis because much work has been put into their development and they seem to be reasonable.

Additional coupling enters through the constraint so that the volume fractions add as

$$\alpha_g + \alpha_\ell = 1 \quad , \tag{10}$$

which means that the volume of vapor and liquid add up to the total pore volume. The heat transferred to each phase is broken into three portions as [20]

$$q^g = q^g_{ext} + q^{gT}_{int} + q^{g\Delta P}_{int} \tag{11}$$

and

$$q^\ell = q^\ell_{ext} + q^{\ell T}_{int} + q^{\ell\Delta P}_{int} \quad . \tag{12}$$

The three terms on the right-hand sides in Eqs. (11) and (12) represent the external and interphase heat transfer resulting from temperature-driving forces and an interphase heat transfer resulting from pressure change.

The mass transfer rate is divided in a similar manner:

$$\dot{m}h_{gs} = \left(\dot{m}^T_{ext} + \dot{m}^T_{int} + \dot{m}^{\Delta P}_{int}\right)h_{gs} \tag{13}$$

and

$$-\dot{m}h_{\ell s} = -\left(\dot{m}^T_{ext} + \dot{m}^T_{int} + \dot{m}^{\Delta P}_{int}\right)h_{\ell s} \quad . \tag{14}$$

At this point, the phases will be assumed to be at the same temperature so that in Eqs. (11) through (14),

$$q_{int}^{gT} = q_{int}^{\ell T} = \dot{m}_{int}^{T} = 0 \quad . \tag{15}$$

It is often convenient to work with the mixture energy equation. This equation will now be obtained from Eqs. (8), (9), and (11) through (15).

The first two terms in Eq. (8) are expanded as

$$\frac{\partial}{\partial t}\left(A\alpha_g\rho_g h_g\right) + \frac{\partial}{\partial x}\left(A\alpha_g\rho_g v^g h_g\right) = A\alpha_g\rho_g\left(\frac{\partial h_g}{\partial t} + v^g \frac{\partial h_g}{\partial x}\right)$$

$$+ h_g\left[\frac{\partial}{\partial t}\left(A\alpha_g\rho_g\right) + \frac{\partial}{\partial x}\left(A\alpha_g\rho_g v^g\right)\right] \quad . \tag{16}$$

The second term on the right side of Eq. (16) is the vapor-phase continuity equation, Eq. (4). Combining Eqs. (4), (8), (11), (15) and (16) results in

$$A\alpha_g\rho_g\left(\frac{\partial h_g}{\partial t} + v^g \frac{\partial h_g}{\partial x}\right) = -A\alpha_g\left(\frac{\partial P}{\partial t} + v^g \frac{\partial P}{\partial x}\right) + A\left(q_{ext}^{gT} + q_{int}^{g\Delta P}\right) \tag{17}$$

The equivalent of Eq. (17) for the liquid energy equation is obtained similarly. The resulting expression is given by

$$A\alpha_\ell\rho_\ell\left(\frac{\partial h_\ell}{\partial t} + v^\ell \frac{\partial h_\ell}{\partial x}\right) = -A\alpha_\ell\left(\frac{\partial P}{\partial t} + v^\ell \frac{\partial P}{\partial x}\right) + A\left(q_{ext}^{\ell T} + q_{int}^{g\Delta P}\right) \quad . \tag{18}$$

In the forms given by Eqs. (17) and (18), the pore area term A cancels out.

The temperature forms of the energy equations are obtained next by the equations of state (eos):

$$h_\ell = h_{\ell eos}(P) \text{ and } h_g = h_{geos}(P), \tag{19}$$

which state that the enthalpies are functions of pressure only since the phase temperatures are equal. Derivatives of the enthalpies appearing in Eqs. (17) and (18) are replaced by temperature derivatives through

$$\partial h_{\ell_{eos}} = \frac{dh_{\ell_{eos}}}{dT}\,\partial T \tag{20}$$

and

$$\partial h_{g_{eos}} = \frac{dh_{g_{eos}}}{dT}\,\partial T \quad . \tag{21}$$

The derivatives of phase enthalpies should strictly be evaluated along the saturation line. They are usually replaced by

$$\frac{dh_{a_{eos}}}{dT} = \lim_{\substack{\alpha_g\to 0 \\ \text{or} \\ \alpha_\ell\to 0}}\left(\frac{\partial ha}{\partial T}\right)_P = C_{pa} \quad . \tag{22}$$

where C_{pa} is the phase heat capacity at constant pressure extrapolated from the single-phase region. By summing Eqs. (17) and (18) and using Eqs. (20), (21), and (22), we obtain

$$(\alpha_g\rho_g C_{pg} + \alpha_\ell\rho_\ell C_{p\ell})\frac{\partial T}{\partial t} + \left(\alpha_g\rho_g C_{pg}v^g + \alpha_\ell\rho_\ell C_{p\ell}v^\ell\right)\frac{\partial T}{\partial x}$$

$$= -\left[\frac{\partial P}{\partial t} + \left(\alpha_g v^g + \alpha_\ell v^\ell\right)\frac{\partial P}{\partial x}\right]$$

$$+ \left(q^g_{ext} + q^\ell_{ext}\right) + \left(q^{g\Delta P}_{int} + q^{\ell\Delta P}_{int}\right) . \tag{23}$$

The sum of the heat transfer rates from internal phase change is related to mass transfer rate by [20]

$$q^{g\Delta P}_{int} + q^{\ell\Delta P}_{int} + (h_{gs} - h_{\ell s})\,\dot{m}^{\Delta P}_{int} = 0 \quad . \tag{24}$$

Because the phases are at saturation, the external heat added can only cause phase change and so the amount of vapor produced by external heat transfer can be computed from [10]

$$q^g_{ext} + q^\ell_{ext} = q_{wg} + q_{w\ell} = \dot{m}^T_{ext}(h_{gs} - h_{\ell s}) \ , \tag{25}$$

where the only external heat sources are through the pore walls. This heat transfer is set up by the solids heat-conduction equation developed in the next section. The functional form of the wall-heat transfer rates is given by [20]

$$q_{wa} = A_{wa}\,h_{wa}(T_w - T) , \tag{26}$$

where h_{wa} is the heat transfer coefficient, $\bar{A}_{wa}$ is the area available for heat transfer to each phase per pore cross sectional control volume, and T_w is the average pore wall temperature. Combination of Eqs. (23) through (26) produces

$$(\alpha_g\rho_g C_{pg} + \alpha_\ell\rho_\ell C_{p\ell})\frac{\partial T}{\partial t} + \left(\alpha_g\rho_g C_{pg}v^g + \alpha_\ell\rho_\ell C_{p\ell}v^\ell\right)\frac{\partial T}{\partial x}$$

$$= -\left[\frac{\partial P}{\partial t} + \left(\alpha_g v^g + \alpha_\ell v^\ell\right)\frac{\partial P}{\partial x}\right]$$

$$- \dot{m}^{\Delta P}_{int}(h_{gs} - h_{\ell s}) + (\bar{T}_w - T)(\bar{A}_{w\ell}h_{w\ell} + \bar{A}_{wg}h_{wg}) \quad . \tag{27}$$

SECTION 4
ENERGY EQUATION FOR THE PORE WALL

The mixture-energy field is coupled to the channel-energy field through the wall-heat transfer that appears on the right hand side of Eq. (27). Because the channel walls are not considered to be imbedded within the two-phase mixture inside the idealized pore, the heat-conduction equation may be averaged independently to obtain a field equation for the average wall temperature $\bar{T}_w$.

The wall-heat conduction equation is written in cylindrical coordinates assuming azimuthal symmetry:

$$\rho_w C_w \frac{\partial T_w}{\partial t} = k_w \left[\frac{1}{r} \frac{\partial}{\partial r} \left(r \frac{\partial T}{\partial r} \right) + \frac{\partial^2 T}{\partial x^2} \right] . \tag{28}$$

Typical spatial boundary conditions are given by

$$k_w \left. \frac{\partial T}{\partial r} \right|_{R_p} \cdot 2\pi R_p L = (h_{wg} A_{wg} + h_{w\ell} A_{w\ell})(T_w - T) \tag{28a}$$

and

$$k_w \left. \frac{\partial T_w}{\partial r} \right|_{R} \cdot 2\pi R L = h_o \, 2\pi R \, L (T_w - T_o) \tag{28b}$$

$$T_w = T_s (x = 0, R_p \leq r \leq R) \tag{28c}$$

$$\frac{\partial T_w}{\partial x} = 0 \; (x = L, \; R_p \leq r \leq R) \; . \tag{28d}$$

Equation (28d) relates the wall heat flux to the fluid through the phase-wall-heat transfer coefficients. Equation (28b) states that there is a heat transfer resistance at the outside wall of the channel.

Equation (28) is integrated over the solid cross-sectional area according to:

$$\int_0^{2\pi} \int_{R_p}^{R} \rho_w \, C_w \frac{\partial T_w}{\partial t} \, r dr d\theta = \int_0^{2\pi} \int_{R_p}^{R} \frac{k_w}{r} \frac{\partial}{\partial r} \left(r \frac{\partial T_w}{\partial r} \right) r dr d\theta + \int_0^{2\pi} \int_{R_p}^{R} \frac{k_w}{r} \frac{\partial^2 T_w}{\partial x^2} \, r dr d\theta \; . \tag{29}$$

Assuming constant physical properties, exchange of integration and differentiation, and defining an average wall temperature by

$$\overline{T}_w = \frac{\int_0^{2\pi} \int_{R_p}^{R} T_w r dr d\theta}{\int_0^{2\pi} \int_{R_p}^{R} r dr d\theta} = \frac{\int_0^{2\pi} \int_{R_p}^{R} T_w r dr d\theta}{\pi \left(R^2 - R_p^2 \right)} \; . \tag{30}$$

results in

$$\rho_w C_w \pi \left(R^2 - R_p^2\right) \frac{\partial \overline{T}_w}{\partial t} = k_w \left(R \left. \frac{\partial T_w}{\partial r} \right|_R - R_p \left. \frac{\partial T_w}{\partial r} \right|_{R_p} \right) \cdot 2\pi$$

$$+ k_w \, 2\pi \left(R^2 - R_p^2\right) \frac{\partial^2 \overline{T}_w}{\partial x^2} \quad . \tag{31}$$

Boundary conditions [Eqs. (28a) and (28b)] allow Eq (31) to be written as

$$\pi \left(R^2 - R_p^2\right) \rho_w C_w \frac{\partial \overline{T}_w}{\partial t} = \pi \left(R^2 - R_p^2\right) k_w \frac{\partial^2 \overline{T}_w}{\partial x^2}$$

$$- \left(h_{wg} A_{wg} + h_{w\ell} A_{w\ell}\right)\left(\overline{T}_w - T\right)$$

$$- 2\pi R \, h_o \left(\overline{T}_w - T\right) \quad . \tag{32}$$

Division of Eq. (32) by πR^2 and use of the definitions of the phase wall areas per unit of pore flow area results in

$$\epsilon_w \rho_w C_w \frac{\partial \overline{T}_w}{\partial t} = \epsilon_w k_w \frac{\partial^2 \overline{T}_w}{\partial x^2} - \left(1 - \epsilon_w\right)\left(h_{wg} \overline{A}_{wg} + h_{w\ell} \overline{A}_{w\ell}\right)\left(\overline{T}_w - T\right)$$

$$- h_o \, \overline{A}_{wo} \left(\overline{T}_w - T_o\right) \quad . \tag{33}$$

where ϵ_w is the volume fraction of the wall given by

$$\epsilon_w = \frac{\pi \left(R^2 - R_p^2\right) L}{\pi R^2 L} \quad . \tag{34}$$

and $(1 - \epsilon_w)$ is the pore volume fraction given by

$$1 - \epsilon_w = \frac{\pi R_p^2 L}{\pi R^2 L} \quad . \tag{34a}$$

The term $\overline{A}_{wo}$ at the end of Eq. (33) is the external wall heat transfer area divided by the entire volume of the pore and wall, $2/R$. At steady state and in the absence of heat conduction, Eq. (33) simply states that all external heat transfer goes into cooling (or heating) the two phase mixture according to:

$$- 2\pi R h_o \left(\overline{T}_w - T_o\right) = \left(h_{wg} A_{wg} + h_{w\ell} A_{w\ell}\right)\left(\overline{T}_w - T\right) = \dot{m}^T_{ext} \left(h_{gs} - h_{\ell s}\right) \quad , \tag{35}$$

or equivalently

$$- h_o \overline{A}_{wo} \left(\overline{T}_w - T_o\right) = \left(1 - \epsilon_w\right) \left(h_{wg} \overline{A}_{wg} + h_{w\ell} \overline{A}_{w\ell}\right) \left(\overline{T}_w - T\right) \quad . \tag{35a}$$

SECTION 5
CLOSURE OF THE EQUATION SET

Once expressions are supplied for the friction and heat transfer correlations, area factors, $\hat{v}$, and physical properties, the set is closed mathematically. Prototypes for these expressions may be found in Ref. 22. The principal variables are $\overline{T}_w$, T, v^ℓ, v^g, α^g, P, and $\dot{m}$. The pressure and temperature are related through an equation of state as

$$T = T_{eos}(P) \text{ or } P = P_{eos}(T) \ . \tag{36}$$

Because there are six field equations for the six principal unknown variables, $\dot{m}$ may be computed explicitly and does not need to be supplied. This expression is derived in Section 6.

Equations (4) through (7), (27) and (33) constitutes the complete two-phase equivalent pore drying model. These equations have been solved for the case of adiabatic walls (no wall heat transfer) in a constant area duct. [23]

SECTION 6
ALTERNATIVE FORMS AND SIMPLIFICATIONS OF THE GENERAL MODEL—COMPARISON WITH OTHER MODELS

Useful alternative forms of the general equations developed in Section 5 are derived in this section. Various simplifications for slow flow are made so that a simple and more tractable model results. The simplified expression also yield much insight into the basic structure of the equations. The simplified models can sometimes be solved analytically. Equation (27) may be rewritten in terms of temperature using Eq. (36) as:

$$(\alpha_g\rho_g C_{pg} + \alpha_\ell\rho_\ell C_{p\ell} + P')\frac{\partial T}{\partial t} + \left[\left(\alpha_g\rho_g C_{pg}v^g + \alpha_\ell\rho_\ell C_{p\ell}v^\ell\right) + P'\left(\alpha_g v^g + \alpha_\ell v^\ell\right)\right]\frac{\partial T}{\partial x}$$

$$= -\dot{m}^{\Delta P}_{int}(h_{gs} - h_{\ell s}) + (\overline{T}_w - T)(\overline{A}_{w\ell}h_{w\ell} + \overline{A}_{wg}h_{wg}) \ , \tag{37}$$

where P′ is a fundamental thermodynamic variable which may be computed from the Clausius-Clapeyron equation as:

$$P' \equiv \frac{dP_{eos}}{dT} = \frac{1}{T}\left(\frac{h_{gs} - h_{\ell s}}{1/\rho_g - 1/\rho_\ell}\right) \ . \tag{38}$$

A useful alternative form of the two energy equations given by Eqs. (33) and (37) is obtained by combining them so as to eliminate the wall heat transfer into the two phase mixture as

$$(1-\epsilon_w)(\alpha_g\rho_g C_{pg} + \alpha_\ell\rho_\ell C_{p\ell} + P')\frac{\partial T}{\partial t} + \epsilon_w\rho_w C_w\frac{\partial \overline{T}_w}{\partial t}$$

$$+ (1-\epsilon_w)\left[\left(\alpha_g\rho_g C_{pg}v^g + \alpha_\ell\rho_\ell C_{p\ell}v^\ell\right) + P'\left(\alpha_g v^g + \alpha_\ell v^\ell\right)\right]\frac{\partial T}{\partial x}$$

$$= \epsilon_w k_w\frac{\partial^2 \overline{T}_w}{\partial x^2} - (1-\epsilon_w)\dot{m}^{\Delta P}_{int}(h_{gs} - h_{\ell s}) - h_o\overline{A}_{wo}(\overline{T}_w - T_o) \ . \tag{39}$$

Equation (39) shows how the grouping of $(1 - \epsilon_w)\,\alpha_\ell$ and $(1 - \epsilon_w)\alpha_g$ arise. These two factors are the area (or volume) fraction of the *total* cross-sectional flow area occupied by each phase. This grouping can be incorporated into Eqs. (4) through (7) by the simple transformation:

$$A\alpha_a = \left(A\,\frac{A_a}{A}\right)\left(\frac{A_T}{A_T}\right) = A_T\,\frac{A_T}{A_T}\,\frac{A_a}{A} = A_T\,(1-\epsilon_w)\,\alpha_a \tag{40}$$

and

$$A\,\bar{A}_{wa} = \left(A\,\frac{A_{wa}}{A}\right)\left(\frac{A_T}{A_T}\right) = A_T\,\frac{A_{wa}}{A_T} = A_T\,\bar{A}'_{wa} \quad . \tag{40a}$$

The terms involving derivatives of the wall temperature and the difference between $\bar{T}_w$ and T_o are all relatable to $\dot{m}^T_{ext}$, the mass transfer rate developed by wall and external heat transfer. Similar to the approach used by Lyczkowski and Solbrig [10] the total mass transfer rate can be associated with the terms in Eq. (39) to develop the constitutive form of this expression as

$$\dot{m} = \dot{m}^{\Delta P}_{int} + \dot{m}^{T}_{ext} \quad , \tag{41}$$

where

$$\dot{m}^{\Delta P}_{ext} = -\,\frac{(\alpha_g\rho_g C_{pg} + \alpha_\ell\rho_\ell C_{p\ell} + P')\,\dfrac{\partial T}{\partial t} + \left[\left(\alpha_g\rho_g C_{pg} v^g + \alpha_\ell\rho_\ell C_{p\ell} v^\ell\right) + P'\left(\alpha_g v^g + \alpha_\ell v^\ell\right)\right]\dfrac{\partial T}{\partial x}}{h_{gs} - h_{\ell s}} \tag{41a}$$

and

$$\dot{m}^{T}_{ext} = \left(\frac{\epsilon_w}{1-\epsilon_w}\right)\left(\frac{k_w\,\dfrac{\partial^2 \bar{T}_w}{\partial x^2} - \rho_w C_w\,\dfrac{\partial \bar{T}_w}{\partial t}}{h_{gs} - h_{\ell s}}\right) - \frac{h_c \bar{A}_{wo}\,(\bar{T}_w - T_o)}{(1-\epsilon_w)\,(h_{gs} - h_{\ell s})} \tag{41b}$$

Equations (41) through (41b) show that the mass-transfer rate is determined from the solution of the system of equations and does not need to be prescribed by some rate expression. To do so would overspecify the system.

The general equation set for slowly varying but finite flows will now be simplified. First, we derive expressions that can be useful for the phase velocity difference. A general form for the transient velocity-difference equation may be derived as follows. First the two-component momentum equations are written in nonconservation law form. The resulting vapor momentum equation is divided by $A\alpha_g$ and the resulting liquid momentum equation is divided by $A\alpha_\ell$. These two equations are subtracted and solved to obtain the slip velocity as:

$$v^g - v^\ell = \frac{\alpha_g\alpha_\ell}{\bar{A}_{g\ell}B_{g\ell}}\left[\left(\rho_\ell\,\frac{\partial v^\ell}{\partial t} + \rho_\ell v^\ell\,\frac{\partial v^\ell}{\partial x} - \rho_g\,\frac{\partial v^g}{\partial t} - \rho_g v^g\,\frac{\partial v^g}{\partial x}\right)\right]$$

$$+ \alpha_g\,\frac{\bar{A}_{w\ell}B_{w\ell}}{\bar{A}_{g\ell}B_{g\ell}}\,v^\ell - \alpha_\ell\,\frac{\bar{A}_{wg}B_{wg}}{\bar{A}_{g\ell}B_{g\ell}}\,v^g + \frac{\alpha_g\dot{m}}{\bar{A}_{g\ell}B_{g\ell}}\,(\bar{v} - v^\ell)$$

$$+ \frac{\alpha_\ell\dot{m}}{\bar{A}_{g\ell}B_{g\ell}}\,(\bar{v} - v^g) + \frac{\alpha_g\alpha_\ell}{\bar{A}_{g\ell}B_\ell}\,(\rho_g - \rho_\ell)\,g_x \quad . \tag{42}$$

The relative velocity is easily related to the volumetric flow j through the expression

$$v^g - v^\ell = (V^g - j)/\alpha_\ell = V_{gj}/\alpha_\ell \ . \tag{42a}$$

or to the difference in volumetric flows as

$$v^g - v^\ell = \alpha_\ell \alpha_g (V_{gj} - V_{\ell j}) \ . \tag{42b}$$

Because the flow is assumed to be slowly varying, inertial forces are expected to be negligible. If we further assume that wall friction and momentum exchange between phases is negligible, the relative velocity may be obtained directly as

$$v^g - v^\varrho = \frac{\alpha_\varrho \alpha_g (\rho_\varrho - \rho_g)\, g_x}{\bar{A}_{g\varrho} B_{g\varrho}} = V_{gj}/\alpha_\varrho \ . \tag{43}$$

An alternative to Eq. (43) is to hypothesize a binary diffusion coefficient by correlating the relative reliability according to [24]

$$v^g - v^\varrho = \frac{-D}{\alpha_\varrho \alpha_g} \frac{\partial \alpha_g}{\partial x} = (V^g - j)/\alpha_\varrho \tag{44}$$

where V^g is the superficial velocity of the vapor. Under the same assumption used to derive Eq. (43), a consistent alternative expression for the relative velocity may be obtained as [21]

$$v^g - v^\varrho = \frac{(\rho_\varrho - \rho_g)\, \alpha_g \alpha_\varrho}{\bar{\rho}\, \bar{A}_{g\varrho} B_{g\varrho}} \left(\frac{\partial P}{\partial x}\right) = V_{gj}/\alpha_\varrho \ . \tag{45}$$

Equations (43) and (45) would be good first estimates of the relative motion between the phases for the expected situation where wall friction predominates.

A most important simplification of the problem is to assume that the heat transfer between the coal and the two-phase mixture is complete so that they are in a state near thermal equilibrium. In this case Eq. (35) becomes in the limit as $\bar{T}_w \to T$, and the phase wall heat transfer coefficients become infinite:

$$\begin{aligned} &[(1 - \epsilon_w)\,(\alpha_g \rho_g C_{pg} + \alpha_\varrho \rho_\varrho C_{p\varrho} + P') + \epsilon_w \rho_w C_w]\, \frac{\partial T}{\partial t} \\ &\quad + (1 - \epsilon_w) \left[\left(\alpha_g \rho_g C_{pg} v^g + \alpha_\varrho \rho_\varrho C_{p\varrho} v^\varrho\right) + P'\left(\alpha_g v^g + \alpha_\varrho v^\varrho\right)\right] \frac{\partial T}{\partial x} \\ &\quad = \epsilon_w k_w \frac{\partial^2 T}{\partial x^2} - (1 - \epsilon_w)\, \dot{m}_{int}^{\Delta P}\, (h_{gs} - h_{\varrho s}) \ . \end{aligned} \tag{46}$$

When the solid-two-phase equal temperature assumption is made, it becomes unclear whether the additional differential terms should continue to be associated with $\dot{m}_{ext}^T$. We define the mean heat capacity by

$$\rho C_{pm} \equiv (1 - \epsilon_w)(\alpha_g \rho_g C_{pg} + \alpha_\varrho \rho_\varrho C_{p\varrho} + P') + \epsilon_w \rho_w C_w \tag{47}$$

so that Eq. (46) becomes

$$\rho C_{pm} \frac{\partial T}{\partial t} + (1 - \epsilon_w) \left[\left(\alpha_g \rho_g C_{pg} v^g + \alpha_\ell \rho_\ell C_{p\ell} v^\ell \right) + P' (\alpha_g \rho_g + \alpha_\ell \rho_\ell) \right] \frac{\partial T}{\partial x}$$

$$= \epsilon_w k_w \frac{\partial^2 T}{\partial x^2} - (1 - \epsilon_w) \dot{m}_{int}^{\Delta P} (h_{gs} - h_{\ell s}) - h_o \bar{A}_{wo} (T - T_o) \quad . \tag{48}$$

Equation (48) corresponds nearly identically with Whittaker's equation VI-1. [16] The minor difference arises from the presence of P′ being retained, the definition of $\dot{m}_{int}^{\Delta P}$, and the presence of an external heat sink which arises because of external heat transfer from the pore.

An equation resembling Darcy's law for the relative motion between the phases has already been derived in Eq. (45). More appropriate expressions can be derived for each of the phase velocities, assuming inertial effects are minimal and wall friction predominates as

$$V^a = (1 - \epsilon_w) \alpha_a v^a = - \left[\frac{(1 - \epsilon_w) \alpha_a^2}{\bar{A}_{wa} B_{wa}} \right] \left(\frac{\partial P}{\partial x} \mp \frac{\dot{m} \hat{v}}{\alpha_a} - \rho_a g_x \right) \quad , \tag{49}$$

where V^a is the seepage or superficial velocities. We define the phase permeabilities as

$$\frac{K_a}{\mu_a} \equiv \frac{(1 - \epsilon_w) \alpha_a^2}{\bar{A}_{wa} B_{wa}} \quad . \tag{50}$$

Equation (49) then becomes

$$V^a = (1 - \epsilon_w) \alpha_a v^a = - \frac{K_a}{\mu_a} \left(\frac{\partial P}{\partial x} \mp \frac{\dot{m} v}{\alpha_a} - \rho_a g_x \right) \quad . \tag{51}$$

In Eq. (50), we clearly show that the phase permeabilities are functions of volume fraction, wall frictions, and flow geometry. Equation (51) is basically Whittaker's equations VI-2 and VI-4. [16] The new term arising is the mass transfer effect upon momentum transfer. The effect, not present in Eq. (51), is the capillary pressure (see the Appendix). A simplified version of Eq. (51), dropping the mass transfer effect and body force, was assumed by Ref. 25 in the analysis of rapidly drying wet-sand molds. Water motion was not considered in that paper.

The next important simplification arises by assuming that the vapor will move appreciably faster than the liquid. If $\hat{v}$ is chosen to be the velocity from which material is coming [8] and $\dot{m}$ is positive most of the time, $\hat{v}$ will also be negligible; the body force on the vapor would also be negligible. In this case, the equations of motion simplify to

$$v^g = 0 \tag{52}$$

and

$$V^g = (1 - \epsilon_w) \alpha^g v^g = - \frac{K_g}{\mu_g} \frac{\partial P}{\partial x} \quad . \tag{52a}$$

Equation (52) allows the liquid continuity equation to be written as

$$\frac{\partial}{\partial t} (A \alpha_\ell \rho_\ell) = -A \dot{m} \tag{53}$$

Because the phase and wall temperatures are nearly equal, $\dot{m}$ is basically $\dot{m}_{int}^{\Delta P}$. Hence, Eq. (53) may be substituted into Eq. (48) to form:

$$\rho C_{pm} \frac{\partial T}{\partial t} + (1 - \epsilon_w) \left[\left(\alpha_g \rho_g C_{pg} v^g \right) + P' \left(\alpha_g \rho_g + \alpha_\ell \rho_\ell \right) \right] \frac{\partial T}{\partial x}$$

$$= \epsilon_w k_w \frac{\partial^2 T}{\partial x^2} + \frac{(1 - \epsilon_w)}{A} (h_{gs} - h_{\ell s}) \frac{\partial}{\partial t} (A \alpha_\ell \rho_\ell) - h_o \bar{A}_{wo} (T - T_o) \quad . \tag{54}$$

If pressure work terms are negligible, Eq. (54) becomes

$$\rho C'_{pm} \frac{\partial T}{\partial t} + (1 - \epsilon_w) \alpha_g \rho_g C_{pg} v^g \frac{\partial T}{\partial x} = \epsilon_w k_w \frac{\partial^2 T}{\partial x^2}$$

$$+ \frac{(1 - \epsilon_w)}{A} (h_{gs} - h_{\ell s}) \frac{\partial}{\partial t} (A \alpha_\ell \rho_\ell) - h_o \bar{A}_{wo} (T - T_o) \quad , \tag{55}$$

where

$$\rho C'_{pm} = (1 - \epsilon_w) (\alpha_g \rho_g C_{pg} + \alpha_\ell \rho_\ell C_{p\ell} + \epsilon_w \rho_w C_w) \quad . \tag{55a}$$

The second term on the right-hand side of Eq. (55) can be written in terms of A_T as

$$\frac{(1 - \epsilon_w)}{A_T (1 - \epsilon_w)} (h_{gs} - h_{\ell s}) \frac{\partial}{\partial t} [A_T (1 - \epsilon_w) \alpha_\ell \rho_\ell] = (h_{gs} - h_{\ell s}) \frac{\partial}{\partial t} [(1 - \epsilon_w) \alpha_\ell \rho_\ell] \quad , \tag{56}$$

provided A_T is not a function of time. This implies that the entire pore space and pore wall do not shrink or expand. Inclusion of coal shrinkage or expansion as a function of dryness can, in principle, be handled by a field equation for the pore wall area as is done in fluid flow within channels having elastic walls.[26] Such a refinement is not justifiable at this point. Combination of Eqs. (52a), (55), and (56) and division through by C'_{pm} produces

$$\frac{\partial T}{\partial t} + \frac{\rho_g C_{pg} v^g}{\rho C'_{pm}} \frac{\partial T}{\partial x} = \frac{\epsilon_w k_w}{\rho C'_{pm}} \frac{\partial^2 T}{\partial x^2} + \left(\frac{h_{gs} - h_{\ell s}}{\rho C'_{pm}} \right) \frac{\partial}{\partial t} [(1 - \epsilon_w) \alpha_\ell \rho_\ell] - \frac{h_o \bar{A}_{wo} (T - T_o)}{\rho C'_{pm}} \quad . \tag{57}$$

Equation (57) is similar to Eq. (i) in Ref. 27. The main difference is that the ratio of $(\rho_g C_{pg} / \rho C'_{pm})$ is taken to be unity there and the heat transfer to the surroundings is zero. A similar formulation occurs in Ref. 28, in which wood pyrolysis was analyzed.

The sum of the two continuity equations may be written as

$$\frac{\partial}{\partial t} [(A_T (1 - \epsilon_w) \alpha_g \rho_g + A_T (1 - \epsilon_w) \alpha_\ell \rho_\ell] + \frac{\partial}{\partial x} (A_T \rho_g v_g) = 0 \quad . \tag{58}$$

If the accumulation of mass of vapor is negligible compared to this liquid, and Eq. (51) is substituted into Eq. (58), the result is

$$\frac{\partial}{\partial t} [A_T (1 - \epsilon_w) \alpha_\ell \rho_\ell] + A_T V^g \frac{\partial \rho_g}{\partial x} = \left(\frac{\rho_g A_T K_g}{\mu_g} \right) \frac{\partial^2 P}{\partial x^2} \quad , \tag{59}$$

assuming K_g/μ_g is constant. Equation (59) is basically Eq. (1) of Reference 25, which has apparently dropped the second term in Eq. (59). Equation (59) can also be written as

$$\frac{\partial}{\partial t}\left[A_T(1-\epsilon_w)\alpha_g\rho_g\right] + A_T V^g \frac{\partial \rho_g}{\partial x} = \left(\frac{\rho_g A_T K_g P'}{\mu_g}\right)\frac{\partial^2 T}{\partial x^2} \quad , \tag{60}$$

assuming P′ is constant. In this form, the mixture continuity equation now resembles Eq. (2) of Ref. 27. The primary difference is apparently in interpreting the concentration of mass. Had there been an assumed diffusion-type relation between the superficial gas velocity V^g and the volumetrix flux j and a Darcey law expression been used to correlate j, a diffusive term would arise in Eq. (60) as it does in Eq. (2) of Ref. 27.

In the limiting situation where the bulk motion became negligible, the theory developed here immediately transforms into the classical drying theory as found in the literature, but with negligible adsorption (bound water). See Refs. 29-31 for examples.

The main point of our manipulations and simplifications is that the model we have developed is reasonable. When simplifying assumptions are made, field equations result, similar to those proposed in the literature. The main difference is that the model rationally incorporates the movement of vapor out of the evaporating pore. The mass transfer rate is computed as part of the solution and does not need to be prescribed. The need for a moving interface with coupled regions is eliminated. The number of phenomonological constants is not as great as Whittaker models.[16,32]

It is useful at this point to summarize the minimum realistic equation set:

vapor continuity

$$\frac{\partial}{\partial x}\left[(1-\epsilon_w)\alpha_g\rho_g v^g\right] = (1-\epsilon_w)\,\dot{m} \quad , \tag{61}$$

liquid continuity

$$\frac{\partial}{\partial t}\left[(1-\epsilon_w)\alpha_g\right] = -(1-\epsilon_w)\,\dot{m}/\rho_g \quad , \tag{62}$$

vapor momentum

$$(1-\epsilon_w)\alpha_g v^g = -\left(\frac{K_g P'}{\mu_g}\right)\frac{\partial T}{\partial x} \quad , \tag{63}$$

and

mixture energy

$$\rho C_{Pm}\frac{\partial T}{\partial t} + (1-\epsilon_w)\alpha_g\rho_g C_{pg} v^g \frac{\partial T}{\partial x} = \epsilon_w k_w \frac{\partial^2 T}{\partial x^2} + (1-\epsilon_w)\,\dot{m}\,(h_{gs}-h_{\ell s}) \quad . \tag{64}$$

The factor $(1-\epsilon_w)$ has been retained even thought it is constant (no shrinkage or chemical reaction). Typical boundary conditions are:

$$\alpha_g(0,x) = 0 \tag{65}$$

$$T(0,x) = T_i \tag{65a}$$

$$\dot{m}\ (0,x) = 0 \tag{65b}$$

$$\frac{\partial T}{\partial x}\ (t,L) = 0 \tag{65c}$$

$$T\ (t,0) = T_s \tag{65d}$$

A typical solution procedure would be as follows.

1. Calculate the temperature of the liquid from Eq. (64) until $T \geq T_s$ where T_s is the saturation temperature.
2. Assume a value for m, set $T = T_s$.
3. Calculate α_ℓ (and hence α_g) from Eq. (62), assuming ρ_ℓ is constant.
4. Calculate the total mass flow of vapor from Eq. (60).
5. Update the temperature using Eq. (64) and the assumed value for $\dot{m}$.
6. Update $\dot{m}$ using the new value of temperatures just obtained using Eq. (64).
7. Repeat steps 3 through 6 until convergence occurs.
8. Compute v^g from Eq. (63).
9. Continue computing m until $\alpha_\ell = 0$, at which point vapor begins to superheat.

The pressure may be obtained from the equation of state.

SECTION 7
A SIMPLE ANALYTICAL EXAMPLE

Assuming m is small and a steady state situation, Eqs. (61) through (64) become

$$\frac{dG^g}{dx} = 0 \tag{66}$$

and

$$\frac{dT}{dx} = \frac{\epsilon_w k_w}{C_{pg} G^g} \frac{d^2T}{dx^2}\ , \tag{67}$$

where $G^g = (1 - \epsilon_w)\, \alpha_g \rho_g v^g$, the flux of vapor per total cross-sectional flow area.

These assumptions are made so that we might estimate the thickness of the zone between the complete vaporization of steam and the beginning of the pyrolysis section, as shown in Fig. 7-1. Equations (66) and (67) may be solved subject to the boundary conditions

$$\epsilon_w k_w \frac{dT}{\partial x} = (h_{gs} - h_{\ell s})\, G^g \qquad x = 0 \tag{67a}$$

$$T = T_1 \qquad x = 0 \tag{67b}$$

$$T = T_2 \qquad x = \ell \tag{67c}$$

Refer to Fig. 7-1 for coordinate positions. Equation (67a) states that all the vaporized steam comes from water vaporizing at $x = 0$. It is a shock-type approximation to the model presented in the previous section for the two-phase region. The solution of Eqs. (66) and (67) subject to boundary conditions (67b) and (67c) is

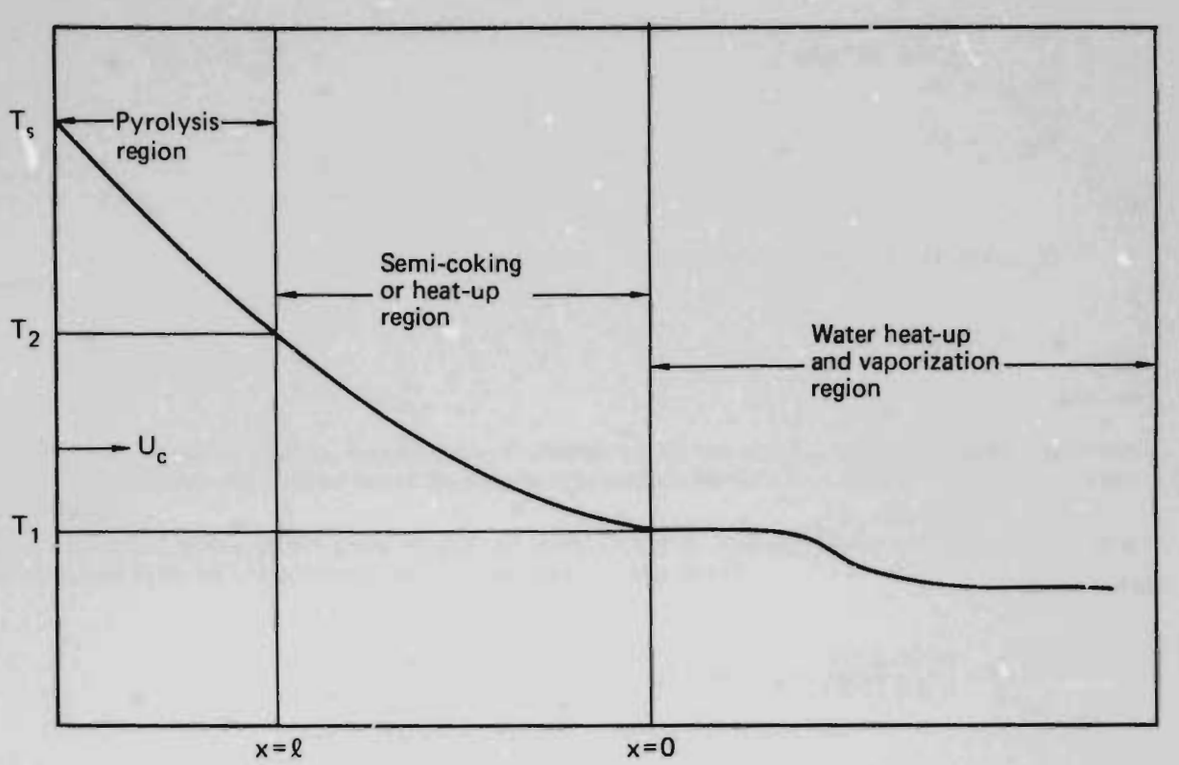

Fig. 7-1. Region of interest and coordinate system for simple analytical example.

$$T = T_1 + \frac{(T_2 - T_1)\,[1 - \exp\,(P_e x/\ell)]}{1 - \exp\,(Pe)} \quad , \tag{68}$$

where Pe is the Peclet number, still to be determined as

$$Pe = \left(\frac{G_g C_{pg}}{\epsilon_w k_w}\right) \ell \quad . \tag{68a}$$

Application of boundary condition Eq. (67a) allows ℓ to be computed from

$$\ell = \left(\frac{\epsilon_w k_w}{G_g C_{pg}}\right) \ln\left[\left(\frac{T_2 - T_1}{h_{gs} - h_{\ell s}}\right) C_{pg} + 1\right] \quad . \tag{69}$$

Assuming a value of the egression rate of the coal face $U_c = 10^{-6}$ m/s [7], the mass flux of water needed to effect this egression rate according to Eq. (3) can be computed as

$$G^{\ell} = 2 \times \epsilon_w \times 10^{-6} \times \rho_c \times M_{H_2O}/M_C \cdot \ell/(m^2\text{-}s) \quad . \tag{70}$$

where ρ_c is the density of coal. and M_{H_2O} and M_C are the molecular weights of water and coal, respectively. Assuming values of

$\epsilon_w = 0.7$,
$\rho_c = 1.28 \times 10^6$ g/m^3,
$M_{H_2O} = 18$,
and
$M_C = 12$,

then

$$G_g = (2)(0.7)10^{-6}(1.28 \times 10^6)(18)/12$$

$$= 2.68 \text{ g/(m}^2\text{-s)}.$$

Assuming

$$k_w = 0.23 \text{ watts/(K - m)}$$

$$C_{pg} = 1.25 \text{ J/(g - K)},$$

then

$$\frac{\epsilon_w k_w}{C_{pg} G^g} = \frac{(0.7)\ (0.23)}{(1.25)\ (2.68)} = 5 \times 10^{-2} \text{ m} \quad .$$

Assuming further that

$T_1 = 100°C$ (temperature at which vapor begins to superheat)
$T_2 = 500°C$ (temperature at which pyrolysis begins),

and

$h_{gs} - h_{fs} = 2270$ J/g,

the length of the zone between dryout and pyrolysis initiation becomes

$$\ell = 5 \times 10^2 \ln \left[\left(\frac{400}{2270} \right) (1.25) + 1 \right] \simeq 10^{-2} \text{ m} = 1 \text{ cm} \quad .$$

This value of 1 cm appears reasonable in light of one of the few controlled laboratory experiments in which a coal monolith was burned and it was found that the semicoking zone, (the region between virgin, but dry coal and coked (char) coal) was 3.5 to 5 cm. [33] Considering the vagaries of describing the experiment, an agreement of this order of magnitude is remarkable.

SECTION 8
EXTENSION TO A GLOBAL DRYING MODEL

The single equivalent pore drying model has gained attributes of a "global" drying model. The pore model is translated into a global model by generalizing the terms ϵ_w and A_o according to

$$\epsilon_w \rightarrow \epsilon_c = \frac{V_c}{V_{TOT}} \quad , \tag{71}$$

$$1 - \epsilon_w \rightarrow 1 - \epsilon_c = \frac{V_p}{V_{TOT}} \quad , \tag{71a}$$

and

$$\bar{A}_o = \frac{A_{sc}}{V_{TOT}} \quad , \tag{71b}$$

where V_c is the volume of char, V_{TOT} is the total control volume size and A_{sc} is the surface area of the coal block. In a global model, the heat loss to the surroundings is much less than for a single pore and therefore can be dropped.

The global drying model given by Eqs. (5), (27), (33), (51), and (61) generalizes the *ad hoc* drying models used in the LLL one-dimensional, packed-bed kinetics model.[34]

SECTION 9
SUMMARY AND CONCLUSIONS

A mechanistic model describing drying of porous media such as wet coal has been developed using two-fluid, two-phase flow theory. The model rationally accounts for the bulk motion of vapor and water through the drying matrix while it contains a minimum number of phenomenological constants such as effective diffusivity and permeability. Comparisons of alternative and simplified forms of the mechanistic model with models assumed or derived in the literature point out their implicit and explicit assumptions while at the same time lending confidence in the reasonableness of the approach adopted here. Most of the literature models appear to be either incorrect, incomplete, or both. An analytic expression was obtained for the mass-transfer (evaporation) rate. A closed-form solution of a highly simplified version of the model yielded an estimate of the semicoking zone length. The global drying model forms the basis for the more general situation of char reacting with hot steam, a subject of current investigation.

ACKNOWLEDGMENTS

The stimulating and valuable discussions with W. R. Airman, R. J. Cena, and C. B. Thorsness contributed to the synthesis of the model. Professor Dimitri Gidaspow assisted in developing the estimate of the semicoking zone length and encouraged the overall approach we adopted.

SYMBOLS

A	Pore cross sectional flow area
A_T	Total channel cross sectional area including pore cross sectional flow area and wall cross sectional area
$A_{g\ell}$	Surface area between vapor and liquid
$\bar{A}_{g\ell}$	Surface area between vapor and liquid phase per unit control volume of pore
$\bar{A}_{wa}$	Surface area of phase "a" in contact with the wall per unit of area control volume
$\bar{A}_{wo}$	External wall area per unit area control volume = VR
$B_{g\ell}$	Friction coefficient between vapor and liquid phases
B_{wa}	Stationary form and viscous drag between wall and phase "a"
C_{pm}	Average heat capacity defined by Eq. (47)
C'_{pm}	Average heat capacity defined by Eq. (55a)
D	Diffusion coefficient defined by Eq. (44)
G_g	Mass flux of vapor = $(1-\epsilon_w)\,\alpha_g\rho_g v^g$
g_x	Axial component of acceleration due to gravity
h_a	Specific enthalpy of phase "a"
h_{as}	Specific enthalpy of saturated "a"
h_{wa}	Wall heat transfer coefficient to phase "a"
h_o	Outside wall heat transfer coefficient
j	Volumetric flux = Q/A
K_a	Permeability of phase "a" defined by Eq. (50)
k_w	Thermal conductivity of the wall
h_{wa}	Wall heat transfer coefficient to phase "a"
$\dot{m}$	Total rate of vapor generation per unit pore control volume
$\dot{m}^{\Delta P}_{int}$	Rate of vapor generation per unit pore control volume due to pressure change
$\dot{m}^{T}_{ext}$	Rate of vapor generation per unit pore control volume due to external temperature difference
$\dot{m}_{int}$	Vapor generation rate per unit pore control volume due to interphase temperature difference
P	Pressure
P'	Fundamental thermodynamic variable defined by Eq. (38)
Q	Volumetric flow
q^a	Total heat flux to phase "a" per unit pore control volume
$q^{a\Delta P}_{int}$	Heat flux to phase "a" per unit pore control volume caused by flashing
q_{wa}	Wall heat flux to phase "a" per unit pore volume
q^{aT}_{int}	Heat flux to phase "a" per unit pore control volume due to phase temperature difference
q^{a}_{ext}	Heat flux to phase "a" per unit pore control volume due to external temperature difference
R	Channel radius
R_p	Pore radius
T_g	Gas phase temperature away from the coal face
T_o	Ambient temperature
T_s	Surface temperature of coal face; saturation temperature
T_w	Area average pore wall temperature
T	Temperature of two-phase mixture in pore
U_c	Velocity of coal face
V^a	Volumetric flux of phase "a" = $(1-\epsilon_w)d_a V^a$
V_{aj}	Drift flux of phase "a" = $V^a - j$
v^a	Velocity of phase "a"
$\hat{v}$	Velocity associated with interphase momentum transfer caused by phase change

x	Spatial dimension
α_g	Vapor volume fraction
α_ℓ	Liquid volume fraction ($\alpha_\ell = 1 - \alpha_g$)
ϵ_c	Volume fraction of coal
ϵ_w	Wall volume fraction defined by Eq. (34)
μ_a	Viscosity of phase "a"
ρ_a	Density of phase "a"
ρ_{as}	Density of phase "a" at saturation pressure
ρ_w	Density of channel wall
$\bar{\rho}$	Average density of two phase mixture = $\alpha_g\rho_g + \alpha_\ell\rho_\ell$
ρ	Average density of channel = $(1 - \epsilon_w)(\alpha_g\rho_g + \alpha_\ell\rho_\ell) + \epsilon_w\rho_w$
σ	Surface tension

REFERENCES

1. D. R. Stephens, R. W. Hill, and C. B. Thorsness, *Highlights of the LLL Hoe Creek No. 2 Underground Gasification Experiment*, Lawrence Livermore Laboratory, Rept. UCRL-80692 (1978).
2. P. P. Klimentov, *Influence of Ground Water on the Process of Underground Gasification of Coal Deposits*, (Izv. vyssh. ucheb zavedenii-Geologiya i razvedka, 1963 No. 4) pp. 106-119, Lawrence Livermore Laboratory, Rept. UCRL-Trans-10869.
3. P. V. Skafa, *Zonal Characteristics of the Process of Gasification of a Coal Seam In a Channel*, (Podzemnaya Gazifikatsiya Uglei, No. 1, pp. 3-10, 1958); Lawrence Livermore Laboratory, Rept. UCRL-Trans-10865.
4. I. Mc C. Stewart and T. F. Wall, "Reaction Rate Analysis of Borehole *In-Situ* Gasification System," *Sixteenth Symposium (International) on Combustion*, The Combustion Institute, Pittsburgh (1976) pp. 525-534.
5. R. C. Forrester III, "Two-dimensional Studies of Coal Pyrolysis: Preliminary Results" Proceedings Second Annual Coal Gasification Symposium, pp. 402-410, MERC/SP-76/3 (1976).
6. J. H. Campbell, Lawrence Livermore Laboratory, private communication (1978).
7. *Underground Coal Gasification Program*, Department of Energy Rept. ERDA 77-51 (1977), p. 26.
8. C. W. Solbrig, G. A. Mortensen, and R. W. Lyczkowski, "An Unequal Phase Velocity, Unequal Phase Temperature Theory Applied to Two-phase Blowdown from a Horizontal Pipe," *Proceeding of the 25th Heat Transfer and Fluid Mechanics Institute* (University of California, Davis, 1976, Stanford Univ. Press, Stanford, 1976), pp. 60-76.
9. R. W. Lyczkowski, "Numerical Techniques for the Computation of Transient Unequal Phase Velocity, Unequal Phase Temperature Two-Phase Flow and Heat Transfer," *Two-phase Transport and Reactor Safety* (T. N. Veziroglu and S. Kakac, Eds., Vol. II, Hemisphere Pub. Co., Washington, 1978), pp. 839-886.
10. R. W. Lyczkowski and C. W. Solbrig, "Constitutive Rate Equations for Flowing Phases Flashing at Unequal Velocities and Temperatures," (*Proceedings of the Topical Meeting on Thermal Reactor Safety, Sur Valley, Idaho, 1977*), Vol 2, pp. 2-424 to 2-442.
11. R. W. Taylor and D. W. Bowen, *Rate of Steam and Carbon Dioxide With Chars Produced From Subbituminous Coals*, Lawrence Livermore Laboratory, Rept. UCRL-52002 (1976).
12. P. N. Thompson, J. R. Mann, and F. Williams, "Underground Gasification of Coal" (National Coal Board, 1976).
13. Dimitri Gidaspow and R. T. Ellington, *Heat Transfer in an Infinite Tube Supporting Surface Combustion*, American Society Mechanical Engineering preprint 61-SA-59 (1961).
14. R. W. Lyczkowski, Dimitri Gidaspow, and C. W. Solbrig, "Simultaneous Convection Diffusion of Reactants, Products, and Heat with a Surface Reaction," *Chemical Engineering Progress Symposium Series*, No. 77, **63** (1967), pp. 1-15.
15. D. U. Olness and S. K. Madsen, *LLL In-Situ Gasification Program Quarterly Report, July through September, 1977*, Lawrence Livermore Laboratory, Rept. UCRL-500026-77-3, Nov. 1 (1977).
16. S. Whittaker, "Simultaneous Heat, Mass and Momentum Transfer in Porous Media. A Theory of Drying," in *Advances in Heat Transfer*, Vol. 15, (J. P. Hartnett and T. F. Irvine, Jr., Eds., Academic Press, New York, 1977), pp 119-203.
17. J. H. Campbell, *Pyrolysis of Subbituminous Coal As It Relates to In-Situ Gasification Part 2: Characterization of Liquid and Solid Products*, Lawrence Livermore Laboratory, Rept. UCRL-52035 Part 2 (1976).
18. C. W. Solbrig and E. D. Hughes, "Governing Equations for a Seriated Continuum: An Unequal Velocity Model for Two-Phase Flow," in *Two-Phase Transport and Reactor Safety* (T. N. Veziroglu and S. Kakac, Eds., Vol. I, pp. 307-362, Hemisphere Pub. Corp., Washington, 1978).
19. C. W. Solbrig and E. D. Hughes, "Two-phase Flow of an Unequal Temperature Fluid," in *Two-Phase Transport and Reactor Safety* (T. N. Veziroglu and S. Kakac, Eds., Vol. II, 1978), pp 561-576.
20. C. W. Solbrig, C. J. Hocevar, and E. D. Hughes, "A Model For a Herogeneous Two-Phase Unequal Temperature Fluid" *Preprints of AICHE Papers 17th National Heat Transfer Conference*, American Institute of Chemical Engineers, New York (1977), pp. 139-151.

21. R. W. Lyczkowski, D. C. Mecham, A. A. Irani, N. Fujita, G. R. Sawtelle, and K. V. Moore, *The Development of RELAP/SLIP For the Semiscale Blowdown Heat Transfer Test S-02-6 (NRC Standard Problem 6)* (Research Project 695-1) Interim Report, EPRI NP-343, 1977.
22. C. W. Solbrig, J. H. McFadden, R. W. Lyczkowski, and E. D. Hughes, "Heat Transfer and Friction Correlations Required to Describe Steam-Water Behavior in Nuclear Safety Studies," AICHE Paper #21, (15th National Heat Transfer Conference, San Francisco, California 1975); Oak Ridge National Laboratory CONF-75084 3, 1976.
23. R. W. Lyczkowski and C. W. Solbrig, "Calculation of the Governing Equations for a Seriated Unequal Velocity, Equal Temperature Two-Phase Continuum," *Preprints of AICHE Papers 17th National Heat Transfer Conference*, American Institute of Chemical Engineers, New York (1977), pp. 100-110.
24. N. Zuber and F. W. Staub, "The Propagation and the Wave Form of the Vapor Volumetric Concentration In Boiling, Forced Convection Sytem Under Oscillatory Conditions," *Int. J. Heat Mass Transfer*, **9**, 871 (1966).
25. H. Saito and N. Seki, "Mass Transfer and Pressure Rise In Moist Material Subjected to Sudden Heating," *J. Heat Transfer*, **99**, No. 1, 105 (1977).
26. Stanley Middleman, *Transport Phenomena In the Cardiovascular System* (Wiley-Interscience, New York, 1972), p. 47.
27. K. N. Shukla, "Heat and Mass Transfer in Combustion and Evaporation Processes' in *Future Energy Production Systems* Vol. I (J. C. Denton and N. H. Afgan, Eds., Academic Press, NY, 1976), pp. 523-547.
28. Hsiang-Cheng Kung, "A Mathematics Model of Wood Pyrolysis," *Combustion and Flame*, **18**, 185 (1972).
29. J. Crank, *The Mathematics of Diffusion* (Oxford University Press, London, 1956), p. 303.
30. Masao Kito and Sachio Sygiyama, "Heat Transfer of Condensible Vapor Diffusing Through Porous Media" *Int. J. Heat Mass Transfer*, **13**, 1705 (1970).
31. C. A. Chase, Jr., Dimitri Gidaspow, and R. E. Peck, "Diffusion of Heat and Mass In a Porous Medium With Bulk Flow," *CEP Symposium Series No. 92*, **65**, 91 (1969).
32. Stephen Whittaker, "Toward a Diffusion Theory of Drying," *Ind. Eng. Fund*, **16**, No. 4, 408 (1977).
33. I. P. Kirichenko and V. S. Ton, *Experiments In Underground Coal Gasification at the Lisichank Mine*, Gornyi Zhurnal, Vol. III, No. 8, 10-21, (1935); UCRL-Trans-1012, (1976).
34. C. B. Thorsness and R. B. Roza, "Lawrence Livermore Laboratory In Situ Coal Gasification Program: Model Calculations and Laboratory Experiments" 51st Annual Fall Technical Conference and Exhibition Soc. Pet. Eng, AIME, New Orleans, (1976).
35. J. D. Ramshaw and J. A. Trapp, "Characteristics, Stability, and Short Wavelength Phenomena In Two-Phase Flow Equation Systems," *Nuclear Sci. and Eng.* **66**, 93 (1978).

CCD

APPENDIX: INCLUSION OF SURFACE TENSION

For the model derived in this paper, we assumed that the pressures of the two phases are equal. The effect of surface tension may easily be included following the approach given by Ramshaw and Trapp.[35]

The pressure between the two phase is given by

$$P_\ell - P_g = \frac{\sigma}{R_c} \quad , \tag{A-1}$$

where σ is the surface tension and R_c is the radius of curvature of the interface given by [35]

$$\frac{1}{R_c} = - R_p \frac{\partial^2 \alpha_g}{\partial x^2} \left[1 + R_p^2 \left(\frac{\partial \alpha_g}{\partial x} \right)^2 \right]^{-3/2} \quad . \tag{A-2}$$

If the assumption is made that

$$R_p^2 \left(\frac{\partial \alpha_g}{\partial x} \right)^2 \ll 1 \quad , \tag{A-3}$$

the phase pressures became related as

$$P_g - P_\ell = - \sigma R_p \frac{\partial^2 \alpha_g}{\partial x^2} \quad . \tag{A-4}$$

UCID- 17859

Lawrence Livermore Laboratory

ANALYSIS OF HANNA II IN-SITU COAL GASIFICATION EXPERIMENTS

R. J. Cena

July 17, 1978

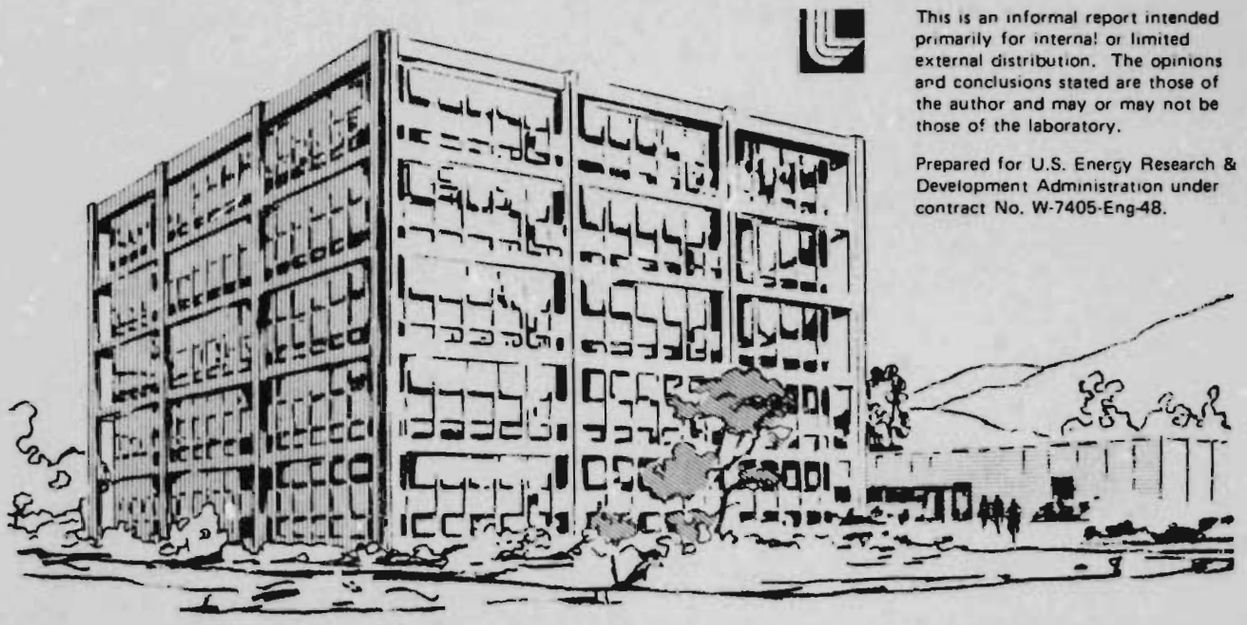

Prepared for U.S. Energy Research & Development Administration under contract No. W-7405-Eng-48.

ANALYSIS OF HANNA II IN-SITU COAL GASIFICATION EXPERIMENTS

by: R. J. Cena

INTRODUCTION

The Laramie Energy Research Center (LERC) has conducted several gasification experiments in recent years, at its Hanna, Wyoming test site.

Herein is an attempt to quantify field test results using material balance calculations consistent with those reported for Hoe Creek. The results of this study are compared with published results for Hanna II Phase I and Phase II[1,2] and with recent Hoe Creek II results.[3]

Background

Two reactions are considered in determining the overall material balance for in-situ gasification:

$$\text{COAL} \xrightarrow{\text{Heat}} X(1)\ \text{CHAR} + [1-X(1)]\ \text{Volatile Products} \qquad (1)$$

and

$$\text{CHAR} + A(1)O_2 + A(2)\ H_2O \rightarrow \text{Products} \qquad (2)$$

Summing these reactions with the product species enumerated we arrive at the overall stoichiometric relation for in-situ gasification reported for Hoe Creek I:[4]

$$\underset{\text{Dry ash-free coal}}{CH_{\alpha_1}O_{\beta_1}} + A(1)O_2 + A(2)H_2O \rightarrow A(3)H_2 + A(4)CH_4 + A(5)CO + A(6)CO_2 + A(7)C_2H_6 + \underset{(\text{Tar})}{A(8)CH_{\alpha_2}O_{\beta_2}} + \underset{(\text{Char})}{A(9)CH_{\alpha_3}O_{\beta_3}} \qquad (3)$$

In Equation (3), A(9) represents the net amount of char left underground, resulting from more char being produced in reaction (1) than consumed in reaction (2).

Assuming the α's and β's are known or can be reasonably estimated, equation (3) contains nine unknown coefficients A(1)-A(9). To solve for the unknown coefficients, nine independent relations must be known. We choose the following set:

A)	Atomic balances	3 equations
	Overall C Balance	
	Overall H Balance	
	Overall O Balance	
B)	Molar ratios of individual product species	5 equations
C)	Molar ratio of O_2 consumed to product species, using O_2 tracer in product gas	1 equation
	TOTAL	9 equations

For air gasification, N_2 provides the necessary O_2 tracer in the product gas. However for burns other than air a suitable inert O_2 tracer must be supplied.

HANNA II EXPERIMENTS

The Hanna II in-situ gasification experiments were conducted in the Hanna #1 coal seam, a 30 foot thick subbituminous coal seam at an approximate depth of 275 feet. The physical properties of this coal pertinent to the solution of Equation (3) are given in Table 1. (See Attachment I)

The Hanna II experiments consisted of three phases. Phase I and II will be discussed here.

TABLE 1. Physical Properties of Hanna II Coal

COAL - $C\ H_{\alpha_1}\ O_{\beta_1}$	M.W.	16.06
α_1 (H/C ratio)		0.9659
β_1 (O/C ratio)		0.1923
TAR - $C\ H_{\alpha_2}\ O_{\beta_2}$	M.W.	13.01
α_2 (H/C ratio)		1.0
β_2 (O/C ratio)		0.0
CHAR - $C\ H_{\alpha_3}\ O_{\beta_3}$	M.W.	12.12
α_3 (H/C ratio)		0.1018
β_3 (O/C ratio)		0.0003
COAL $\rightarrow$ X(1) CHAR + [1-X(1)] VOLATILE		X(1) = 0.6533

HANNA II PHASE I

The Hanna II Phase I experiment consisted of reverse combustion linking of two wells 52 ft. apart followed by 38 days of forward gasification.

Published results[1] summarizing the forward gasification are presented in Table 2.

TABLE 2. HANNA II Phase I Summary

Overall Average Composition of Product Gas
(volume percent)

N_2	-	51.0
H_2	-	17.3
CO	-	14.7
CO_2	-	12.4
CH_4	-	3.3
C_2-C_4	-	0.6

Average Operational Parameters

Heating Value of Gas (Gross)	152 Btu/scf
Daily Gas Production	2.7 MM scf
Daily Air Injection	1.9 MM scf
Daily Btu Production	420 MM Btu

HANNA II PHASE II

The Hanna II Phase II experiment consisted of reverse combustion linking of two wells 60 ft. apart followed by a 27 day period of forward gasification. The average forward burn gas composition and operating parameters, derived from daily averages,[5] are presented in Table 3.

TABLE 3. HANNA II Phase II Summary

Overall Average Composition of Product Gas
(volume percent)

N_2	-	49.08
H_2	-	16.421
CO	-	15.913
CO_2	-	11.900
CH_4	-	5.416
C_2-C_4	-	0.4506

Average Operational Parameters

Daily Gas Production	6.59 MM scf
Daily Air Injection	4.13 MM scf

Material Balance Calculations

Using the physical properties in Table 1 in conjunction with reported Phase I results, Equation (3) is solved for the unknown coefficients A(1) - A(9). The results of this calculation are presented in Table 4.

TABLE 4. Stoichiometric Coefficients for Hanna II Phase I

A(1)	O_2	=	0.2732	
A(2)	H_2O	=	0.0474	
A(3)	H_2	=	0.3443	
A(4)	CH_4	=	0.0657	
A(5)	CO	=	0.2925	
A(6)	CO_2	=	0.2468	
A(7)	C_2H_6	=	0.0119	
A(8)	TAR	=	0.0	(assumed)
A(9)	CHAR	=	0.3711	

For completeness a second calculation, disregarding the O_2 tracer information and assuming no net CHAR formation A(9) = 0 is presented in Table 5.

TABLE 5. Stoichiometric Coefficients for Hanna II Phase I, Assuming No Net CHAR Formation

A(1)	O_2	=	0.3762	
A(2)	H_2O	=	0.3291	
A(3)	H_2	=	0.5475	
A(4)	CH_4	=	0.1044	
A(5)	CO	=	0.4652	
A(6)	CO_2	=	0.3924	
A(7)	C_2H_6	=	0.0190	
A(8)	TAR	=	0.0	(assumed)
A(9)	CHAR	=	0.0	(assumed)

Similarly, Equation (3) is solved for Phase II using product compositions in Table 3. These results are presented in Table 6. Table 7 corresponds to the case where no char is assumed.

TABLE 6. Stoichiometric Coefficients for Hanna II Phase II

A(1)	O_2	=	0.2333	
A(2)	H_2O	=	0.0419	
A(3)	H_2	=	0.2897	
A(4)	CH_4	=	0.0955	
A(5)	CO	=	0.2807	
A(6)	CO_2	=	0.2099	
A(7)	C_2H_6	=	0.0080	
A(8)	TAR	=	0.0	(assumed)
A(9)	CHAR	=	0.3979	

TABLE 7. Stoichiometric Coefficients for Hanna II Phase II, Assuming No Net CHAR Formed

A(1)	O_2	=	0.3081	
A(2)	H_2O	=	0.3552	
A(3)	H_2	=	0.4811	
A(4)	CH_4	=	0.1587	
A(5)	CO	=	0.4662	
A(6)	CO_2	=	0.3487	
A(7)	C_2H_6	=	0.0132	
A(8)	TAR	=	0.0	(assumed)
A(9)	CHAR	=	0.0	(assumed)

Results

Two interesting results are evident from the material balances presented in Tables 4 and 6:

(1) A large, unreacted CHAR zone is calculated to remain following gasification, in both cases,

and,

(2) Very little water is calculated to enter into the overall reaction.

The fraction of coal carbonized only to the total amount of coal affected, carbonized and gasified is A(9)/X(1).

For Hanna II coal, X(1) = 0.6533 which yields for Phase I, 57% carbonized and for Phase II, 61% carbonized.

Thus total coal consumption, on a dry ash free (DAF) basis, can be calculated from the operating results in Tables 2 and 3. For Phase I a total of 1143 tons of coal were affected with 493 tons gasified and 649 tons carbonized only. LERC reports[1] 538 tons gasified and 475 tons carbonized which agrees reasonably well.

For Phase II, a total of 2124 tons of coal were affected with 830 tons gasified and 1293 tons carbonized. Here LERC reports[2] 2190 tons of coal burned on a wet with ash basis, which corresponds to 1367 tons (DAF). This value was not determined from consideration of a complete material balance but rather by summing carbon in the product gas, which tacitly assumes that no net Char is left underground. This is in obvious conflict with material balance results.

Hoe Creek II Results

Material balance results for Hoe Creek II are presented in Table 8.

TABLE 8. Stoichiometric Coefficients for Hoe Creek II

A(1)	O_2	=	0.449
A(2)	H_2O	=	0.189
A(3)	H_2	=	0.404
A(4)	CH_4	=	0.067
A(5)	CO	=	0.221
A(6)	CO_2	=	0.527
A(7)	C_2H_6	=	0.023
A(8)	TAR	=	0.039
A(9)	CHAR	=	0.099

The fraction of carbonized to total coal affected for Hoe Creek II is 0.099/0.6725 or 14.7 percent. This compares with 57 and 61 percent carbonization for Phases I and II, respectively.

Also, the amount of water entering into gasification is two to four times that calculated for the Hanna experiments.

Sensitivity Study

Before any conclusions can be derived from the above results, the matter of sensitivity should be considered. Presented in Figures 1 through 3 are plots showing the variation in the amount of unreacted char versus variations in 1) product gas composition, 2) tar composition and amount and, finally, 3) coal composition.

In Figure 1, we see that large changes in the product gas composition does affect the amount of unreacted char. However, for reasonable ranges of variation, $\pm$ 0.5 mole percent, very little change occurs.

In Figure 2 we see that no reasonable assumptions as to the amount or composition of unreacted tar serves to significantly reduce the amount of char formed.

And finally, in Figure 3 we see that the amount of unreacted char is sensitive to coal composition.

However, a deviation of greater than 10 percent for the H/C ratio coupled with a 50 percent change for the O/C ratio from reported values is necessary to bring the Char estimates to zero.

Conclusions

The results of this analysis show that large amounts of unreacted char may be left underground following gasification. Also, very little water is calculated to enter into the overall gasification reaction at Hanna II. In view of the heterogeneous nature of Hanna coal, the apparent conclusion of a large char zone may be partially offset by differences in the composition of coal actually entering into gasification.

However, since coal composition is one of the few parameters which can be measured in a field experiment, it is felt that uncertainties in this area should be eliminated, so that more abstract parameters such as unreacted char formed may be addressed.

References

1. Brandenburg, C. F., et al., "Interpretation of Chemical and Physical Measurements From an In Situ Coal Gasification Experiment," SPE 5654, presented at the SPE Fall Meeting of AIME, Dallas, Tex., Sept. 28-Oct. 1, 1975, 28 pp.

2. Fischer, D. D., C. F. Brandenburg, S. B. King, R. M. Boyd, and H. L. Hutchinson, "Status of the Linked Vertical Well Process in Underground Coal Gasification," paper FS-4, presented at 2nd Annual Underground Coal Gasification Symposium, Morgantown, WV, Aug. 10-12, 1976.

3. Aimen, W. R., Thorsness, C. B., Hill, R. W., et al., "The Hoe Creek II Field Experiment On Underground Coal Gasification, Preliminary Results," Lawrence Livermore Laboratory Rept., UCRL - 80592, February 27, 1978.

4. Hill, R. W. and Thorsness, C. B., "Results from an In Situ Coal Gasification Experiment Involving Explosive Fracturing: Hoe Creek Experiment No. 1," Lawrence Livermore Laboratory Rept., UCRL - 52229, February 15, 1977.

5. Private Communication, Daily Averaged Gas Composition, Flow Rates, Heating Values and Coal Consumption for Period 4/17/78 (day 106) through 7/31/78 (day 211) Laramie Energy Research Center.

ATTACHMENT I

Analysis of Coal Taken from Hanna No. 1 Seam

	Hanna I Site			Hanna II Site
	As received	Moisture-free	Moisture-and ash-free	As Received
Proximate analysis: (wt %)				
Moisture	9.51	-	-	8.62
Volatile matter	32.64	36.07	48.91	31.66
Fixed carbon	34.09	37.67	51.09	30.78
Ash	23.76	26.26	-	28.92
	100.00	100.00	100.00	99.98
Ultimate analysis: (wt %)				
Hydrogen	5.09	4.45	6.04	4.64
Carbon	49.60	54.81	74.33	45.34
Nitrogen	1.29	1.43	1.94	1.14
Oxygen	19.58	12.30	16.67	19.27
Sulfur	.68	.75	1.02	0.69
Ash	23.76	26.26	-	28.92
	100.00	100.00	100.00	100.00
Heating Value (Btu/lb)	8,660	9,580	12,990	8,600

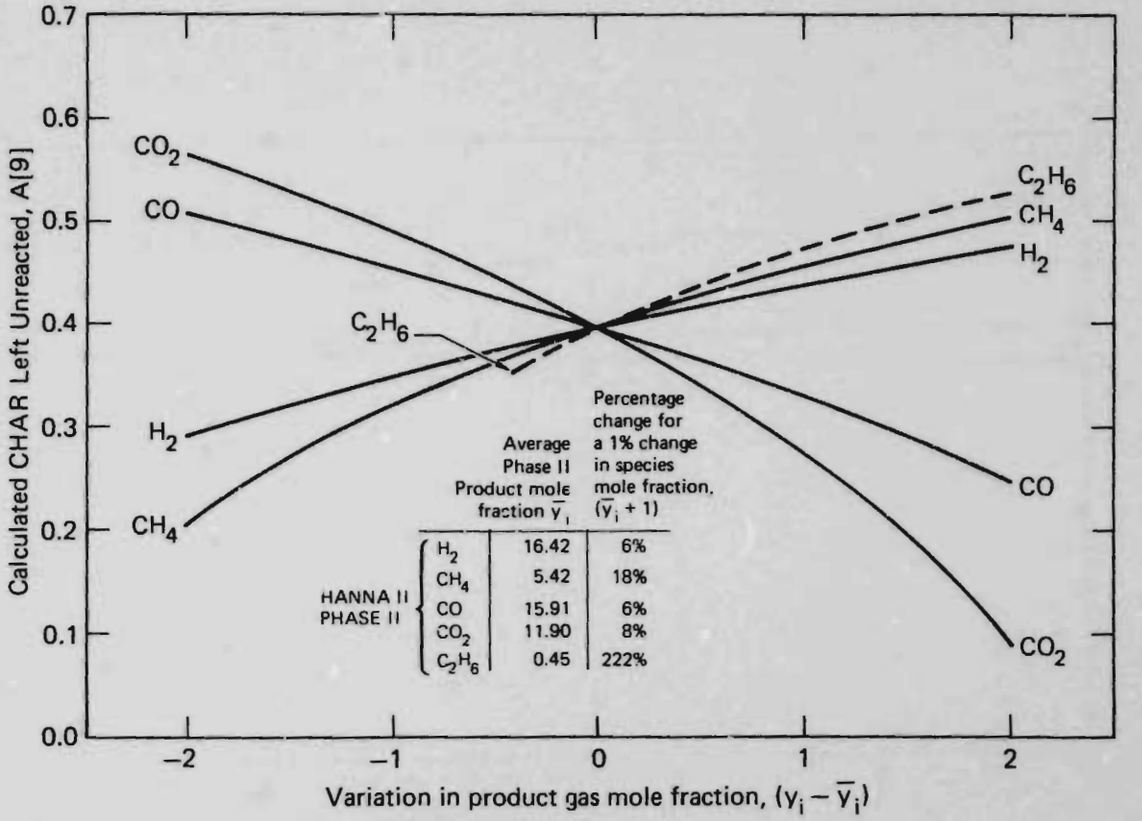

Fig. 1 Effect of Gas Composition on Char Formation

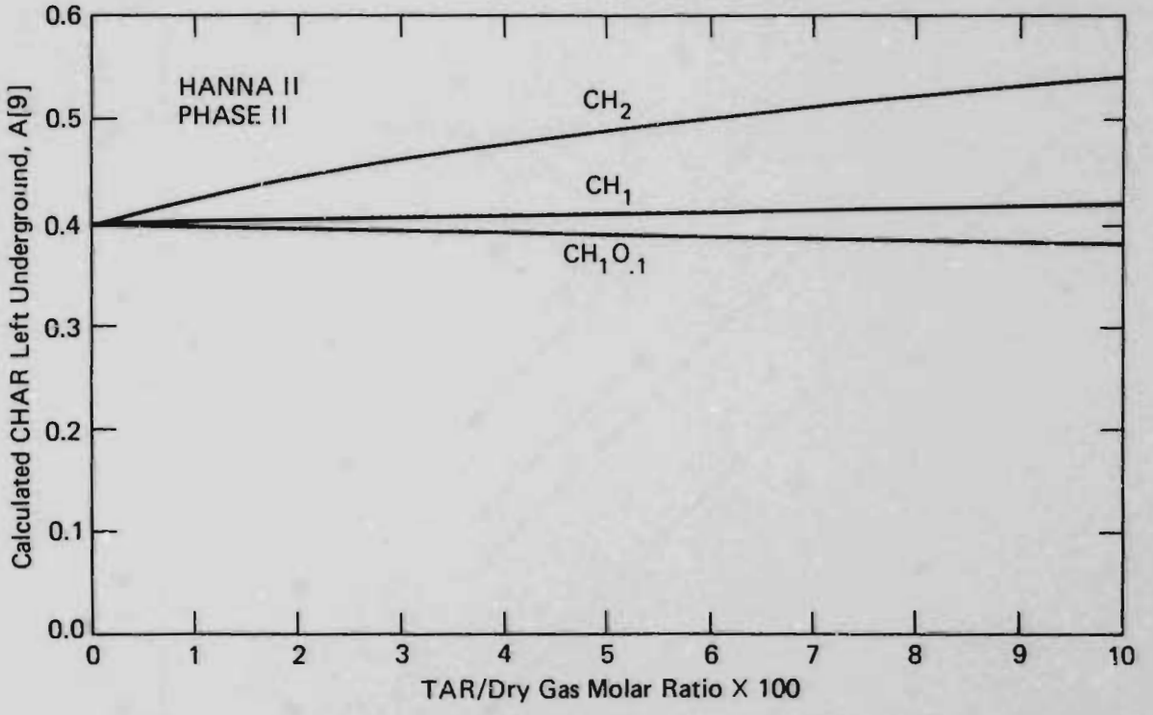

Fig. 2 Effect of Tar Amount and Composition on Char Formation

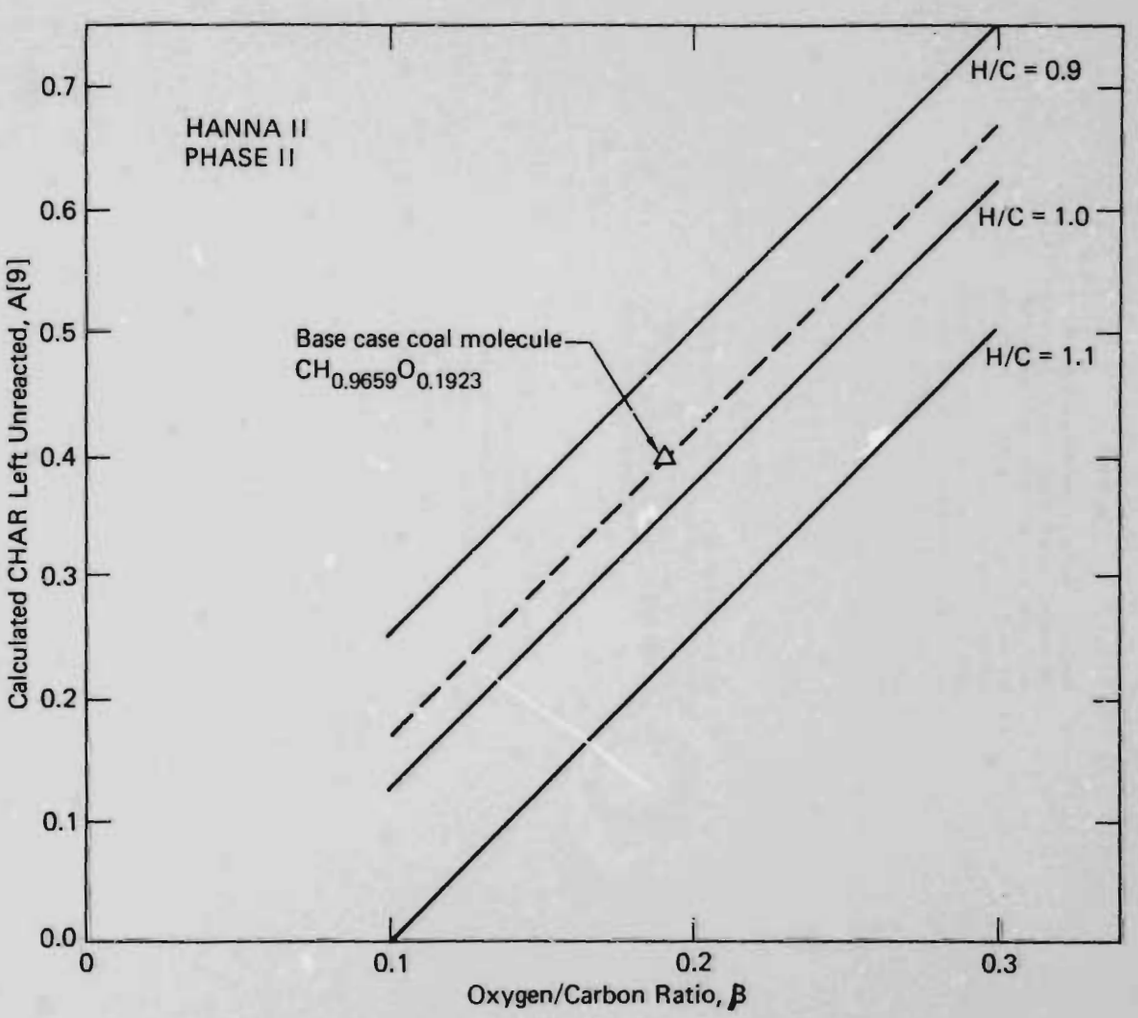

Fig. 3 Effect of Coal Molecule on Char Formation $CH_\alpha O_\beta$

NOTICE

"This report was prepared as an account of work sponsored by the United States Government. Neither the United States nor the United States Department of Energy, nor any of their employees, nor any of their contractors, subcontractors, or their employees, makes any warranty, express or implied, or assumes any legal liability or responsibility for the accuracy, completeness or usefulness of any information, apparatus, product or process disclosed, or represents that its use would not infringe privately-owned rights."

NOTICE

Reference to a company or product name does not imply approval or recommendation of the product by the University of California or the U.S. Department of Energy to the exclusion of others that may be suitable.

Printed in the United States of America
Available from
National Technical Information Service
U.S. Department of Commerce
5285 Port Royal Road
Springfield, VA 22161
Price: Printed Copy $; Microfiche $3.00

Page Range	Domestic Price	Page Range	Domestic Price
001-025	$ 4.00	326-350	$12.00
026-050	4.50	351-375	12.50
051-075	5.25	376-400	13.00
076-100	6.00	401-425	13.25
101-125	6.50	426-450	14.00
126-150	7.25	451-475	14.50
151-175	8.00	476-500	15.00
176-200	9.00	501-525	15.25
201-225	9.25	526-550	15.50
226-250	9.50	551-575	16.25
251-275	10.75	576-600	16.50
276-300	11.00	601-up	[1]
301-325	11.75		

[1] Add $2.50 for each additional 100 page increment from 601 pages up.

47. 1 Library copy.

[redacted]

UCRL-52524

MOVING EQUILIBRIUM FRONT MODEL FOR *IN SITU* GASIFICATION

C. B. Thorsness
A. E. Sherwood

July 25, 1978

Work performed under the auspices of the U.S. Department of Energy by the UCLLL under contract number W-740E-ENG-48.

LAWRENCE
LIVERMORE
LABORATORY
University of California/Livermore

Distribution Category
UC-90c

LAWRENCE LIVERMORE LABORATORY
University of California Livermore, California 94550

UCRL-52524

MOVING EQUILIBRIUM FRONT MODEL FOR *IN SITU* GASIFICATION

C. B. Thorsness

A. E. Sherwood

MS. date: July 25, 1978

CONTENTS

NOMENCLATURE

$h_g^i \mid T_j$	Enthalpy of gas species "i" at temperature T_j (cal/g-mole)
$h_s^i \mid T_j$	Enthalpy of solid species "i" at temperature T_j (cal/g)
y_j^i	Gas mole fraction of species "i" at location "j"
T_j	Temperature at location "j" (K)
G_j	Gas flux at location "j" $\left(\frac{\text{g-mole}}{\text{cm}^2\,\text{s}}\right)$
L_j	Liquid water flux at location "j" $\left(\frac{\text{g}}{\text{cm}^2\,\text{s}}\right)$
S^k	Density of solid species "k" $\left(\frac{\text{g}}{\text{cm}^3}\right)$
M_s^k	Molecular weight of solid species "k"
M_g^i	Molecular weight of gas species "i"
W_R	Reaction front velocity $\left(\frac{\text{cm}}{\text{s}}\right)$
W_D	Drying front velocity $\left(\frac{\text{cm}}{\text{s}}\right)$
W_S	Steam front velocity $\left(\frac{\text{cm}}{\text{s}}\right)$

Gas species:
1 – N_2
2 – O_2
3 – H_2O(g)
4 – H_2
5 – CH_4
6 – CO
7 – CH_2
8 – Tar

Solid species:
1 – Coal
2 – Char
3 – H_2O(M)
4 – H_2O(F)
5 – Ash

MOVING EQUILIBRIUM FRONT MODEL FOR *IN SITU* GASIFICATION

ABSTRACT

We have developed a simple model for forward-combustion *in situ* coal gasification. The model treats chemical and thermal problems of gasification by considering macroscopic material and energy balances written around the moving fronts associated with the process. At various points in the system, we assume thermodynamic equilibrium to exist, thus allowing the thermal and mass balances to be coupled in such a way that the performance of the system is completely specified. We have done sample calculations for a number of feed compositions using various assumptions about the thermodynamic properties of the solid-phase char and system operating pressures. The equilibrium assumptions used are most appropriate for high oxygen-feed concentrations and for coals with a mole ratio of water to carbon in the char below 0.35. The usefulness of the model is limited by two primary considerations: predicted hot gas equilibrium temperatures can be so low that rate limitations in reaching equilibrium can be severe; and energy release into the wet coal may not be high enough to ensure that the predicted rate of drying will exceed the predicted rate of coal consumption.

INTRODUCTION

To gasify coal *in situ*, the bed is first prepared and then ignited and a steam-oxygen and/or air mixture is injected into it to sustain combustion. This report presents a simple model of the response of the bed to gasification. We feel that the model amplifies our understanding of the gasification process and thereby helps us to achieve maximum results. One approach to modeling *in situ* gasification process involves writing out differential equations describing the rate processes involved and solving the resulting set of equations. This leads to a detailed description of the process[1-4] but at the same time requires detailed submodels to be generated to describe reaction rates, transport coefficients, etc. The complexity of these models, and the gasification process itself, suggests that the development of simpler models be explored.

We treat chemical and thermal problems of gasification by examining the macroscopic material and energy balances associated with moving fronts. We assume a one-dimensional adiabatic model in which heat and mass are only transported in the system by convection. We also assume that equilibrium exists at various points with respect to chemical changes. Thus, thermal and mass balances can be coupled to completely specify the performance of the system.

Stephens[5,6] previously explored the use of an equilibrium assumption to help understand gasification. Our work is different from Stephens' in that we consider gasification to be a continuous process rather than a batch process. In addition, we use energy balances to couple equilibrium temperatures to available energy, which Stephens did not.

The moving fronts--bed temperatures--important to this model are sketched in Fig. 1. Each is associated with a strong heat effect and each front moves at its own velocity. The reaction front represents the face of the unconsumed char, the drying-pyrolysis front is where coal is dried and then pyrolyzed to char, and the condensation front is where the coal is heated, primarily by steam condensation, to an appropriate steam-plateau temperature. We assume that the processes involved in the vicinity of these fronts are rapid, and we thus treat changes in this area essentially as step changes. In previous work[7] a similar model was used to investigate pressure drop in the system. However, here we assume pressure drop to be unimportant and emphasize the chemical makeup of the produced gas as well as the relative motion of thermal fronts.

The gas species we consider are O_2, N_2, H_2O, H_2, CH_4, CO, CO_2, and tar; the nongaseous species are coal, char, $H_2O(F)$, $H_2O(M)$, and ash. Char is the basic solid product of coal pyrolysis and tar represents a pseudo-component incorporating all products of pyrolysis that are not among the listed gas species. $H_2O(F)$ is "fixed" or bound water contained in the coal and released in the drying process, and $H_2O(M)$ is "mobile" water contained in the flow-carrying porosity of the system.

MODEL EQUATIONS

The basic model equations involve the mass and energy balances of the three moving control volumes shown in Fig. 1. Between control volumes we assume that no change in the system occurs and that gases and solids are the same temperature. Figure 2 shows these control volumes in reference frames moving at the velocity of the individual fronts. Major inflow and outflow streams are shown for each of the control volumes R, D, and S. We assume that the gas velocity is much greater than the front velocities and as a consequence we need not consider relative motion of the control volumes when dealing with gas streams.

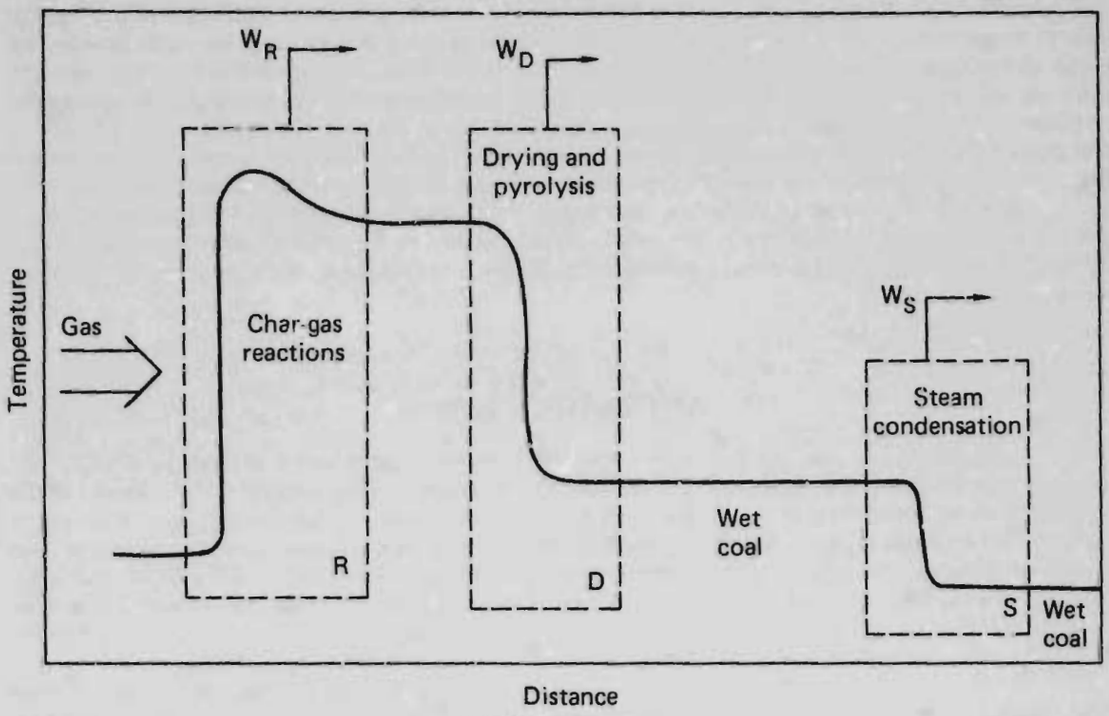

Fig. 1. Fronts with moving control volumes.

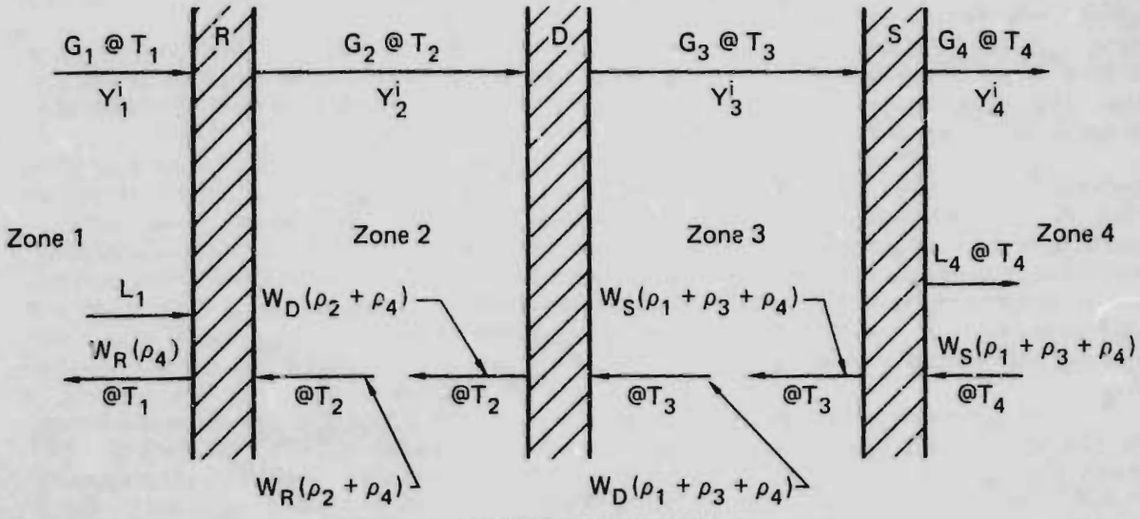

Fig. 2 Flow streams for mass and energy balances.

Zone 1 represents the inlet region where we assume that the inlet gas is in thermal equilibrium with ash. Zone 2 represents the region where the gas-phase that contains reaction products is assumed to be in thermal and chemical equilibrium with solid containing char and ash. Zone 3 is the steam plateau region where a solid phase that contains undried coal and ash are assumed to be in thermal and water-vapor/liquid equilibrium with the flowing gas stream. Zone 4 represents the unheated coal bed, also assumed to be in thermal and water-vapor/liquid equilibrium with the flowing gas stream. Also present in Zone 4 is a liquid water stream. All char/gas reactions are assumed to occur within the confines of control volume R. In control volume D we assume that water in the wet coal is dried and that solid coal is pyrolyzed to yield gaseous species and a solid char. In control volume S we assume that the steam condenses to liquid water.

Reaction-Front Control Volume R

The mass balance for species i in control volume R can be written

$$\frac{\delta_{i,3} L_1}{18} + G_1 y_1^i + \frac{W_R \rho^2 R_R^i}{M_s^2} = G_2 y_2^i, \tag{1}$$

$$\delta_{i,3} = 0 \ (i \neq 3), \ \delta_{3,3} = 1,$$

where the numerical subscripts refer to the zone from which or into which a given stream is flowing, the superscript "i" is the gas species, G is the molar gas fluxes, Y is the gas mole fraction, and W_R is the velocity of the reaction front. A separate equation is written for each gas species. The R_R's represent stoichiometric coefficients defined for the overall reaction of char (CH_aO_b)

$$CH_aO_b + \alpha O_2 + \beta H_2O \rightarrow R_R^1 H_2 + R_R^5 CH_4 + R_R^6 CO + R_R^7 CO_2. \tag{2}$$

An enthalpy balance around control volume R yields

$$L_1 h_s^1 + G_1 \sum_{i=1}^{8} y_1^i h_g^i \mid_{T_1} + W_R \left[\rho^2 h_s^2 \mid_{T_2} + {}^5h_s^5 \mid_{T_2} - \rho^5 h_s^5 \mid_{T_1} \right]$$

$$= G_2 \sum_{i=1}^{8} y_2^i h_g^i \mid_{T_2}, \tag{3}$$

where the gas enthalpy h_i^g is defined per mole of species "i" while the solid species are defined per gram of material. We assume that the enthalpies are only a function of temperature.

The following problem must be solved: given ρ^2, ρ^5, y_1^i, G_1, and T_1, find R_R^i, α, β, W_R, y_2^i, G_2, and T_2. The solution is obtained by first rearranging Eq. (3) so that

$$W_R = G_2 \left[\sum_{i=1}^{8} y_2^i h_g^i \mid_{T_2} - G_1 \sum_{i=1}^{8} y_1^i h_g^i \mid_{T_1} - L_1 h_s^1 \mid_{T_1} \right]$$

$$\left[\rho^2 h_s^2 \mid_{T_2} + \rho^5 h_s^5 \mid_{T_2} - \rho^5 h_s^5 \mid_{T_1} \right]^{-1}; \tag{4}$$

Eq. (1) must then be summed over i so that

$$W_R = \left[G_2 - G_1 - \frac{L_1}{18} \right] \left[\rho^2 \sum_{i=1}^{8} R_R^i \right]^{-1}. \tag{5}$$

The rest of the solution then involves an iterative process that proceeds in the following manner: T_2 is estimated and equilibrium assumption then allows the calculation of R_R^i, G_2, and y^i (see Appendix A). Equations (4) and (5) are then used to calculate two values for W_R. If they do not agree, a new estimate of the T_2 is made and the procedure is repeated.

A computer program has been written (see Appendix B) for the computations outlined above, as well as for those given below for the other fronts.

Drying-Pyrolysis-Front Control Volume D

The mass balance around control volume D is given for each of the eight gas species as

$$G_2\, y_2^i + W_D \left[\frac{\rho^1 R_p^i}{M_s^1} + \frac{\rho^3 R_D^i}{M_s^3} \right] = G_3\, y_3^i \,. \tag{6}$$

where R_p^i is the coefficient of the overall reaction for pyrolysis and

$$\begin{aligned} CH_cO_d(\text{coal}) \rightarrow\ & \eta CH_aO_b + R_p^3 H_2O + R_p^4 H_2 \\ & + R_p^5 CH_4 + R_p^6 CO + R_p^7 CO_2 \\ & + R_p^8\, C_eH_f\,(\text{tar}) \,. \end{aligned} \tag{7}$$

Also note that the effective char density is defined as

$$\rho^2 = \frac{M_s^2}{M_s^1}\, \eta\, \rho^1 \,, \tag{8}$$

where R_D^i is the coefficient for the drying reaction and is simply

$$R_D^3 = 1$$

and $$R_D^i = 0 \text{ for } i \neq 3 \,.$$

The enthalpy balance around the control volume is

$$\begin{aligned} G_2 \sum_{i=1}^{8} \left(y_2^i\, h_s^i \,|\, T_2 \right) + W_D \Big[& \rho^1 h_s^1 \,|\, T_2 + \rho^4 h_s^4 \,|\, T_3 + \rho^5 h_s^5 \,|\, T_3 \\ & - \rho^2 h_s^2 \,|\, T_2 - \rho^5 h_s^5 \,|\, T_2 \Big] = G_3 \sum_{i=1}^{8} \left(y_3^i\, h_s^i \,|\, T_3 \right) \,. \end{aligned} \tag{9}$$

The following problem must be solved: given G_2, y_2^i, T_2, R_p^i, R_D^i, ρ^1, ρ^4, and ρ^5, find W_D, G_3, y_3^i, and T_3. The solution is obtained by first combining Eqs. (6) and (9) to produce an equation for W_D and eliminating the unknowns $G_3 y_3^i$. Thus,

$$W_D = G_2 \left\{ \sum_{i=1}^{8} \left[y_2^i \left(h_v^i \mid_{T_3} - h_v^i \mid_{T_3} \right) \right] \right\} \left\{ \rho^1 h_s^1 \mid_{T_3} + \rho^4 h_s^4 \mid_{T_3} + \rho^5 h_s^5 \mid_{T_3} - \rho^2 h_s \mid_{T_2} - \rho^5 h_s^5 \mid_{T_2} - \sum_{i=1}^{8} \left[\left(\frac{\rho_1 R_p^i}{M_s^1} + \frac{\rho_3 R_D^i}{M_s^3} \right) h_v^i \mid_{T_3} \right] \right\}^{-1} . \tag{10}$$

An equation for G_3 is generated by summing Eq. (6) over all i:

$$G_3 = G_2 + W_D \left[\rho^1 \left(\frac{\sum_{i=1}^{8} R_p^i}{M_s^1} \right) + \rho^3 \left(\frac{\sum_{i=1}^{8} R_D^i}{M_g^3} \right) \right] . \tag{11}$$

The remaining part of the solution procedure is iterative. An estimate is made for T_3, Eq. (10) is solved for W_D, and Eq. (6) is used with i = 3 to calculate y_3^i. The assumption of water-vapor/liquid equilibrium in zone 3 allows a relation to calculate T_3:

$$P_{H_2O} = y_3^3 P ,$$

and, assuming $P_{H_2O} = \exp \left(12.61 - \frac{4690}{T_3} \right)$,

then

$$T_3 = 4690 \left[12.61 - \ln(P_{H_2O}) \right]^{-1} . \tag{12}$$

Here P_{H_2O} is the vapor pressure of water (atm) at T_3. If this calculated T_3 agrees with the estimated value, a solution has been obtained and the remaining concentrations are found using Eq. (8). If it does not agree, this value is used as a new estimate for T_3 and the procedure repeated until agreement is obtained.

Steam Condensation Front-Control Volume S

The gas species mass balances for these control volumes lead to the following:

$$G_3 y_3^i = G_4 y_4^i + \delta_{i,3} \frac{L_4}{18} . \tag{13}$$

The only change allowed in this control volume is steam condensation that causes an effluent liquid water stream L_4. We assume that the solid phase composition does not change while traversing this front.

The enthalpy balance is

$$G_3 \sum_{i=1}^{8} \left(y_3^i h_g^i \mid T_3 \right) + W_s \left[\rho^1 \left(h_s^1 \mid T_4 - h_s^1 \mid T_3 \right) + \rho^4 \left(h_s^4 \mid T_4 - h_s^4 \mid T_3 \right) \right.$$

$$\left. + \rho^5 \left(h_s^5 \mid T_4 - h_s^5 \mid T_5 \right) \right] = G_4 \sum_{i=1}^{8} \left(y_4^i h_g^i \mid T_4 \right) + L_4 h_s^3 \mid T_4 . \tag{14}$$

The following problem must be solved: given G_3, y_3^i, T_3, and T_4, find W_s, G_4, y_4^i, and L_4. Unlike the previous solutions, these result. an be found directly. First the water vapor concentration in zone 4 is found by assuming water vapor/liquid equilibrium in zone 4:

$$y_4^3 = \frac{P_{H_2O} \mid T_4}{P} . \tag{15}$$

Equation (13) with i = 3 is then used along with Eq. (13) summed over i to find the liquid water rate

$$L_4 = 18\, G_3 \left(y_3^3 - y_4^3\right) \left(1 - y_4^3\right)^{-1} . \tag{16}$$

The equation for gas flow in zone 4 is

$$G_4 = G_3 \left(1 - y_3^3\right) \left(1 - y_4^3\right)^{-1} . \tag{17}$$

Equation (13) is then used for each species to determine y_4^i. Finally, Eqs. (14), (16), and (17) lead to an equation for the rate of front movement

$$W_s = G_3 \left\{ - \sum_{\substack{i=1 \\ i \neq 3}}^{8} \left(y_3^i h_g^i \mid T_3 \right) + \left[y_4^3 h_g^3 \mid T_4 \right] \left[1 - \frac{\left(y_3^3 - y_4^3\right)}{\left(1 - y_4^3\right)} \right] \right.$$

$$\left. + 18 \frac{\left(y_3^3 - y_4^3\right)}{\left(1 - y_4^3\right)} h_s^3 \mid T_4 \right\} \left\{ \rho^1 \left(h_s^1 \mid T_4 - h_s^1 \mid T_3 \right) \right.$$

$$\left. + \rho^4 \left(h_s^4 \mid T_4 - h_s^4 \mid T_3 \right) + \rho^5 \left(h_s^5 \mid T_4 - h_s^5 \mid T_3 \right) \right\}^{-1} \tag{18}$$

THE REACTION FRONT

In the equations that describe the moving fronts (1 through 18), upstream fronts are, for the most part, uncoupled from the downstream fronts. Thus, the motion of the reaction front and accompanying gas composition and temperature in zone 2 can be investigated without reference to the other fronts. The primary variables that influence the reaction front are the gas-feed stream composition and temperature, the system operating pressure, the ash content of the char, and the exact nature of the assumed equilibrium in zone 2. Total gas flow rate and total solid density influence only the magnitude of W_R but not reaction temperature or composition.

To calculate equilibrium composition (as outlined in Appendix A), several equilibrium constants must be calculated and the number and composition of chemical species allowed in the equilibrium mixture must be estimated. The equilibrium constants are calculated from the thermodynamic properties of the species present in the system. The properties of gas species are well known. On the other hand, the properties of the char in zone 2 are not well known, because its exact structure is unknown. Consequently, we have estimated the thermodynamic properties of char (heat of formation, absolute entropy, and heat capacity) that cover a range of possible specifications, including β-graphite and a much less ordered substance with a nonzero standard free-energy of formation. Appendix B describes the nature of char thermodynamics as well as the thermodynamics of the other substances.

In general, the reacting species allowed in the equilibrium mixture of zone 2 consist of char in the solid phase and N_2, O_2, H_2O, H_2, CH_4, CO, and CO_2 in the gas phase. This list is modified for some calculations by omitting CH_4 because it appears in zone 2 via a reaction whose rate is considerably lower than those for other constituents.

We performed a series of calculations to investigate the influence of the important parameters on the behavior of the reaction front. The results of some of these calculations are presented to illustrate the possible range of behavior. These results are divided into five cases that show the influence of particular variables. Because oxygen concentration is the dominant variable we present a series of concentrations for each of the five cases. Table 1 presents the pertinent input data required for each case.

Table 1. Input data for cases A through E: gas flow rate for all cases $1X10^{-4}$ $\frac{mol}{s\ cm^2}$.

Case	T_{IN}	CH_4 present	Pressure, atm	Char		Ash Density, g/cm^3
				Density, g/cm^3	Chemistry	
A	Dew point	Yes	1	0.245	$CH_{.09}O_{.016}$	0.0408
B	Dew point	Yes	1	0.238	C	0.0408
C	Dew point	No	1	0.245	$CH_{.09}O_{.016}$	0.0408
D	Dew point	Yes	30	0.245	$CH_{.09}O_{.016}$	0.0408
E	300K	Yes	1	0.245	$CH_{.09}O_{.016}$	0.0408

Case A is a standard against which the influence of other assumed conditions can be compared. We used a char typical of that obtained from subbituminous coal and low-pressure operation. Figure 3 shows the calculated gas composition and temperature in zone 2 as a function of the oxygen mole fraction. Steam is the other reactant that flows into the reaction zone along with the oxygen. The inlet temperature changes slightly with oxygen content because we assume the inflowing reactants to be at the dew point. The gas composition of the product gas responds as expected to the change in oxygen concentration. At low oxygen concentrations the temperature is relatively low and rather large amounts of CH_4 and CO_2 are present. As oxygen concentration increases, the temperature also increases and CO and H_2 become the dominant gases. Note the rather complete decomposition of H_2O at all conditions. In addition, the calculated equilibrium temperatures are relatively low at low oxygen concentration. To establish a low-temperature equilibrium mixture would require very long residence times in the char zone.

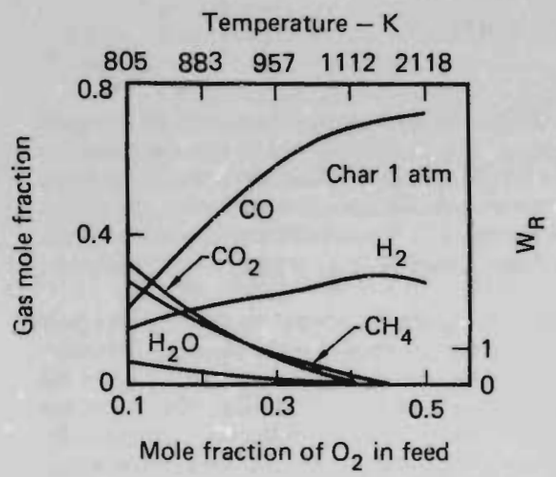

Fig. 3. Char adiabatic equilibrium, at 1 atm with methane; y^i, T vs mole fraction O_2 in the feed.

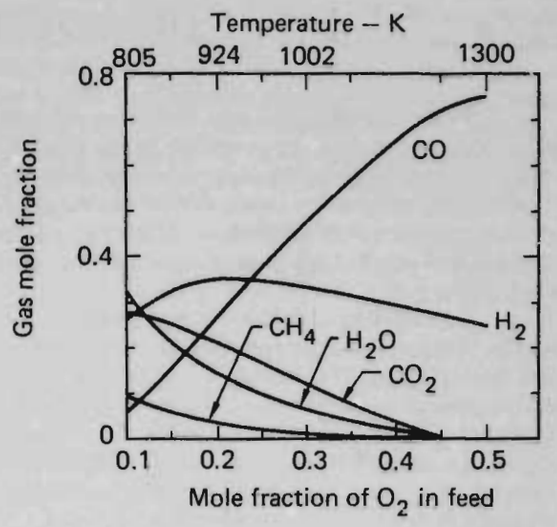

Fig. 4. Graphite adiabatic equilibrium, at 1 atm; y^i, T, vs mole fraction O_2 in the feed.

Case B shows the results assuming that the char thermodynamics correspond to β-graphite. Figure 4 gives the calculated gas composition and temperature for this case. The CH_4 concentration is much lower than that for Case A and H_2 is higher. At low oxygen concentrations the amount of steam decomposition is considerably less than that of case A. The equilibrium temperatures are in general somewhat higher than those of Case A.

Case C shows the influence of suppressing CH_4 on the computed gas composition and temperature (see Fig. 5). Gas compositions are similar to Case B but the equilibrium temperatures are lower, primarily as a result of the slight increase in steam decomposition.

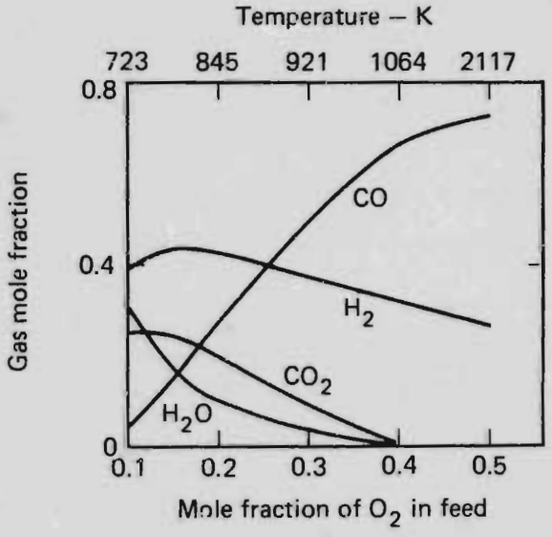

Fig. 5. Char adiabatic equilibrium, at 1 atm no methane; y^i, T, vs mole fraction O_2 in the feed.

Figure 6 gives the calculated gas compositions and temperatures for Case D. We can find the influence of increased pressure by comparing these results with Case A. The higher pressure operation slightly increases the methane concentration and substantially increases the equilibrium temperature.

Case E illustrates the influence of changing the feed stream from oxygen/steam to oxygen/water. Figure 7 shows the calculated gas composition and temperatures. When we compare these results to Case A we see a considerable reduction in the equilibrium temperature caused by the additional heat load of vaporizing water. The concentrations of CH_4 and CO_2 increase in response to the lower temperatures.

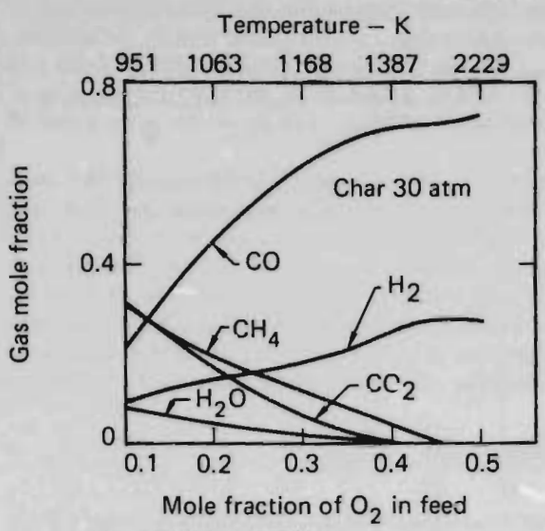

Fig. 6. Char adiabatic equilibrium, at 30 atm with methane; y^i, T, vs mole fraction O_2 in the feed.

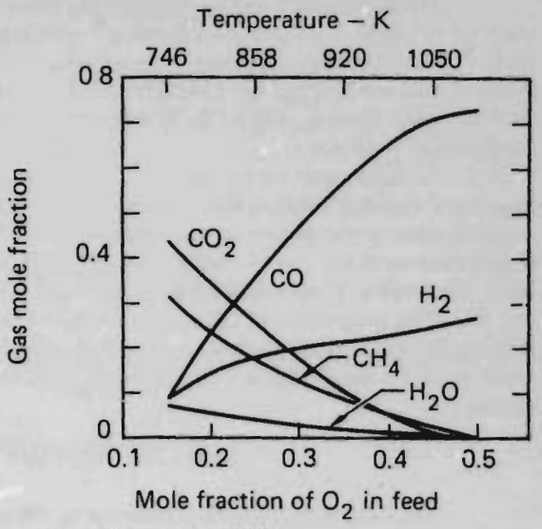

Fig. 7. Char adiabatic equilibrium, at 1 atm with methane for liquid H_2O feed; y^i, T, vs mole fraction O_2 in the feed.

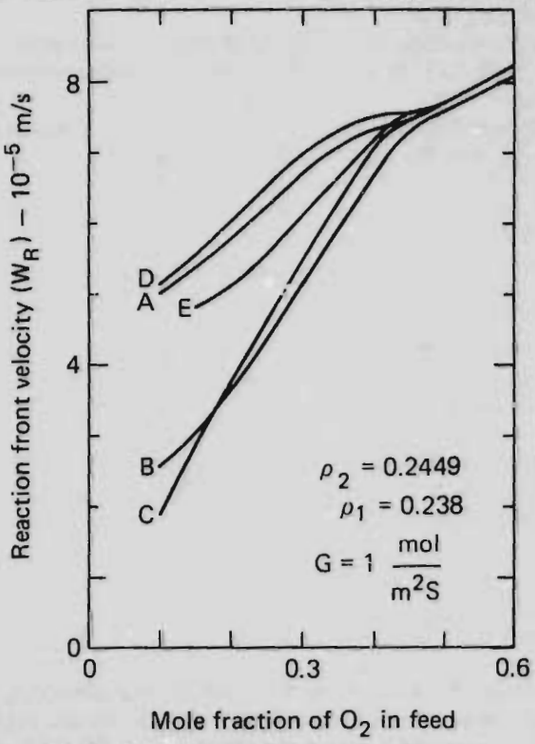

Fig. 8. Reaction front velocity for cases A through E vs mole fraction O_2 in the feed.

The ash content of the char is the only remaining variable that could influence the reaction front. However, when we removed all the ash from Case A we did not find any significant change in calculated gas composition or temperature.

Figure 8 shows the velocity of the reaction front for each case as a function of oxygen feed concentration. At high oxygen concentrations all cases reach the same asymptote corresponding to the formation of H_2 and CO as the only reaction products. The slight offset of Case B stems from the lower value of char density used in the calculations.

The computed gas compositions as shown in Figs. 3 through 7 are not a function of the magnitude of the total gas flow. For a constant char/ash ratio they are not a function of absolute solid density. In addition, we have found that W_R at a given oxygen feed concentration is directly proportional to the total feed rate and inversely proportional to the solid density. Figure 8 can be used to determine W_R for any value of reactant flow or solid density. Appendix D summarizes additional runs including some in which air is assumed for the feed stream.

In summary, we can make several conclusions about the performance of the model. The most important variable influencing the calculated results is the oxygen/steam ratio in the feed gas. The next consideration is the nature of the char thermodynamics and the presence or absence of methane in the equilibrium mixture. The operating pressure is less important. The remaining variable, ash content, is of very little importance. Low oxygen-feed concentrations favor CH_4 and CO_2 while high oxygen feeds favor H_2 and CO. The temperatures calculated for low oxygen concentrations probably invalidate the assumption that the system would reach such an equilibrium in a reasonable amount of time. However, for reasonably reactive chars many of the higher oxygen-feed concentrations may approach the calculated equilibrium states.

THE DRYING/PYROLYSIS FRONT

The heat required to turn wet coal to dry/hot char and the rate at which heat is supplied to the front controls the rate of movement of the drying/pyrolysis front. This heat is supplied by the hot gas that emerges from the reaction zone; consequently, the rate of movement of the drying/pyrolysis front is necessarily coupled to the upstream reaction front.

The change in gas composition and temperature when crossing the front is of less interest than changes across the reaction front because we are not considering any reactions other than the evolution of pyroysis products and steam.

A discussion of the drying/pyrolysis front must define the solid phase in zone 3 and the pyrolysis reaction. The solid is wet coal. For the zone 3 solid we take:

$$\rho^1 \text{ (coal)} = 0.415 \ \frac{g}{cm^3}, \tag{19}$$

$$\rho^4 \text{ (fixed water)} = \ldots \frac{g}{cm^3} \tag{20}$$

$$\rho^5 \text{ (ash)} = 0.0408 \frac{g}{cm^3}, \tag{21}$$

as well as a coal molecule of $CH_{0.912}\ O_{0.194}$. The assumed pyrolysis reaction is given by

$$CH_{0.912}\ O_{0.194} \rightarrow 0.776\ CH_{0.09}\ O_{0.016} + 0.078\ H_2O + 0.083 H_2 + 0.044 CH_4 + 0.103\ CO + 0.037 CO_2 + 0.014\ C_9H_{25.3}\text{(tar)}. \tag{22}$$

These values are for a particular subbituminous coal from the Wyodak mine in Wyoming.

We can see that the ratio of the drying/pyrolysis front velocity and the reaction front velocities for a particular system are independent of both gas feed rate and the total solid density. Thus, the calculated results for W_D/W_R shown in Fig. 9 are independent of total flow rate and solid density and are shown

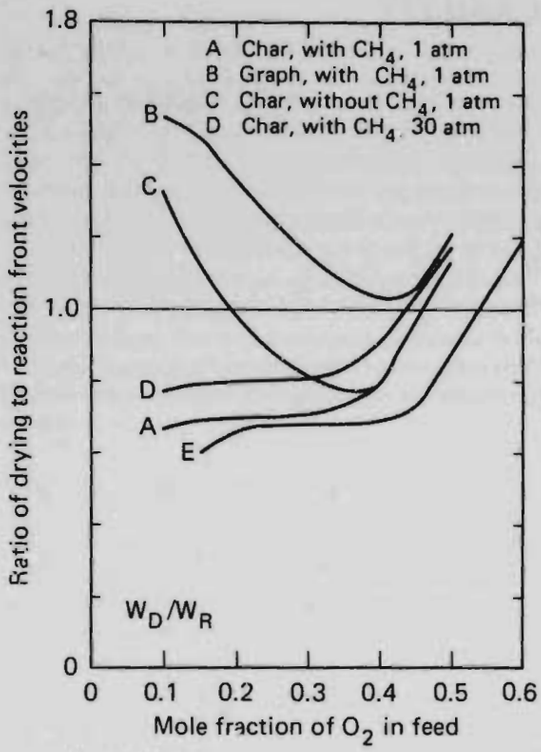

Fig. 9. W_D/W_R **vs mole fraction** O_2 **in the feed for cases A through E.**

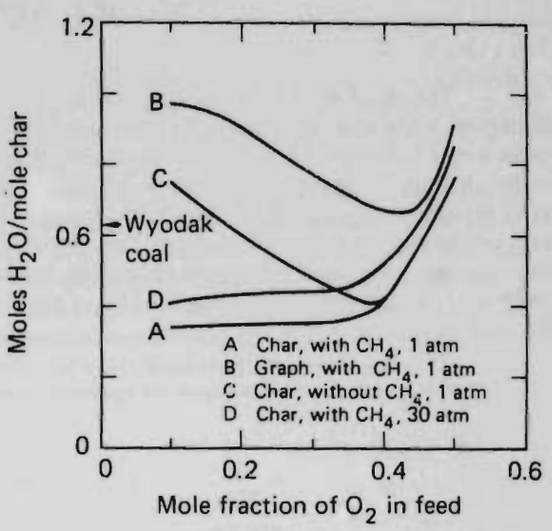

Fig. 10. ρ_{H_2O}/ρ_{char} **vs mole fraction** O_2 **in the feed for cases A through D in which** $W_D/W_R > 1$.

corresponding to the reaction front performances in cases A, B, C, and D.

For the initial physical picture of the process to be valid, the ratio W_D/W_R must be greater than, or equal to, one to ensure the presence of a hot char zone in equilibrium with the flowing gases in zone 2. A value less than one indicates that heat convected downstream from the reaction zone is insufficient to dry and pyrolyze the coal rapidly enough to supply the char requirements of the reaction zone. Figure 9 shows that for many of the cases the model calculates $W_D/W_R < 1$. We can only model systems with reaction-front properties that correspond to cases A and D for high oxygen-feed concentrations. However, if char behaves more like graphite (case B), the model predicts possible solutions over the entire range of oxygen concentration. In any case, the lower water decomposition and low methane concentrations reduce the effective carbon-carrying ability of the gas stream and thus slow the reaction front enough to always allow W_D to be greater than W_R.

Certainly, real systems with feed compositions and char thermodynamics that yield W_D/W_R less than one would perform as adequate gasification schemes. The above results only indicate that they would not operate with equilibrium compositions and temperature in the hot char zone. Rate processes would be important in these systems.

The primary parameter influencing the speed of the drying/pyrolysis front for a given gas flow rate is the total amount of water that must be removed from the wet coal. The reaction front speed, on the other hand, is related to the effective char density. Consequently, the ratio W_D/W_R for a given system is a function of the ratio of water in the coal to char formed from the coal. To determine how the model applies to coals of varying wetness we made a series of runs. We ran cases A, B, C, and D using the same assumptions as before except that we varied the amount of water in the coal. Figure 10 shows the results of these runs. The lines represent the conditions for which $W_D/W_R = 1$ as a function of oxygen feed concentration and coal wetness. Coal systems with water contents on or below any particular line would have calculated $W_D/W_R > 1$. This would indicate the possible presence of a hot char bank in equilibrium with the reacted gas mixture. For all four cases, coals with a mole ratio of water to char less than 0.33 would yield $W_D/W_R > 1$, and thus would represent (at least theoretically) possible system performance.

MODEL APPLICABILITY

The number of possible coal system properties and gasification operating conditions is large. However, we have established some general guide lines to indicate when the present model might apply. The three major variables that influence the W_D/W_R ratio are gas-feed composition, char thermodynamics, and water/char ratio. Figure 11 defines regions where the model could be at least theoretically applied. Boundaries are shown separating the figure into regions. Two of these boundaries represent a system where we assume the char to behave like β-graphite; the other two represent a system where the char is a more active species with thermodynamic properties estimated for the char $CH_{0.99}O_{0.016}$. (A system in which methane is suppressed acts much like that of the β-graphite system.) Boundaries for two pressure levels for each system are shown.

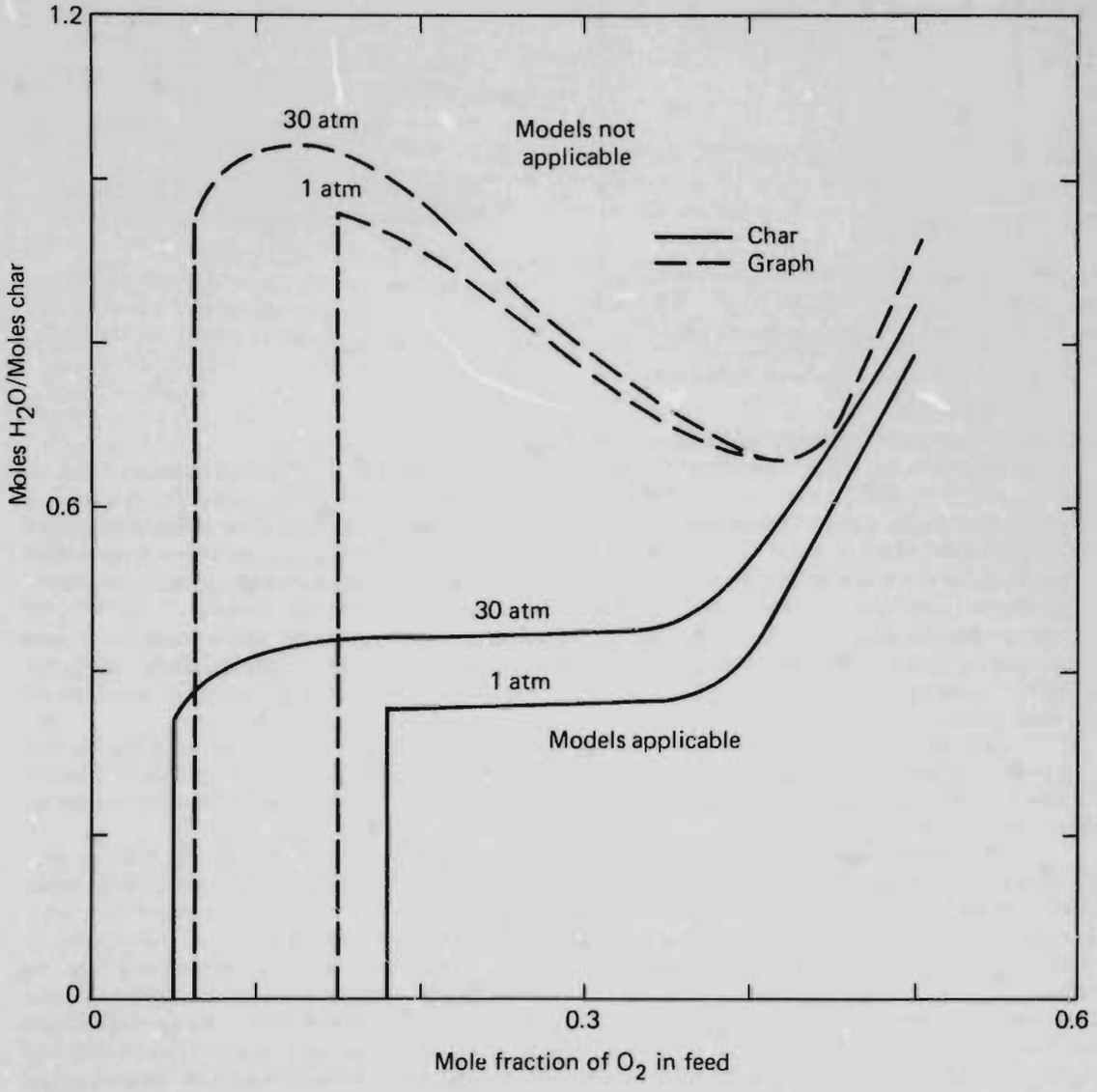

Fig. 11. Range of model applicability for char and graphite, ρ_{H_2O}/ρ_{char} vs mole fraction O_2 in the feed.

We used an additional factor, beyond the consideration of W_D/W_R ratio, to establish the boundaries shown in Fig. 11. While the portion of the boundaries with a horizontal component only require $W_D/W_R \geq 1$, the vertical boundaries are based on a temperature limitation. This limitation is an attempt to recognize the fact that equilibrium will not be achieved in the hot char zone if the calculated equilibrium temperature is not high enough to promote rapid reaction rates. In Fig. 11 we drew the vertical boundaries somewhat arbitrarily at the point where calculated hot char temperature was 900K.

For a given set of assumptions about char thermodynamics, the more the system is below and to the right of the corresponding boundary, the more likely an equilibrium description of the process would apply. In this regard, distance from the vertical boundary is more important because it represents a hotter char zone. Because most reaction rates are exponential in temperature, shifts to the right are accompanied by large increases in reaction rates in the hot char zone, and thus a greater probability of equilibrium. Increased distance below the more horizontal portion of the line represents larger values of W_D/W_R that translate into the development of larger hot char banks. This increase also increases residence time in the hot char zone as well as the chances of reaching equilibrium. However, it is not as important a factor as increased temperature.

THE STEAM CONDENSATION FRONT

The steam condensation front is a thermal front driven primarily by steam condensation. The only gas composition change allowed in the model across the front is the removal of steam from the gas phase accompanied by the appearance of a water phase. We assume the water phase to move out of the system at a rate identical to its generation rate.

The speed of movement of the front is primarily a function of initial solid temperature, average solid heat capacity, and water saturation of the gas arriving at the front. In all cases in which a reasonable amount of water is present in the system, the velocity of the steam condensation front is much greater than that of the other fronts. Figure 12 shows a typical result of the ratio of the steam condensation front velocity to that of both the drying/pyrolysis front and the reaction front. As with the other fronts, W_s is directly proportional to the injected gas flow rate and inversely proportional to the total density. Thus, for a given system the results in Fig. 11 are independent of total flow and total solid density. These particular results are for a char that we assume to behave as a β-graphite and for which the other input variable are those of case B with the additional assumption that $\rho_s = 0.224$ g/cm^3.

The movement of the steam front is not important in considerations of dry gas production or model applicability. However, it does allow us to estimate the arrival of steam at the production end of a system. The size of zone 3 (the region between the drying/pyrolysis and steam condensation fronts) may influence the overall pressure drop in the system.[7]

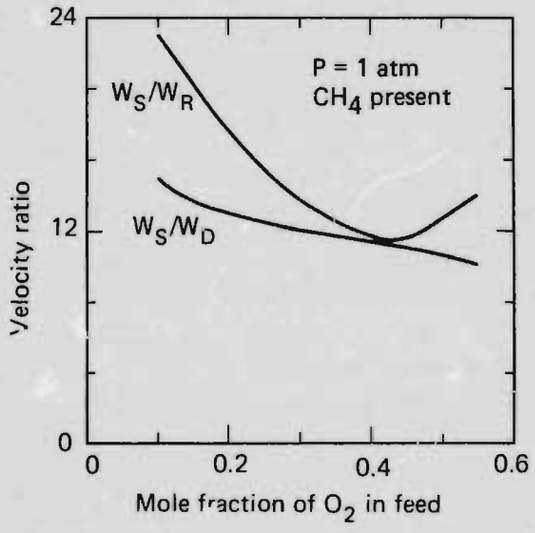

Fig. 12. W_s/W_D, W_s/W_R vs mole fraction O_2 in the feed for graphite.

ENERGY RECOVERY FROM REACTION ZONE

As an example of the results that can be obtained from the model, we calculated several parameters that are important in the optimization of the gasification process. We limited our consideration to products from the reaction zone for cases A, B, C, and D described in the earlier section.

Figure 13 shows calculated values of energy recovery in the gas as a function of oxygen feed concentration. The two sets of curves represent two methods of reporting the results. One is the ratio of the heat of combustion of the produced gas to the heat of combustion of the char consumed. The other relates the energy produced in the gas to the amount of oxygen required. The calculated energy recovery as a fraction of that in the char is nearly constant, decreasing slightly for higher oxygen-feed concentrations. This decrease results from the increase in waste-sensible heat at the higher oxygen concentration. Values of this ratio greater than one arise because steam feed is used in these examples and because heats of combustion of the product gases use water at 298K as the combustion product. A latter example, which accounts for the energy delivered into the system by the steam, always gives values of the heat-recovery ratio less than unity.

The gas heat of combustion per mole of oxygen feed shows more variation than the fraction recovery ratio. The trend for all four cases favors lower oxygen concentration. This trend is more pronounced in cases A and D where substantial amounts of methane are present. As more oxygen is used, the temperature increases and the methane drops rather rapidly. The dotted portion of the curves represent systems with a calculated char temperature less than 900K.

Another important consideration in gasification performance is the heating value of the dry produced gas. Figure 14 presents calculated dry gas heating values reported here as heats of combustion with final products at 25°C and water in the liquid form. Here we can see two different trends. The models using char as $CH_{0.09}O_{0.016}$ show a decrease in the gas heating value as oxygen concentration is increased. In these systems, this decrease corresponds to the decrease in methane at higher oxygen concentrations, as methane has a strong influence on the heating value. On the other hand, models using either graphite thermodynamics or those that suppress methane show the opposite trend. Because little or no methane is present in these systems, the CO_2 level is the dominant factor that controls the heating value. At higher oxygen concentrations, the CO_2 concentration decreases and thus the heating value increases.

Figure 15 compares the relative energy recovery using steam and water feed. For the steam calculations we assumed that the oxygen/steam feed was at its dew point. For the liquid calculations, we assumed that the oxygen/liquid water feed was at 300K. We completed this calculation for char that behaved like β-graphite at a pressure of 30 atm. For the steam feed case there are two bases for the relative energy recovery: a gross value based solely on the heating value of the produced gas at 298K, and a result calculated by subtracting from the gross gas heating value the energy required to generate the steam/oxygen feed from an oxygen/liquid water feed at 300K.

Even with the energy cost of generating the steam feed, Fig. 15 shows the net cold-gas energy recovery to be greater than that for the liquid feed over a considerable range of oxygen feed compositions. However, we have not considered any inefficiency in steam generation. Also, the greatest differences appear at low oxygen concentrations where the computed equilibrium temperatures are lowest and where the equilibrium assumption is most likely to break down. We found that the calculated results showed a similar trend at low pressure (1 atm), but for systems with substantial amounts of methane (e.g., the char of case A), we did not compute any difference in corrected steam-feed systems and liquid feed systems.

In all the above computations, the inclusion of the drying/pyrolysis front in the system would influence the results. Including the pyrolysis gas in the system generally softens trends in the computed energy recovery as a function of oxygen because it is more or less a constant additive term.

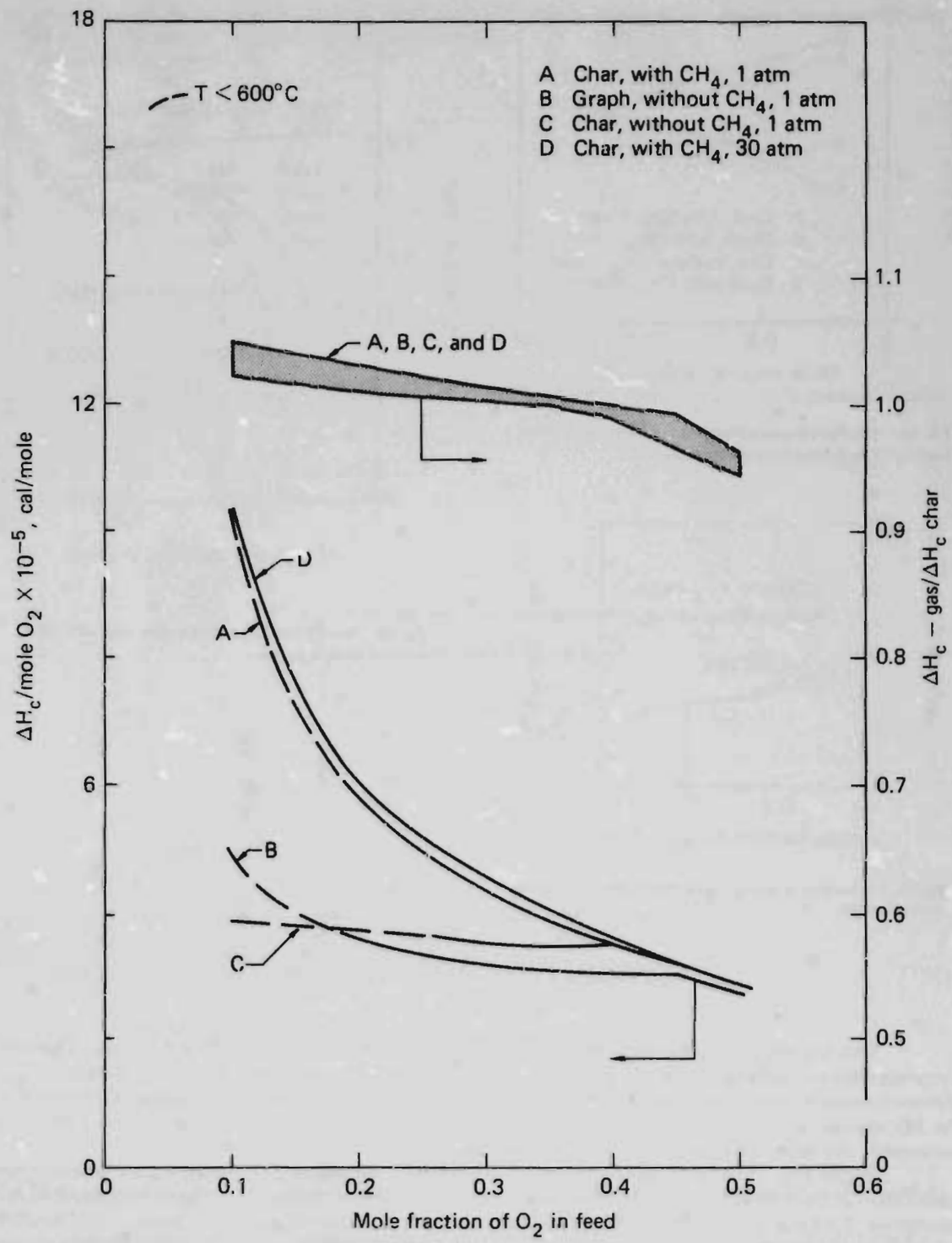

Fig. 13. Energy recovery from reaction zone vs mole fraction O_2 in the feed for cases A through D.

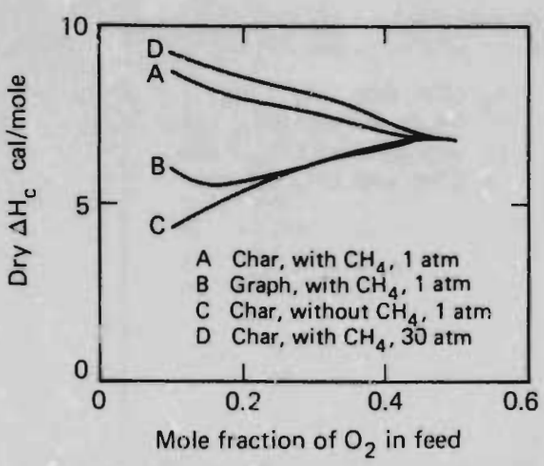

Fig. 14. Gas heat of combustion from reaction zone vs mole fraction O_2 in the feed for cases A through D.

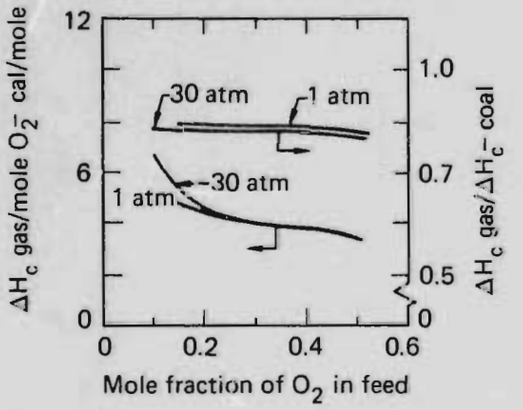

Fig. 16. Wyodak coal energy recovery assuming β-graphite char properties.

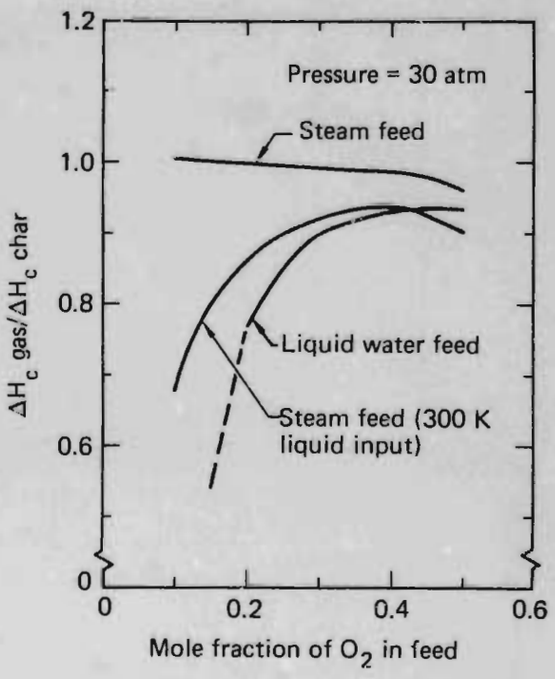

Fig. 15. Energy recovery from reaction zone with liquid water or steam injection.

WYODAK COAL CALCULATIONS

This section presents some examples of calculated results for a typical overall system. The coal properties and pryrolsis behavior are those of subbituminous coal from the Wyodak mine.[8,9] We assume the thermodynamic properties of the char to be those of β-graphite, primarily because they allow calculations on the full system to be carried out over a complete range of oxygen/steam ratios, not because they are necessarily the recommended values for the char obtained from this coal.

Figure 16 shows the calculated energy recovered in the form of combustible gas after the complete gasification of a quantity of coal. In this calculation we assume that the components treated here as tar do not contribute to the energy recovered. The results shown are not a function of the total amount of coal gasified because the results are presented in the form of ratios. We have only shown the results for which the hot char zone had a temperature of 900K. The fractional energy recovery is reasonably constant at 0.75 to 0.8 over the range of oxygen concentrations. The calculated ratio of total gas heat of combustion per mole of oxygen put into the system again shows more variation and again favors lower oxygen concentrations. The system pressure is shown to have little influence in the 1-to-30-atm range.

Figure 17 shows calculated velocities of each of the three fronts. We performed these calculations using a particular gas rate and set of solid concentrations:

$$G_1 = 1 \times 10^{-4} \ \frac{\text{g-mole}}{\text{cm}^2\ \text{s}}$$

$$\rho_1 = 0.415 \quad \text{g/cm}^3$$
$$\rho_2 = 0.238 \quad \text{g/cm}^3$$
$$\rho_4 = 0.224 \quad \text{g/cm}^3$$
$$\rho_5 = 0.0408 \quad \text{g/cm}^3$$

$$\rho = \sum_{i=1}^{5} \int_i = 0.918 \ \text{g/cm}^3$$

However, as we previously pointed out, velocities of each front for other flow rates and total densities can be calculated using

$$W_{new} = W_{old} \frac{G_{new}}{G_{old}} \frac{\rho_{old}}{\rho_{new}} .$$

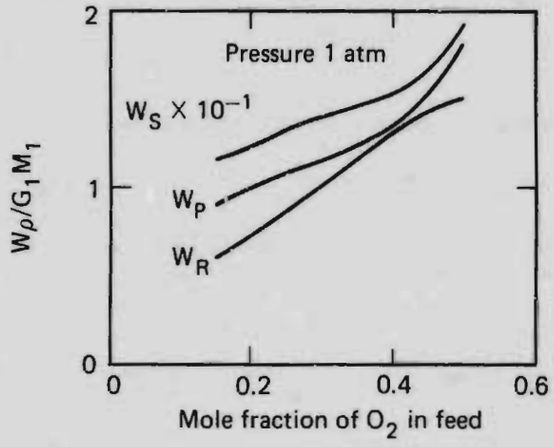

Fig. 17. Wyodak coal front velocities assuming β-graphite char properties.

The front velocities are shown for a system operating at 1 atm. The results are not strong functions of pressure.

As a final example, Figs. 18 and 19 show typical temperature, flow rate, and gas compositions for a single run as a function of time. The coal system used is that given above. In the results, we use dimensionless units so that the assumed length, absolute flow rate, and total solid density are not important. This particular run used an oxygen feed-stream mole fraction of 0.2. The rest of the feed stream was steamed at its dewpoint (432K); pressure was taken at 30 atm.

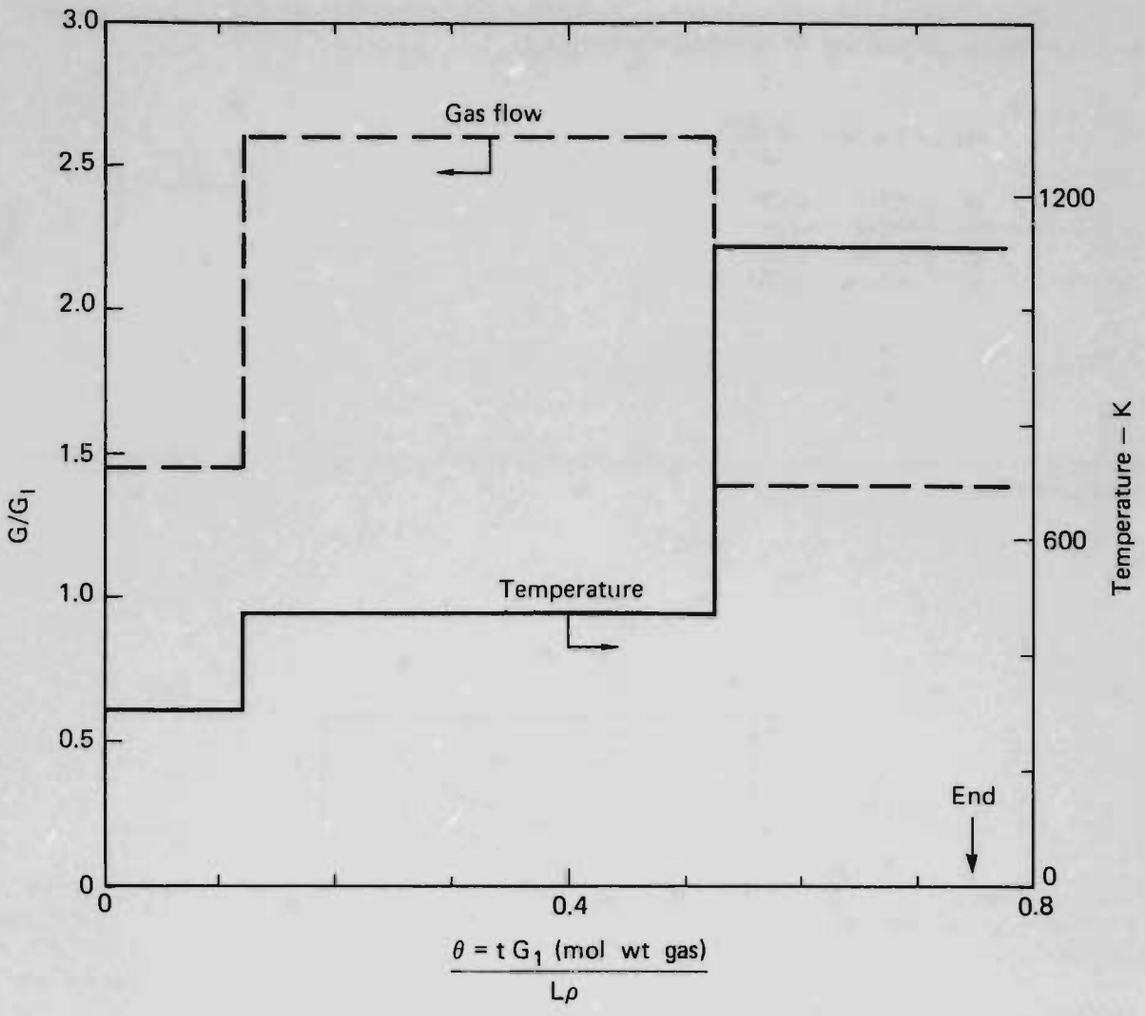

Fig. 18. Wyodak coal calculated gas flow and exit temperature assuming β-graphite char properties.

Exit gas flow rates and temperatures are shown in Fig. 18. The changes in the variables occur in stepwise curves that correspond to the arrivals of the three fronts at the exhaust end of the system. The change in exhaust gas composition also occurs in the same stepwise fashion as shown in Fig. 19.

The curves shown above as well as water production rates and gas heating value can be generated for any coal system and gas feed composition using the computer program given in Appendix B.

CONCLUSIONS

We have developed an equilibrium model to describe the *in situ* gasification process. The model is most appropriate for high oxygen-feed concentrations and for coals with a mole ratio of water to char

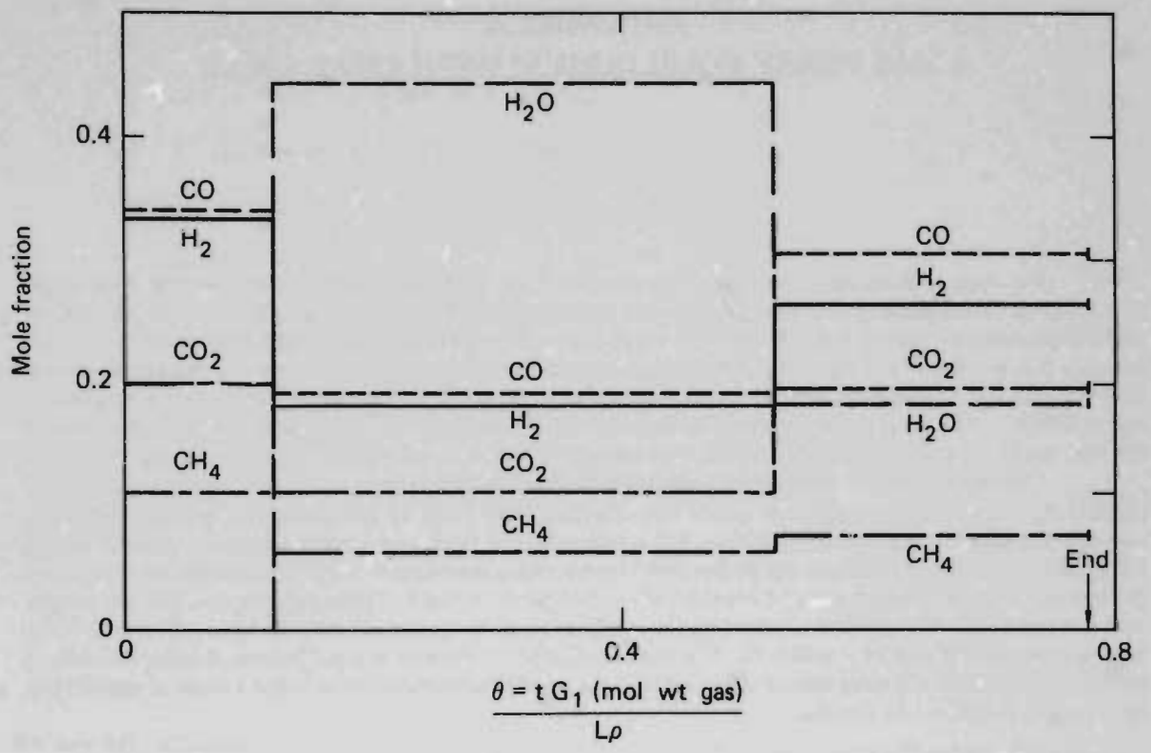

Fig. 19. Wyodak coal calculated gas exit composition assuming β-graphite char properties.

below 0.35. The usefulness of the model is limited by two considerations: inadequate temperature of the equilibrium gas hot-char mixture that would lead to rate limitations in reaching equilibrium, and the problem of generating enough energy in wet coal so that the predicted rate of drying exceeds the predicted rate of char consumption.

For systems where the model is applicable, the overall predicted energy recovery is rather insensitive to the process variables considered. The energy recovery per unit of oxygen consumed is somewhat more sensitive, and favors low oxygen-feed concentrations. Under certain assumptions the energy recovery per unit of oxygen may be higher for steam feeds than for water feeds, even when considering the energy debt incurred in generating the steam.

The calculated gas compositions obtained from this equilibrium model for a given coal system are influenced by the following (given in order of importance):

- Feed stream composition.
- Char thermodynamics and/or assumed presence of CH_4 in the hot char zone equilibrium.
- System operating pressure.

The pressure is much less important than the first two factors.

Future work should include an examination of alternate pseudo-equilibrium assumptions that can be applied to the hot char zone. Some assumption based on a minimum temperature and assumed water-gas-shift equilibrium might allow an extension of the range of applicability of the model.

APPENDIX A
A GAS PHASE EQUILIBRIUM WITH COAL CHAR

We want to determine the phase composition for a C,H,O,N system in equilibrium with a carbonaceous solid containing hydrogen and oxygen and represented by the formula CH_aO_b. For a Wyoming subbituminous coal[10] dried at 400 K, a ≃ 0.8, b ≃ 0.2. Pyrolysis of this coal at about 800K gives a coal char with a ≃ 0.4, b ≃ 0.1. Hyrdrogen and oxygen content continue to diminish as temperature increases, leading eventually to the formation of graphite. Graphitization, however, is a slow process requiring temperatures above 2000K.[11] For our present purposes, we assume that the composition and thermodynamic properties of the char are know and that it reaches equilibrium with a feed stream containing oxygen, steam, and nitrogen.

The phase rule tells us that there are 3 deg of freedom in a system containing four "components" (C,H,O,N) and two phases (gas and solid). The system is then fixed by specifying temperature, pressure, and two gas-phase composition variables. For composition variables we choose the molar ratio of steam/oxygen (s) and nitrogen/oxygen (n) in the feed stream. As a convenient basis for calculation, we take 1 mole of equilibrium product gas and consider the eight species noted in Table A-1. Oxygen will not be present at equilibrium in a significant amount and we list it as a trace species. The initial moles of oxygen in the feed stream are defined as y moles O_2. We require char to be present at equilibrium. A trace quantity is sufficient because it is a solid species. The initial amount of char required to produce 1 mole of equilibrium product gas is defined as z moles.

Table A-1. Initial and equilibrium species

Gas species	Initial moles	Equilibrium moles
O_2	y	Trace
CO	0	x_1
CO_2	0	x_2
H_2	0	x_3
CH_4	0	x_4
H_2O	sy	x_5
N_2	ny	x_6
Solid	y(1+s+n)	1
CH_aO_b	z	Trace

We have a total of eight unknowns listed in Table A-1, including the equilibrium composition variables x_1 to x_6, and the initial oxygen and char y and z. Five of these may be eliminated by the four-element balances and the definition $x_1 = 1$.

From a carbon balance,

$$z = x_1 + x_2 + x_4. \tag{A-1}$$

From an oxygen balance,

$$y = (x_1 + 2x_2 + x_5 - bz)/(2 + s). \tag{A-2}$$

From a nitrogen balance,

$$x_6 = \alpha y \tag{A-3}$$

where $\alpha = n/(2+s)$. (A-4)

Using the above with a hydrogen balance gives,

$$x_5 = C_0 - C_1x_1 - C_2x_2 - C_3x_3, \tag{A-5}$$

$$x_4 = D_0 - D_1x_1 - D_2x_2 - D_3x_3, \tag{A-6}$$

where:

$$C_0 = C_3/C_4, \tag{A-7}$$

$$C_1 = \{C_5[1+\alpha(1-b)] + \beta(1-b) + s/2\}/C_4, \tag{A-8}$$

$$C_2 = \{C_5[1+\alpha(2-b)] + \beta(2-b) + a/2\}/C_4, \tag{A-9}$$

$$C_3 = (C_5 - 1)/C_4, \tag{A-10}$$

$$C_4 = C_5(1+\alpha) - 1 + \beta, \tag{A-11}$$

$$C_5 = (2 - a/2 + \beta b)/(1-\alpha b), \tag{A-12}$$

$$\beta = s/(2+s), \tag{A-13}$$

$$D_0 = [1 - (1+\alpha)C_0]/D_4, \tag{A-14}$$

$$D_1 = [1 + \alpha(1-b) - (1+\alpha)C_1]/D_4, \tag{A-15}$$

$$D_2 = [1 + \alpha(2-b) - (1+\alpha)C_2]/D_4, \tag{A-16}$$

$$D_3 = [1 - (1+\alpha)C_3]/D_4, \tag{A-17}$$

$$D_4 = 1 - \alpha b. \tag{A-18}$$

We are left with three unknowns, x_1, x_2, and x_3 that require three independent reaction-equilibrium expressions involving the unknown species. For these we take:

(1) $CO + H_2O \gtrless CO_2 + H_2$, (A-19)

(2) $CH_aO_b + (1-b)\,CO_2 \quad (2-b)\,CO + \left(\frac{a}{2}\right) H_2$, (A-20)

(3) $CH_aO_b + \left(2 - \frac{a}{2} - b\right) H_2 \quad CH_4 + (b)H_2O$. (A-21)

Let K_1, K_2, and K_3 represent the equilibrium constants at a given temperature and pressure for the above three reactions and define

$$f_1 \equiv K_1 x_1 x_5 - x_2 x_3, \tag{A-22}$$

$$f_2 \equiv K_2 x_2^{1-b} - x_1^{2-b} x_3^{a/2}, \tag{A-23}$$

$$f_3 \equiv K_3 x_3 \quad 2 - \frac{a}{2} + b \quad - x_4 x_5^b. \tag{A-24}$$

The f_i defined above will be zero if the correct equilibrium compositions are chosen. We solve these equations by Newton-Raphson iteration. If we assume trial estimates of x_1, x_2, and x_3 on the jth iteration and call these x_k, we can form new estimates x_k^{j+1} by solving the linear equations

$$f_i + \sum_{k=1}^{3} \frac{\partial f_i}{\partial x_k}(x_k^{j+1} - x_k) = 0, \; i = 1,2,3. \tag{A-25}$$

The derivatives $\frac{\partial f_i}{\partial x_k}$ are available from Eqs. (A-22)–(A-24) with x_4 and x_5 replaced by Eqs. (A-5) and (A-6).

The above method of determining the equilibrium composition has been programmed for computer solution and converges quite rapidly. We have found that a single starting estimate,

$x_1 = 0.30,\ x_2 = 0.15,\ x_3 = 0.10,$

suffices over the range of conditions of interest to us:

$$500 \leq T \leq 2000\ \text{K},$$
$$1 \leq P \leq 100\ \text{Atm},$$
$$1 \leq s \leq 5,$$
$$0 \leq n \leq 4.$$

For an accuracy of within $\pm 10^{-5}$ in mole fraction, about five iterations are needed at 2000 K increasing to about 15 iterations at 500 K. Calculated results from this gas/char equilibrium computer program are discussed elsewhere in this report.

In our calculations we have not considered hydrocarbon gases other than methane on the grounds that they will not be present in significant amounts except at low temperatures where we do not expect equilibrium to prevail. One can argue that methane may not be present because the methane formation reaction is not rapid without a catalyst. A modification of the program to suppress methane is simply to set $K_3 = 0$ in Eq. (A-24). The calculation then proceeds smoothly to converge with methane suppressed.

A second modification allows for an arbitrary feed gas composition. Let

h_1 = moles initial CO/mole O_2, (A-26)

h_2 = moles initial CO_2/mole O_2, (A-27)

h_3 = moles initial H_2/mole O_2, (A-28)

h_4 = moles initial CH_4/mole O_2. (A-29)

One can show from element balances that the only change needed in the program is to redefine α and β [(Eqs. (A-4) and (A-13))] to read:

$$\alpha = n/\left[2+s+h_1(1-b) + h_2(2-b) - h_4 b\right], \tag{A-30}$$

$$\beta = \frac{s - h_1 a/2 - h_2 a/2 + h_3 + h_4(2-a/2)}{2 + s + h_1(1-b) + h_2(2-b) - h_4 b}. \tag{A-31}$$

APPENDIX B
COMPUTER PROGRAM

The solution of the equations outlined in the body of the report are obtained through the use of a FORTRAN computer code written to run on LLL's DCD 7600 computers. The program consists of a main program and a number of subroutines. Below is a short summary of the main functions carried out by each unit of the program.

MAIN Program

The main program is responsible for the overall control of the problem solution. It reads all required input data and initializes all parts of the program through subroutine calls. It also contains the overall logic for obtaining solutions around the drying/pyrolysis and the steam condensation front.

Subroutine TBURN

This subroutine is responsible for obtaining a solution to the equations written to describe the reaction front. It iterates the solution to obtain a consistent gas composition and gas temperature in the hot char zone as well as a reaction front velocity. It is called by MAIN.

Subroutine EQUILX

This subroutine calculates gas composition in equilibrium with excess coal char, given temperature pressure, and inlet gas composition. It is called by TBURN.

Function ROOT

This is a routine written by A. C. Hindmarsh[1] that is used by MAIN as a root-finding routine to calculate the steam-plateau temperature. It is called by MAIN.

Function FUN

This is a routine called by ROOT to establish the function, in this case a relation for the steam-plateau temperature, that ROOT is solving.

Subroutine HREACT

This subroutine contains the specifications of all the thermodynamic properties. Depending on the type of call, it calculates equilibrium constants or enthalpies of each of the chemical species at a particular temperature. The routine is initialized by a call form MAIN. It is called by MAIN, FUN, TBURN, and EQUILX.

Subroutine AIJ

This subroutine calculates stiochiometric coefficients required by the problem solution. It also specifies and/or calculates molecular weights for all species. It is called only once by MAIN.

Subroutine OUT

This subroutine calculates values for gas composition, gas flow rates, temperatures, and heating values existing in the system as a function of time. This routine is only entered if $W_D > W_R$. It is called by MAIN.

Subroutine PNT

This subroutine writes most of the output generated by the program. It is called by MAIN. Following is an example of a computer source program.

```
2
      PROGRAM EMOD (INPUT,EOUT,TAPE2=INPUT,TAPE3=EOUT)
C*****************************************************************
C
C    THIS PROGRAM WILL CALCULATE GAS COMPOSITIONS,TEMPERATURES,AND
C       VELOCITIES OF A GASIFICATION PROCESS DIVED INTO THREE ZONES.
C       THESE INCLUDE A REACTION ZONE,A STEAM PLATEAU ZONE,AND
C       A UNHEATED COAL ZONE.  EQUILIBRIUM RELATIONS ARE USED
C       TO CALCULATE THE REACTION ZONE GAS COMPOSITON AND TEMPREATURE
C       CONTSTRAINTED BE MATERIAL AND ENERGY BALANCE CONSIDERATIONS.
C       THE FORMATION OF METHANE IN THIS ZONE MAY BE SUPPRESSED IF
C       DESIRED.  GAS COMPOSITION IN THE STEAM PLATEAU ZONE IS FOUND
C       BY DETERMINING THE AMOUNT OF DRYING AND PYROLYSIS
C       ASSOCIALTED WITH THE COOLING OF THE HOT REACTION GAS.  FINALLY
C       IN THE UNHEATED ZONE THE GAS COMPOSITION IS CALCULATED BASED
C       ON REMOVAL OF THE APPROPRIATE AMOUNT OF WATER FROM
C       THE GAS PHASE.
C
C      A HEAT LOSS TERM MAY BE ASSOCIATED WITH THE REACTION ZONE
C      BY SPECIFYING QLOSS AND TLOSS, WHERE
C            HEAT LOSS=QLOSS(TREACTION-TLOSS)
C
C
C    INPUT:
C            A1-H/C RATIO IN CHAR
C            B1-O/C RATIO IN CHAR
C            A2-H/C RATIO IN COAL
C            B2-O/C RATIO IN COAL
C            A3-H/C RATIO IN TAR
C            ETA2-RATIO C-CHAR/C-COAL
C            ETA3-RATIO C-TAR/C-COAL
C            ROB-EFFECTIVE DENSITY OF COAL BED
C            FCOAL-WEITGHT FRACTION C IN DAF COAL
C            FH2OF-WEIGHT FRACTION FIXED WATER IN TOTAL SOLID
C            FH2OM-WEIGHT FRACTION MOBILE WATER IN TOTAL SOLID
C            FASH-WEIGHT FRACTION ASH IN TOTAL SOLLID
C            GI-FEED RATE (MOL/S)
C            TO-FEED TEMPERATURE (K)
C            TI-INITIAL COAL TEMPERATURE (K)
C            XL-BED LENGTH (CM)
C            PRES-SYSTEM PRESSURE (ATM)
C            FS-INJECTED STEAM/O2 RATIO
C            FN-INJECTED N2/O2 RATIO
C            FL-INJECTED LIQ H2O/O2 RATIO
C            GV(7)-.GT.O NO CH4 IN REACTION ZONE
C                  .LE.O CH4 IN REACTION ZONE
C            QLOSS-HEAT LOSS COEFICIENT IN REATION ZONE
C                        CAL/K/MOL OF PRODUCT GAS
C            TLOSS-TEMPERATURE PARAMETER IN REACTION ZONE HEAT LOSS (K)
C            THERM-.LE.O WILL USE A1 AND B1 FOR THERMODYNAMIC PROPERTIS
C                  OF EXCESS SOLID IN REACTION ZONE
C                  .GT.O WILL USE A4 AND B4 FOR THERMO PROPERTIES
C            A4-H/C RATIO FOR SPECIAL THERMO PROPERTIES
C            B4-O/C RATIO FOR SPECIAL THERMO PROPERTIES
C
C*****************************************************************
      EXTERNAL FUN
      COMMON/GIVE/ GV(20),TK(20)
      COMMON/ROOTCOM/ XX(20),YY(20)
      COMMON/PNT/IRUN,G,Y(8),TR,X(8),RO(5),TI,TS,U,V,W,XL,S,GC
     1   ,FW,FP,PRES,GI,GEND(100,12)
     2      ,BZ(5),HOB(3)
     3      ,YIG(9),QLOSS,TLOSS
      COMMON/PAR/A(13,8),WM(13),F(8),HF298(13),ROS(5),XXL,PX
      COMMON/STOIC1/A1,B1,A2,B2,A3,A4,B4,ETA1,ETA2,ETA3,WW,WA,ITHERM
      COMMON/ENTHAL/ ENT(13)
      COMMON/ONE/T1,T5,T6
      DIMENSION DUM(8)
      CALL CHANGE (5H+EQMD)
      LW=20000
      CALL CREATE (4HEOUT,LW,MIW)
```

```
      ERR=0.1
      READ (2,02) A1,B1,A2,B2,A3,ETA2,ETA3
      READ (2,02) ROB,FCOAL,FH2OF,FH2OM,FASH
      WW=FH2OM+FH2OF
      WA=FASH
      ETA1=FH2OF/FCOAL
      TS=300.
      CALL AIJ
      CALL HREACT (0,TS,TS,TS,DUM,PRES)
      SS=0.
      DO 10 J=1,8
   10 SS=SS+A(J,3)
      DO 11 J=1,8
   11 X(J)=A(J,3)/SS
      RO(1)=ROB*FCOAL
      RO(2)=RO(1)*WM(10)/WM(9)*A(10,3)
      RO(3)=ROB*FH2OM
      RO(4)=ROB*FH2OF
      RO(5)=ROB*FASH
      FP=SS*RO(1)/WM(9)
      FW=(RO(3)+RO(4))/18.
      IRUN=0
      CALL PNT(1)
  100 READ (2,02) GI,TO,TI,XL,PRES
      IF (GI.LT.0) GO TO 1000
      READ (2,02) FS ,FN,FL,GV(7),QLOSS,TLOSS
      READ (2,02) THERM,A4,B4
      ITHERM=THERM
      GV(4)=FS
      GV(6)=FL
      GV(5)=FN
      IRUN=IRUN+1
   01 FORMAT (I2,F10.0)
   02 FORMAT (8F10.0)
      GV(1)=RO(5)/RO(1)
      GV(2)=PRES
      GV(3)=TO
      GV(10)=FCOAL
      GV(11)=FH2OF
      GV(12)=FH2OM
      GV(13)=FASH
      DO 6000 I=1,8
 6000 YIG(I)=0.
      DEN=1.+FS+FN+FL
      YIG(1)=FN/DEN
      YIG(2)=1./DEN
      YIG(3)=FS/DEN
      YIG(9)=FL/DEN
      CALL PNT(2)
      CALL TBURN
      GC=TK(1)+TK(2)+TK(4)
      Y(1)=TK(6)
      Y(2)=0.
      Y(3)=TK(5)
      Y(4)=TK(3)
      Y(5)=TK(4)
      Y(6)=TK(1)
      Y(7)=TK(2)
      Y(8)=0.
      TR=TK(7)
      G=GI*TK(8)
      CALL HREACT (3,TR,TR,TR,DUM,PRES)
      HG=0.
      DO 20 J=1,8
   20 HG=HG+Y(J)*ENT(J)
      T1=G*HG
      T5=RO(2)*ENT(10)/WM(10)
      T6=RO(5)*ENT(13)/WM(13)
      J=16
      XX(1)=TS
      XX(2)=0.99*TS
C
CC    USE ROOT SUBROUTINE TO FIND ZERO OF FUNCTION FUN.  THIS
CC         WILL YIELD THE STEAM PLATEUA TEMPERATURE.
C
      TS=ROOT (FUN,ERR,ERR,J)
      CALL HREACT (3,TS,TS,TS,DUM,PRES)
      HG=0.
      DO 30 J=1,8
   30 HG=HG+Y(J)*ENT(J)
      T2=G*HG
      HG=0.
      DO 40 J=1,8
   40 HG=HG+X(J)*ENT(J)
      T3=FP*HG
       T4=FW*ENT(3)
      T7=RO(5)*ENT(13)/WM(13)
      T8=RO(1)*ENT(9)/WM(9)
      T9 =RO(4)*ENT(12)/WM(12)
      T10=RO(3)*ENT(11)/WM(11)
      T11=RO(2)*ENT(10)/WM(10)
```

```
      V=(T1-T2)/(T3+T4+T5+T6-T7-T8-T5-T10)
      P=V*FP
      GDR=G*(1.-Y(3))
      PDR=P*(1.-X(3))
      VPR=EXP(12.61-4690./TI)
      S=VPR/(PRES-VPR)
      R8=T8
      R10=T7
      R12=T9
      R14=T10
      WG=S*(GDR+PDR)
      WV=Y(3)*G+X(3)*P+V*FW
      WLG=WV-WG
      R1=T2-Y(3)*G*ENT(3)
      R3=T3*V-X(3)*P*ENT(3)
      R5=WV*ENT(3)
      CALL HREACT(3,TI,TI,TI,DUM,PRES)
      HG=-Y(3)*ENT(3)
      DO 50 J=1,8
   30 HG=HG+Y(J)*ENT(J)
      R2=G*HG
      HG=-X(3)*ENT(3)
      DO 60 J=1,8
   60 HG=HG+X(J)*ENT(J)
      R4=P*HG
      R6=WG*ENT(3)
      R7=WLG*ENT(11)
      R9=RG(1)*ENT(9)/WM(9)
      R11=RG(5)*ENT(13)/WM(13)
      R13=RG(4)*ENT(12)/WM(12)
      R15=RG(3)*ENT(11)/WM(11)
C
CC    BASED ON CALCULATED STEAM TEMPERATURE AND ON GAS FLOW
CC        RATES FIND THE DRYING/PYRILYSIS AND THE STEAM
CC        CONDENSATION FRONT VELOCITIES.
C
      U=(R1-R2+R3-R4+R5-R6-R7)/(R8-R9+R10-R11+R12-R13+R14-R15)
      W=G*GC*WM(10)/RG(2)
      FG2=1./(1.+GV(4)+GV(5)+GV(6))
      GEND(IRUN,1)=GV(4)
      GEND(IRUN,2)=FG2
      GEND(IRUN,3)=PRES
      GEND(IRUN,4)=TG
      GEND(IRUN,5)=TR
      GEND(IRUN,6)=TS
      GEND(IRUN,7)=W
      GEND(IRUN,8)=V
      GEND(IRUN,9)=U
      GEND(IRUN,10)=V/W
      HCHAR=HF298(10)+94052.+A1/2.*68317.
      BZ(1)=Y(4)*68317.+Y(5)*212800.+Y(6)*67636.
      BZ(2)=BZ(1)/HCHAR/GC
      FTG=GV(4)+GV(6)+1.+GV(5)
      TT=GV(3)
      CALL HREACT (3,TT,TT,TT,DUM,PRES)
      HGFF=GV(4)/FTG*ENT(3)+GV(6)/FTG*ENT(11)+1./FTG*ENT(2)
     1    +GV(5)/FTG*ENT(1)
      HGFF=HGFF-1./FTG*13.-(GV(4)/FTG+GV(6)/FTG)*(-68300.)-GV(5)/FTG*13.
      BZ(3)=(BZ(1)*G/GI-HGFF)
      BZ(4)=BZ(3)/GC/HCHAR*GI/G
      BZ(3)=BZ(3)/GEND(IRUN,2)
      BZ(1)=BZ(1)*G/GI/GEND(IRUN,2)
      BZ(5)=HGFF
      IF (V.LT.W) GO TO 70
      CALL OUT
   70 CONTINUE
      CALL PNT(3)
      GO TO 100
 1000 CONTINUE
      CALL PNT (4)
      CALL EXIT
 4000 FORMAT (5(2X,E12.3))
      END
      SUBROUTINE TBURN
C*****************************************************************
C
C     CALCULATES THE REACTION ZONE TEMPERATURE.
C
C*****************************************************************
      COMMON/GIVE/ GV(20),TK(20)
      COMMON/ISIG/ NXCH4
      COMMON/STOIC1/A1,B1,A2,B2,A3,A4,B4,ETA1,ETA2,ETA3
     1   ,XXX,XXXX
      COMMON /CAP/ C(13,5)
      COMMON/PAR/A(13,8),WM(13),F(8),HF298(13),ROS(5),XL,PO
      COMMON /ENTHAL/ HI(13)
      DIMENSION X(6) ,ID(12),HIO(13),HR(8)
      TG=2500.
      IF ((FS+FL).LT.1.5) TG=5000.
      DT=-100.
```

```
      T=TO-DT
      DTO=DT
      NT=50
      NLOOK=-1
      GP=GV(1)
      P=GV(2)
      NXCH4=GV(7)+0.001
      FS=GV(4)
      FN=GV(5)
      TO=GV(3)
      FL=GV(6)
      FCOAL=GV(10)
      FH2OF=GV(11)
      FH2OM=GV(12)
      FASH=GV(13)
C  FT IS TOTAL H2O/O2 RATIO
      FT=FL+FS
      TOUT=GV(8)
      NTRY=0
      NLAST=0
      LAP=0
      DO 700 M=1,NT
      LAP=LAP+1
      T=T+DT
      CALL EQUILX (T,P,FT,FN,X,Z,Y,PF)
C
CC  MATERIAL BALANCE-BASIS ONE MOLE PRODUCT GAS
C
CC  SOLIDS IN
CC        CHAR AND ASH
C
      CHAR=Z
      ASH=CHAR/ETA2*WM(9)/FCOAL*FASH/WM(13)
CC  INPUT GAS LIQUIDS
C        O2,H2O(G),H2O(L),N2
      O2IN=Y
      XN2IN=Y*FN
      H2OGIN=Y*FS
      H2OLIN=Y*FL
CC  GAS PRODUCTS OUT
C    H2O,H2,CO,CO2,CH4
      COOT=X(1)
      CO2OT=X(2)
      H2OT=X(3)
      CH4OT=X(4)
      H2OOT=X(5)
      XN2OT=X(6)
CC
CC   SOLID OUT
C     ASH EQUAL TO ASH IN
C
CC  ENERGY BALANCE
      CALL HREACT (3,TO,TO,TO,HR,PRES)
      HIN=O2IN*HI(2)+XN2IN*HI(1)+H2OGIN*HI(3)+H2OLIN*HI(11)
      HOUT=ASH*HI(13)
      CALL HREACT(3,T,T,T,HR,PRES)
      HIN=HIN+CHAR*HI(10)+ASH*HI(13)
      HOUT=HOUT+COOT*HI(6)+CO2OT*HI(7)+H2OT*HI(4)+CH4OT*HI(5)
     *     +H2OOT*HI(3)+XN2OT*HI(1)+QLOSS*(T-TLOSS)
      IF (HIN-HOUT) 700,750,400
  400 IF (NTRY) 750,420,450
  420 NTRY=1
      T=T-DT
      DT=DTO/10.
      GO TO 700
  450 IF (NLAST) 750,460,750
  460 NLAST=1
      T=T-DT
      DT=DTO/100.
  700 CONTINUE
  750 CONTINUE
C
CC   IF LAP.LT.NT THEN SUCCESSFULLY FOUND BURN TEMPERATURE AND
CC        GAS COMPOSITION
C
      IF (LAP.LE.NT) GO TO 760
      WRITE (3,1000) LAP,T
 1000 FORMAT (1X,30HNO SOLUTION FOUND IN TBURN    ,I5,5X,F8.2)
      CALL EXIT
  760 CONTINUE
      DO 790 L=1,6
  790 TK(L)=X(L)
      TK(7)=T
      TK(8)=PF
  800 CONTINUE
      RETURN
      END
      SUBROUTINE EQUILX(T,P,FS,FN,X,Z,Y,PF)
```

```
C*****************************************************************************
C
C     CALCULATES EQUILIBRIUM GAS COMPOSITION AT A PRESSURE OF P
C          AND A TEMPERATURE OF T.  EXCESS SOLID CHAR IS ASSUMED
C          TO BE PRESENT.
C
C     INPUTS:   T-TEMPERATURE (K)
C               P-PRESSURE (ATM)
C               FS-RATIO H2O TO O2 IN FEED
C               FN-RATIO OF N2 TO O2 IN FEED
C               NXCH4-IF.LE.0 SUPPRESSES CH4 IN REACTION ZONE BY
C                     SETTING EK3=EK(7)=0.
C                     IF .GT.0 CH4 ASSUMED PRESENT IN REACTION ZONE.
C
C     OUTPUTS: X(K)-PROD. GAS COMPOSITION
C                    1-CO
C                    2-CO2
C                    3-H2
C                    4-CH4
C                    5-H2O
C                    6-N2
C              Z-MOLES OF CHAR (ONE CARBON) REACTED PER MOLE GAS PRODUCED
C              Y-MOLES OF O2 PER MOLE OF PRODUCT GAS
C              PF-MOLES OF PRODUCT GAS PER MOLE OF FEED
C
C*****************************************************************************
      COMMON/ISIG/ NXCH4
      COMMON/STOIC1/A1,B1,A2,B2,A3,A4,B4,ETA1,ETA2,ETA3
     1   ,XXX,XXXX
      DIMENSION EK(8),X(6)
      DIMENSION DF(3,3),F(3),DX(3),BS(9),RS(3),WS(3),VS(3)
      AH=0.5*A1
      ALFA=FN/(2.0+FS)
      BETA=FS/(2.0+FS)
      C5=(2.0-AH+BETA*B1)/(1.0-ALFA*B1)
      C4=C5*(1.0+ALFA)-1.0+BETA
      CO=C5/C4
      C1=(C5*(1.0+ALFA*(1.0-B1))+BETA*(1.0-B1)+AH)/C4
      C2=(C5*(1.0+ALFA*(2.0-B1))+BETA*(2.0-B1)+AH)/C4
      C3=(C5-1.0)/C4
      D4=1.0-ALFA*B1
      DO=(1.0-(1.0+ALFA)*CO)/D4
      D1=(1.0+ALFA*(1.0-B1)-(1.0+ALFA)*C1)/D4
      D2=(1.0+ALFA*(2.0-B1)-(1.0+ALFA)*C2)/D4
      D3=(1.0-(1.0+ALFA)*C3)/D4
      DUM2=1.0-B1
      DUM3=2.0-B1
      DUM4=2.0-AH+B1
      CALL HREACT (2,T,T,T,EK,P)
      EK1=EK(8)
      EK2=EK(5)/(EK(8)**DUM2)
      EK3=0.0
      IF (NXCH4.LE.0) EK3=EK(7)
      EPS=1.0E-06
      EPSH2=0.001
      X1=0.30
      X2=0.15
      X3=0.10
      X4=0.01
      X5=0.01
      NTRY=0
   30 CONTINUE
      LAP=1
      DO 50 J=1,30
      IF(J-1) 44,44,40
   40 CONTINUE
      X1=X1+DX(1)
      X2=X2+DX(2)
      X3=X3+DX(3)
      X4=DO-D1*X1-D2*X2-D3*X3
      X5=CO-C1*X1-C2*X2-C3*X3
      IF(X3) 42,42,44
   42 X3=EPSH2
   44 CONTINUE
      DUM=X3**AH
      F(1)=-EK1*X1*X5+X2*X3
      DF(1,1)=EK1*(X5-X1*C1)
      DF(1,2)=-EK1*X1*C2-X3
      DF(1,3)=-EK1*X1*C3-X2
      F(2)=-EK2*X2**DUM2+X1**DUM3*DUM
      DF(2,1)=-DUM3*X1**DUM2*DUM
      IF(X2) 440,440,445
  440 DF(2,2)=EK2
      GO TO 450
  445 DF(2,2)=DUM2*EK2*X2**(-B1)
  450 CONTINUE
      DF(2,3)=-AH*X1**DUM3*DUM/X3
      IF(X5) 460,460,465
  460 F(3)=-EK3*X3**DUM4+X4
      DF(3,1)=D1
      DF(3,2)=D2
```

```
      DF(3,3)=DUM4*EK3*X3**(DUM4-1.0)+D3
      GO TO 470
  465 F(3)=-EK3*X3**DUM4+X4*X5**B1
      DF(3,1)=B1*C1*X4*X5**(-DUM2)+D1*X5**B1
      DF(3,2)=B1*C2*X4*X5**(-DUM2)+D2*X5**B1
      DF(3,3)=DUM4*EK3*X3**(DUM4-1.0)+B1*C3*X4*X5**(-DUM2)+D3*X5**B1
  470 CONTINUE
      CALL MLR(3,3,3,DF,F,DX,BS,RS,WS,VS)
      IF(ABSF(DX(1))+ABSF(DX(2))-EPS)      60,60,49
   49 LAP=LAP+1
      IF(X1   +DX(1)) 501,502,502
  501 DX(1)=-X1
  502 CONTINUE
      IF(X2   +DX(2)) 503,504,504
  503 DX(2)=-X2
  504 CONTINUE
      IF(X3   +DX(3)) 505,505,50
  505 DX(3)=-X3   +EPSH2
   50 CONTINUE
   60 CONTINUE
      X6=ALOG((1.0-B1)*X1+(2.0-B1)*X2-B1*X4+X5)
      IF(LAP-30) 70,70,65
   65 WRITE(3,950) T,P,FS,FN
   70 CONTINUE
      X(1)=X1
      X(2)=X2
      X(3)=X3
      X(4)=X4
      X(5)=X5
      X(6)=X6
      DO 200 J=1,6
      IF(X(J)) 100,200,200
  100 IF(X(J)+1.0E-05) 120,180,180
  120 IF(NTRY) 130,130,140
  130 NTRY=1
      X1=0.1
      X2=0.1
      X3=0.1
      X4=0.10
      X5=0.1
      GO TO 30
  140 WRITE(3,952) T,P,FS,FN,X(J)
  180 X(J)=0.0
  200 CONTINUE
      SUM=0.0
      DO 300 J=1,6
  300 SUM=SUM+X(J)
      SUM=1.0/SUM
      DO 400 J=1,6
  400 X(J)=X(J)*SUM
      Z=X(1)+X(2)+X(4)
      Y=(DUM2*X(1)+DUM3*X(2)-B1*X(4)+X(5))/(2.0+FS)
      IF(Z) 620,620,630
  620 WRITE(3,954)
      Z=1.0
  630 IF(Y) 640,640,650
  640 WRITE(3,956)
      Y=1.0
  650 CONTINUE
      PF=1.0/(Y*(1.0+FS+FN))
      RETURN
  950 FORMAT("30 LAPS EXCEEDED IN EQUIL",10X,4E15.4//)
  952 FORMAT("NEGATIVE X(J) IN EQUIL",10X,5E15.4//)
  954 FORMAT("Z IS NEG OR ZERO, SET=1.0")
  956 FORMAT("Y IS NEG OR ZERO, SET=1.0")
      END
      FUNCTION ROOT(FUNC,DX,DY,J)
C*************************************************************************
C
C     ROOT FINDING SUBROUTINE.  FINDS THE ZEROS OF FUNCTION FUNC.
C
C*************************************************************************
      COMMON/ROOTCOM/X(20),Y(20)
      DIMENSION C(20),P(20)
      JMAX=J$    J=2
      DIF=X(1)-X(2)$    IF(DIF)1,11,1
1     Y(1)=FUNC(X(1))$    Y(2)=FUNC(X(2))
      XNOW=X(1)
      IF(Y(1)-Y(2))2,11,2
2     C(2)=DIF/(Y(1)-Y(2))
      P(2)=-Y(1)
      GO TO 6
3     R=1.$    S=0.
      JJ=J-1
      DO 4 K=2,JJ
      S=S+C(K)*R
4     R=P(K)+(YNOW-Y(K))*R
      P(J)=-P(J-1)*Y(J-1)
      Q=P(J)+YNOW*R
      IF(Q)5,11,5
5     C(J)=-YNOW*S/Q
```

```
6       DIF=C(J)*P(J)
        J=J+1$    X(J)=XNOW=XNOW+DIF
        IF(DIF)8,7,8
7       Y(J)=Y(J-1)
        IF(ABSF(Y(J))-DY)13,11,11
8       Y(J)=YNOW=FUNC(XNOW)
        IF(ABSF(DIF)-DX)9,10,10
9       IF(ABSF(YNOW)-DY)13,10,10
10      IF(J-JMAX)3,12,12
11      ROOT=X(J)$    J=0$    RETURN
12      ROOT=X(J)$    J=-1$    RETURN
13      ROOT=X(J)$    RETURN
        END
        FUNCTION FUN(TST)
C*****************************************************************
C
C    FUNCTION USED BY ROOT.  ZERO OF FUNCTION WILL YIELD STEAM
C         PLATEAU TEMPERATURE
C
C*****************************************************************
        COMMON/PNT/IRUN,G,Y(8),TR,X(8),RO(5),TI,TS,U,V,W,XL,S,GC
       1   ,FW,FP,PRES,GI,QEND(100,12)
        COMMON/PAR/A(13,8),WM(13),F(8),HF298(13),ROS(5),XXL,PX
        COMMON/ENTHAL/ ENT(13)
        COMMON/ONE/T1,T5,T6
        DIMENSION DUM(8)
        CALL HREACT(3,TST,TST,TST,DUM,PRES)
        HG=0.
        DO 30 J=1,8
   30   HG=HG+Y(J)*ENT(J)
        T2=G*HG
        HG=0.
        DO 40 J=1,8
   40   HG=HG+X(J)*ENT(J)
        T3=FP*HG
        T4=FW*ENT(3)
        T7=RO(5)*ENT(13)/WM(13)
        T8=RO(1)*ENT(9)/WM(9)
        T9 =RO(4)*ENT(12)/WM(12)
        T10=RO(3)*ENT(11)/WM(11)
        T11=RO(2)*ENT(10)/WM(10)
        V=(T1-T2)/(T3+T4+T5+T6-T7-T8-T9-T10)
        PP=PRES*(V*FW+Y(3)*G+X(3)*V*FP)/(G+V*FP+V*FW)
        FUN=TST-4690./(12.61-ALOG(PP))
        RETURN
        END
        SUBROUTINE HREACT (N,T,TG,TS,HR,P)
C*****************************************************************
C
C    THIS SUBROUTINE CALCULATES ALL THERMODYNAMIC PROPERTIES.
C         ENTHALPY OF CHAR AND COAL AS WELL ENTROPY GIVEN AS
C         A FUNCTION OF HYDROGEN AND OXYGEN CONTENT.
C           H AND O CONTENT ARE ZERO THEN PROPERTIES ARE THOSE OF
C         GRAPHITE.  CONSTANTS A4 AND B4 WILL BE USED TO CALCILATE
C         THE THERMODYNAMIC PROPERTIES OF CHAR IF ITHERM IS .GT. 0.
C         CHAR IS THE SUBSTANCE ASSUMED TO BE IN EXCESS IF THE
C         REACTION ZONE EQUILIBRIUM PROBLEM.  NOTE HOWEVER THAT IN
C         MATERIAL BALANCE CONSIDERATIONS THE A2 B2 STOICHIOMETRY
C         OF CHAR WILL ALWAYS BE RETAINED.
C
C        INPUTS: N-.EQ.0 FOR INTIALIZATION
C                  .EQ.1 CALCULATES HEATS OF REACTION
C                  .EQ.2 CALCULATES  EQUILIBRIUM CONSTANTS
C                  .EQ.3 CALCULATES ENTALPIES OF ALL SPECIES
C                T-TEMPERATURE AT WHICH TO CALCULATE EQUILIBRIUM CONSTANTS
C                    AND HEATS OF REACTION
C                TG-GAS TEMPERATURES USED TO CALCULATE GAS SPECIES
C                  ENTHALPIES
C                TS-TEMPERATURE USED TO CALCULATE SOLID SPECIES ENTHALPIES.
C             A1,A2,A3,A4,B1,B2,B3,B4-STOICHIOMETRIC PARAMETERS
C                  FOR SOLID SPICIES
C             A(I,J)-STOICHIOMETRIC COEFICIENTS FOR REACTIONS
C   OUTPUTS: HR(K)-FOR N.NE.2 HEATS OF REACTION
C              HR(K)-FOR N.EQ.2 EQYILIBRIUM CONSTANTS
C               HI(K)-ENTALPY OF SPEICIES K FOR N.EQ.3
C
C*****************************************************************
        COMMON/PAR/A(13,8),WM(13),F(8),HF298(13),ROS(5),XL,PO
```

```
      COMMON/STOIC1/A1,B1,A2,B2,A3,A4,B4,ETA1,ETA2,ETA3
     1   ,XXX,XXXX,ITHERM
      COMMON /CAP/ C(13,5)
      COMMON /ENTHAL/ H1(13)
      DIMENSION HR(8),D(8,5)
      DIMENSION HRO(8),EO(8),E(8,6)
      DIMENSION S298(13),G(8),PE(8)
      DIMENSION TOXK(5),TDF(5)
      IF(N.EQ.1) GO TO 800
      IF(N.EQ.2) GO TO 700
      IF(N.EQ.3) GO TO 900
C-------- INITIALIZATION ----------------
C        S298(I) IS ABSOLUTE ENTROPY, CAL/MOL-K, AT 298.15 K
C        HF298(I) IS ENTHALPY OF FORMATION, CAL/MOL, AT 298.15 K
C        C(I,K) ARE HEAT CAPACITY COEFFICIENTS, CP IN CAL/MOL-K
      DO 100 I=1,13
      S298(I)=0.0
      HF298(I)=0.0
      DO 100 K=1,5
  100 C(I,K)=0.0
C        N2
      C(1,1)=6.524
      C(1,2)=1.250E-03
      C(1,3)=-0.001E-06
C        O2
      S298(2)=49.00
      C(2,1)=6.148
      C(2,2)=3.102E-03
      C(2,3)=-0.923E-06
C        H2O
      S298(3)=45.106
      HF298(3)=-57798.
      C(3,1)=7.256
      C(3,2)=2.298E-03
      C(3,3)=0.283E-06
C        H2
      S298(4)=31.21
      C(4,1)=6.947
      C(4,2)=-0.200E-03
      C(4,3)=0.481E-06
C        CH4
      S298(5)=44.48
      HF298(5)=-17895.
      C(5,1)=3.381
      C(5,2)=18.044E-03
      C(5,3)=-4.300E-06
C        CO
      S298(6)=47.21
      HF298(6)=-26417.
      C(6,1)=6.420
      C(6,2)=1.665E-03
      C(6,3)=-0.196E-06
C        CO2
      S298(7)=51.07
      HF298(7)=-94054.
      C(7,1)=6.214
      C(7,2)=10.396E-03
      C(7,3)=-3.545E-06
C        TAR (1,3,5 TRIMETHYLBENZENE, C9H12)
      S298(8)=92.15
      HF298(8)=-3840.
      C(8,1)=20.1
      C(8,2)=0.0532
C        DAF COAL
      S298(9)=1.359+3.17*A2+4.0*B2
      HF298(9)=-8710.
      C(9,1)=-1.5865+A2*0.87*1.008+B2*0.36*16.0
      C(9,2)=1.58050E-02
      C(9,3)=-1.38974E-05
      C(9,4)=5.7677E-09
      C(9,5)=-9.2008E-13
C        CHAR
      AT=A1
      BT=B1
      IF (ITHERM.LE.0) GO TO 105
C
CC  SET TO SPECIAL THERMO PARAMETERS
C
      AT=A4
      BT=B4
  105 CONTINUE
      S298(10)=1.359+3.17*AT+4.0*BT
      IF(AT) 120,120,110
  110 HF298(10)=2600.-68000.*BT
  120 CONTINUE
      C(10,1)=-1.5865+AT*0.87*1.008+BT*0.36*16.0
      C(10,2)=C(9,2)
      C(10,3)=C(9,3)
      C(10,4)=C(9,4)
      C(10,5)=C(9,5)
C        H2O(L)
```

```
      HF298(11)=-68317.
      C(11,1)=1.03*WM(11)
C        H2O(F)
      HF298(12)=HF298(11)
      C(12,1)=C(11,1)
C        ASH
      C(13,1)=0.142*WM(13)
      C(13,2)=1.4E-04*WM(13)
C
      DO 200 J=1,8
      DO 200 K=1,5
  200 D(J,K)=0.0
      DO 210 J=1,8
      DO 210 K=1,5
      DO 210 I=1,13
  210 D(J,K)=D(J,K)+A(I,J)*C(I,K)/FLOATF(K)
      TO=298.15
      DO 320 J=1,8
      HRO(J)=0.0
      DO 300 K=1,5
  300 HRO(J)=HRO(J)-D(J,K)*TO**K
      DO 310 I=1,13
  310 HRO(J)=HRO(J)+A(I,J)*HF298(I)
  320 CONTINUE
C
      R=1.9872
      DO 420 J=4,8
      EO(J)=HRO(J)/TO-D(J,1)*LOGF(TO)
      DO 400 K=2,5

  400 EO(J)=EO(J)-D(J,K)*TO**(K-1)/FLOATF(K-1)
  420 EO(J)=EO(J)/R
      DO 520 J=4,8
      E(J,1)=-HRO(J)/R
      E(J,2)=D(J,1)/R
      DO 500 K=3,6
  500 E(J,K)=D(J,K-1)/(FLOATF(K-2)*R)
  520 CONTINUE
      T=TO
      T2=TO*TO
      T3=T2*TO
      T4=T3*TO
      T5=T4*TO
      DO 650 J=4,8
      HR(J)=HRO(J)+D(J,1)*T+D(J,2)*T2+D(J,3)*T3+D(J,4)*T4+D(J,5)*T5
      G(J  )=HR(J)/TO
      PE(J  )=0.0
      DO 600 I=2,10
  600 G(J)=G(J)-A(I,J)*S298(I)
      DO 620 I=2,7
  620 PE(J)=PE(J)-A(I,J)
  650 G(J  )=G(J  )/R
      DO 660 K=1,5
  660 TOXK(K)=TO**K
      RETURN
C
C------- CALCULATES INTEGRAL OF DELH/RT**2 FROM 298 TO T ---
C        AND THEN CALCULATES EK(J); REFERRED TO AS HR(J)
  700 CONTINUE
      T2=T*T
      T3=T2*T
      T4=T3*T
      XL=LOGF(T)
      DO 750 J=4,8
      DUM=  EO(J)+E(J,1)/T+E(J,2)*XL+E(J,3)*T+E(J,4)*T2+E(J,5)*T3
     1       +E(J,6)*T4
      HR(J  )=EXPF(-G(J  )+DUM)*P**PE(J)
  750 CONTINUE
      RETURN
C
C------- CALCULATES HEAT OF REACTION --------
C
  800 CONTINUE
      T2=T*T
      T3=T2*T
      T4=T3*T
      T5=T4*T
      DO 850 J=1,8
  850 HR(J)=HRO(J)+D(J,1)*T+D(J,2)*T2+D(J,3)*T3+D(J,4)*T4+D(J,5)*T5
      RETURN
C
C------- CALCULATES ENTHALPY OF SPECIES I -------
C
  900 CONTINUE
      TXK=TG
      DO 910 K=1,5
      XK=K
      TDF(K)=(TXK-TOXK(K))/XK
  910 TXK=TXK*TG
      DO 950 I=1,8
```

```
      HI(I)=HF298(I)
      DO 950 K=1,5
  950 HI(I)=HI(I)+C(I,K)*TDF(K)
      TXK=TS
      DO 960 K=1,5
      XK=K
      TDF(K)=(TXK-TOXK(K))/XK
  960 TXK=TXK*TS
      DO 980 I=9,13
      HI(I)=HF298(I)
      DO 980 K=1,5
  980 HI(I)=HI(I)+C(I,K)*TDF(K)
      RETURN
      END
      SUBROUTINE AIJ
C*****************************************************************
C
C     REACTION STOICHIOMETRIC COEFFICIENTS SET, AS WELL SPECIES
C        MOLECULAR WEIGHTS.
C
C*****************************************************************
      COMMON/PAR/A(13,8),WM(13),F(8),HF298(13),ROS(5),XL,PO
      COMMON/STOIC1/A1,B1,A2,B2,A3,A4,B4,ETA1,ETA2,ETA3
     1  ,XXX,XXXX
      COMMON/STOIC2/IDS(13),IDR(8)
C-------- DEFINE:ATOMIC WTS,   II,JJ ----------------------------
      AWC=12.011
      AWH=1.0080
      AWO=15.9994
      AWN=14.0067
      II=13
      JJ=8
      NC=9
C-------- SPECIES ID SETUP AND MOLECULAR WT CALCULATION ---------
      IDS(1)=8H N2
      WM(1)=2.0*AWN
      IDS(2)=8H O2
      WM(2)=2.0*AWO
      IDS(3)=8H H2O
      WM(3)=2.0*AWH+AWO
      IDS(4)=8H H2
      WM(4)=2.0*AWH
      IDS(5)=8H CH4
      WM(5)=AWC+4.0*AWH
      IDS(6)=8H CO
      WM(6)=AWC+AWO
      IDS(7)=8H CO2
      WM(7)=AWC+2.0*AWO
      IDS(8)=8H TAR
      WM(8)=AWC+A3*AWH
      WM(8)=WM(8)*NC
      IDS( 9)=8H DC(S)
      WM( 9)=AWC+A2*AWH+B2*AWO
      IDS(10)=8H CHAR(S)
      WM(10)=AWC+A1*AWH+B1*AWO
      IDS(11)=8H H2O(L)
      WM(11)=WM(3)
      IDS(12)=8H H2O(F)
      WM(12)=WM(3)
      IDS(13)=8H ASH(S)

      WM(13)=180.0
C-------- STOICHIOMETRIC COEFFICIENTS ------------
      DO 200 J=1,JJ
      DO 100 I=1,II
  100 A(I,J)=0.0
  200 CONTINUE
      A(3,1)=1.0
      A(11,1)=-1.0
      A(3,2)=1.0
      A(12,2)=-1.0
C       USES H2O,CO2,AND CO TO BALANCE
      A(9,3)=-1.
      A(10,3)=ETA2
      A(4,3)=0.083
      A(5,3)=0.044
      A(8,3)=ETA3/NC
      A(3,3)=(A2-A1*ETA2-2.*A(4,3)-4.*A(5,3)-A3*ETA3)/2.
      A(7,3)=B2-1.-B1*ETA2+ETA2-A(3,3)+A(5,3)+ETA3
      A(6,3)=1.-ETA2-A(7,3)-A(5,3)-ETA3
      A(2,4)=-(1.0+A1/4.-B1/2.)
      A(3,4)=A1/2.0
      A(7,4)=1.0
      A(10,4)=-1.0
      A(3,5)=-1.0+B1
      A(4,5)=1.0+A1/2.-B1
      A(6,5)=1.0
      A(10,5)=-1.0
      A(3,6)=A1/2.0
      A(6,6)=2.0+A1/2.0-B1
      A(7,6)=-1.0-A1/2.0+B1
```

```
      A(10,6)=-1.0
      A(3,7)=B1
      A(4,7)=-(2.0-A1/2.0+B1)
      A(5,7)=1.0
      A(10,7)=-1.0
      A(3, 8)=-1.0
      A(4, 8)=1.0
      A(6, 8)=-1.0
      A(7, 8)=1.0
C--------- REACTION RATE ID SETUP --------
      IDR( 1)=10H    11=3
      IDR( 2)=10H    12=3
      IDR( 3)=10H     9=10+
      IDR( 4)=10H 10+2= 7+3
      IDR( 5)=10H 10+3= 4+6
      IDR( 6)=10H 10+7= 6+3
      IDR( 7)=10H 10+4= 5+3
      IDR( 8)=10H  6+3= 4+7
      RETURN
      END
      SUBROUTINE OUT
C*************************************************************
C
C     CALCULATES EXHASUST FLOWS TEMPERATURES,AND COMPOSITIONS
C           FOR THE COMPLETE SYSTEM.  ONLY DONE IF ALL FRONT
C           VELOCITIES ARE INTERNALLY CONSISTANT. (IE WR.LE.WD)
C
C*************************************************************
      COMMON/PNT/IRUN,G,Y(8),TR,X(8),RO(5),TI,TS,U,V,W,XL,S,GC
     1   ,FW,FP,PRES,GI,OEND(100,12)

     2      ,BZ(5),HOB(3)
      COMMON/PAR/A(13,8),WM(13),F(8),HF298(13),ROS(5),XXL,PX
      COMMON/STOIC1/A1,B1,A2,B2,A3,A4,B4,ETA1,ETA2,ETA3,WW,WA,ITHERM
      COMMON/GIVE/ GV(20),TK(20)
      COMMON/PNT1/ TM(3),FL(3),TEMP(3),GF(3),GFD(3),YW(3,8),YD(3,8),
     1  HV(3),YGI(3,8),GFI(3),HVI(3),FLI(3),HCOAL
      DIMENSION YGIO(8),DT(3)
      DIMENSION DUM(8)
      TM(1)=XL/U
      TM(2)=XL/V
      TM(3)=XL/W
      P=V*FP
      GDR=G*(1.-Y(3))
      PDR=P*(1.-X(3))
      FL(1)=V*FW-S*(GDR+PDR)+Y(3)*G+X(3)*P
      FL(2)=0.
      FL(2)=0.
      TEMP(1)=TI
      TEMP(2)=TS
      TEMP(3)=TR
      GF(3)=G
      GF(2)=G+P+V*FW
      GF(1)=GF(2)-FL(1)
      DO 10 J=1,8
   10 YW(3,J)=Y(J)
      DO 20 J=1,8
   20 YW(2,J)=(G*Y(J)+X(J)*P)/GF(2)
      YW(2,3)=YW(2,3)+V*FW/GF(2)
      DO 25 J=1,8
   25 YW(1,J)=YW(2,J)*GF(2)/GF(1)
      YW(1,3)=(YW(2,3)*GF(2)-FL(1))/GF(1)
      DO 40 I=1,3
      DO 30 J=1,8
   30 YD(I,J)=YW(I,J)/(1.-YW(I,3))
      YD(I,3)=0.
      GFD(I)=GF(I)*(1.-YW(I,3))
   40 HV(I)=YD(I,4)*68317.+YD(I,5)*212800.+YD(I,6)*67636.
      DO 50 J=1,8
   50 YGIO(J)=0.
      GFIO=0.
      HVIO=0.
      DT(1)=TM(1)
      DT(2)=TM(2)-TM(1)
      DT(3)=TM(3)-TM(2)
      DO 70 I=1,3
      TFLW=GF(I)*DT(I)
      GFI(I)=GFIO+TFLW
      GFIO=GFI(I)
      HVI(I)=HVIO+GFD(I)*DT(I)*HV(I)
      HVIO=HVI(I)
      DO 60 J=1,8
      YGI(I,J)=YGIO(J)+YW(I,J)*TFLW
   60 YGIO(J)=YGI(I,J)
   70 CONTINUE
      HCOAL=94052.+A2/2.*68317.+HF298(9)
      HCOAL=RO(1)*XL*HCOAL/WM(9)
      OEND(IRUN,11)=HVI(3)/HCOAL
      OEND(IRUN,12)=HVI(3)/(TM(3)*GI*OEND(IRUN,2))
      HOFF=BZ(5)
      HOB(1)=(HVI(3)-GI*TM(3)*HOFF)
```

```
      HOB(2)=HOB(1)/HCOAL
      HOB(1)=HOB(1)/OEND(IRUN,2)/GI/TM(3)
      RETURN
      END
      SUBROUTINE PNT (NN)
C*****************************************************************
C
C     PROVIDES MOST OF THE PRINTED OUTPUT.
C
C*****************************************************************
      COMMON/STOICI/A1,B1,A2,B2,A3,A4,B4,ETA1,ETA2,ETA3,WW,WA,ITHERM
      COMMON/PAR/A(13,8),WM(13),F(8),HF298(13),ROS(5),XXL,PX
      COMMON/PNT/IRUN,G,Y(8),TR,X(8),RO(5),TI,TS,U,V,W,XL,S,GC
     1  ,FW,FP,PRES,GI,OEND(100,12)
     2     ,BZ(5),HOB(3)
     3     YIG(9),QLOSS,TLOSS
      COMMON/PNT1/ TM(3),FL(3),TEMP(3),OF(3),GFD(3),YW(3,8),YD(3,8),
     1  HV(3),YGI(3,8),GFI(3),HVI(3),FLI(3),HCOAL
      COMMON/GIVE/ ADD(20),ADDD(20)
      IF (NN.EQ.4) GO TO 4000
      IF (NN.EQ.3) GO TO 3000
      IF (NN.EQ.2) GO TO 2000
      WRITE (3,400)
  400 FORMAT (1X///30X,17HSYSTEM PROPERTIES///)
                  WRITE(3,22) A2,B2,ETA2,ETA3,WW,WA
   22 FORMAT(5X,22HCOAL PROPERTIES-  H/C=,F5.3,6H,  O/C=,F5.3,
     1  9H,  CHAR/C=,F5.3,8H,  TAR/C=,F5.3,6H,  H2O=,F5.3,6H,  ASH=,F5.3/)
      WRITE(3,23) A1,B1,HF298(10),A3
   23 FORMAT(5X,22HCHAR PROPERTIES-  H/C=,F5.3,6H,  O/C=,F5.3,1H,,
     1    7H HFORM=,F8.0,10X,
     2  21HTAR PROPERTIES-  H/C=,F5.3/)
      WRITE (3,05)
   05 FORMAT (5X,13HPYROLYSIS GAS/)
      WRITE (3,03) X
      WRITE (3,06) RO
   06 FORMAT (1X/5X,15HSOLID DENSITIES,15H (GM/CC OF BED)/
     2                10X,5HCOAL ,F7.4/10X,5HCHAR ,
     1    F7.4/10X,5HH2OM ,F7.4/10X,5HH2OF ,F7.4/10X,5HASH  ,F7.4//)
      WRITE (3,401)
      WRITE (3,402) WM
  401 FORMAT (1X/,5X,17HMOLECULAR WEIGHTS/)
  402 FORMAT (10X,7F8.2/10X,F8.2)
      WRITE (3,403)
  403 FORMAT (1X//,5X,18HHEATS OF FORMATION/)
      WRITE (3,404) HF298
  404 FORMAT (1X/10X,7F10.1/10X,7F10.1)
      WRITE (3,429)
  429 FORMAT (2X,27HSTOICHIOMETRIC COEFFICIENTS//10X,8HREACTION,40X,
     1   9HCOMPONENT/18X,42H  N2      O2      H2O    H2      CH4     CO    ,
     2   49H  CO2     TAR     COAL    CHAR  H2OM    H2OF     ASH  /)
      DO 430 J=1,8
  430 WRITE (3,411) J,(A(I,J),I=1,13)
  411 FORMAT (14X,I2,2X,13(F6.3,1X))
      RETURN
 2000 CONTINUE
      WRITE (3,01) IRUN
   01 FORMAT (1H1//     50X,4HRUN ,I2)
      WRITE (3,2001) GI
 2001 FORMAT (5X,11HFEED RATE =,E12.2,14H (MOL/CM2/SEC)/)
      WRITE (3,03) (YIG(I),I=1,8)

      WRITE (3,2002) YIG(9)
      WRITE (3,04) ADD(3)
 2002 FORMAT (19X,10HLIQUID H2O,F7.4)
   07 FORMAT (1X////5X,20HINITIAL COAL TEMP =,F12.2,4H (K))
      RETURN
 3000 CONTINUE
      WRITE (3,07) TI
      WRITE (3,10) PRES
   10 FORMAT(5X,8HPRESSURE,F10.2,6H (ATM)/)
      WRITE (3,08) XL
   08 FORMAT (5X,7HLENGTH=,F10.2,5H (CM)/)
      IF (ADD(7).GT.0.) WRITE (3,3010)
 3010 FORMAT (5X,18HMETHANE SUPPRESSED)
      WRITE (3,02) G
   02 FORMAT ( 1X///5X,23HREACTION GAS PROPERTIES/10X,6HFLOW= ,E12.2,
     1    13H(MOL/CM2/SEC))
      WRITE (3,3300) QLOSS,TLOSS
 3300 FORMAT (10X,20HHEAT LOSS PARAMS     ,5X,7HQLOSS= ,E15.3,
     *      5X,7HTLOSS= ,F8.2)
      WRITE (3,03) Y
   03 FORMAT (10X,27HCOMPOSITION (MOLE FRACTION)/,26X,
     1                                  4HN2  ,F7.4/26X,4HO2  ,F7.4/
     1    26X,4HH2O ,F7.4/26X,4HH2  ,F7.4/26X,4HCH4 ,F7.4/26X,4HCO  ,
     2   F7.4/26X,4HCO2 ,F7.4/26X,4HTAR ,F7.4)
      WRITE (3,04) TR
   04 FORMAT (10X,12HTEMPERATURE ,F10.2,4H (K)/)
      WRITE (3,2010)
 2010 FORMAT (1X//5X,22HFOR REACTION ZONE ONLY//)
      WRITE (3,99) (BZ(I),I=1,4)
```

```
 99 FORMAT ( 20X,13HHCOMB/MOLE O2,10X,20HHCOMB GAS/HCOMB CHAR/
    1    22X,9H(CAL/MOL)//
    1    10X,5HAT TI,5X,E12.3,10X,F8.4//3X,16HWRT H2O(L) 300 K,3X,
    2  E12.3,  9X,F8.3/10X,4HFEED)
     WRITE (3,09) W,V,U
 09 FORMAT (////5X,30HCALCULATED VELOCITIES (CM/SEC)//9X,9HREACTION ,
    1     E12.3/9X,9HDRYING    ,E12.3/9X,9HSTEAM     ,E12.3)
     IF (V.LT.W) RETURN
     WRITE (3,100)
100 FORMAT (1H1///5X,13HSYSTEM OUTPUT/38X,9HWET BASIS//7X,4HTIME,27X,
    1   11HCOMPOSITION,20X,4HTEMP,4X,3HGAS,6X,3HLIQ/
    2    7X,5H(SEC),10X,2HO2,4X,2HN2,
    3   4X,3HH2O,3X,2HH2,4X,3HCH4,3X,2HCO,4X,3HCO2,3X,3HTAR,
    4    3X,3H(K),3X,4HFLOW,6X,4HFLOW/7X,3H0.0,70X,13H(MOL/CM2/SEC))
     DO 40 I=1,3
 40 WRITE (3,101) (YW(I,J),J=1,8),TEMP(I),GF(I),FL(I),TM(I)
101 FORMAT (18X,8F6.3,F8.1,2E10.3/5X,E13.4)
     WRITE (3,102)
102 FORMAT (1X/38X,9HDRY BASIS/60X,4HHEAT,8X,3HGAS/68X,5HVALUE,8X,
    1   4HFLOW/7X,3H0.0,58X,9H(CAL/MOL))
     DO 50 I=1,3
 50 WRITE (3,103) (YD(I,J),J=1,8),HV(I),GFD(I),TM(I)
103 FORMAT (18X,8F6.3,2E11.3/5X,E13.4)
     WRITE (3,104)
104 FORMAT (1X//34X,21HINTEGRATED QUANTITIES//10X,4HTIME,9X,2HN2,8X,
    1   2HO2,8X,3HH2O,7X,2HH2,8X,3HCH4,
    2                7X,2HCO,8X,3HCO2,7X,3HTAR,5X,8HHEAT VAL/
    3   10X,5H(SEC),40X,9H(MOL/CM2),37X,9H(CAL/CM2))
     DO 60 I=1,3
 60 WRITE (3,105) TM(I),(YGI(I,J),J=1,8),HVI(I)
105 FORMAT (5X,E13.4,  8E10.3,E12.4)

     WRITE (3,106) HCOAL
106 FORMAT (1X//40X,19HCOAL HEATING VALUE ,E12.3,10H (CAL/CM2))
     WRITE (3,107) HOB(1),HOB(2)
107 FORMAT (1X///,17X,17HBASE H2O(L) 300 K,3X,
    1    17HHCOMB GAS/MOLE O2,E12.3/
    1    20X,4HFEED,
    2   14X,20HHCOMB GAS/HCOMB COAL,F8.3)
     RETURN
4000 CONTINUE
     WRITE (3,300)
300 FORMAT (1H1,1X///,40X,7HSUMMARY///,
    2   5X,53HRUN      FS       FO2       PRESS       TO       TB       TS,
    3    54H       WR       WP       WS       WP/WR       HG/HC   HG/O2//)
     DO 303 J=1,IRUN
     WRITE (3,301) J,(OEND(J,L),L=1,12)
301 FORMAT (2XI3,2X, 2F8.4,4F9.1,3F9.6,2F9.3,E12.3)
303 CONTINUE
     RETURN
     END
```

INPUT

The following card images demonstrate the required input for running a problem, or set of problems. All formats are F 10.0.

Card 1. Chemistry parameters
- A. a (char H/C ratio).
- B. b (char O/C ratio).
- C. c (coal H/C ratio).
- D. d (coal O/C ratio).
- E. f/e (tar H/C ratio).
- F. η (moles char produced per mole of coal pyrolyzed).
- G. $e \cdot R_p^s$ (atoms of C in tar per mole of coal pyrolyzed).

Card 2. Solid composition:
- A. Effective solid density of bed, $\frac{g}{cm^2}$.
- B. Weight fraction dry coal.
- C. Weight fraction fixed water.
- D. Weight fraction mobile water (generally 0).
- E. Weight fraction ash.

Card 3. System operating parameters:
- A. $G_1 + L_1$ (Feed flux), $\frac{mole}{cm^2\ s}$.
- B. T_1 (Feed temperature, K).
- C. T_4 (initial coal temperature, K).
- D. L (system length, cm).
- E. P (system pressure, atm).

Card 4. Feed composition and equilibrium assumption:
- A. $\frac{y_1^3}{y_1^2}$ (steam/oxygen mole ratio).
- B. $\frac{y_1^1}{y_1^2}$ (Nitrogen/oxygen mole ratio).
- C. $\frac{L_1}{y_1^2 G_1}$ (Liquid water/oxygen mole ratio).
- D. Y: $= -1$. Methane allowed in zone 2,
  $= +1$. Methane not allowed in zone 2.

The set formed by cards 3 and 4 can be repeated as many times as desired.

Card 5. Terminator
- A. Supply a negative number to terminate input.

APPENDIX C
CHAR THERMODYNAMICS

The equilibrium calculations described in Appendix A require equilibrium constants at given temperatures and pressure for reactions involving coal char and several common gas species. The basic thermodynamic information required for each species is the heat of formation and absolute entropy at 298 K, and the heat capacity from 298 K to the temperature of interest. For the gaseous species these data are available in the JANAF tables[12]. For coal char, however, the thermodynamic functions must be estimated.

Representing char as CH_aO_b, the following empirical relations are used:

$$\Delta H^{\circ}_{f,298} = \begin{cases} 0 & , a = 0 \\ 2.6 - 68.0b & , a > 0 \end{cases} \quad \text{(kcal/mole)}, \qquad \text{(C-1)}$$

$$S^{\circ}_{298} = 1.359 + 3.17a + 4.0b \quad \text{(cal/mole-K)}, \qquad \text{(C-2)}$$

$$C_p(T) = C_p(T,\text{graphite}) + 0.88a + 5.8b \ \text{(cal/mole-K)} \qquad \text{(C-3)}$$

Equation (C-1) for the heat of formation, with $a > 0$, is based on the Dulong formula[13] for the heat of combustion of coal. The formula is simply back-solved for the heat of formation of char, knowing the heats of formation of carbon dioxide and liquid water. The Dulong formula has been found by Thibaut[14] to work well for cokes containing varying amounts of hydrogen (a) and oxygen (b). To generate the quoted heat of formation of amorphous carbon, (2600 kcal/mole), we set $b = 0$ and $a \approx 10^{-6}$ in Eq. (C-1). To generate graphite with a zero heat of formation, we set $a = b = 0$.

Equation (C-2) for the absolute entropy of coal char comes from a Krikorian[15] correlation based on the entropies of high-molecular-weight solid aromatic hydrocarbons. For $a = b = 0$, the entropy reduces to the value for graphite.

Equation (C-3) for char-heat capacity is essentially a Kopp's law additive atomic component relation, except that the carbon component is assumed to have the normal graphite temperature dependence. For graphite we use a polynomial in the temperature that accurately represents the JANAF tables from 298 to 2000K. We have taken the Kopp's Law coefficients for hydrogen and oxygen from Gomez, Gayle, and Taylor,[10] who determined these from a variety of British coals at room temperature. Over a temperature range from 300 to 2000K, the heat capacity of graphite increases by almost a factor of three while hydrogen and oxygen increase only about 20%. It therefore seems reasonable that the heat capacity of a char should follow the graphite temperature curve with small, essentially temperature-independent corrections caused by the presence of hydrogen and oxygen. This procedure is consistent with the findings of Kirov and Stephens[16]. Equation (C-3) also gives a plausible heat capacity estimate over a wide temperature range, unlike the equations given in either Ref. 9 or 16 which give unreasonable results at higher temperatures.

Table C-1. Calculated equilibrium properties of a carbonaceous solid, CH_aO_b, at 1000K, 3 atm, and a steam/oxygen molar feed ratio of 2.

Solid	a	b	Moles O_2 mole solid	Composition, mole %					Heating value, Btu/SCF
				CO	CO_2	H_2	CH_4	H_2O	
Equilibrium methane									
Graphite	0	0	0.38	37	21	28	2	12	260
Amorphous carbon	10^{-6}	0	0.29	53	13	24	6	4	320
High-temp char	0.15	.02	0.23	62	6	19	12	1	380
Low-temp char	0.40	.10	0.17	69	1	8	21	1	460
Methane suppressed									
Graphite	0	0	0.40	35	21	31	—	13	240
Amorphous carbon	10^{-6}	0	0.32	51	11	33	—	5	280
High-temp char	0.15	0.02	0.27	57	5	36	—	2	300
Low-temp char	0.40	0.10	0.23	60	1	39	—	—	310

It should be clear from the above discussion that our scheme for char thermodynamics is quite approximate, and based on very limited data. One use for the formalism is to explore the sensitivity of calculated equilibrium results to the hydrogen and oxygen content of the char. Table C shows calculated results for carbonaceous solids ranging from graphite to a low-temperature char with a high hydrogen and oxygen content. The calculations have been carried out both with and without methane in the equilibrium gas.

With methane present, the calculated heating value of the equilibrium gas increases as the hydrogen and oxygen content of the char increase. The oxygen requirement also decreases substantially (moles O_2 required/mole solid consumed), as a and b increase. The differences between graphite and amorphous carbon stem from the finite heat of formation of amorphous carbon. With methane suppressed, the calculated heating values are reduced and the sensitivity to the char hydrogen and oxygen content is diminished.

APPENDIX D SUMMARY OF RUNS

The following tables show the calculated results for reaction zone temperatures, gas compositions, and relative velocity for a variety of assumed conditions. Included are runs for char having a $CH_{0.09}O_{.016}$ and a C stoichiometry as well as results for pressures of 1 and 30 atm with and without methane in the equilibrium mixture. In addition to pure oxygen/water feeds, a number of results are given for air and air/water feeds. Results for both steam and liquid water feeds are also included. The velocity ratio shown for each case assumes an ash weight fraction of 0.06 and a water weight fraction of 0.33 in the wet coal.

Table D-1. Char, $CH_{0.09}O_{.016}$; O_2/steam feed.
A. Pressure = 1 atm; CH_4 present.

Feed			Reaction zone gas						Velocity ratio
Temp,	Mole fraction		Temp,	Mole fraction					
K	O_2	H_2O	K	H_2O	H_2	CH_4	CO	CO_2	W_D/W_R
320	0.10	0.90	805	0.060	0.145	0.278	0.195	0.322	0.664
327	0.15	0.85	848	0.047	0.184	0.211	0.314	0.244	0.689
334	0.20	0.80	883	0.035	0.210	0.160	0.421	0.175	0.697
339	0.25	0.75	915	0.026	0.228	0.118	0.510	0.119	0.698
343	0.30	0.70	951	0.017	0.244	0.083	0.587	0.070	0.702
346	0.35	0.65	1000	0.009	0.261	0.052	0.648	0.031	0.717
350	0.40	0.60	1112	0.002	0.286	0.019	0.687	0.005	0.780
352	0.45	0.55	1533	0.000	0.293	0.001	0.706	0.000	0.977
355	0.50	0.50	2118	0.000	0.272	0.000	0.728	0.000	1.133
359	0.60	0.40	3022	0.000	0.226	0.000	0.774	0.000	1.313

B. Pressure = 30 atm; CH_4 present.

Feed			Reaction zone gas						Velocity ratio
Temp,	Mole fraction		Temp,	Mole fraction					
K	O_2	H_2	K	H_2O	H_2	CH_4	CO	CO_2	W_D/W_R
407	0.10	0.90	951	0.079	0.092	0.304	0.211	0.315	0.766
422	0.15	0.85	1013	0.063	0.121	0.244	0.339	0.234	0.791
432	0.20	0.80	1063	0.049	0.142	0.195	0.448	0.166	0.796
441	0.25	0.75	1112	0.035	0.162	0.153	0.541	0.109	0.797
450	0.30	0.70	1168	0.024	0.183	0.116	0.616	0.061	0.803
456	0.35	0.65	1215	0.013	0.209	0.081	0.671	0.026	0.828
462	0.40	0.60	1387	0.005	0.247	0.042	0.700	0.006	0.896
467	0.45	0.55	1707	0.001	0.271	0.010	0.711	0.001	1.033
472	0.50	0.50	2229	0.000	0.268	0.002	0.730	0.000	1.169
480	0.60	0.40	3075	0.000	0.225	0.000	0.774	0.000	1.353

C. Pressure—1 atm; CH_4 not present.

Feed			Reaction zone gas						Velocity Ratio
Temp, K	Mole fraction O_2	Mole fraction H_2O	Temp, K	Mole fraction H_2O	Mole fraction H_2	Mole fraction CH_4	Mole fraction CO	Mole fraction CO_2	W_D/W_R
320	0.10	0.90	723	0.311	0.397	—	0.042	0.250	1.316
327	0.15	0.85	797	0.172	0.438	—	0.147	0.244	1.114
334	0.20	0.80	845	0.103	0.428	—	0.269	0.200	0.975
339	0.25	0.75	884	0.063	0.403	—	0.386	0.148	0.878
343	0.30	0.70	921	0.037	0.374	—	0.491	0.098	0.811
346	0.35	0.65	967	0.018	0.345	—	0.586	0.550	0.770
350	0.40	0.60	1064	0.005	0.318	—	0.667	0.010	0.776
352	0.45	0.55	1524	0.000	0.295	—	0.705	0.000	0.975
355	0.50	0.50	2117	0.000	0.272	—	0.728	0.000	1.133
359	0.60	0.40	3022	0.000	0.226	—	0.774	0.000	1.313

D. Pressure = 30 atm; CH_4 not present.

Feed			Reaction zone gas						Velocity ratio
Temp, K	Mole fraction O_2	Mole fraction H_2O	Temp, K	Mole fraction H_2O	Mole fraction H_2	Mole fraction CH_4	Mole fraction CO	Mole fraction CO_2	W_D/W_R
407	0.10	0.90	866	0.407	0.324	—	0.061	0.208	1.645
422	0.15	0.85	953	0.259	0.370	—	0.168	0.203	1.350
432	0.20	0.80	1014	0.170	0.375	—	0.285	0.170	1.162
441	0.25	0.75	1065	0.110	0.366	—	0.394	0.129	1.039
450	0.30	0.70	1117	0.068	0.350	—	0.495	0.087	0.956
456	0.35	0.65	1178	0.037	0.332	—	0.582	0.049	0.906
462	0.40	0.60	1288	0.013	0.314	—	0.658	0.015	0.900
467	0.45	0.55	1644	0.001	0.294	—	0.704	0.001	1.020
472	0.50	0.50	2218	0.000	0.272	—	0.728	0.000	1.168
480	0.60	0.40	3074	0.000	0.226	—	0.774	0.000	1.353

Table D-2. Char, C (β-graphite); O_2/Steam feed

A. Pressure = 1 atm; CH_4 present.

Feed			Reaction zone gas						Velocity ratio
Temp, K	Mole fraction O_2	Mole fraction H_2O	Temp, K	Mole fraction H_2O	Mole fraction H_2	Mole fraction CH_4	Mole fraction CO	Mole fraction CO_2	W_D/W_R
320	0.10	0.90	805	0.314	0.262	0.090	0.057	0.277	1.527
327	0.15	0.85	875	0.211	0.331	0.051	0.154	0.253	1.486
334	0.20	0.80	924	0.143	0.351	0.030	0.264	0.212	1.364
339	0.25	0.75	964	0.096	0.348	0.018	0.371	0.167	1.246
343	0.30	0.70	1002	0.061	0.334	0.011	0.473	0.121	1.158
346	0.35	0.65	1043	0.036	0.315	0.006	0.565	0.077	1.074
350	0.40	0.60	1101	0.017	0.293	0.003	0.650	0.036	1.025
352	0.45	0.55	1254	0.003	0.273	0.001	0.719	0.005	1.043
355	0.50	0.50	1803	0.000	0.250	0.000	0.750	0.000	1.209
359	0.60	0.40	2873	0.000	0.201	0.000	0.799	0.000	1.385

B. Pressure = 30 atm; CH_4 present.

Feed			Reaction zone gas						Velocity ratio
Temp, K	Mole fraction O_2	Mole fraction H_2O	Temp, K	Mole fraction H_2O	Mole fraction H_2	Mole fraction CH_4	Mole fraction CO	Mole fraction CO_2	W_D/W_R
407	0.10	0.90	959	0.337	0.170	0.139	0.082	0.271	1.618
422	0.15	0.85	1048	0.248	0.230	0.097	0.190	0.236	1.590
432	0.20	0.80	1111	0.182	0.259	0.069	0.298	0.193	0.149
441	0.25	0.75	1165	0.130	0.272	0.048	0.401	0.149	1.385
450	0.30	0.70	1217	0.089	0.275	0.033	0.495	0.108	1.294
456	0.35	0.65	1274	0.057	0.273	0.022	0.578	0.070	1.223
462	0.40	0.60	1352	0.030	0.268	0.013	0.653	0.036	1.174
467	0.45	0.55	1506	0.009	0.262	0.005	0.714	0.010	1.172
472	0.50	0.50	1934	0.001	0.248	0.001	0.750	0.001	1.263
480	0.60	0.40	2939	0.000	0.200	0.000	0.799	0.000	1.434

C. Pressure = 1 atm; CH_4 not present.

Feed			Reaction zone gas						Velocity ratio
Temp, K	Mole fraction O_2	Mole fraction H_2O	Temp, K	Mole fraction H_2O	Mole fraction H_2	Mole fraction CH_4	Mole fraction CO	Mole fraction CO_2	W_D/W_R
320	0.10	0.90	785	0.418	0.321	—	0.037	0.224	2.262
327	0.15	0.85	865	0.253	0.380	—	0.130	0.237	1.772
334	0.20	0.80	918	0.162	0.386	—	0.243	0.209	1.489
339	0.25	0.75	960	0.105	0.372	—	0.356	0.167	1.304
343	0.30	0.70	999	0.066	0.350	—	0.462	0.122	1.176
346	0.35	0.65	1040	0.039	0.325	—	0.557	0.079	1.087
350	0.40	0.60	1099	0.018	0.299	—	0.647	0.037	1.030
352	0.45	0.55	1254	0.003	0.274	—	0.718	0.005	1.044
355	0.50	0.50	1803	0.000	0.250	—	0.750	0.000	1.209
359	0.60	0.40	2873	0.000	0.201	—	0.799	0.000	1.385

D. Pressure = 30 atm; CH_4 not present.

Feed			Reaction zone gas						Velocity ratio
Temp, K	Mole fraction O_2	Mole fraction H_2O	Temp, K	Mole fraction H_2O	Mole fraction H_2	Mole fraction CH_4	Mole fraction CO	Mole fraction CO_2	W_D/W_R
407	0.10	0.90	933	0.505	0.257	—	0.051	0.188	2.882
422	0.15	0.85	1031	0.341	0.313	—	0.148	0.198	2.181
432	0.20	0.80	1099	0.235	0.330	—	0.258	0.177	1.792
441	0.25	0.75	1155	0.161	0.328	—	0.366	0.144	1.548
450	0.30	0.70	1208	0.107	0.318	—	0.466	0.108	1.383
456	0.35	0.65	1265	0.067	0.304	—	0.557	0.073	1.270
462	0.40	0.60	1342	0.035	0.287	—	0.640	0.039	1.195
467	0.45	0.55	1492	0.011	0.270	—	0.709	0.011	1.175
472	0.50	0.50	1929	0.001	0.250	—	0.749	0.001	1.263
480	0.60	0.40	2938	0.000	0.201	—	0.799	0.000	1.434

1172 GANOW H
PRELIMINARY RESULTS OF THE GEOTECHNICAL INSTRUMENTATION PROGRAM F

Table D-3. Char, $CH_{0.09}O_{0.16}$; O_2/H_2O (liq) feed.

A. Pressure − 1 atm; CH_4 present.

Feed			Reaction zone gas						Velocity ratio
Temp, K	Mole fraction O_2	Mole fraction H_2O	Temp, K	Mole fraction H_2O	Mole fraction H_2	Mole fraction CH_4	Mole fraction CO	Mole fraction CO_2	W_D/W_R
300	0.15	0.85	746	0.070	0.087	0.317	0.088	0.438	0.593
300	0.20	0.80	815	0.056	0.145	0.232	0.232	0.335	0.660
300	0.25	0.75	858	0.043	0.179	0.172	0.361	0.246	0.677
300	0.30	0.70	894	0.031	0.201	0.125	0.474	0.169	0.679
300	0.35	0.65	928	0.021	0.216	0.089	0.566	0.108	0.678
300	0.40	0.60	972	0.012	0.231	0.057	0.646	0.054	0.684
300	0.45	0.55	1056	0.004	0.252	0.026	0.705	0.013	0.720
300	0.50	0.50	1395	0.000	0.268	0.002	0.729	0.000	0.890
300	0.60	0.40	2664	0.000	0.226	0.000	0.774	0.000	1.200

B. Pressure = 30 atm; CH_4 present.

Feed			Reaction zone gas						Velocity ratio
Temp, K	Mole fraction O_2	Mole fraction H_2O	Temp, K	Mole fraction H_2O	Mole fraction H_2	Mole fraction CH_4	Mole fraction CO	Mole fraction CO_2	W_D/W_R
300	0.15	0.85	850	0.091	0.046	0.339	0.075	0.449	0.659
300	0.20	0.80	954	0.077	0.087	0.264	0.228	0.344	0.754
300	0.25	0.75	1018	0.060	0.114	0.207	0.369	.251	0.774
300	0.30	0.70	1071	0.045	0.135	0.161	0.488	0.172	0.775
300	0.35	0.65	1122	0.032	0.152	0.124	0.584	0.108	0.773
300	0.40	0.60	1186	0.020	0.173	0.089	0.663	0.055	0.781
300	0.45	0.55	1287	0.009	0.201	0.055	0.717	0.018	0.816
300	0.50	0.50	1533	0.002	0.241	0.018	0.738	0.002	0.928
300	0.60	0.40	2667	0.000	0.225	0.001	0.774	0.000	1.214

C. Pressure = 1 atm; CH_4 not present.

Feed			Reaction zone gas						Velocity ratio
Temp, K	Mole fraction O_2	Mole fraction H_2O	Temp, K	Mole fraction H_2O	Mole fraction H_2	Mole fraction CH_4	Mole fraction CO	Mole fraction CO_2	W_D/W_R
300	0.15	0.85	632	0.515	0.237	—	0.006	0.243	1.243
300	0.20	0.80	754	0.241	0.382	—	0.080	0.297	1.102
300	0.25	0.75	819	0.134	0.398	—	0.211	0.257	0.967
300	0.30	0.70	865	0.078	0.380	—	0.347	0.195	0.864
300	0.35	0.65	903	0.046	0.353	—	0.467	0.135	0.794
300	0.40	0.60	947	0.026	0.323	—	0.578	0.075	0.745
300	0.45	0.55	1020	0.009	0.296	—	0.668	0.027	0.735
300	0.50	0.50	1382	0.000	0.272	—	0.728	0.000	0.886
300	0.60	0.40	2664	0.000	0.226	—	0.774	0.000	1.200

D. Pressure = 30 atm; CH_4 not present.

Feed			Reaction zone gas						Velocity ratio
Temp,	Mole fraction		Temp,	Mole fraction					
K	O_2	H_2O	K	H_2O	H_2	CH_4	CO	CO_2	W_D/W_R
300	0.15	0.85	733	0.620	0.162	—	0.008	0.210	1.466
300	0.20	0.80	887	0.357	0.296	—	0.089	0.258	1.351
300	0.25	0.75	971	0.222	0.332	—	0.217	0.229	1.165
300	0.30	0.70	1031	0.142	0.333	—	0.345	0.180	1.031
300	0.35	0.65	1083	0.089	0.322	—	0.460	0.129	0.940
300	0.40	0.60	1141	0.051	0.305	—	0.566	0.079	0.879
300	0.45	0.55	1227	0.022	0.228	—	0.659	0.032	0.852
300	0.50	0.50	1446	0.003	0.270	—	0.723	0.004	0.909
300	0.60	0.40	2664	0.000	0.226	—	0.774	0.000	1.214

Table D-4. Char, $CH_{0.09}O_{0.016}$; Air/H_2O (liquid) feed.

A. Pressure = 1 atm; CH_4 present.

Feed			Reaction zone gas							Velocity ratio
Temp,	Mole fraction		Temp,	Mole fraction						
K	O_2	H_2O	K	N_2	H_2O	H_2	CH_4	CO	CO_2	W_D/W_R
300	0.10	0.52	720	0.351	0.045	0.053	0.208	0.045	0.298	0.774
300	0.15	0.29	860	0.454	0.016	0.109	0.062	0.253	0.105	1.108
300	0.21	0.00	1919	0.639	0.000	0.016	0.000	0.345	0.000	2.303

B. Pressure = 30 atm; CH_4 present.

Feed			Reaction zone gas							Velocity ratio
Temp,	Mole fraction		Temp,	Mole fraction						
K	O_2	H_2O	K	N_2	H_2O	H_2	CH_4	CO	CO_2	W_D/W_R
300	0.10	0.52	802	0.359	0.057	0.024	0.222	0.032	0.306	0.815
300	0.15	0.29	1011	0.470	0.025	0.068	0.083	0.238	0.116	1.241
300	0.21	0.00	1919	0.639	0.000	0.016	0.000	0.345	0.000	2.314

C. Pressure = 1 atm; CH_4 not present.

Feed			Reaction zone gas							Velocity ratio
Temp,	Mole fraction		Temp,	Mole fraction						
K	O_2	H_2O	K	N_2	H_2O	H_2	CH_4	CO	CO_2	W_D/W_R
300	0.10	0.52	615	0.345	0.337	0.152	—	0.003	0.164	1.684
300	0.15	0.29	840	0.446	0.038	0.203	—	0.196	0.118	1.390
300	0.21	0.00	1919	0.639	0.000	0.016	—	0.345	0.000	2.303

D. Pressure = 30 atm; CH_4 not present.

Feed			Reaction zone gas							Velocity ratio
Temp,	Mole fraction		Temp,	Mole fraction						
K	O_2	H_2O	K	N_2	H_2O	H_2	CH_4	CO	CO_2	W_D/W_R
300	0.10	0.52	697	0.356	0.410	0.093	—	0.003	0.138	1.939
300	0.15	0.29	980	0.462	0.076	0.171	—	0.173	0.118	1.684
300	0.21	0.00	1919	0.639	0.000	0.000	—	0.345	0.000	2.314

Table D-5. Char, C (β-graphite); Air/H_2O(liquid) feed.

A. Pressure = 1 atm; CH_4 present.

Feed			Reaction zone gas							Velocity ratio
Temp,	Mole fraction		Temp,	Mole fraction						
K	O_2	H_2O	K	N_2	H_2O	H_2	CH_4	CO	CO_2	W_D/W_R
300	0.10	0.52	668	0.363	0.292	0.064	0.075	0.004	0.202	1.700
300	0.15	0.29	907	0.470	0.059	0.164	0.008	0.168	0.131	2.073
300	0.21	0.00	1832	0.653	0.000	0.000	0.000	0.347	0.000	2.658

B. Pressure = 30 atm; CH_4 present.

Feed			Reaction zone gas							Velocity ratio
Temp,	Mole fraction		Temp,	Mole fraction						
K	O_2	H_2O	K	N_2	H_2O	H_2	CH_4	CO	CO_2	W_D/W_R
300	0.10	0.52	726	0.371	0.304	0.024	0.095	0.002	0.204	1.571
300	0.15	0.29	1056	0.488	0.089	0.115	0.022	0.153	0.133	2.374
300	0.21	0.00	1833	0.653	0.000	0.000	0.000	0.347	0.000	2.702

C. Pressure = 1 atm; CH_4 not present.

Feed			Reaction zone gas							Velocity ratio
Temp,	Mole fraction		Temp,	Mole fraction						
K	O_2	H_2O	K	N_2	H_2O	H_2	CH_4	CO	CO_2	W_D/W_R
300	0.10	0.52	660	0.361	0.413	0.086	—	0.002	0.138	3.169
300	0.15	0.29	903	0.468	0.065	0.175	—	0.160	0.132	2.161
300	0.21	0.00	1832	0.652	0.000	0.000	—	0.347	0.000	2.658

D. Pressure = 30 atm; CH_4 not present.

Feed			Reaction zone gas							Velocity ratio
Temp,	Mole fraction		Temp,	Mole fraction						
K	O_2	H_2O	K	N_2	H_2O	H_2	CH_4	CO	CO_2	W_D/W_R
300	0.10	0.52	740	0.367	0.453	0.054	—	0.002	0.124	3.597
300	0.15	0.29	1049	0.484	0.110	0.139	—	0.141	0.128	2.661
300	0.21	0.00	1833	0.653	0.000	0.000	—	0.347	0.000	2.702

REFERENCES

1. C. B. Thorness and R. B. Rozsa, *Lawrence Livermore Laboratory In-Situ Coal Gasification Program: Model Calculations and Laboratory Experiments*, Lawrence Livermore Laboratory, Rept. UCRL-78302 (1976).
2. A. A. Winslow, *Numerical Model of Coal Gasification in a Packed Bed*, Lawrence Livermore Laboratory, Rept. UCRL-77627 (1976).
3. W. K. Sawyer and L. Z. Shuck, "Numerical Simulation of Mass and Energy Transfer in the Longwall Process of Underground Gasification of Coal," in *Proc. of 4th Symposium of Numerical Simulation of Reservoir*.
4. O. D. Gunn and D. L. Whitman, *An In-Situ Coal Gasification Model (Forward Mode) For Feasibility Studies and Design*, Laramie Energy Research Center, Laramie, Wyoming, Rept. LERC/R1-76/2 (1976).
5. D. R. Stephens, *Thermodynamic Equilibrium for Wyoming Coal*, Lawrence Livermore Laboratory, Rept. UCID-16094 (1972).
6. D. R. Stephens, and G. D. Miller, *Thermodynamic Equilibrium for Wyoming Coal: New Calculations*, Lawrence Livermore Laboratory, Rept. UCID-17044 (1976).
7. C. B. Thorsness, *Estimates of Thermal Front Movements and Pressure-Drop-vs-Flow-Rate Relations in Forward In-Situ Coal Gasification*, Lawrence Livermore Laboratory, Rept. UCID-17007 (1976).
8. J. H. Campbell, *Pyrolysis of Subbituminous Coal as it Relates to In-Situ Gasification (Part 1: Gas Evolution)*, Lawrence Livermore Laboratory, Rept. UCRL-52035 (1976).
9. M. Gomez, J. B. Gayle, and A. R. Taylor, Jr., *Heat Content and Specific Heat of Coals and Related Products*, U. S. Bureau of Mines, RI 6607 (1965).
10. P. L. Walker, Jr., Ed., *Chemistry and Physics of Carbon* (M. Decker, New York, 1971).
11. A. C. Hindmarsh, Lawrence Livermore Laboratory, CIC Rept. C.21-1-004 (1970). Readers outside the Laboratory who desire further information on LLL internal documents should address their inquiries to the Technical Information Department, Lawrence Livermore Laboratory, Livermore, California 94550.
12. D. R. Stall, *JANAF Thermochemical Tables 2nd Edition* Washington, D. C. (1971).
13. O. A. Hougen and K. M. Watson, *Chemical Process Principles, Past Due* (J. Wiley, New York, 1948) p. 327.
14. Thibant, p. 497, *Chemistry of Coal Utilization*, H. H. Lawry, Ed. (J. Wiley and Sons, 1963).
15. O. H. Krikorian, *Thermodynamic Properties of Wyoming Coals, CDTN* 72-18, (1972).
16. N. Y. Kirov and J. N. Stephens, *Physical Aspects of Coal Carbonization*, University of New South Wales Research Monograph, Sydney, Australia (1967).

MLD

PREPRINT UCRL- 81814

Lawrence Livermore Laboratory

HIGH-BTU GAS VIA IN-SITU COAL GASIFICATION

D. R. STEPHENS, R. W. HILL, AND E. L. BURWELL

OCTOBER, 1978

THIS PAPER WAS PREPARED FOR SUBMISSION TO:
10th SYNTHETIC PIPELINE GAS SYMPOSIUM
OCTOBER 30 - NOVEMBER 1, 1978, DES PLAINES, IL.

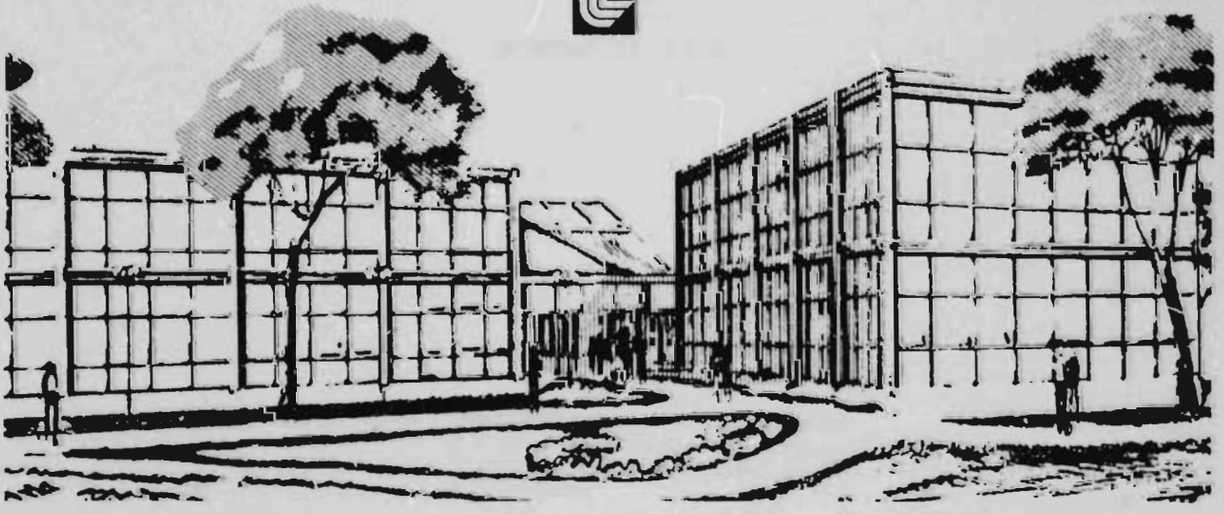

HIGH-BTU GAS VIA IN-SITU COAL GASIFICATION

Douglas R. Stephens

Richard W. Hill

Edward L. Burwell

October 30, 1978

"Work performed under the auspices of the U.S. Department of Energy by the Lawrence Livermore Laboratory under contract number W-7405-ENG-48."

HIGH-BTU GAS VIA IN-SITJ COAL GASIFICATION

D. R. Stephens*, R. W. Hill* and E. L. Burwell**

ABSTRACT

Underground coal gasification offers a relatively low cost, environmentally sound method to produce SNG from coal. The resource is huge and widely distributed. The results of recent underground coal gasification tests in the U.S. have been very encouraging. A brief review of the technology is given followed by a description of Lawrence Livermore Laboratory's recent underground coal gasification experiment, Hoe Creek #2, in which gas of 100-150 Btu/scf was produced using air injection, and 250-300 Btu/scf when injecting steam and oxygen. Plans for future experiments are also described.

*Lawrence Livermore Laboratory, P. O. Box 808, Livermore, California.
**Branch Chief, UCG, Division of Fossil Fuel Extraction, DOE, Washington, D.C. 20545.

INTRODUCTION

A major objective of the U. S. energy program is the development of environmentally acceptable ways to use coal. Thus, development of processes to produce clean fuels from coal is a high priority task. In-situ coal gasification is one of the most promising of these processes. It offers three major potential advantages as a source of synthetic fuel: (1) pipeline quality gas at costs competitive with or lower than that of other synfuels, (2) use of as much as 1.8 trillion tons of coal (quadruple the present coal reserves) that would not be economical to strip or deep mine, and (3) possible environmental advantages.

The DOE underground coal gasification (UCG) program has been described in detail by Wieber.[1] A brief update will be given in this paper followed by a more detailed description of LLL's project to produce high Btu gas via in-situ coal gasification.

History

Underground coal gasification has existed as a concept since 1868 and field tests have been conducted since 1912.[2] The Soviets have executed a field program for over 40 years, and have operated semi-commercial UCG plants for over 20 years. USBM tests in the 1940's and 1950's in the U.S. were quite unsuccessful but did not take advantage of the proven Russian experience.

The USBM resumed UCG testing in 1972, which grew into the current DOE program. A number of major milestones have been accomplished, including the following:

- Air injection producing low Btu gas (165 Btu/scf) at 8.5 million SCFD. This experiment was conducted by the Laramie Energy Technology Center and was in operation continuously for 55 days.

- Steam/oxygen injection producing medium Btu gas (265 Btu/scf) at 1.7 million SCFD. This experiment was conducted by the Lawrence Livermore Laboratory and was in operation for 58 days of air gasification with a scheduled 2 day oxygen test.

BASIC PRINCIPLES

Coal is gasified underground by drilling boreholes into the seam and injecting air (or oxygen and steam) into the underground reaction zone. The hot gases are forced through the seam to the exit borehole and are carried to the surface where they are cleaned and upgraded for use.

The coal-bed permeability must be increased since the natural permeability is too low for gasification. The bed is prepared by reverse combustion, directional drilling, shaped charges or other techniques to form a linkage path between the array of boreholes near the bottom of the seam. This helps to maximize resource recovery by undercutting the coal as it is gasified. The existence of a long hot linkage channel ensures the product gas is properly reduced and has a high heating value that remains fairly uniform with time. Figure 1 shows a side view of a gasification zone.[3] The linkage path has been formed at the bottom of the coal seam. As gasification proceeds from right to left, coal falls into the gasified cavity and creates a highly reactive rubble zone. As the system expands the gasification zone gradually encompasses the full thickness of the coal seam and moves in a broad front towards the outlet well.

Figure 2 shows a plan view of a field development as applied by the Soviets near Moscow which allows extraction of the entire coal resource.[3] The dotted lines show the location of the underground linkage channels formed

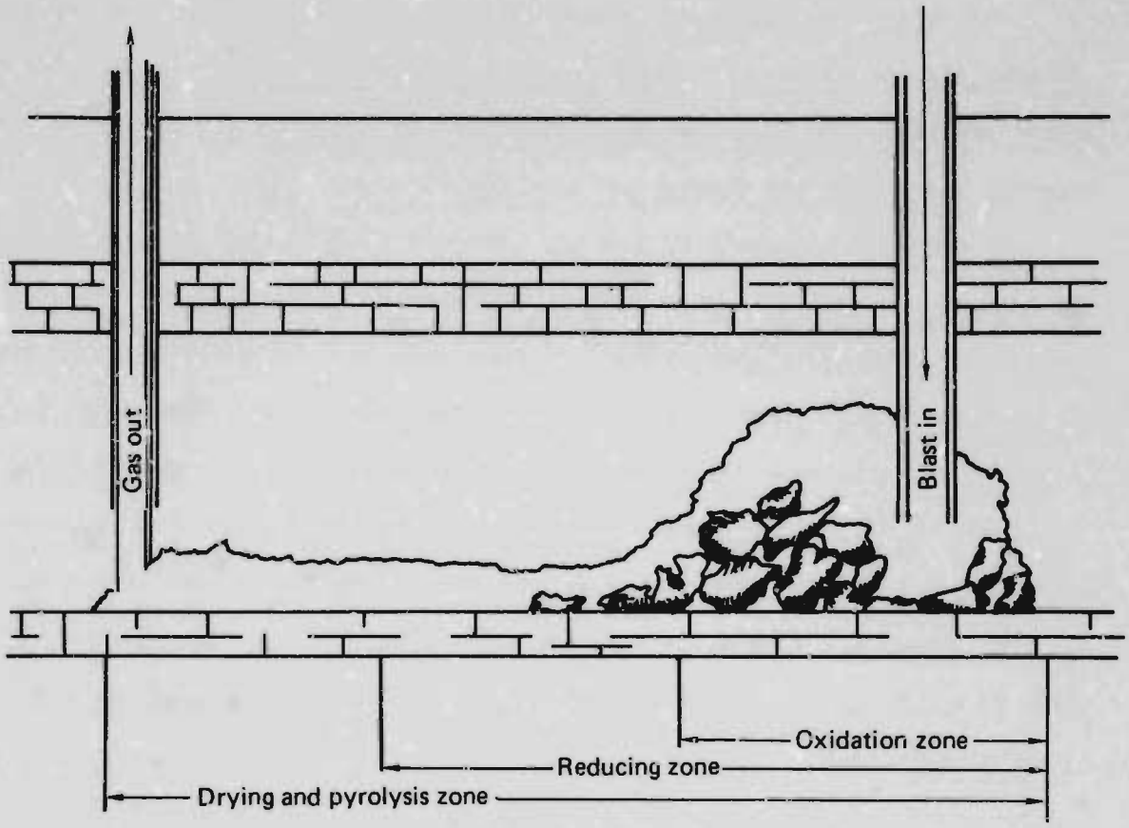

Fig. 1. Conceptual view of a channel during gasification.

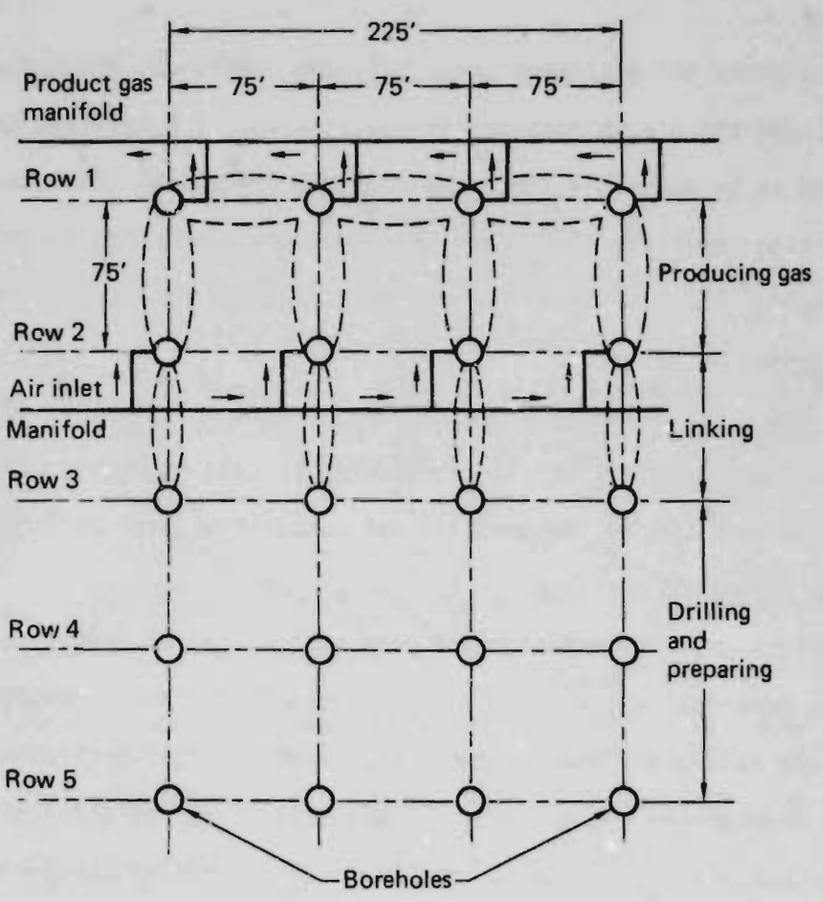

Fig. 2. Plan of an underground coal gasification plant near Moscow.

in the coal by reverse combustion in preparation for gasification. The production phase of gasification is carried out by forward gasification in the channels. Commercially attractive well spacings are believed to be longer than the 75 ft shown in this figure; spacings of 100-150 ft would be more appropriate in the U.S.

Resource

Figure 3 shows the estimated total U.S. coal resource, the resource amenable to UCG, and the proven reserves of coal. Almost 1.8 trillion tons of coal are believed to be available for commercial UCG processes. This huge resource would more than quadruple the U.S. proven reserves and is equivalent to more than 3000 quads (10^{15} Btu) after process efficiencies and inaccessibility of some of the coal is assumed.(4)

Coal seams suitable for UCG are found at depths of 300 ft to 2000 ft. Most of the new coal mines utilize strip-minable coal at depths of less than 200 ft. Therefore UCG is, in general, not competitive with coal mining but utilizes an alternate resource.

The western coal is predominantly deep, thick, sub-bituminous or lignite, and thus is very desireable for UCG. These coals are highly reactive and tend to shrink and fall apart when heated. This tends to self-rubble the coal and produce an underground packed bed. The midwestern and eastern coals tend to be thin and bituminous, and swell upon heating, decreasing the permeability, and thus present a greater challenge for UCG.

Cost Estimates

Independent cost estimates, which were not funded by DOE, have been made for underground coal gasification by Bechtel, Gulf, SRI, the Resource Sciences Corporation, Amoco and PG&E which show that product gas from underground coal

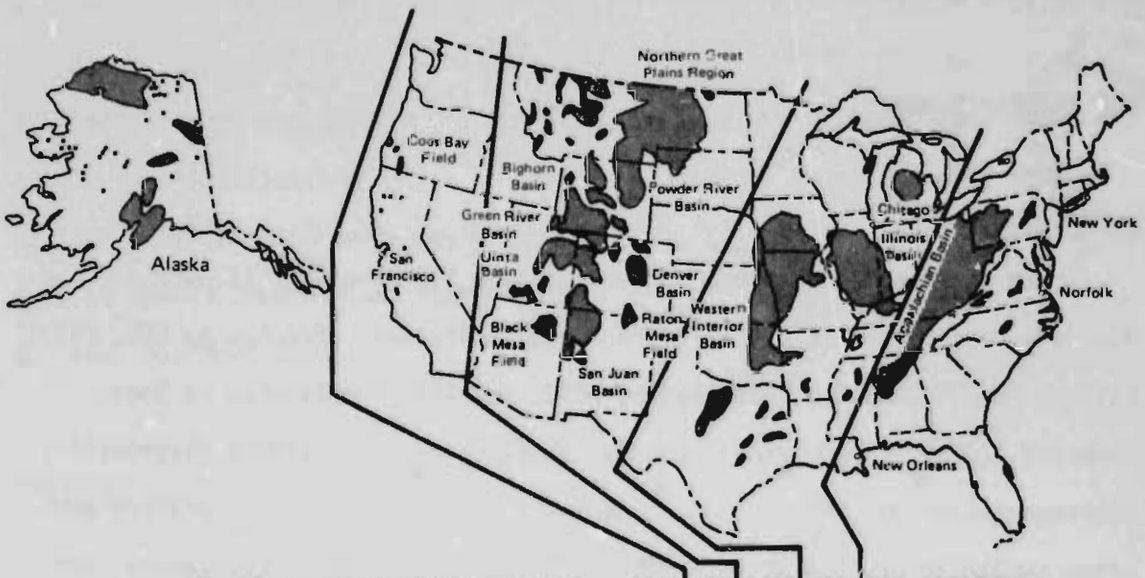

Total Coal to 6000 feet (billions of tons):*	2030	100	3,260	620	350	6,360	Total
Estimated Mineable Reserve Base (Billions of tons):	10	2	200	110	110	432	Total
Estimated UCG Resource (Billions of tons):*	640	20	920	140	80	1,800	Total

*Divide these numbers by 1.1 to obtain tonnes.

Fig. 3. Coal Resources for Underground Coal Gasification.

gasification is projected to cost some 65-75% as much as that produced by strip mining and aboveground coal gasification.[5]

Table 1 presents projected cost data of SNG from underground coal gasification compared with other methods. Synthetic natural gas produced by underground coal gasification cannot economically compete with conventionally produced natural gas. However, underground coal gasification is competitive with LNG, the Northwest Alaskan pipeline, surface coal gasification, and with much of the unconventional sources of gas.

DOE PROGRAM SUMMARY

Projects

There are four major field projects in the DOE Program: (1) Western Low-Btu Gas, directed by LETC, (2) Western Medium Btu Gas, directed by LLL, (3) Eastern Coal Technology, directed by METC, and (4) Steeply Dipping Beds, directed by Gulf R&D Company. Sandia Laboratories is providing diagnostic instrumentation to LETC and LLL. There also is a supporting laboratory program, including participation by ORNL, ANL, LASL, U. Texas, U. Alabama, and other universities.

Results

Since 1972 the Laramie Energy Technology Center has been applying the reverse combustion (linked vertical well) process to underground coal gasification in the Hanna field in Wyoming, as summarized in Table 2.[6-8] Some of the data from the Hanna 2, phase 2 test is shown in Fig. 4; as can be seen, a very constant and high heating value of product gas was obtained.

Table 1

Cost of Pipeline Gas from Alternate Domestic Sources (as Produced)

	1978 Cost/10^6 Btu
• Alaskan Gas[1]	$4.20 - $4.50
• LNG[1]	$3.20 - $5.00
• Devonian Shale[1] and Tight Sands[1]	$2.00 - $4.00
• SNG from Naptha[1]	$5.00 - $7.40
• Geopressured Methane[1]	$4.50
• Surface Gasification[1]	$4.00 - $4.80
• UCG (MOPPS Reston Workshop)	$2.70 - $3.40
• UCG (MOPPS Intermediate Supply Gp.)	$1.75
• UCG (Gulf R&D Co.)	$2.10 - $3.10

[1] DOE Commercialization Task Force, Oct. 1978

In five of the six field tests after Hanna 1, the reverse combustion link propagated at the bottom of the seam. Lateral deviations and in some cases multiple links were observed. As can be seen from the table, these tests produced high quality gas. During Hanna 4 an override situation developed using reverse combustion and low quality gas was produced when linking across a spacing of 100 ft. At present Hanna 4 is shut down to effect repairs, drill additional process wells and additional instrumentation wells. It is planned to relay a reverse combustion link in stages across a total length of 120 ft.

Since 1972 the Lawrence Livermore Laboratory has been studying permeability enhancement (linking) techniques and steam-oxygen gasification. We have completed two underground coal gasification tests at the Hoe Creek site near Gillette, Wyoming as shown in Table 3.[9, 10] Explosive fracturing was used to link Hoe Creek #1 while reverse combustion was used to link Hoe Creek #2. The LLL project will be described in more detail in the following section.

The Sandia Laboratories is providing valuable diagnostic information predominantly to LETC and recently to LLL. They have diagnosed all the Hanna burns and will participate in the Hoe Creek #3 test. They have successfully developed both downhole (thermocouples, pressure and gas sampling, subsidence and acoustic) and remote (electrical) techniques to analyze the propagation of the burn front to aid in understanding and control of the underground process.[11, 12] It is expected that commercial operators would prefer less costly surface diagnostics rather than downhole instrumentation. Sandia has also been active in site characterization for LETC.

The Morgantown Energy Technology Center is studying the gasification of bituminous coal near Pricetown, West Virginia, as shown in Table 4.[13, 14]

Table 2

Underground Coal Gasification Project at the

Laramie Energy Technology Center

The project features low Btu (air) gasification, using reverse combustion (LVW), in the Hanna Basin, Wyoming.

Hanna I:	Linked by hydraulic fracture and reverse combustion. HHV 126 Btu/scf, good resource recovery.
Hanna II, 01:	Linked by reverse combustion, 152 Btu/scf, good resource recovery, 83% thermal recovery.
Hanna II, 02:	Linked by reverse combustion, 175 Btu/scf, high resource recovery, 89% thermal recovery.
Hanna II, 03:	Linked by reverse combustion, 138 Btu/scf, high resource recovery, 76% thermal recovery.
Hanna III:	Linked by reverse combustion, 130 Btu/scf, high resource recovery.
Hanna IV:	Linked by reverse combustion, active.
Hanna V:	Multiple process well sweep test, planned.
Pilot Test:	Planned.

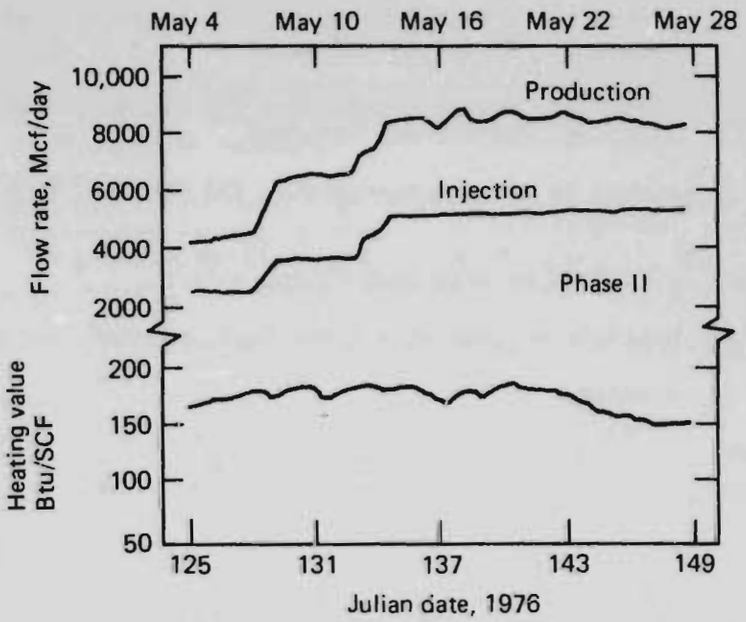

Fig. 4. Production rates and heating value of gas from LERC experiment Hanna II, Phase 2.

Table 3

Underground Coal Gasification Project at the

Lawrence Livermore Laboratory

The project features steam/oxygen gasification and linking techniques, in the Powder River Basin, Wyoming

Characterized Hoe Creek site, near Gillette, Wyoming in 1975

Hoe Creek #1	Linked by explosive fracturing 1975, gasified with air in 1976 product heating value = 110 Btu/scf, 73% thermal recovery, 15% resource recovery.
Hoe Creek #2:	Linked by reverse combustion, gasified with air (two-day oxygen burn), in 1977 product heating value - 106 Btu/scf (263 Btu/scf with oxygen/ steam), 68% thermal recovery, very high resource recovery.
Hoe Creek #3:	Linked by directional drilling, to be gasified with oxygen/ steam, July 1979.
Deep Test #4:	Deep linear burn, steam/oxygen, planned.
Deep Sweep #5:	Deep multiple process well sweep test, planned.
Pilot Test:	Planned.

Table 4

Underground Coal Gasification Project at the

Morgantown Energy Technology Center

The project features low Btu (air) gasification of a swelling bituminous coal near Pricetown, West Virginia.

Pricetown I:	To be linked by reverse combustion (LVW), early 1979.
Pricetown II:	To be linked by directional drilling, 1980.
Future Tests:	To be determined.

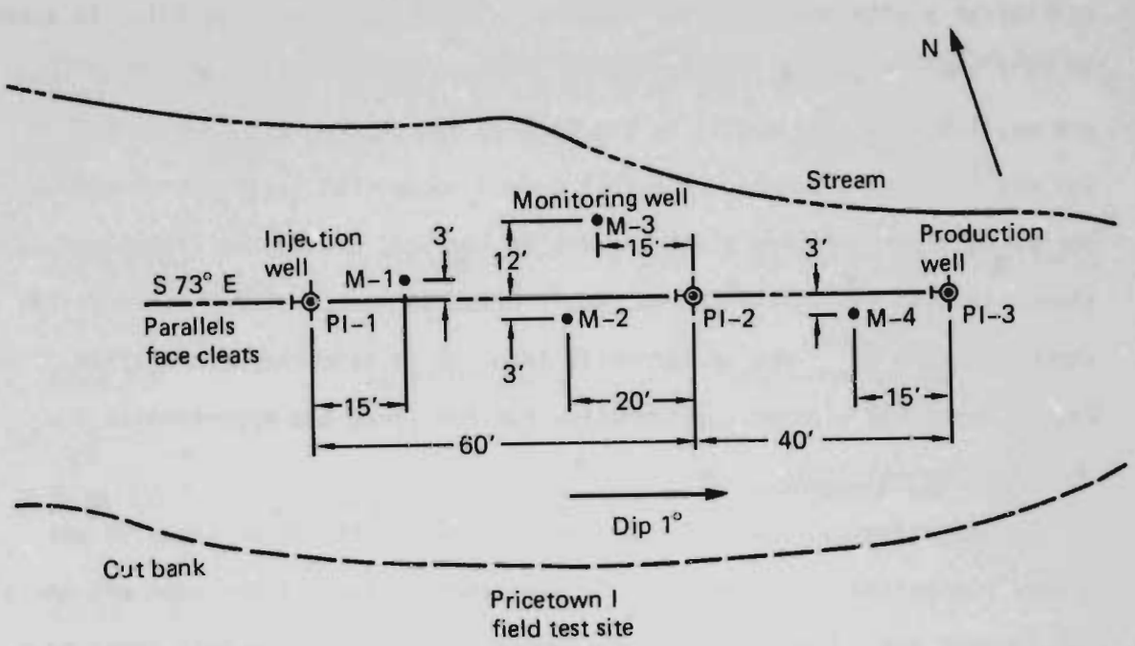

Fig. 5. Well placement for Pricetown I.

Their earlier work was primarily in laboratory experimentation but emphasis has now shifted to the field. They are currently fielding Pricetown I which applies reverse combustion experience gained in the west to eastern coal: see Fig. 5. The test will be ignited in early 1979. It is to be followed by Pricetown II, which is to be linked by directional drilling in 1980.

The underground gasification of steeply dipping coal beds is under development by the Gulf Research and Development Company and TRW Systems, Inc., working at a site near Rawlins, Wyoming. Steeply dipping beds (dips in excess of 35^{o}) are, in general, uneconomical to mine, yet 100 billion tons of coal are available to UCG, mostly in the Rockies and the Pacific Coast. The Soviets[15] have described in detail a very successful gasification method employing slant drilling along the dip of the bed, and so the technology is almost in hand for this resource. Gulf plans to execute three field tests, as shown in Table 5[16] and is currently involved in site characterization. Fig. 6 shows the planned configuration for the first two experiments.

Experimental Scale

The experimental scale of these underground gasification tests is not always recognized. At present, U.S. experiments have not included end use of the product gas. However, all experiments are continuous - most tests have been for 30-60 consecutive days, which illustrates the simplicity and reliability of the UCG process. Coal consumption rates have been 20-120 tons per day, producing 2-12 mmscfd of 110-170 Btu/scf gas. LLL's Hoe Creek #2 oxygen phase utilized 30 tpd of coal, producing 3 mmscfd of 260 Btu/scf gas.

Thus the scale of operations and size of equipment are of the order of DOE/Fossil Energy pilot plants, and in general the length of runs without interruption are greater.

Table 5

Underground Coal Gasification Project at

the Gulf Research and Development Company, with

TRW Systems as Subcontractor

The project features low Btu (air) gasification of steeply dipping coal beds, near Rawlins, Wyoming, linked by slant drilling.

Burn #1:	July 1980	Simple initial experiment.
Burn #2:	September 1980	Instrumented test.
Burn #3:	September 1981	Sweep test.
Pilot Scale Test:	Planned.	

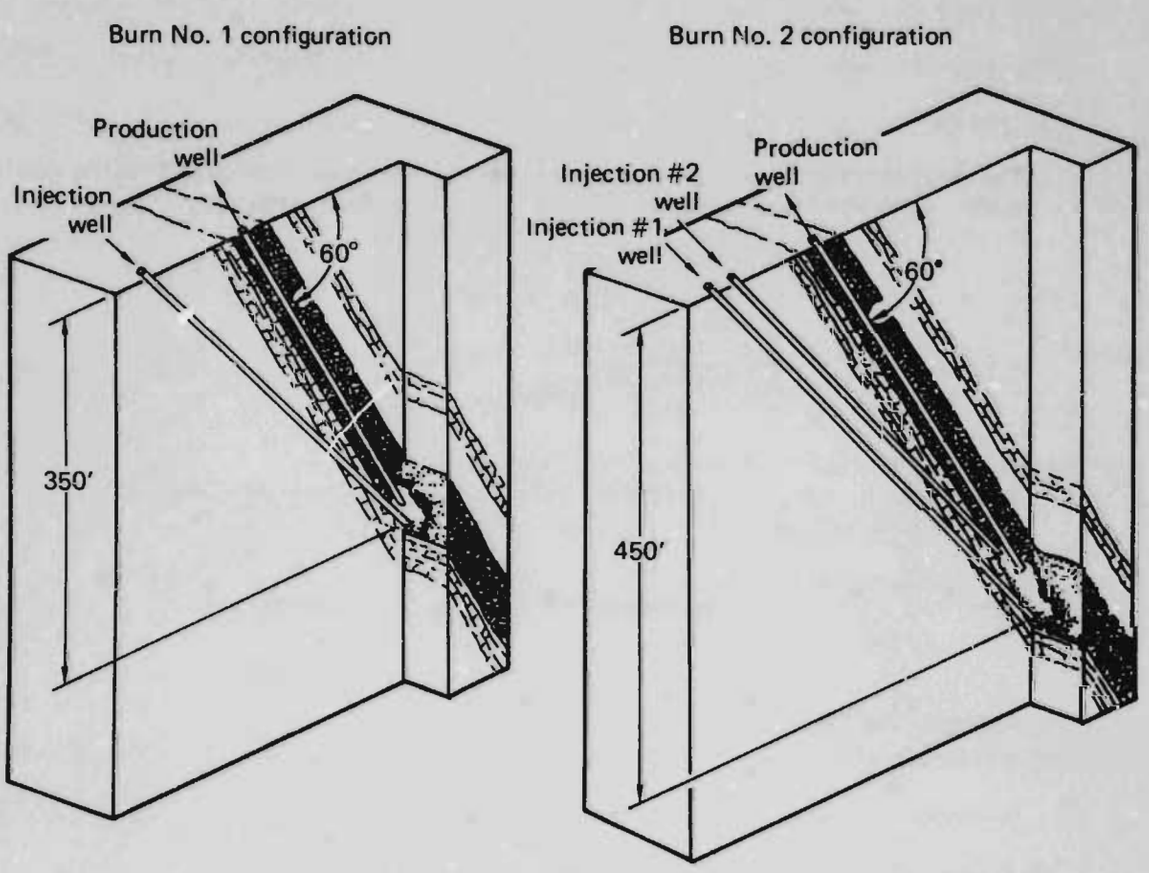
Burn No. 1 configuration
Production well
Injection well
60°
350'
Burn No. 2 configuration
Injection #2 well
Production well
Injection #1 well
60°
450'

Fig. 6.

Environmental Issues and Control

Environmental issues with UCG include air quality, subsidence, and water quality. The air quality issue is similar to aboveground processing with respect to fugitive emissions from the plant and can be minimized by good engineering practice. The underground process itself should have no significant impact upon air quality. This issue will not be described further.

Efficient coal extraction will cause surface subsidence. Regions of surface cultural activity, such as towns, roads, pipelines, etc., should be avoided. This is a problem with any type of efficient coal extraction, including strip mining and underground mining.

Surface subsidence can be minimized by wide spacings of the rows of process wells. In this way pillars of unburned coal will support the overburden above the gasified zones, and surface subsidence should be small. This technique limits resource recovery but has little effect upon process economics. Eventually a decision will be necessary on this issue: whether subsidence is to be minimized or resource extraction is to be maximized.

In general, all coal beds are aquifers. Dangerous coal derived contaminants such as phenols are introduced into the coal aquifer during and following the coal gasification process. Fortunately, coal itself absorbs the contaminants and confines them near the burn zone. Data from the LLL's Hoe Creek #1 experiment, which has been monitored for over a year, show that the contaminants produced from this test are immobilized and have decreased in concentration by a factor of 100: see Fig. 7.[17] Thus, predictions made in the laboratory experimentally and by calculations have been thus far verified in the field, although more work remains to be done.

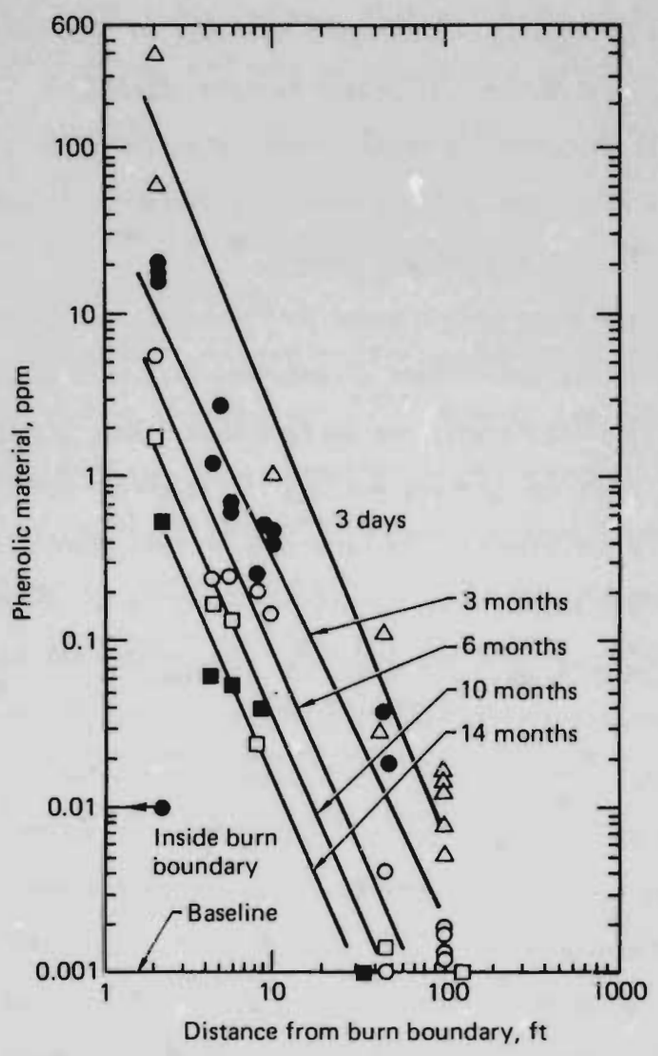

Fig. 7. Concentrations of phenolic materials as a function of distance from the nearest burn boundary of the Hoe Creek I in-situ coal gasification experiment. Times are measured from the end of gasification. Sampling wells are completed in the gasified coal seam and located in various directions from the gasification zone.

THE LLL PROJECT

The major objective of the LLL project is to develop a commercial in-situ coal gasification process which produces medium Btu product suitable for upgrading to pipeline quality gas. The process involves first increasing the coal bed permeability, since the natural permeability of the coal in-place is too low for gasification, followed by injection of mixtures of oxygen with steam or carbon dioxide. A second objective for the project is to develop improved techniques to increase the coal bed permeability. Methods under investigation include chemical explosive fracturing, reverse combustion, shaped charges and directional drilling.

Previous underground coal gasification experiments, using oxygen/steam or enriched air/steam have been analyzed.[18] Most of the tests were conducted in Soviet-Bloc countries. These experiments were operated for a month or more, consumed up to 20,000 tons of coal, with no serious technical problems reported. The Soviets reported that if air gasification was efficient, then an oxygen or steam-oxygen process was also efficient. This was confirmed in the U.S. by the USBM tests in Gorgas, Alabama.

Data for these test are summarized in Table 6. The results from Gorlovskaya, Podmoskovnaya, and Poland suggest that a medium-Btu gas suitable for upgrading to pipeline quality gas can be obtained from underground coal gasification, particularly if steam-oxygen rather than enriched air and steam are used. On a nitrogen-free basis, the following gas quality was obtained in the experiments: CH_4, 2-6%; H_2, 37-42%; CO, 18-27%; CO_2, 25-34%, with a higher heating value of 220 to 270 Btu/scf.

Hoe Creek #2

The major objectives of the Hoe Creek #2 underground coal gasification experiment were:

Table 6.

Enriched Air and Steam-Oxygen Underground Coal Gasification Test Data.

Station and Generator	Blast composition (%) O_2	N_2	Moles steam per mole blast	CH_4	H_2	CO	CO_2	N_2	H_2S	C_nH_m	O_2	Higher heating value Btu/scf
Gorlovskaya, #1, USSR	45	55	-	2.8	29.4	19.5	18.3	27.8	-	-	-	187
Lisichansk, #24, USSR	44.8	55.2	-	2.38	15.8	7.62	32.2	38.33	2.09	0.19	0.37	103
Podmoskovnaya, #VNII, USSR	65	35	-	1.9	35.0	15.3	28.1	16.2	2.9	0.4	0.2	190
Podmoskovnaya, #VNII, USSR	65	35	0.42	1.8	35.0	15.6	28.4	15.7	2.9	0.4	0.2	190
Mars Mine, Poland	100	0	-	6.3	37.0	25.8	28.8	1.4	-	-	0.7	267
Gorgas, Alabama, USBM	100	0	-	4.1	24.5	21.2	47.8	-	-	0.3	0.2	195

1. Investigate reverse combustion process in a uniform, wet, hydrologically active coal seam.
2. Determine forward gasification parameters with injected air flows of 2000-4000 scfm.
3. Conduct a short steam-oxygen burn with the Hoe Creek #2 air burn.
4. Evaluate diagnostic instrumentation.
5. Evaluate operational parameters.
6. Evaluate environmental concerns.

All of the objectives were accomplished successfully.

Site stratigraphy is shown in Fig. 8 and a plan view of the well layout is shown in Fig. 9.

We gasified the Felix #2 coal seam, which is a wet (30% H_2O), low ash (4%) subbituminous coal. The seam is 25 ft. thick at a nominal depth of 125 ft. The wells I-1 through I-12 each contain six thermocouples in the Felix #2 coal seam and at least one thermocouple in the overburden. In addition to the thermocouples, each instrument well, except I-10, contained a stainless steel tube, open at the end, seven feet from the bottom of the coal seam, for pressure measurement and gas sampling during the burn. Wells I-1, I-5 and I-10 included additional inconel tubes for a traveling thermocouple. Well A was the injection well, B was the production well, while C-well was planned as a dewatering well. We linked C with B using reverse combustion.

The wells designated H-1 through H-6 and SI-1, SI-2 and SI-3 were used for high frequency electromagnetic (HFEM) transmission measurements for burn front detection. Wells Ex-1, Ex-2, SS-1, SS-2, SI-1, SI-2, SI-3, and PZ-1 were used for subsurface ground motion measurement. Wells WS-1 through WS-9 were used for post burn water sampling.

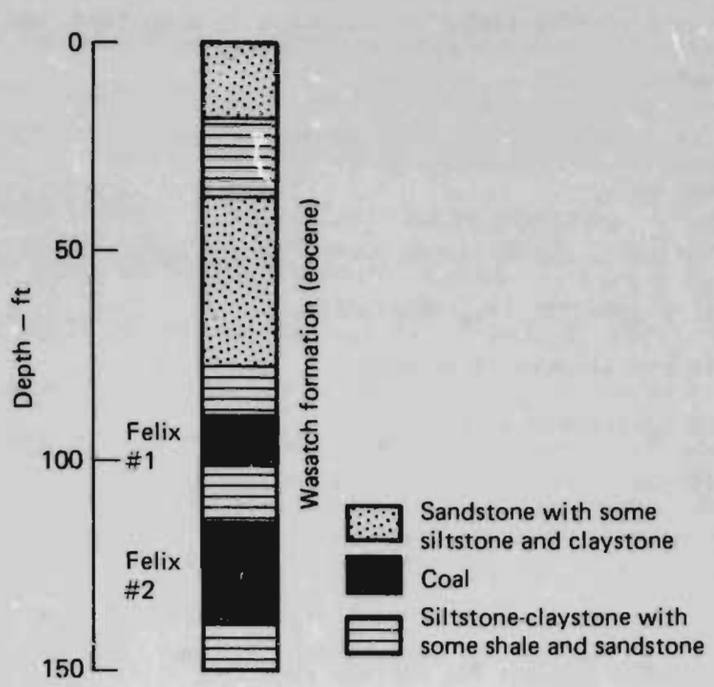

Fig. 8. Site stratigraphy obtained from cored wells.

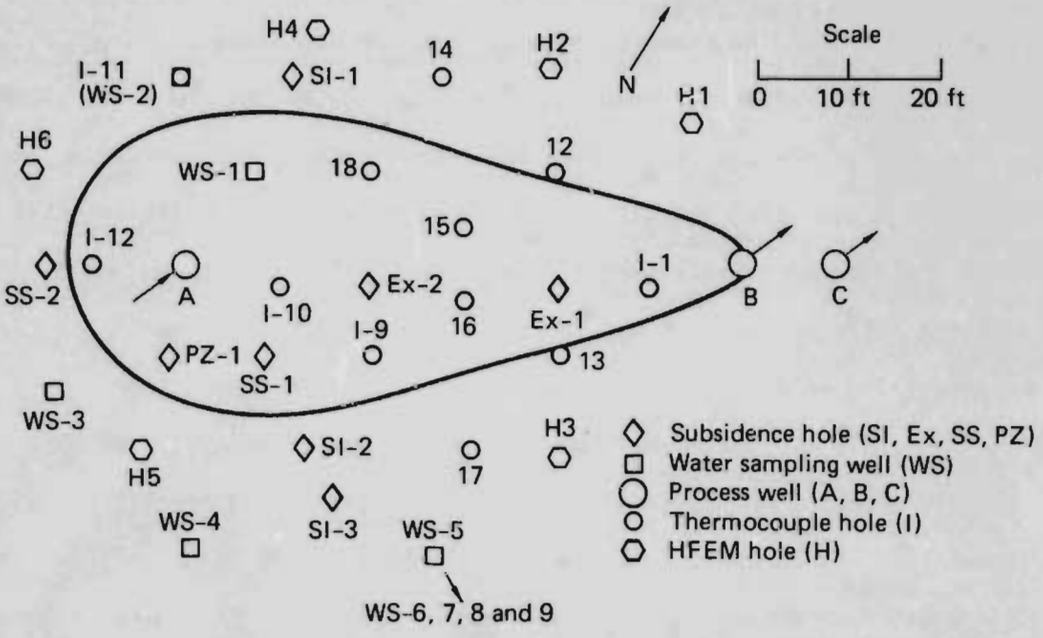

Fig. 9. Hoe Creek experiment No. 2 layout. The predicted sweep is shown as the enclosed tear drop-shaped region.

All instrumentation worked well.

All the data taken were stored on magnetic disc and tape by an HP-21 MX-E computer, which allowed instant access to both raw and processed data with a large number of plotting and tabulating routines. Field work took place from June to October, 1977. Air flow tests began on October 4 and showed that product flow rates of 35-40 scfm could be produced with a backpressure of 53 psia. On October 14 the coal was ignited in Well B, with injection in Wells A and C, and two reverse burn links simultaneously initiated toward the injection and dewatering wells. Data from traveling thermocouples, fixed thermocouples and HFEM indicated that there were several reverse burn paths which appeared to be near the bottom of the seam.

The reverse burn link to the injection well was completed on October 28, and forward gasification was then carried out through December 25, a period of 58 days. A scheduled two-day oxygen burn was executed which produced a more efficient gasification with air with no safety or operational problems.

An override situation developed after a few days of forward gasification, causing a rapid decline in product heating value: see Fig. 10, which shows the product gas heating value over the entire forward gasification period. This appeared to be due to damage to the casing and the presence of multiple gasification paths, some near the bottom of the coal and some near the top. The injection casing had been completed within the bottom 5 ft. of the coal. This problem was overcome in 1977 day 311 by injecting air near the bottom of the coal seam using an auxiliary stainless steel dewatering line. As can be seen in Fig. 10, the heating value increased to over 100 Btu/scf. Following this phase, the steam-oxygen test was carried out. We injected the oxygen through a 3-in. stainless steel pipe completed inside the A well casing and

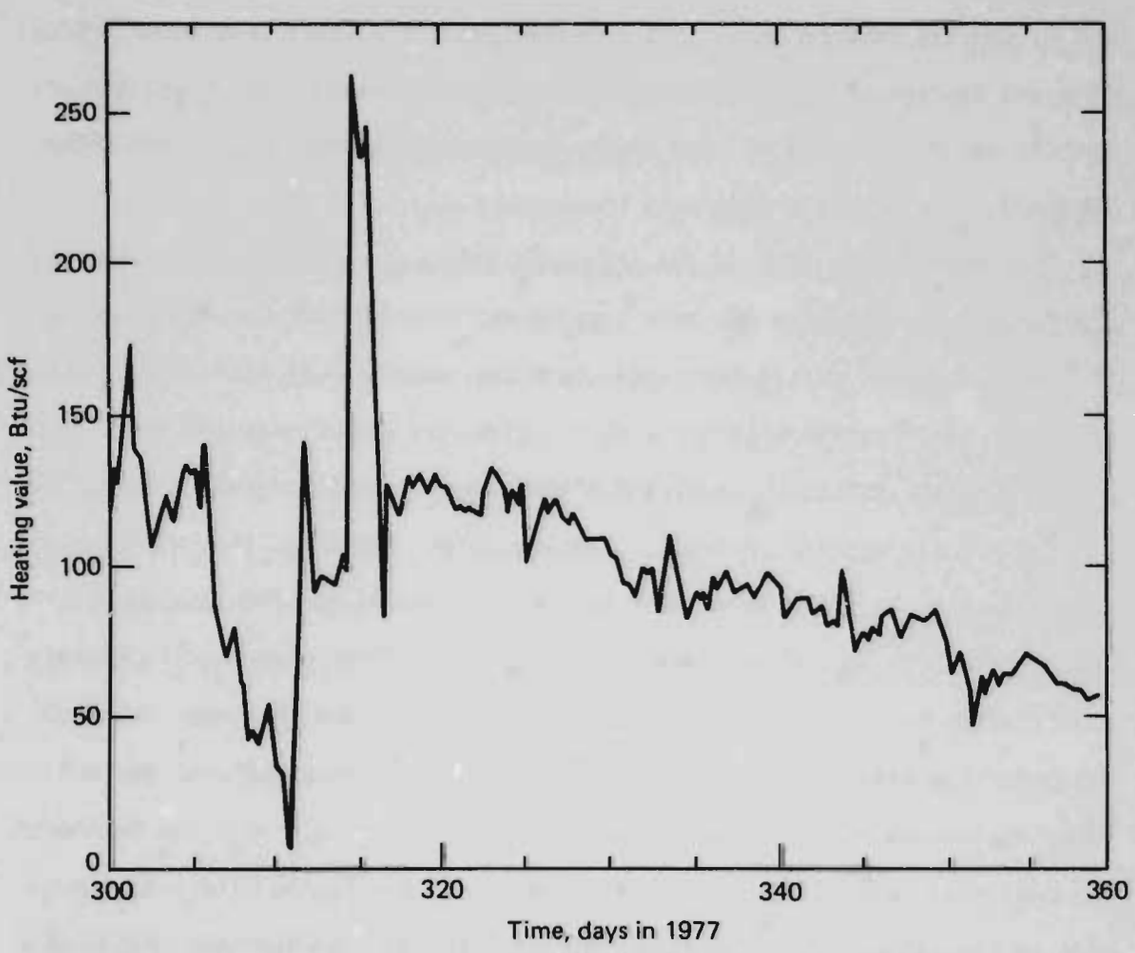

Fig. 10. Heating value of the produced gas during the forward burn period, Hoe Creek No. 2.

injected the steam through the space between the 3-in. pipe and well casing. Since the 3-in. pipe was completed near the top of the coal seam, and since the main casing was almost certainly burned off at this time we believe that the oxygen emerged near the top of the coal seam.

For several hours after we started oxygen injection, the heating value of the product gas decreased as the burn zone moved to the top of the coal seam. As the underground temperature rose, however, the heating value increased steadily to over 280 Btu/scf and remained fairly constant throughout the rest of the test. Figure 11 outlines the changes in the heating value of the product gas from the beginning of the oxygen burn.

Figure 12 shows the concentrations of the three main combustible gases before, during, and after the oxygen-steam burn. The dip in carbon monoxide production (and in heating value as shown in Fig. 11) occurred at the start of the oxygen-steam burn, when the burn zone was changing position. Good quality gas was produced using oxygen in the same injection geometry that, with air, produced very poor gas which suggests that the oxygen gasification produced a much hotter burn, consuming the oxygen close to the injection well. If this is the case, better control over product gas quality may be obtained with oxygen gasification compared to that with air. These results are quite encouraging for steam-oxygen gasification.

After the oxygen/steam test, air injection was returned to the auxiliary dewatering line. Gasification continued for another 43 days. During this time the product heating value decreased more-or-less linearly with time, from 140 to 67 Btu/scf, when gasification was terminated by shutting off the compressors on Christmas Day. Burn through had not occurred and ungasified coal remained near the production wells. The decline in heating value apparently was due to increases in heat loss to inert materials underground.

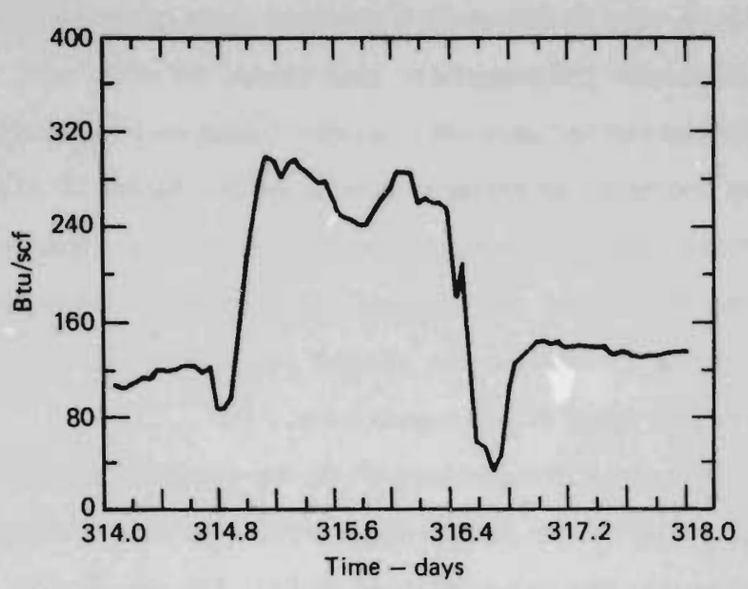

Fig. 11. Heating value of gas produced during steam-oxygen phase of Hoe Creek No. 2.

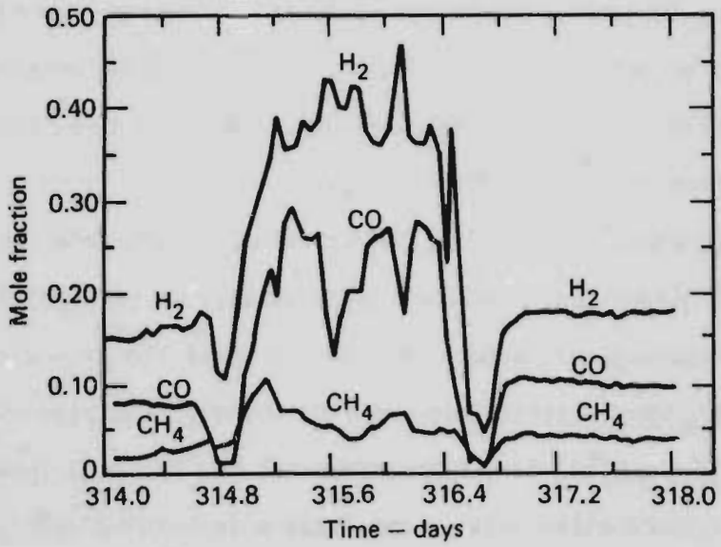

Fig. 12. Combustible gas concentrations during steam-oxygen phase of Hoe Creek No. 2.

During forward gasification, 2300 tons of coal were consumed, producing product gas of an average heating value of 108 Btu/scf with air injection and 264 Btu/scf with oxygen and steam injection. The sweep width was approximately 50 ft. Gas losses during the test averaged 20%. The energy balance for the consumed coal is shown in Fig. 13. The results for the Hoe Creek #2 experiment are described in more detail in Ref. 10.

PLANS

Issues

A number of key issues must be resolved in UCG to move the technology into the commercial sector. The major issues are:

- Demonstration of reliable link at bottom of coal seam.
- Control of water influx.
- Minimize gas losses.
- Subsidence control.
- Process control with good gas quality.
- Environmental control.
- Technology transfer to industry.

Hanna IV and Hoe Creek #2 have shown that, at times, reverse combustion links do not propagate at the bottom of the coal seam, as required for efficient gasification. The demonstration of a reliable link at the bottom of the coal seam is being approached in two ways. LETC and SLA, together with the other laboratories, are developing improved site characterization techniques to determine the geologic factors which determine whether reverse combustion will stay at the bottom of the coal seam or not. Hanna IV was shut down in

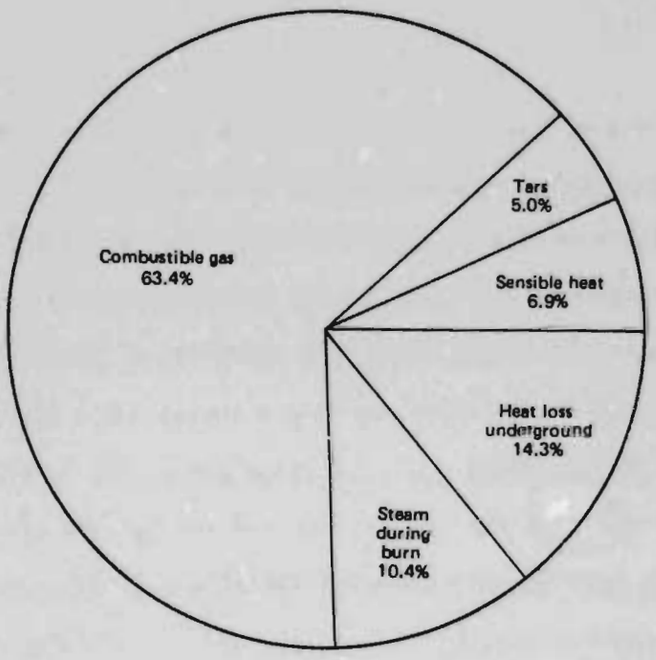

Fig. 13. Energy distribution, for the Hoe Creek No. 2 experiment.

part for this purpose, and the second phase of this test will provide additional information on the reliability and control of reverse combustion.

LLL and METC, together with the other laboratories, are investigating the use of mechanical links which can effect the link at the bottom of the coal seam independent of geology. LLL is working on directional drilling and the use of shaped charges while METC is working on directional drilling and hydrofracturing.

Hoe Creek #3

The first gasification test using a mechanical link in the U.S. will be LLL's Hoe Creek #3. This experiment is co-sponsored by DOE and GRI.

In order to ensure a single link near the bottom of the coal seam, we have used directional controlled drilling to construct a known gasification channel.

The deviated hole was drilled during July-August, 1978, using a 2-3/8" diameter Dyna-Drill mud motor to drill a 3" diameter hole. Initially the drilling angle was inclined 30^{0} to the horizontal and deviated at a rate of approximately 5^{0} per 100 feet of travel.

Despite some difficulties with drill sticking in the unconsolidated sand above Felix #1, a hole 710 ft. long was completed with the bottom half of the coal seam for a distance of 200 ft. An elevation view of this hole is shown in Fig. 14.

Vertical wells will be drilled and linked to this channel in October of 1978 as the first step in the drilling program for Hoe Creek #3. A high pressure water jet casing cutter will be used to make the links.

After the linking phase is completed the rest of the wells will be drilled to complete the pattern for Hoe Creek #3, as shown in Fig. 15. Surface piping and process systems will be constructed starting early in 1979 and should be completed by early summer. Gasification is scheduled for July-August 1979.

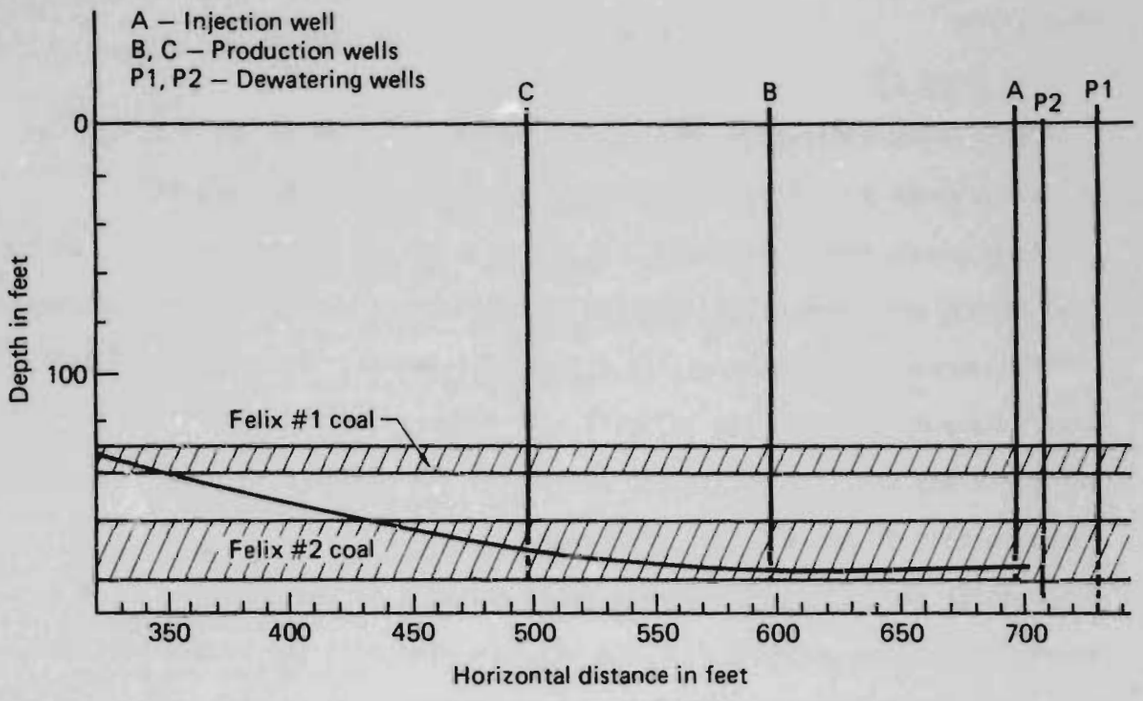

Fig. 14. Hoe Creek No. 3 process wells [illegible] channel.

Since the directional hole is only 3" in diameter, reverse burn will be used to enlarge the hole to allow for the high production flow rates desired. This step should take two or three days and will be followed by up to two weeks of forward burn with air to allow a direct comparison to be made with Hoe Creek #2 results.

Following the air burn we plan to gasify with steam and oxygen at a coal consumption rate of 80-100 TPD for up to six weeks.

Future Plans

In all UCG projects the intent is to perform linear (two-to-three process well) experiments such as Hanna IV, Hoe Creek #3, Pricetown I and SDB burn #1, to: demonstrate reliable linking, show that water influx can be minimized while also minimizing gas losses, obtain good gas quality and good process control which is vital for favorable economics, and demonstrate acceptable environmental impact. With success at this level, it is then necessary to scale up to sweep tests to demonstrate at a significant scale that all the above criteria are met, including acceptable subsidence control.

A schedule for the LLL medium Btu UCG project is shown in Fig. 16. A deep site (coal seam at 500-1000 ft.) of potential commercial interest would be selected and characterized. A three-process well, steam-oxygen test, designated experiment #4, would be designed, fielded, and tested at the 100 TPD, 5×10^6 scfd of medium Btu gas level. Test #5 would be a sweep experiment involving up to three simultaneous burns in a six-to-nine well pattern. The test would be carried out on a sufficiently large scale (300 TPD coal consumption, 15×10^6 scfd product) to verify technical, environmental and economic predictions. We anticipate executing tests #4 and #5 in conjunction with an industrial partner, under joint DOE/GRI sponsorship. Following the

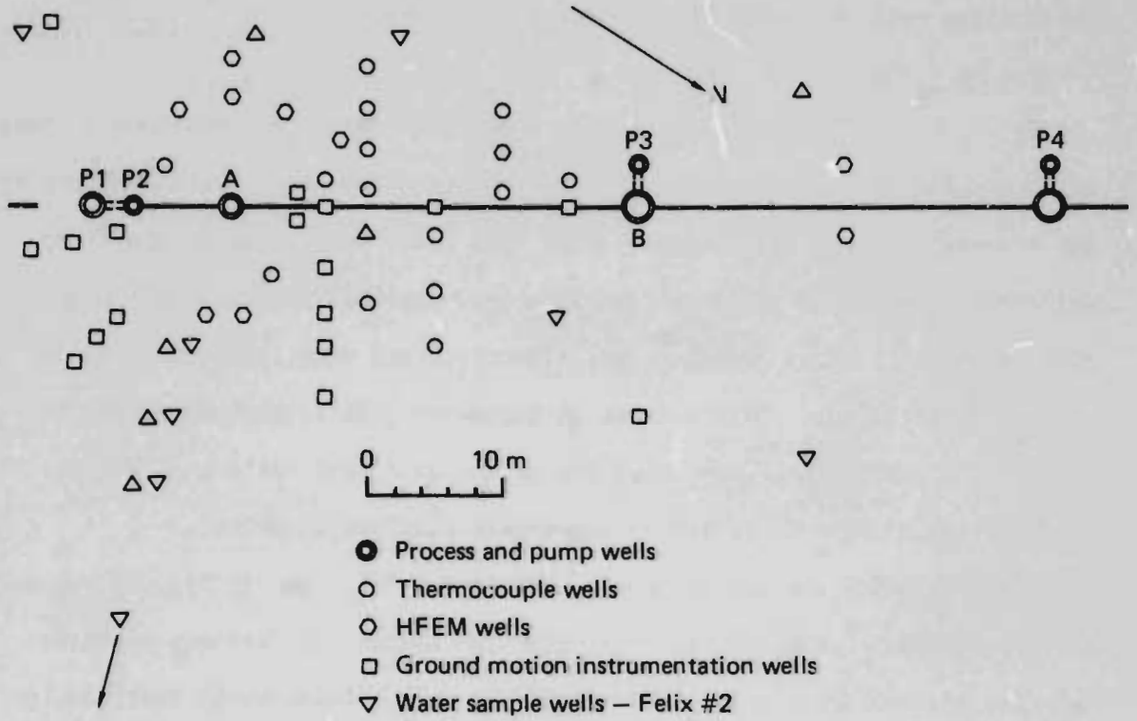

Fig. 15. Hoe Creek No. 3 plan view of well array.

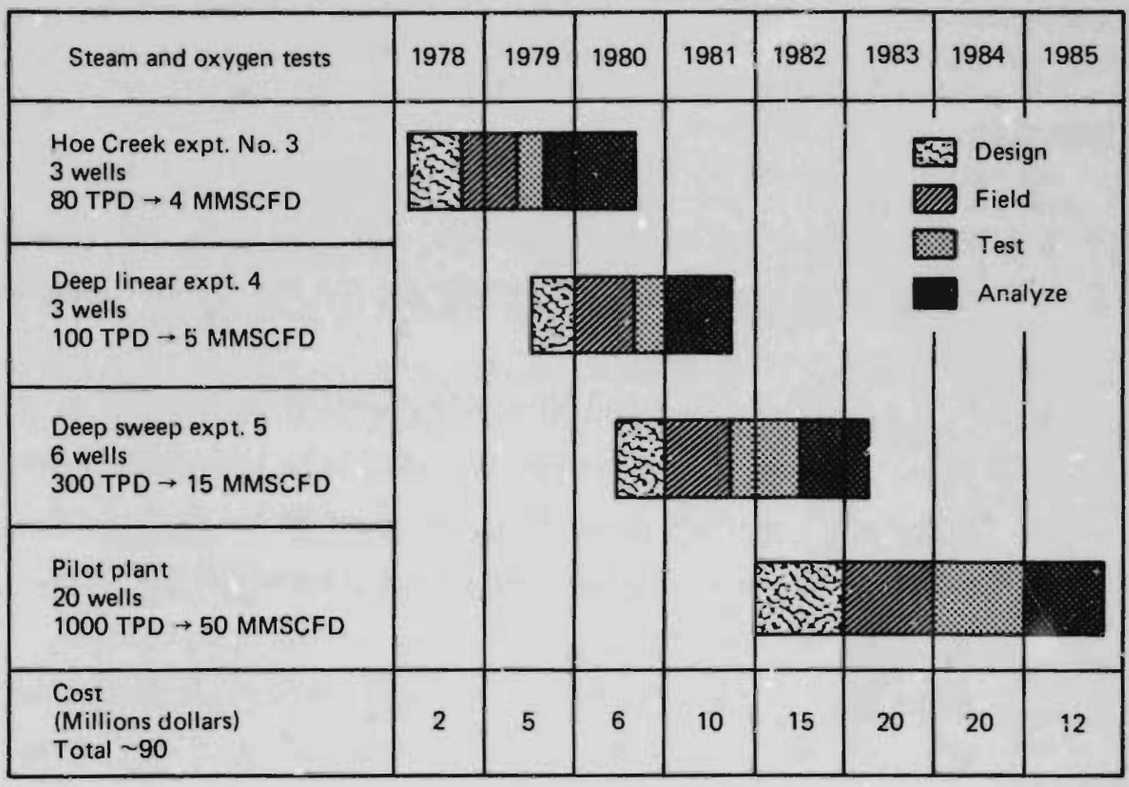

Medium – Btu in-situ coal gasification project

Fig. 16. Schedule for the LLL medium – Btu in-situ coal gasification project.

successful execution of this test, the industrial partner would carry out the ensuing pilot scale test with support, as appropriate, from LLL and other DOE laboratories.

This is a success-oriented schedule; it may be necessary to repeat some test. In addition, it would be desirable to perform some linear tests similar to #3 or #4 in other coal deposits to extend the technology to a wider resource base.

CONCLUSION

- UCG can recover the energy in unminable coal seams. The coal reserve for UCG is vast and widely distributed and could ultimately supply at least 3000 quads of energy.
- Tests to date confirm potential economic and environmental advantages. Economic studies indicate UCG costs to be approximately 75% of that for mining and conventional coal gasification.
- Results of previous steam/enriched air and steam/oxygen UCG tests, and of the Hoe Creek #2 test are very encouraging in that steam-oxygen gasification is technically feasible and produces product gas at least as efficiently as from air gasification. Thus much of the more extensive data base with air gasification using UCG is applicable to high Btu gasification.
- Demonstration of reliable linking at the bottom of the coal seam is crucial in obtaining good quality gas. Hoe Creek #3 will be the first UCG test in the U.S. to use presumed reliable link and will also be the first long term steam-oxygen test in UCG.

References

1. P. R. Wieber, "Prospects of Producing Synthetic Natural Gas Through Undergound Coal Gasification," Proceedings of the Ninth Synthetic Pipeline Gas Symposium, AGA, (1977).

2. D. U. Olness and D. W. Gregg, "The Historical Development of Underground Coal Gasification," Lawrence Livermore Laboratory, Rept. UCRL-52283, (1977).

3. D. W. Gregg, R. W. Hill and D. U. Olness, "An Overview of the Soviet Effort in Underground Coal Gasification," Lawrence Livermore Laboraotry, Rept. UCRL-52004, (1976).

4. "Underground Coal Gasification Program," Division of Oil, Gas, and Shale Technology, The Energy Research and Development Administration, ERDA 77-51, (March 1977).

5. Refer to the process economics papers in (a) Proceedings of the 2nd Annual Underground Coal Conversion Symposium, L. Z. Shuck, Ed., Rept. MERC/SP-76/3 (1976). (b) Proceedings of the 3rd Annual Underground Coal Conversion Symposium, D. R. Stephens, Ed., Rept. CONF-770652 (1977). (c) Proceedings of the 4th Annual Underground Coal Conversion Symposium, D. A. Northrop and W. L. Noll, Eds., Rept. SAND-78-0941 (1978).

6. C. F. Brandenburg, D. D. Fischer, D. A. Northrop and L. A. Schrider, "Results and Status of the Second Hanna In Situ Coal Gasification Experiment," in Proceedings of the 2nd Annual Underground Coal Conversion Symposium, L. A. Shuck, Ed., Rept. MERC/SP-76/3 (1976).

7. C. F. Brandenburg, D. D. Fischer, R. M. Boyd, S. B. King and A. E. Humphrey, "A Review of LERC's In Situ Coal Gasification Project," in Proceedings of the 3rd Annual Underground Coal Conversion Symposium, D. R. Stephens, Ed., Rept. CONF-770652 (1977).

8. T. C. Bartke, L. Dockter, T. E. Sterner, J. E. Virgona and L. F. Wojdac, "Status Report on the Hanna III and Hanna IV Underground Coal Gasification Experiments," in Proceedings of the 4th Annual Underground Coal Conversion Symposium, D. A. Northrop and W. L. Noll, Eds., Rept. SAND-78-0941, (1978).

9. R. W. Hill, D. R. Stephens and C. B. Thorsness, "The LLL In Situ Coal Gasification Project," in Proceedings of the 3rd Annual Underground Coal Conversion Symposium, D. R. Stephens, Ed., Rept. CONF-770652, (1977).

10. R. W. Hill, C. B. Thorsness, D. R. Stephens, D. S. Thompson and W. R. Aiman, "The LLL Underground Coal Gasification Project: 1978 Status," in Proceedings of the 4th Annual Underground Coal Conversion Symposium, D. A. Northrop and W. L. Noll, Eds., Rept. SAND-78-0941 (1978).

11. D. A. Northrop, et al, "Instrumentation for In Situ Coal Gasification: An Assessment of Techniques Evaluated on the Hanna II Experiment," Sandia Laboratories, SAND 77-0669, (September 1977).

12. P. J. Hommert and D. A. Northrop, "Sandia Laboratories Project Review: Instrumentation and Process Control Development for In Situ Coal Gasification," in Proceedings of the 4th Annual Underground Coal Conversion Symposium, D. A. Northrop and W. L. Noll, Eds., Rept. SAND-78-0941, (1978).

13. L. D. Strickland, "A Status Report on MERC's Program for In Situ Gasification of Bituminous Coals," Proceedings of the Third Annual Symposium on Underground Coal Conversion, D. R. Stephens, Ed., Rept. CONF-770652, (1977).

14. L. D. Strickland, J. W. Martin, A. J. Liberatore and D. W. Gilmore, "The MERC Program for In Situ Gasification of Eastern Coals," in Proceedings of the 4th Annual Underground Coal Conversion Symposium, D. A. Northrop and W. L. Noll, Eds., Rept. SAND-78-0941, (1978).

15. E. Kreinin and M. Revva, "Underground Gasification of Coal," UCRL-Trans-10810, (1966).

16. J. H. Daniel and P. Alexander, "Underground Gasification for Steeply Dipping Coal Beds," in Proceedings of the 4th Annual Underground coal Conversion Symposium, D. A. Northrop and W. L. Noll, Eds., Rept. SAND-78-0941, (1978).

17. S. W. Mead, H. C. Ganow and F.T. Wang, "Groundwater and Subsidence Investigations of the LLL In Situ Coal Gasification Experiments," in Proceedings of the 4th Annual Underground Coal Conversion Symposium, D. A. Northrop and W. L. Noll, Eds., Rept. SAND 78-0941, (1978).

18. D. R. Stephens and D. G. Miller, "Soviet-Block Underground Coal Gasification Results Using Enriched Air and Steam," Rept. UCID-17245, (1976).

Ted Cherk

PREPRINT UCRL- 81887

Lawrence Livermore Laboratory

CONTROL ASPECTS OF UNDERGROUND COAL GASIFICATION: LLL INVESTIGATIONS OF GROUND-WATER AND SUBSIDENCE EFFECTS

S. WARREN MEAD, FRANCIS T. WANG, AND HAROLD C. GANOW

NOVEMBER 10, 1978

THIS PAPER WAS PREPARED FOR SUBMISSION TO:
DOE ENVIRONMENTAL CONTROL SYMPOSIUM, WASHINGTON, D.C., NOVEMBER 28-30, 1978

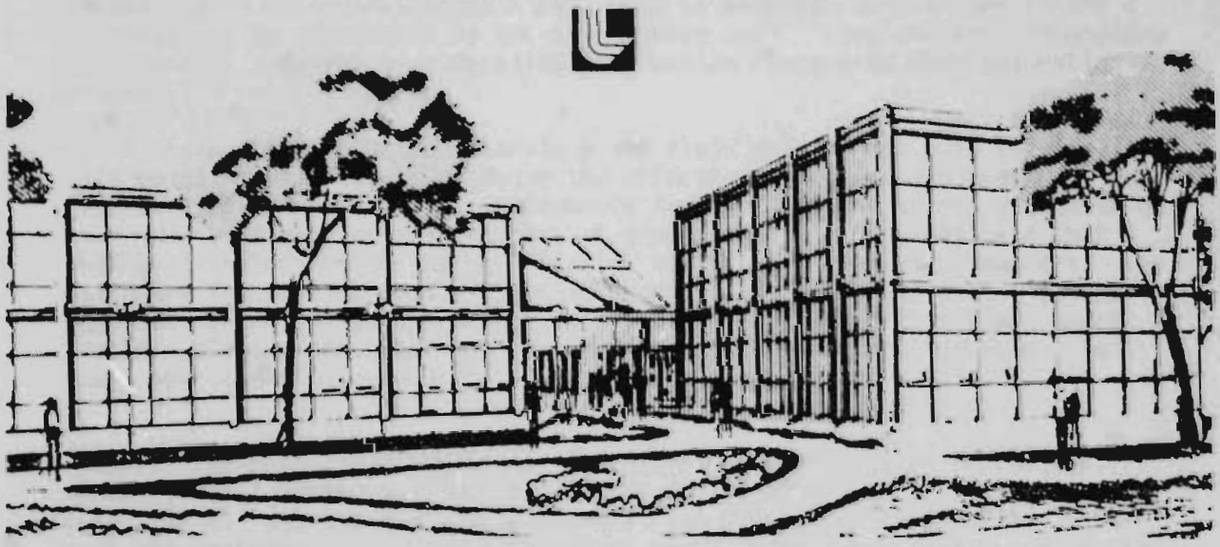

CONTROL ASPECTS OF UNDERGROUND COAL GASIFICATION:

LLL INVESTIGATIONS OF GROUND-WATER AND SUBSIDENCE EFFECTS*

S. Warren Mead, Francis T. Wang, and Harold C. Ganow
Lawrence Livermore Laboratory
P. O. Box 808
Livermore, CA 94550

ABSTRACT

The conversion of coal into combustible gases promises to become an important method of coal utilization. If this conversion is carried out with the coal in place underground - in situ coal gasification - additional environmental and economic advantages can be realized. Our investigations are designed to evaluate some of the environmental implications of this alternative energy technology, and to identify appropriate environmental controls.

Changes in ground-water quality and the possible effects of subsidence and ground movement induced by the underground gasification cavity represent significant environmental concerns associated with the in situ gasification process. We have measured these effects at the sites of two in situ coal gasification experiments conducted in northeastern Wyoming by the Lawrence Livermore Laboratory. Our measurements of ground-water quality in the vicinity of the gasification experiments indicate that the reaction products, such as ash and some coal tars, that remain underground following gasification, are a potential source of localized ground-water contamination. However, the concentration of important contaminants, such as phenols, show a significant decrease due to adsorption by the surrounding coal. Complementary laboratory measurements are providing detailed information concerning this adsorption process.

We have also conducted laboratory and field measurements, in conjunction with modeling studies, to evaluate the effects of subsidence phenomena. Data from subsurface geotechnical instruments installed at the second gasification experiment, as well as measurements of ground-water levels, indicate that roof collapse connected the gasification cavity with overlying aquifers. The environmental implications of this interconnection are being investigated. Our results suggest that hydrogeological site-selection criteria may be of considerable environmental importance in choosing locations for commercial-scale operations.

*Support for these investigations is provided by the Division of Environmental Control Technology (DOE/ASEV), the Office of Research and Development (EPA/IERL-CI) and the Division of Fossil Fuel Extraction (DOE/ASET). This work was performed under the auspices of the U.S. Department of Energy by the Lawrence Livermore Laboratory under contract number W-7405-ENG-48.

INTRODUCTION

The production of combustible gases or chemical feedstock by means of coal gasification promises to become an important method of coal utilization. If the gasificaton of coal is accomplished with the coal in place underground - in situ gasification - additional environmental and economic advantages can be realized. For example, in situ coal gasification can be carried out without the need for underground mine workers, and it may make recovery of very deep coals economically attractive.

In situ coal gasification generally involves a complex series of chemical reactions, but it can be simply characterized as the heating of coal in the presence of gasifying agents such as oxygen and steam. Some of the coal is burned to provide heat to drive the gasification reactons. In the simplest form of in situ gasification, two or more process wells drilled into the coal seam are used, after the coal is ignited, to inject air or other gasifying agents and to withdraw the resulting combustible gas mixture (Fig. 1). In most cases, the coal's permeability must be enhanced, before gasification, along a path connecting the process wells. (The need to achieve this preliminary connection reliably and economically represents an important current challenge in the development of a practicable in situ technology.) The product gas generally requires some form of clean-up in a surface plant and, if synthetic natural gas is the desired product, an upgrading process to achieve higher energy density.

Although in situ coal gasification offers important environmental advantages when compared with more conventional methods of coal utilization, there are significant environmental concerns that need to be investigated. If these concerns are addressed now, in parallel with the development of the in situ method, it will be possible to identify appropriate control technologies in a timely manner and, perhaps, influence process development such as to preclude or minimize adverse environmental effects.

In order to insure that realistic and effective control methods will be identified, it is essential to develop a quantitative understanding of potential environmental effects as they would occur in connection with large, commercial-sized operations. Some of these possible effects are peculiar to underground gasification and have not been previously investigated in detail. Futhermore, important environmental consequences may require decades to develop. We are therefore concentrating our present efforts on the accumulation of basic data concerning the potential sources of environmental effects, and on the development of reliable, predictive modeling capabilities. With this background, it should be possible to isolate control technologies that are realistically applicable to this promising method of coal recovery.

Two characteristic features of the in situ coal gasification process have led to particular environmental concern: first, the fact that some of the reaction products remain underground as potential ground-water contaminants and, second, the cavity (and possible subsidence) produced by the extraction of the gasified coal. Our in situ coal environmental group at the Lawrence

Livermore Laboratory (LLL) is concentrating special attention on these two aspects of the in situ process. We hope to assess their environmental significance and identify methods for controlling any adverse environmental consequences. Our approach involves a combination of field measurements near in situ gasification experiments, laboratory investigations, and predictive modeling studies.

LLL has conducted two in situ coal gasification experiments[1,2] at its Hoe Creek site in northeastern Wyoming. These experiments have given us the opportunity to measure changes in ground-water quality and subsidence effects associated with two underground gasification operations.

The Hoe Creek site is located in a sparsely populated region of gently rolling semi-arid rangeland. This area is part of the Powder River basin of northeast Wyoming and southeast Montana - a region that may contain half a trillion tons of coal suitable for in situ gasification. The coal gasified in the Hoe Creek experiments (the Felix II Coal) is 25 ft thick and lies at a depth of about 125 ft - well below the static water level. The Felix II Coal is an aquifer and is overlain by two additional aquifers. A detailed evaluation of the hydraulic characteristics of the Felix Coal and the near-by strata at the Hoe Creek site will be found in reference 3.

The first Hoe Creek experiment[1] took place in the fall of 1976. The two process wells - for injecting air and extracting product gas - were about 33 ft apart, and chemical explosives were used to produce enhanced permeability in the Felix II coal. Approximately 120 tons of coal were gasified in an 11-day experiment.

A second experiment, Hoe Creek II, was conducted during the fall and winter of 1977. The process wells were located approximately 60 ft apart and the required path of enhanced permeability was achieved using a preliminary "reverse combustion" technique, developed in this country by the Laramie Energy Technology Center. The gasification operation lasted 58 days, during which approximately 2000 tons of coal were converted to gas and extracted through the production well. The average energy content of this gas was 108 Btu/scf. Gas losses during this experiment averaged 20%.

Perhaps the most significant environmental concern associated with the underground gasification of coal stems from the existence of gasification reaction products that remain underground. These residual materials include coal ash, char, some of the coal tars, and approximately 10-15% of the product gases which are not extracted through the production wells. When ground water returns to the gasification zone, the ash is leached, producing inorganic contaminants, and some of the other residual materials, including organics are dissolved. The contaminated water moves through the coal seam in the general direction of the natural ground-water flow. Fortunately, there are other natural phenomena - for example, the filtering and adsorption properties of coal itself - which tend to purify the ground water and to restrict the contaminants to a localized region. Nevertheless, the ultimate environmental significance of the residual underground products is not yet known.

The ground movement and potential subsidence associated with the creation of a gasification cavity are also of significant environmental concern - in part, because these phenomena may affect the dispersal of the reaction-product contaminants. In particular, fissuring and roof collapse, which result from cavity formation, can destroy the integrity of the underground "reaction vessel" and permit the escape of pollutants to the surface or into overlying aquifers. Large areal gasification operations could also lead to significant surface subsidence, with results that may be important environmentally, and in their effects on process facilities.

WATER SAMPLING AT HOE CREEK I

Measurements of changes in ground-water quality near in situ coal gasification experiments are of importance, initially, in that they help to define the contaminant source. That is, they permit a description of the composition, concentration, and early-time distribution of the underground contaminants. Such measurements also provide information concerning short-term changes in concentration and composition that are a result of chemical reactions, sorption by coal and other media, or biological action. Over a period of several years, the water quality measurements will begin to yield information concerning the possible development of a plume of contaminated ground water that may spread outward from the gasification site in the direction of natural ground-water flow.

We have carried out extensive ground-water quality investigations at the sites of both LLL in situ coal gasification experiments. Approximately a dozen wells in the vicinity of the first gasification experiment (Hoe Creek I) were monitored before, during, and after gasification.[4,5] The samples were analyzed in the field and, much more extensively, at the laboratories of the U. S. Geological Survey, the Research Triangle Institute, and LLL. A simplified summary of the data is given in Table I.

TABLE I. A simplified summary of data for contaminants that showed a large increase following gasification (Hoe Creek I).

Species	Pre-gasification value (mg/l)	Inside burn zone Concentration Increase (mg/l)		Outside burn zone Concentration Increase (mg/l)	
Phenols	0.001	0.1	100 x	500	5×10^5 x
CN^-	0.01	0.4	40 x	300	3×10^4 x
NH_4^+	0.5	20	40 x	70	100 x
DOC	6	4	-	200	40 x
Br^-	0.1	1.0	10 x	4	40 x
Pb^{+2}	0.001	0.001	-	0.04	40 x
Ba^{+2}	0.1	-	-	1.0	10 x
K^+	5	60	10 x	45	8 x
Li^{+1}	0.03	0.3	10 x	0.2	6 x
Mg^{+2}	10	50	5 x	60	6 x
SO_4^{-2}	200	2000	10 x	1000	5 x
Ca^{+2}	40	600	20 x	200	5 x
B (III)	0.1	0.7	7 x	0.5	5 x

Among the chemical species that show a large increase as a result of the gasification experiment are the phenolic materials, which represent the largest group of organic contaminants introduced into the underground environment by this experiment. The changes in concentration of the phenolic materials, as a function of time and distance from the boundary of the gasified zone, are shown in Fig. 2. Notice that the phenol concentrations have decreased by roughly two orders of magnitude at all distances from the burn zone. Although most other contaminants are also decreasing[5], their rates of decrease are not, in general, as rapid as those indicated in Fig. 2.

The water from selected wells was analyzed by the Research Triangle Institute using a method that combines gas chromotography and mass spectrometry (GC-mass spec). This technique (now also employed at LLL) provides detailed information concerning volatile and semi-volatile organic contaminants. The coal gasification process produces an enormous variety of such organic by-products. The more volatile aromatic materials such as benzene, toluene, xylenes, and napthalene penetrate into the porous media surrounding the gasification zone.[5] As illustrated in Fig. 3, the species of lower molecular weight (more volatile) are transported further from the gasification zone. A discussion of some limitations that apply to quantitative comparisons of the GC-mass spec data with results obtained by other methods will be found in Ref. 5.

It is important to point out that the natural rate of ground-water movement in the gasified coal seam (Felix II) may be only a few meters per year. Consequently, data such as those presented in Fig. 2 do not, as yet, provide evidence concerning changes in contaminant concentrations that may occur as a result of natural ground-water flow. In principal, phenol concentrations in the outer wells might ultimately increase. Nevertheless, the rapid and uniform decrease in the concentrations of phenolic materials over a period of more than a year is an encouraging example of the self-cleansing capabilities of coal aquifers.

LABORATORY AND COMPUTATIONAL STUDIES

A clearer and more quantitative understanding of the ground-water changes near an underground gasification operation can be achieved by means of laboratory investigations carried out in conjunction with the field measurements. Of particular interest, are the nature and magnitude of the cleansing actions that occur when contaminated water is exposed to coal. Results such as those shown in Fig. 4 leave little doubt that phenol is rapidly adsorbed by coal. More elaborate experiments involving the flow of contaminants through a column of coal (Fig. 5) are also underway. They establish values of the distribution coefficient, K_d, which is a measure of the fractional adsorption of a dissolved contaminant and an essential ingredient in contaminant transport modeling. Our modeling efforts include the development of a 2-dimensional computer code capable of predicting transient dispersion of contaminants introduced continuously from a line source. The model includes convection, longitudinal and lateral dispersion, and adsorption.[6]

GROUND-WATER EFFECTS AT HOE CREEK II

Nine ground-water sampling wells were provided for measuring ground-water quality changes resulting from the second Hoe Creek experiment. Since the second experiment involved the gasification of 20 times as much coal as Hoe Creek I, it would be of considerable interest to compare ground-water changes near the two sites. Such a comparison might help to establish the dependence of the contaminant source strength on the amount of coal gasified. In particular, the comparison might indicate whether the concentrated "shell" of phenolic materials just outside the burn zone is a surface effect or dependent on the entire gasified volume. Unfortunately, a straightforward and meaningful comparison of ground-water measurements at the two sites is impossible, for reasons discussed below.

We have sampled the ground-water near the Hoe Creek II site before, during, and several times after gasification. Some analyses are performed in the field, and preserved samples are sent for extensive analysis to U.S. Geological Survey laboratories, Gulf South Research Institute, and LLL. The

highest measured concentration of phenolic materials (as determined by field analysis) is less than 30 ppm. By contrast, we measured phenol concentrations of more than 400 ppm near the Hoe Creek I experiment. Of course, the phenol concentrations are expected to depend very strongly on well locations relative to the burn boundary (Fig. 2), and this effect could account for large differences in measured concentrations. However, a more important difference stands in the way of a simple comparison of contaminant levels near the two sites. Water level data (Fig. 6), subsurface geotechnical measurements, and post-burn coring investigations show that cavity roof collapse connected the gasification cavity with overlying aquifers (The Felix I Coal and a coarse channel sand above it). Since the Hoe Creek site is a recharge area (hydraulic head decreasing with depth), water from the overlying aquifers is flowing into the gasification cavity and producing an abnormally high hydraulic head within the cavity. Calculations based on the data of Fig. 6 suggest that ground-water flow rates in the immediate vicinity of the cavity exceed normal flow rates by at least an order of magnitude. Preliminary data on phenol concentrations (Fig. 7) showed a temporary increase in concentration in some of the sampling wells, which are completed in the Felix II Coal. Evidently, source concentrations and source geometry were significantly affected by the aquifer interconnection. The environmental implications of the altered contaminant distribution are being investigated.

Another question whose importance is emphasized by the aquifer interconnection at the Hoe Creek II site concerns the possibility that contaminants from the gasification zone may migrate into overlying aquifers. Additional sampling wells recently completed in the Felix I aquifer will help to answer this question. It may be that the downward flow of water in a recharge area will minimize the spread of contaminants into overlying aquifers. In any case, the importance of an enlightened choice of site selection criteria is becoming increasingly apparent.

SUBSIDENCE STUDIES

Since ground deformations induced by the gasification cavity may play an important role in determining contaminant dispersal and may, in addition, lead to significant surface subsidence, an improved understanding of these subsidence phenomena is of outstanding importance. We are attempting to extend out knowledge of these effects and develop a reliable predictive capability through a combination of laboratory tests of overburden cores, geotechnical measurements at the site of ongoing gasification experiments, and finite element modeling.

A preliminary modeling study of the subsidence induced by underground coal gasification was conducted in preparation for the first Hoe Creek experiment.[7] In the treatment employed, a stratified overburden is stressed by gravity loading and by the removal of coal seam elements in a manner simulating coal combustion. The resulting stresses, strains, and displacements are determined for the duration of the excavation process and for subsequent quiescent periods during which plastic deformation and stress relaxation gradually take place in the rock and soil strata. Inelastic

procedures are employed, which require the use of measured or assumed physical properties for the various strata. The results of these calculations indicated that surface subsidence would be small - a few inches at most. Within the accuracy of our surface-monument measurements, no post-burn surface subsidence was detected.

An augmented version of the above method was used in an effort to predict subsidence and ground movement for the Hoe Creek II experiment.[8] Two sets of assumed values of material properties were employed, termed "probable" and "lower bound". We also added a new feature to our method of modeling the excavation process associated with gasification. As the computations proceeded, roof material that developed tensile stress was mathematically removed in a subsequent iteration. In other words: as coal elements were "gasified" and zones of tensile stress appeared in the roof, those zones were "spalled" or allowed to collapse. This procedure produces a shallow arched roof, free of tensile stress, such as might be expected to occur naturally.

This augmented model also predicted surface subsidence of only an inch or so. On the other hand, relatively large deformations, and considerable roof caving were predicted below the surface. It seemed clear that subsurface measurements would produce the most helpful data - both for understanding the implications of subsidence for the in situ gasification process, and as a guide in checking and improving our subsidence modeling capabilities. Subsequent measurements have shown that a combination of roof caving and combustion (in the overlying Felix I Coal) caused portions of the cavity to be extended some 70 ft above the top of the Felix II Coal, much higher than predicted.

In an effort to provide subsurface data, we designed an array of geotechnical instruments for installation in the overburden at the site of the Hoe Creek II experiment (Fig. 8). The instruments included two 6-position borehole extensometers (Fig. 9), two electrical shear strips, a multiple piezometer installation, and a borehole deflectometer apparatus that was utilized in six specially cased boreholes. Provisions for surface measurements included specially designed isolation bench marks, an optical level, and a precision tape extensometer. A detailed description of these instruments, their deployment at the Hoe Creek II site, and some preliminary results are reported by Ganow et al. in reference 9. An analysis of the geotechnical data (obtained before, during, and after the Hoe Creek II experiment) has provided a relatively clear picture of the overburden deformation and roof collapse that occurred in response to the growth of the gasification cavity. Of particular interest, is the fact that the extensometers and piezometers documented the interconnection of the gasified coal seam with the overlying Felix I and channel sand aquifers.

Since a variety of measurements have shown that roof collapse extended significantly higher than predicted, we are attempting to develop modeling methods that take account of process-related phenomena that may be significant. Roof spalling due to shrinkage effects induced by heating may be an important factor in determining the utlimate cavity size. A prelimirary attempt to incorporate these shrinkage effects into the calculations is described by Greenlaw et al. in reference 10.

We have also carried out extensive triaxial strength tests on core samples obtained from the Felix II overburden at Hoe Creek. The material properties obtained from these tests will be used in future modeling studies. The usefulness of 3-dimensional solutions will also be explored. We are hopeful that an improved knowledge of subsidence behavior in actual gasification experiments, used in conjunction with properly measured overburden characteristics, can permit the development of predictive modeling capabilities that will be a reliable guide to the subsidence phenomena that may accompany large scale in situ coal gasification.

ACKNOWLEDGMENTS

The continuing cooperation and assistance of Dr. D. R. Stephens, Project Director of LLL's In Situ Coal Program, is particularly important to the success of our environmental studies. We are also grateful for the assistance of Dr. Stephens' scientific and engineering staff. John Campbell (LLL) and John Busby (USGS) made essential contributions to the water quality studies carried out in conjunction with the Hoe Creek I experiment. Our finite element modeling effort is conducted by Robert Langland and Russell Greenlaw, and the GC-mass spec analysis at LLL is under the direction of Daniel Stuermer.

REFERENCES

1. R. W. Hill and C. B. Thorsness, Results from an In Situ Coal Gasification Experiment Involving Explosive Fracturing: Hoe Creek Experiment No. 1, Lawrence Livermore Laboratory, Rept. UCRL-52229, Feb. 1977.

2. W. R. Airman, et al., The Hoe Creek II Field Experiment on Underground Coal Gasification, Preliminary Results, Lawrence Livermore Laboratory, Rept. UCRL-80592, Feb. 1978.

3. R. Stone and D. F. Snoeberger, Evaluation of the Native Hydraulic Characteristics of the Felix Coal (Eocene, Wasatch Formation) and Associated Strata, Hoe Creek Site, Campbell County, Wyoming, Lawrence Livermore Laboratory, Rept. UCRL-51992 (1976).

4. S. W. Mead, et al., LLL Environmental Studies of In Situ Coal Gasification, Annual Report Fiscal Year 1977, Lawrence Livermore Laboratory, Rept. UCRL-50032-78 (1978).

5. J. H. Campbell, E. D. Pellizzari and S. D. Santor, Results of a Ground Water Quality Study Near an Underground Coal Gasification Experiment, (Hoe Creek 1), Lawrence Livermore Laboratory, Rept. UCRL-52405, 1978.

6. Robert V. Homsy, Two-Dimensional Transient Convective Dispersion and Adsorption in Porous Media, Lawrence Livermore Laboratory, UCRL, to be published (1978).

7. R. T. Langland and D. Fletcher, Predicting Subsidence over Coal Gasification Sites, Lawrence Livermore Laboratory, Rept. UCID-17326 (1976).

8. R. C. Greenlaw, H. C. Ganow, and R. T. Langland, Subsidence and Stability Studies for Underground Coal Gasification, Lawrence Livermore Laboratory Rept. UCID-17674 (1977).

9. H. C. Ganow, R. C. Greenlaw, and R. T. Langland, "Geotechnical Instrumentation Applied to In Situ Coal Gasification Induced Subsidence," Proceedings of the Fourth Annual Underground Coal Conversion Symposium, July 17-20, 1978. Also published as Lawrence Livermore Laboratory, Rept. UCRL-81267 (1978).

10. R. C. Greenlaw, H. C. Ganow, and R. T. Langland, "Non-Linear Subsidence Modeling at Hoe Creek," Proceedings of the Fourth Annual Underground Coal Conversion Symposium, July 17-20, 1978.

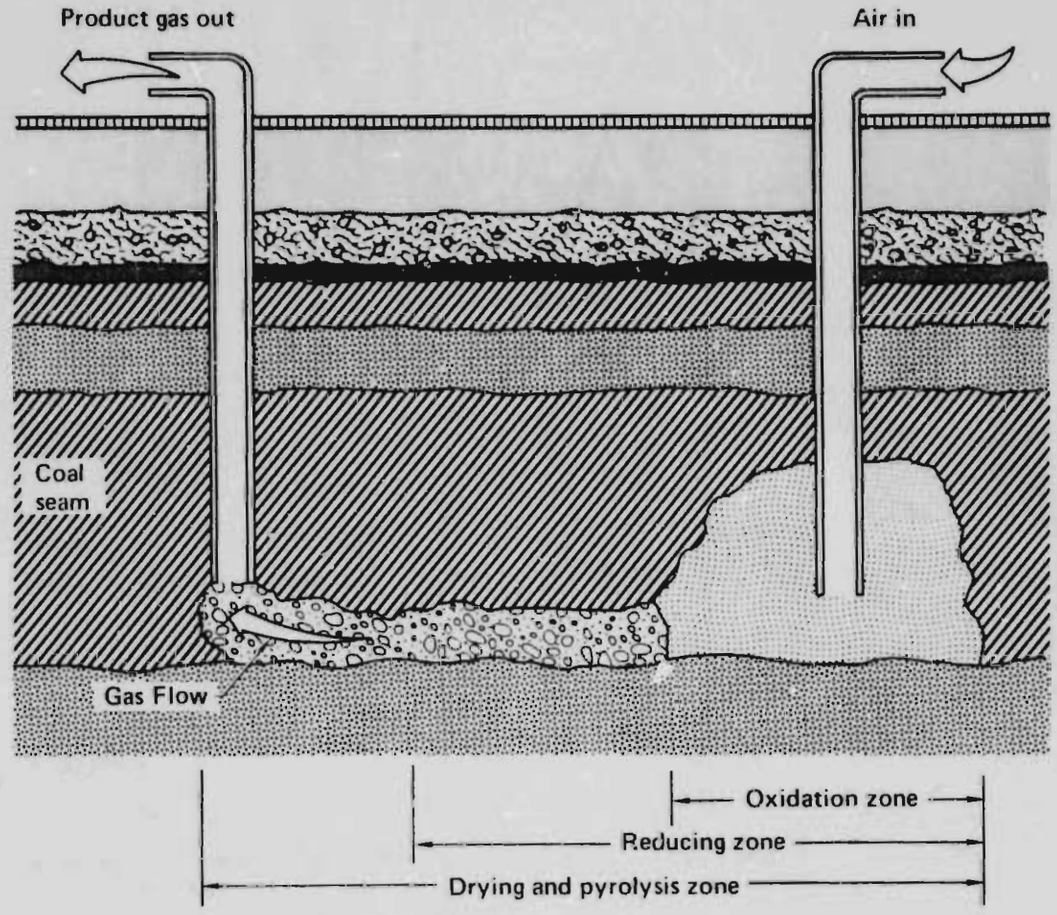

Figure 1. Schematic representation of the *in situ* coal gasification process. The region ahead of the oxidation zone has been modified before gasification to provide a path of increased permeability that will permit adequate gas flow.

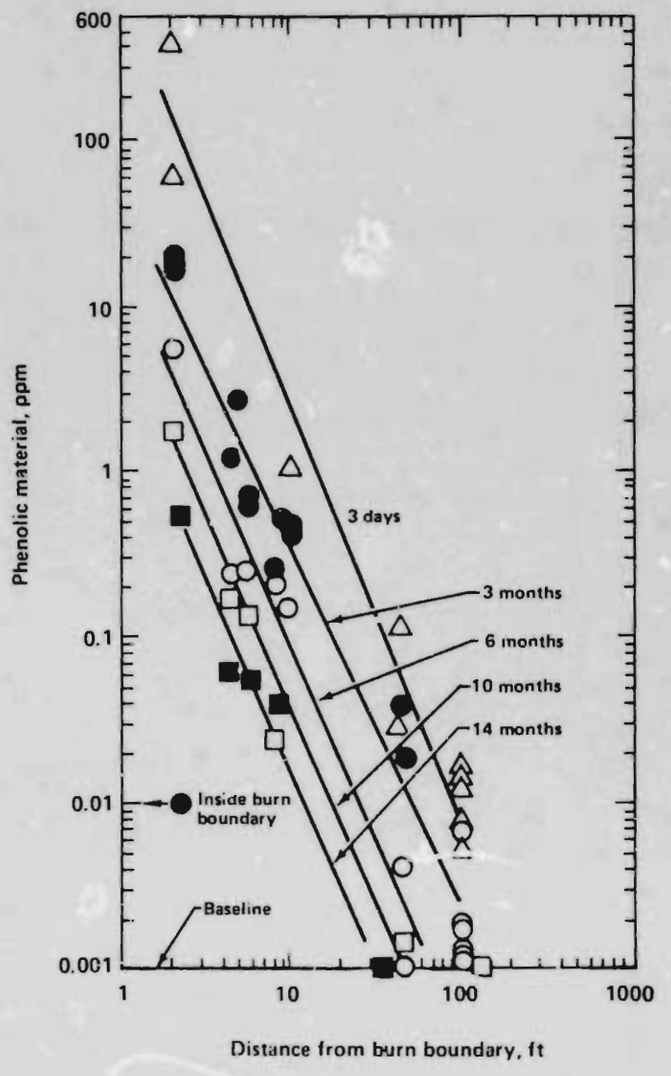

Figure 2. Concentrations of phenolic materials as a function of distance from the nearest burn boundary of the Hoe Creek I *in situ* coal gasification experiment. Times are measured from the end of gasification. Sampling wells are completed in the gasified coal seam and located in various directions from the gasification zone.

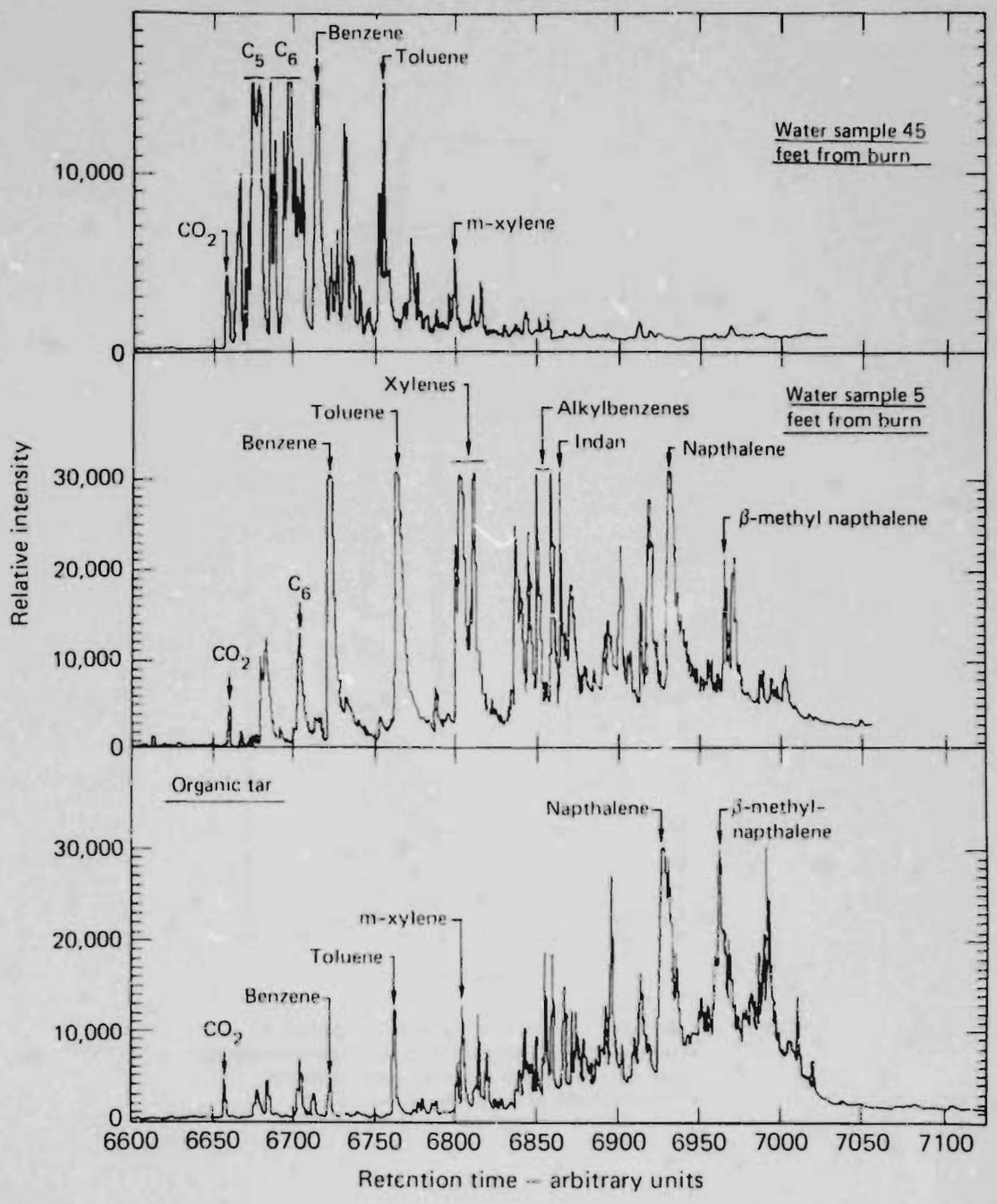

Figure 3. Chromatograms of volatile organics found in product tar and in water obtained 5 ft and 45 ft from the burn zone. The numbers on the abscissa are related to the chromatograph retention times. Note that the lower-molecular-weight (more volatile) species move much further out into the formation, and that the organics in the nearby water are more like the product stream tar.

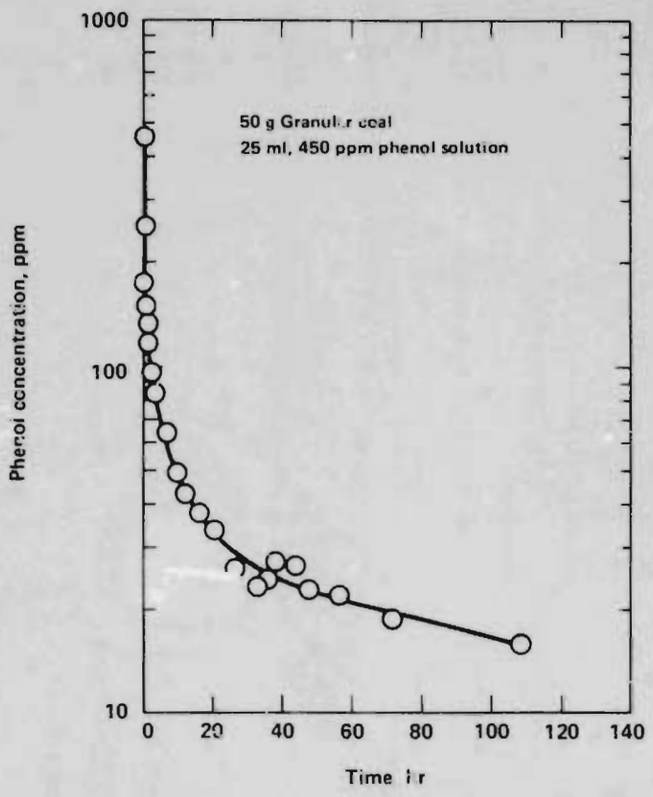

Figure 4. Laboratory measurements of phenol adsorbed by granular coal as a function of time. The data represent the analysis of a large number of equivalent phenol solutions agitated with a shaker table.

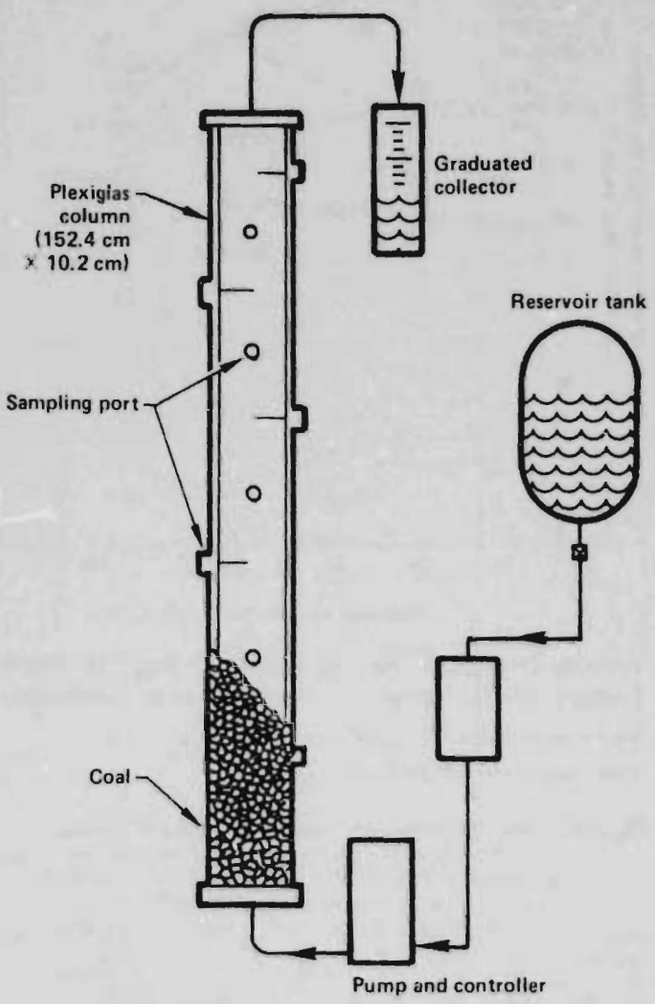

Figure 5. Coal column apparatus used to simulate the flow of contaminated ground water through a coal seam. During operation, samples are extracted through rubber septa using a hypodermic syringe.

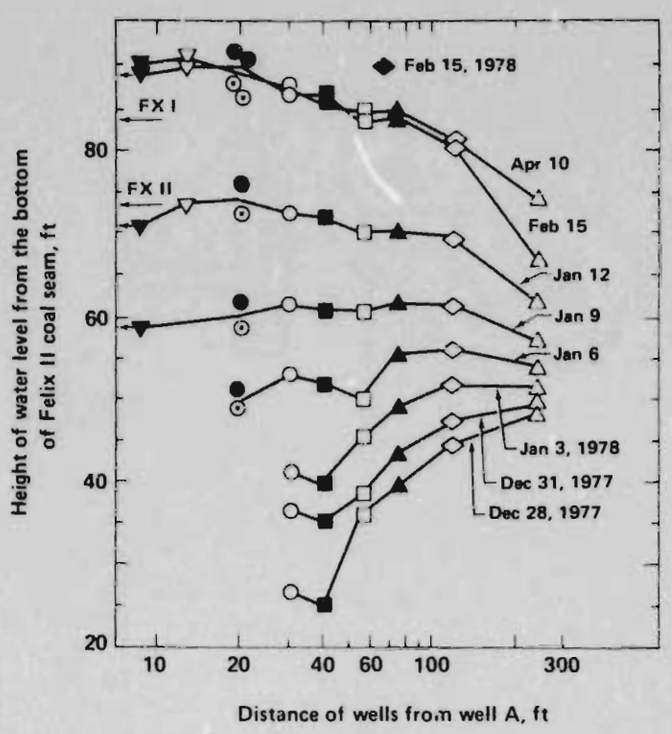

Figure 6. Water levels in wells near the Hoe Creek II *in situ* coal gasification experiment. The water levels are plotted as a function of distance from the injection well "A" at various times following gasification. (A logarithmic distance scale is used to avoid data crowding for the close-in wells.) All wells are completed in the gasified Felix II coal seam except WS-1, which was completed in the overlying Felix I coal aquifer. The data show how water levels have changed since air injection was terminated at the conclusion of the gasification experiment on December 25, 1977. The elevated water levels in the vicinity of the gasification zone suggest that the gasification cavity has been interconnected with the overlying Felix I coal aquifer, which lies about 20 feet above the Felix II Coal, and with another aquifer above the Felix I Coal.

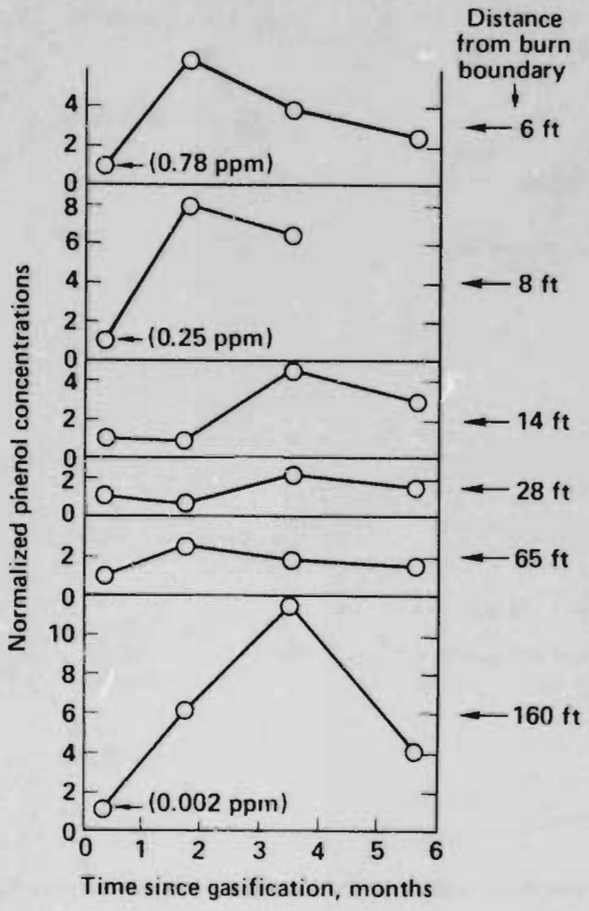

Figure 7. Changes in the measured concentrations of phenolic materials in the Felix II coal aquifer as a function of time after gasification. The measurements were made in some of the wells shown in Figure 5. These and other data suggest that the contaminants are moving outward away from the gasification zone. This movement appears to be much exaggerated in the immediate vicinity of the gasification zone as a result of an interconnection with an overlying aquifer. (Note that the actual magnitudes of the phenol concentrations measured in the close-in wells are hundreds of times greater than those in the outermost well.)

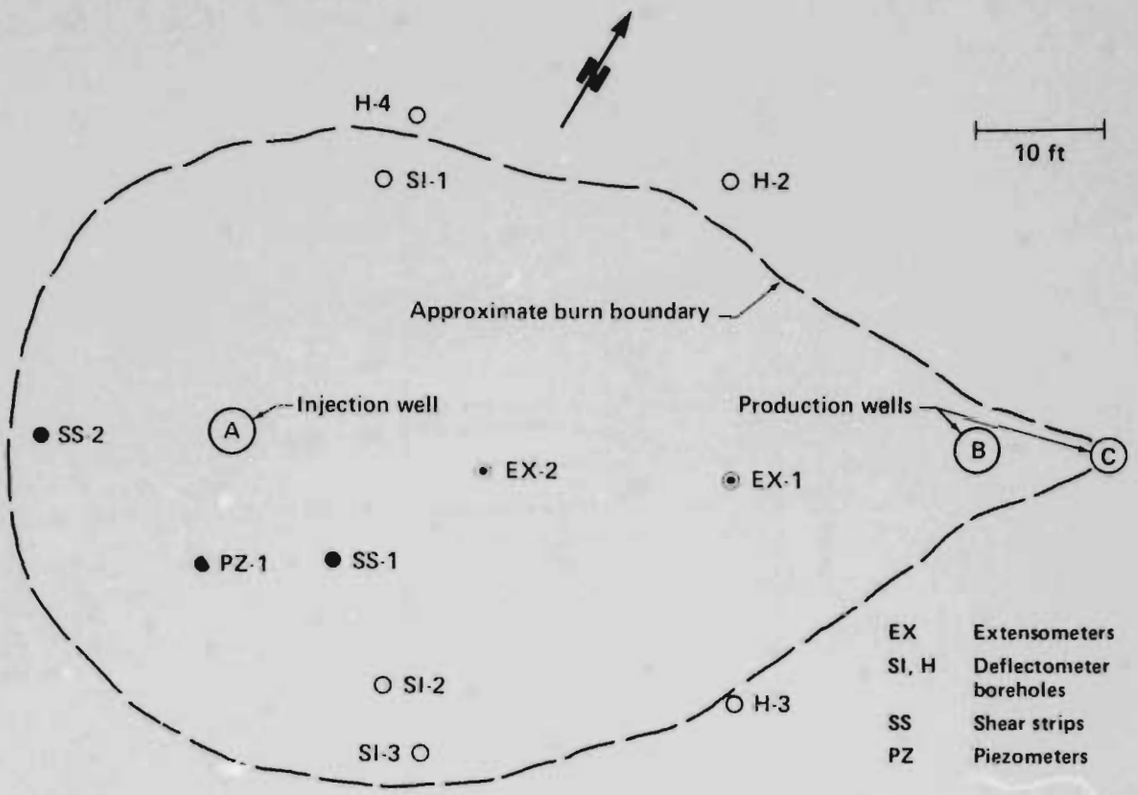

Figure 8. Plan view showing process wells and subsidence instrumentation boreholes at Site II.

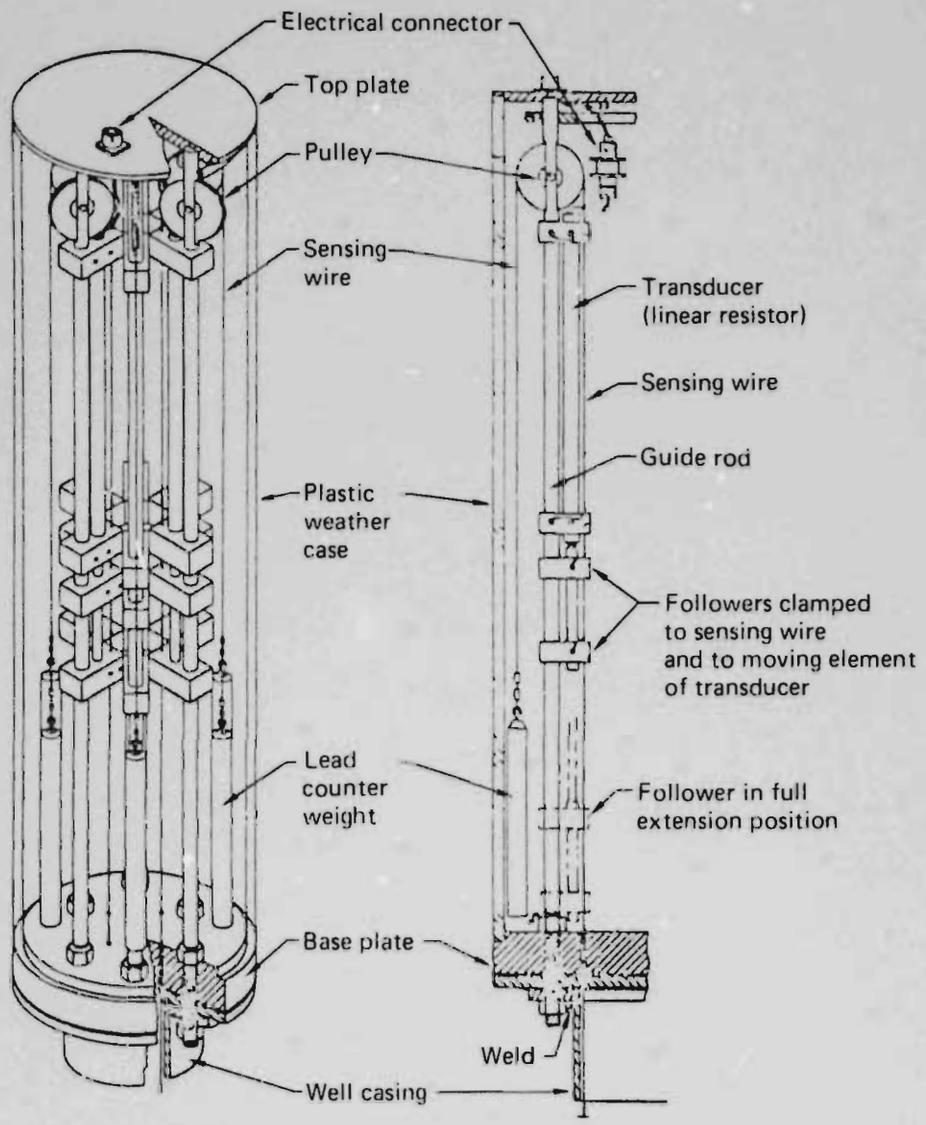

Figure 9. **Multiple-position borehole extensometer sensing head. Cables from the sensing head extend down to expandable mechanical anchors located at various positions in the overburden. Displacements measured at the sensing head are the integrals of vertical strains occurring between the head and the various anchor points.**

UCID- 18013

Lawrence Livermore Laboratory

HOE CREEK NO. 3 PRE OPERATIONAL REPORT

R. W. Hill

December 29, 1978

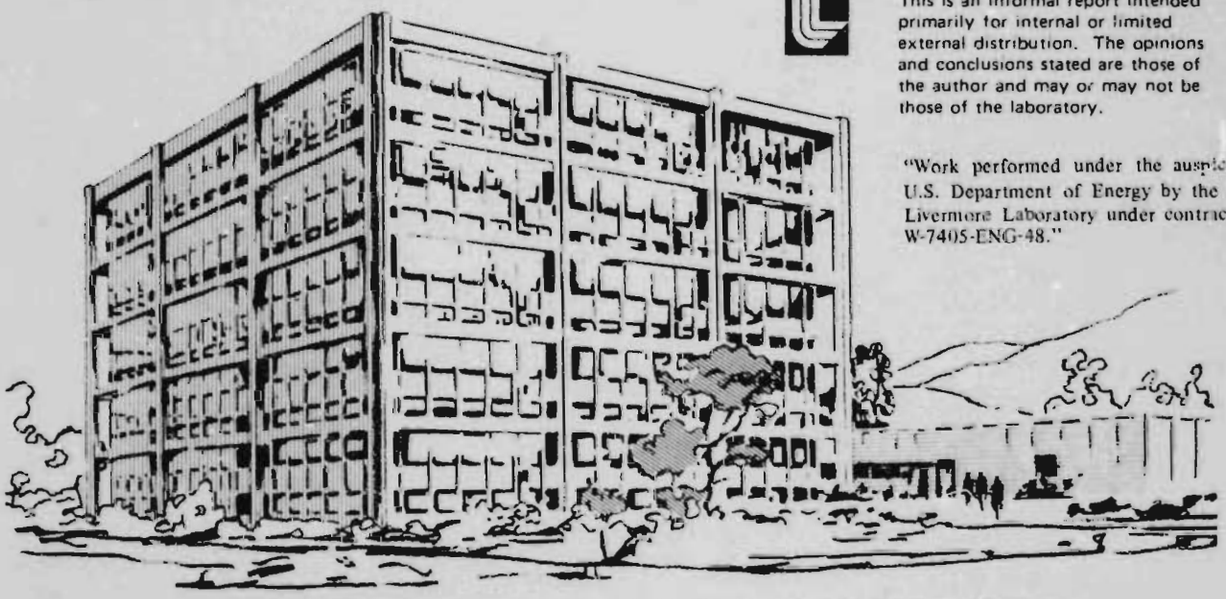

"Work performed under the auspices of the U.S. Department of Energy by the Lawrence Livermore Laboratory under contract number W-7405-ENG-48."

HOE CREEK NO. 3

PRE OPERATIONAL REPORT

R. W. Hill

TABLE OF CONTENTS

I. Scientific Design Outline

R. W. Hill

The basic goal of the LLL In-Situ Coal Gasification Project is to develop a process for producing medium heating value gas that can be an economical source of pipeline quality gas (SNG). The gas produced by gasifying coal with air is contaminated with the nitrogen contained in the air, thus lowering the heating value. Although it is possible to remove the nitrogen from the product, it is more economical to remove the nitrogen from the air and use oxygen as the injectant.

Our first two field experiments were designed to test two different coal permeability enhancement techniques, explosive fracturing in the case of Hoe Creek No. 1 and reverse combustion linking in Hoe Creek No. 2. Both were air burns for reasons of economy.

Hoe Creek No. 3 is to be our first full oxygen gasification. The major goals of this experiment are to:

1. Carry out forward gasification with a known, reliable link at the bottom of the coal seam.
2. Determine steam/oxygen gasification efficiencies at coal consumption rates up to 100 tons/day.
3. Gasify at commerical process well spacings (100-200 ft).
4. Determine burn zone configuration
5. Minimize gas losses and water influx.
6. Determine water quality and subsidence effects.

There was strong evidence that in both Hoe Creek No. 1 and No. 2, channels were created at the coal-overburden interface allowing gas override to occur. In both cases the override led to a reduction in produced gas heating value due to excessive heat loss to the overburden and to a reduction

in the total amount of coal consumed due to the unfavorable burn front geometry. It is possible that the Felix No. 2 seam at the Hoe Creek site has a high permeability zone at the top of the seam. The tests done so far show that such a zone does not extend uniformly over the site, however it may exist locally.

Since the major goal of the Hoe Creek No. 3 experiment is to do a successful oxygen/steam forward burn, it is very important to try to insure a proper linking channel and to prevent gas override. Therefore, in order to insure a single link near the bottom of the coal seam, we have used directionally controlled drilling to construct the channel.

The deviated hole was drilled during July 1978, using a 2 3/8" diameter Dyna-Drill mud motor to drill a 3" diameter hole. Initially the drilling angle was inclined 30^{o} to the horizontal and deviated at a rate of approximately 5^{o} per 100 feet of travel.

Despite some difficulties with the drill sticking in the unconsolidated sand above Felix No. 1, a hole 710 feet long was completed with the last 200 feet in the bottom half of the coal seam. An elevation view of this hole is shown in Figure 1.

Using the logging data provided by the driller, we have attempted to intersect the deviated hole (DD-1) with several vertical holes. We planned to contact DD-1 by using a water jet tool loaned to us by the Bureau of Mines.

After several unsuccessful tries an HFEM transmitting antenna was inserted in the plastic pipe inside DD-1 and a receiving antenna was placed in several holes drilled close to the predicted location of the C-well. The received signals indicated that DD-1 was almost 50 feet further west than predicted by the driller's log. One of the holes used for HFEM location was indicated to be only 1-2 feet away from DD-1. This was confirmed by inserting a 2.5 curie Cs γ-ray source into DD-1 and using the γ log detector in the vertical hole. Additional HFEM and γ logging has been used to locate the far end of DD-1.

It is expected that all of the HFEM wells, water wells and some of the cased instrumentation wells will be drilled by the end of January 1979. The remainder

of the drilling program will be completed starting in March or April.

Instrumentation Plan

A. Underground Thermal and Pressure Instrumentation.

A plan view of the well layout for the Hoe Creek No. 3 experiment, is shown in Figure 2.

Wells A, B, and C are all process wells. Well A is designated as the injection well and Well B as the main production well. Well C will be used as an auxilliary production well to allow measurement of gas composition changes over a long production path and to determine what operational problems are involved with long underground channels. Although there are no plans to change the injection point, Wells B and C will be designed to allow such a change although not without a prolonged shutdown of the system.

The thermocouple types and emplacements are given in Table 1. The design philosophy is to try a number of ideas to try to increase the lifetime of the thermocouples in the high temperature environment. The results from Hoe Creek No. 2 show that we can expect to collapse up into Felix No. 1 and perhaps higher. Therefore, thermocouples are also to be placed in and above the upper seam for Hoe Creek No. 3.

Most of the thermocouples will be installed in open holes using a wire rope messenger cable as was done for Hoe Creek No. 2. Cement grout will be used to stem the holes. Three wells will be equipped with 4" heavy duty steel casing and the thermocouples will be grouted inside the casing.

We will attempt to fill these pipes with some sealing material that will prevent gas flow in the event of pipe failure but will not cause damage to the thermocouple sheathing.

Three wells, I-6, I-7, and I-8, will be used to test three combinations of thermocouple sheathing material, insulation and wire thickness.

Bubbler tubes similar to those used on Hoe Creek No. 2; but made of ordinary iron pipe will be installed in most instrument wells in the bottom one meter of the Felix No. 2 seam. In addition, bubbler tubes will also be installed at the top of the seam I-1 and I-3.

HOE CREEK NO. 3 -- ELEVATION VIEW

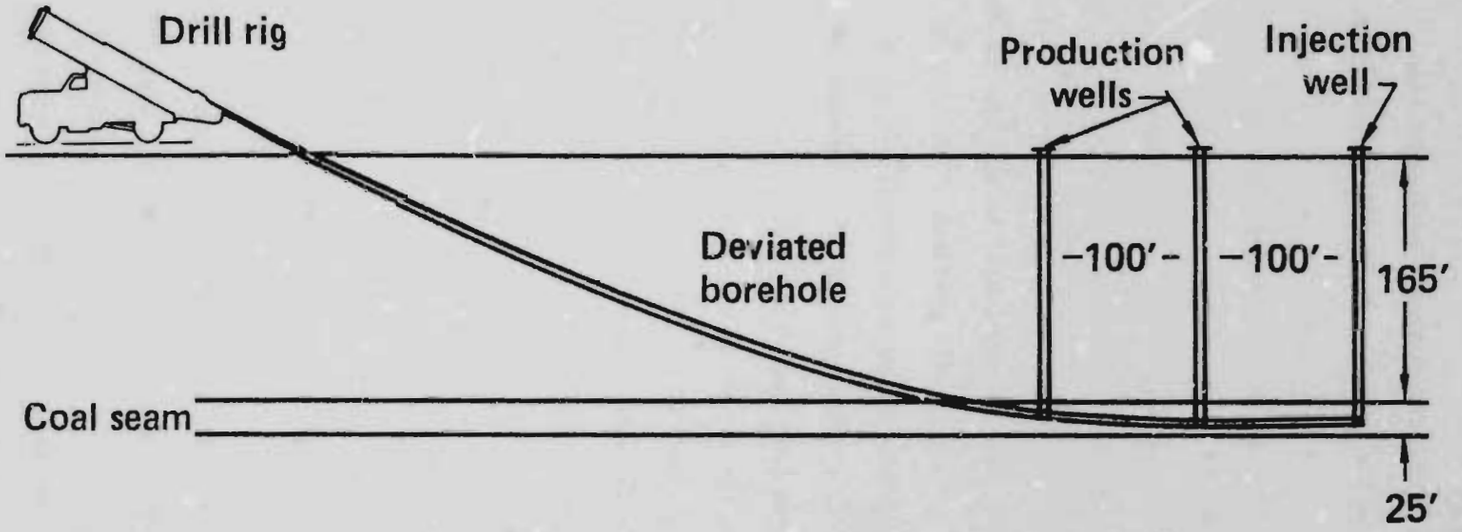

Figure 1. Process Wells and Directionally Drilled Channel

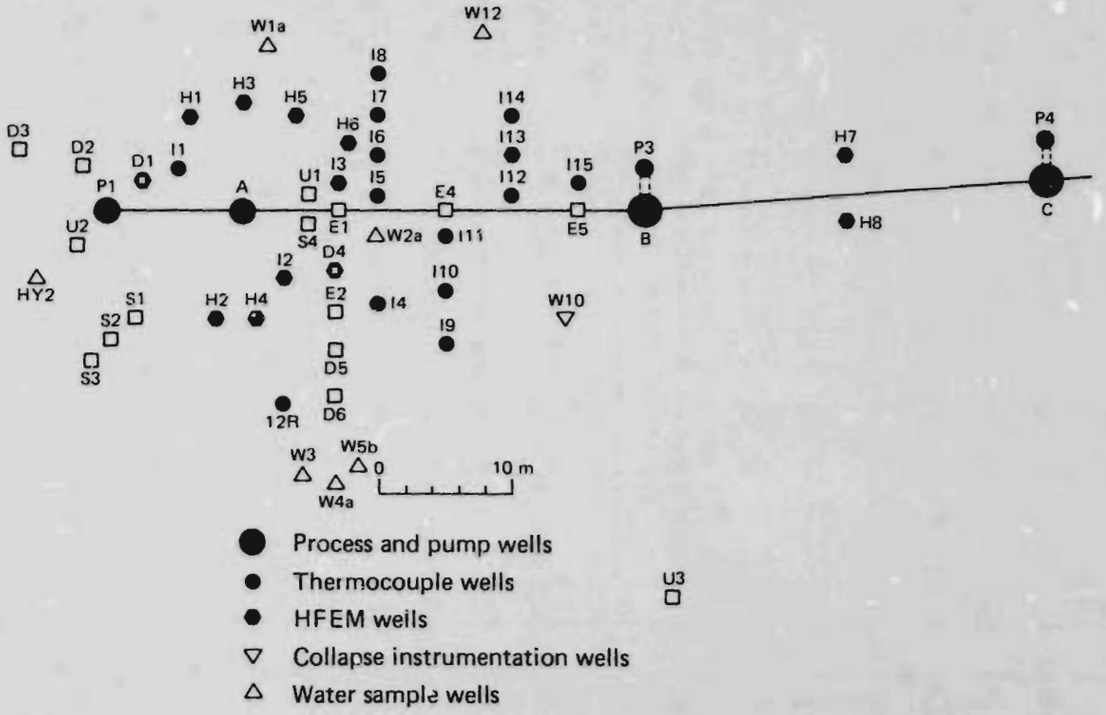

Figure 2. Hoe Creek 3 Plan View

X = 310SS, 1/8" D
O = 310SS, 1/8" D outside casing
# = 310SS, 1/8" D on pump line

I = Incalloy 800, 1/8" D
A = 310SS, 1/8" D Alumina ins.
L = 310SS, 1/4" D

B = Bubbler, Gas Sample Tube
* = 4" Steel Cased
** = Sandia Inverted TC plus standard TC string

Hoe Creek # 3 Downhole Thermocouple Array

Height Above Seam Botton Meters	TC Length	I1	I2 **	I3	I4	I5	I6 *	I7 *	I8 *	I9	I10	I11	I12	I13	I14	I15	A	B	C	P1	P2	P3	P4	H7	H8	Total Req'd	No. cut to length	Additional Required	Special Materials
30	28			X		X						X	X				0	0	0	0						8	3	5	
25	33			X		X						X	X													4	2	2	
20	38	X	X	X		X						X	X			X	0	0	0	0						11	8	3	
17	41	X	X	X		X						X	X			X										7	7	0	
15	43	X	X	X	X	X	X	X	X	X	X	X	X	X	X	X	0	0	0	0	0	0	0	X	X	24	20	4	
14	44	X	X	X		X						X	X			X										7	7	0	
13	45	X	X	X	X	X	X	X	X	X	X	X	X	X	X	X	0	0	0	0	0	0	0	X	X	24	20	4	
11.5	46.5	X	X	X		X						X	X			X										7	7	0	
10	48	X	X	X	X	X	X	X	X	X	X	X	X	X	X	X	0	0	0	0	0	0	0	X	X	24	23	1	
8.5	49.5	X	X	X		X						X	X													7	7	0	
7	51	XB	X	XB	X	X	X	X	X	X	X	X	X	X	X	X	0	0	0	0	0	0	0	X	X	24	20	4	
6	52	X	X	X	X	X	X	X	X	X	X	X	X	X	X	X	0	0		0	0	0	0	X	X	23	21	2	
5	53	X	X	X	X	X	XO	XO	XO	X	X	X	X	X	X	X	0	0		0	0	0	0	X	X	26	23	3	
4	54	X	X	X	X	X	X	X	X	X	X	X	X	X	X	X	0	0		0	0	0	0	X	X	23	22	1	
3	55	X	X	X	X	X	XO	XO	XO	XI	XL	XA	X	X	X	X	#	#	#	#	0			X	X	28	20	5	3
2	56	X	X	X	X	X	X	X	X	XA	XI	XL	X	X	X	X	#	#	#	#	#	#	#	X	X	27	23	1	3
1	57	XB	X	XB	XB	XB	XB	XB	XB	XLB	XAB	XIB	XB	XB	XB	XB								X	X	20	20	-3	3
0	58																									--	--		
-1	59																			#		#	#			3	4	-1	
-3	61																									--	--		
-5	63																			#		#	#			3	4	-1	
No. 310SS in string		15	15	17	10	17	10	10	10	10	10	17	17	10	10	15	-	-		-		-	-	10	10				
No. TC special		-	-	-	-	-	-	-	-	3	3	3	-	-	-	-	-	-		-	-	-	-	-	-				
No. TC outside casing		-	-	-	-	-	2	2	2	-	-	-	-	-	-	-	9	9	6	9	8	7	7	-	-				
No. TC on pumpline		-	-	-	-	-	-	-	-	-	-	-	-	-	-	-	2	2	2	4	1	3	3	-	-				
No. TC Total		15	15	17	10	17	12	12	12	13	13	20	17	10	10	15	11	11	8	13	9	11	11	10	10	300	261		

All of these tubes will be provided with nitrogen flow and pressure transducers for continuous computer monitoring of the down hole pressure. They will also be provided with valves and fittings to allow gas samples to be taken manually when desired.

We are currently planning to try a downhole Freon tracer system. This will consist of 5-10 containers, probably some laboratory type gas sample bottles, filled with different varieties of Freon and arranged to open at a preset temperature or pressure. These containers will be grouted in place in some of the instrument wells. An on-line Freon detector will sound an alarm when a container bursts and a sample will be collected for analysis. Thus a positive indication will be given that the temperature reached the preset value at a particular point in the formation.

All wells that have pipes coming to the surface, must have some sort of sealing mechanism to prevent blowout in the case of pipe failure.

B. Resistivity Net and Inverted Thermocouple.

Sandia Laboratories will field a surface resistivity network experiment for the Hoe Creek No. 3. This will be designed to give us an alternative method of locating the burn zone. It is expected that the data can be analyzed via a phone link to the Sandia Albuquerque computer and relayed back to Hoe Creek with a reasonable turn around time.

Sandia will also field an up-side-down thermocouple string where the temperature will be measured, digitized, FM multiplexed and transmitted to a receiving antenna underneath the coal seam and outside the burn zone. This system will be battery operated to prevent loss of signal by override burn off.

C. HFEM Well Placement.

The high frequency electromagnetic burn front location technique (HFEM) was tested successfully on Hoe creek No. 2. The present experiment will utilize

the HFEM technique to monitor the reverse burn of the drilled channel and then to measure the initial cavity growth around the injection well. This will allow us to determine the cavity size and position without having any wells penetrating the coal in the immediate vicinity of the injection well. This should minimize the probability of inducing fractures in the coal and the possibility of creating an override path.

D. Environmental Measurements

Both collapse instrumentation and water sampling will be done for Hoe Creek No. 3 in essentially the same manner as for Hoe Creek No. 2. A well layout plan view showing all of the wells is shown in Figure 2.

A monitoring program for air quality is also being planned. This program will be designed to give us reasonable assurance that we are complying with the appropriate state and federal regulations.

E. Gas Analysis, Water and Particulates

Gas analysis will be similar to that done on Hoe Creek No. 2. A new process gas chromatograph and a process mass spectrometer have been purchased. They will be used on the clean gas stream to give fast turn around analysis for essentially continuous display.

Water content of the gas will be determined by a humidity meter similar to but improved from that used on Hoe Creek No. 2. This will allow continuous humidity measurements to compliment the gas analysis.

Particulates in the gas stream will be determined in two ways. A large knock-out tank will be used in the production gas stream. Periodic sampling of the collected particulates will be done. A separate, small gas stream sample will be used to get a more accurate particulate sample at more frequent intervals.

We will attempt to determine the fraction of injected steam that reacts with the coal by using deuterated water as a tracer in the steam boiler. The process mass spectrometer should be capable of on-line analysis for deuterium.

Reverse Burn Widening of Channel

According to Kreinin and Revva (UCRL-Trans 10810) the standard way of enlarging a directionally drilled hole, (and linking it to vertical wells) is by reverse combustion. Although the data they give are for a harder bituminous coal the order of magnitude of their measurements ought to be about right.

Reverse burn along a 120 meter-long drilled hole 7.5 cm in radius (6" diam) took approximately 72 hours or 1.7 m/hr (5.6 ft/hr, 130 ft/day). The hole was enlarged to .5 m diameter. The average flow rate during reverse burn was 1740 m^3/h or 1024 scfm.

Since our directionally drilled hole has a 3 inch diameter, we would expect to operate in the 200-300 scfm range. A series of laboratory tests is scheduled to get better data on the rates in question.

Reverse burn of the directionally drilled hole will be necessary to increase its air acceptance even if it has been mechanically linked to the vertical wells.

Air flow and hydrology testing will precede ignition. The coal seam will be ignited at the bottom of Well C with air injection into Well A, assuming Wells A, B, and C are already satisfactorily linked to the directionally drilled hole. If the wells are not already linked, then the injection point will be moved from well to well as required to draw the burn zone along the desired path.

When the burn reaches Well A, the forward burn phase will be started. A short period of forward burn with air injection (up to one week) will be used to establish a hot burn zone at the bottom of the coal seam before oxygen/steam flow is started. A period of one week of air burn would allow a direct comparison to be made with the results from Hoe Creek No. 2.

At the start of forward burn, both air flow and pressure will be raised very gradually in small steps to insure that the flow remains in the channel and no override is precipitated.

Oxygen-steam injection will be started in Well A at the end of the air burn period. Current plans are to use a high percentage of steam as a dilutant for the oxygen during the first part of the experiment. This will provide a test of the hypothesis that the width of the burn zone is directly related to the input flow rate. However, we will adjust the steam/oxygen ratio as needed to maximize the gas heating value and minimize the amount of oxygen used per ton of coal consumed.

A forward burn with oxygen-steam from Well A to Well B will satisfy all of the goals outlined earlier. A planned program of flow rate and operating pressure changes will be used. The majority of the experiment will be conducted under the flow conditions that give the best gas composition, or if that is not practical, at the maximum oxygen flow available.

The experiment planned is a forward burn from well A to well B with gas production from both B and C. We do not plan to continue the burn from B to C. However, the design will include a provision for converting well B into an injection well with a short shut down period if necessary. This would allow continuation of the burn if additional funds become available.

We want to determine the effect of the oxygen/steam ratio on the burn geometry. In order to do this we will plan to inject at as high a steam flow as practical (50% to 80% steam) for a period of time long enough to determine the cavity growth rates in both width and length before changing the oxygen/steam ratio.

The average oxygen injection rate planned is 20 moles/sec (1000 scfm). Short periods (one or two days) of operation at double this rate are being planned for.

Although we hope to have better performance for Hoe Creek #3 than was achieved during the oxygen burn during Hoe Creek #2, all estimates are based on Hoe Creek #2 results. Table II is a summary of the parameters expected for Hoe Creek #3 assuming similar performance.

TABLE 2

Performance Estimates Based on Hoe Creek No. 2 Results

Coal Consumption - 5280 tons - 3550 m^3

Average Injection Flow Rate Oxygen 20 mol/s = 1000 scfm

Steam 80 mol/s = 4000 scfm

Burn Period at Average Rate = 45 Days

Total Oxygen Consumption = 2780 Tons

Total Steam Consumption = 6220 Tons

Steam Generation Water Feed Rate = 33,000 gal/day

Produced gas Flow Rate = 148 mol/s = 7430 scfm

Produced Gas Temperature 650°C

Produced Gas Flow Rate After Cooling 181 mol/s = 9086 scfm

Cooling Water Needed for Gas Temperature of 350°C = 9.4 gpm

Produced Gas:

Wet Heat of Combustion = 101 KJ/mol = 114 Btu/ft^3

Dry Heat of Combustion = 235 KJ/mol = 164 Btu/ft^3

Produced Gas Composition

	Before Cooling Mol Fraction	After Cooling Mol Fraction
H	0.530	0.617
H_2	0.178	0.145
CH_4	0.026	0.021
CO	0.105	0.085
CO_2	0.156	0.127
C_2H_4	1.7×10^{-4}	1.4×10^{-4}
C_2H_6	10.8×10^{-4}	8.8×10^{-4}
C_3H_6	1.4×10^{-4}	1.2×10^{-4}
C_3H_8	2.2×10^{-4}	1.8×10^{-4}
C_5H_{12}	13.5×10^{-4}	11.0×10^{-4}
Tar	28.4×10^{-4}	23.2×10^{-4}

The Wells P1, P2, P3 and P4 are designed to be directly connected to the drilled channel. If it is possible to have water pumps survive in wells connected to the channel, we may be able to operate at low backpressure and still keep the area dewatered. In any case, we will be able to observe the effect of water influx on gas quality for a burn with the production channel at the bottom of the coal seam.

A report will be issued at a later date giving the operating plans in more detail.

II. Data Acquisition and Storage

R. Cena and C. B. Thorsness

A. Experimental Data

The Hoe Creek III data acquisition and storge system will build upon the computer operating system developed for Hoe Creek II. The experimental data to be collected fall into three catagories:

1) Process Data
2) Compositional Dta
3) Diagnostic Data

1. Process Data

Parameters which determine the state of operation of the above ground facility constitute process data. The specific data include:

- System pressures and temperatures throughout the above ground process piping.
- Pressure temperature and differential pressure for each process flow metering station.
- Parameters pertinent to process geometry, e.g., orifice size, active metering station, etc.
- Parameters pertinent to specific process equipment, e.g., boiler, compressors, incinerator, flare, etc.

As discussed earlier, the process consists of air or oxygen/steam injection into the coal seam with production from the coal seam 100 meters from injection. The product gas travels through a particle removal device and is then sampled before passing to the incinerator and flare for disposal.

2. Compositional Data

The flow rates of all streams entering or leaving the system will be computed from the process data. Compositional data will be collected for

the product stream, four instrument well sample streams, and the oxygen injection stream. Details of the analysis system are discussed in Section 3--Chemical Analysis System. The process stream flow rates and compositions will be used in energy and material balances to calculate variables which can not be measured directly such as char accumulation and heat loss to inert materials underground.

Diagnostic Data

The state of the process beneath the ground will be monitored using diagnostic tools. These include:

- Downhole thermocouples at fixed locations in each I-well, process well, and pump well.
- HFEM probing techniques.
- Electrical resistivity measurements.
- Geophysical measurements.
- Tracer measurements.

The downhole thermocouples located throughout the coal seam and in the overburden represent a large portion of our diagnostic data. The locations of the wells are shown in Fig. 2 and the specific locations for TC's in each well is shown in Table I. Each thermocouple will be routinely measured for junction voltage, loop resistance, and resistance to ground, thus providing not only temperatures but diagnostics concerning TC failure.

Tracer techniques will be used to obtain information concerning the fluid dynamics in the system and the propagation of the burn zone through the coal seam. Two types of tracer information will be utilized during Hoe Creek III:

1) Helium tracers
2) Flurocarbon tracers

A pulse of Helium tracer gas will be injected along with the injection stream periodically with the resultant response measured in the production stream. Continuous

Data will be collected from the first response to a point where little or no detectable Helium remains. The will data provide measurements of the active volume and dispersiveness of the underground system.

Flurocarbon tracer canisters will be placed at various locations underground to help identify the extent of burn propagation under ground. Detection of flurocarbons in the product gas will signal the arrival of burn or subsidence at the canister location.

B. Experimental Hardware

The hardware components (Fig. 3) of the data acquisition and storage system fall into two catagories:

- Data Acquisition Hardware.
- Data Management Hardware.

1. Data Acquisition Hardware

The bulk of the process and diagnostic data will be routinely collected via two COMUX digital voltmeter scanners, each equipped with 252 channels.

The COMUX, supplied by Sandia Laboratory, is designed such that each channel is capable of measuring a thermocouple junction's voltage, loop resistance, and resistance to ground.

This feature allows complete monitoring of each thermocouple using only a single channel. 285 downhole thermocouples will be connected to the COMUX as well as most above ground TCs.

In addition to the thermal couples several other data gathering instruments will be directly linked to the COMUX for routine data acquisition. These include:

- Pressure transducers to measure the above ground and down hole pressure throughout the system.
- Two humidity meters to measure the water content in the produced gas and the ratio of water to organic liquid.

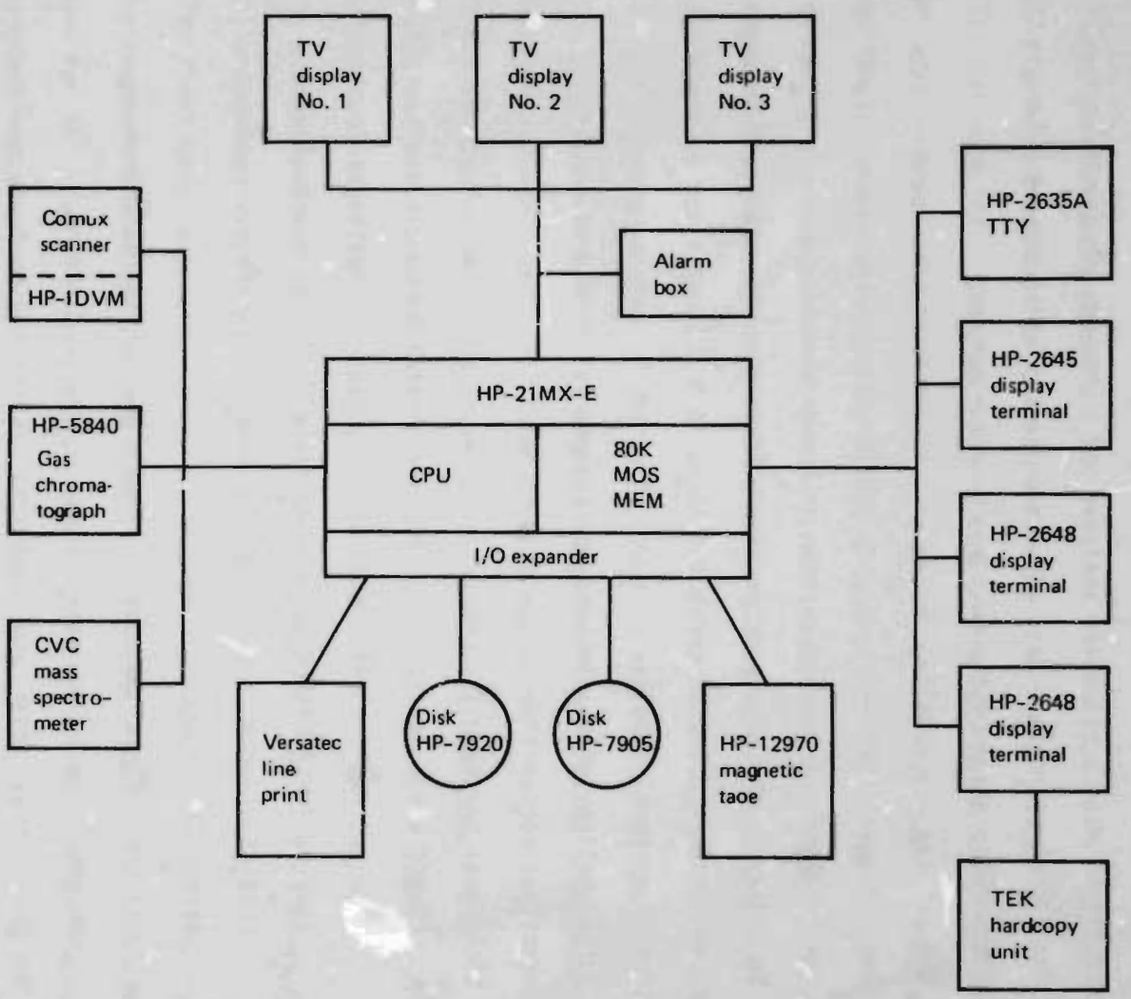

Figure 3. Data Acquisition and Storage System

- Several geophysical instruments to measure ground movement discussed in detail elsewhere.

Much of the constituent data will be analyzed in the field via an online time of flight mass spectometer analyzer and a process gas chromatograph.

The gas chromatograph data will be collected at 60 minute intervals for backup and calibration of the mass spectrometer system.

The primary gas sampling system will be the mass spectrometer with sampling times as short as 10 seconds. This will provide essentially real time analysis of the composition of the product gas.

In addition, the mass spectrometer will sample injected gas for oxygen to tracer ratios and may be connected to up to 4 - I-wells for downhole gas sampling on an hourly basis.

During helium tests, the mass spectrometer will determine helium concentrations versus time in the product gas.

Additional hardware includes:

- Liquid condenser system will provide batch backup to the humidity meter system for water and organic content and will provide liquid samples for in field and Laboratory analysis of trace elements, tritiated water, and organic components. All liquid condenser data will be gathered manually.
- On line analyzer to monitor product gas for the detection of flurocarbons in the product gas.

The geophysical, HFEM, and electrical resistivity hardware are discussed elsewhere in this report.

2. Data Management Hardware

All of the data collected via the COMUX scanner, gas chromatographs, and mass spectral analyzer will be automatically recorded at regular intervals

using a Hewlett-Packard 21MX-E Computer. The primary responsibilities of the computer include:

1) Real time acquisition and archiving of all relevent process data.

2) Real time data reduction

3) Real time data display and retrieval.

The software for the system has as its base the HP RTE IV operating system. Built on top of this base is a series of system and user programs to perform the tasks mentioned above. System programs are defined as those routines which perform the basic data acquisition and archival tasks, while user programs are those codes which perform data display and manipulation functions.

Of the three major aims of the system that of the highest priority is the acquisition and archiving (on magnetic tape) of all relevant process variables at regular intervals.

The second major aim is to provide real time data reduction. This capability is provided by system programs which convert all incoming analog or digital signals to useful engineering units and by user programs which perform a number of heat and mass balances and pressure drop/flow calculations useful in interpreting the performance of the gasification process.

The final major objective ot the system is to provide the capability to display the raw and reduced data on demand showing either current values of selected variables, or the time history or any variable throughout the course of the experiment.

System Operation

The COMUX scanner will routinely report information to the computer via hardware interface cards and software drivers.

The COMUX will be scanned at 15 minute intervals for system flows and water/gas ratios and at 30 minute intervals for system flows and water/gas ratios and at 30 minute intervals for all other data.

The computer will control the mass spectrometer in several ways. First, the mass spectrometer will queried at 2 second intervals to provide real time analysis of product gas composition. Second, the computer will request automatic standarizartion sampling at hourly intervals. Third, samples from the oxygen injection stream and from up to 4 connected I-wells, may be analyzed hourly.

The gas chromatograph will report product compositions directly to the computer at 60 minute intervals.

Additional data is entered into the computer manually via software programs. These include:

- manual input of condenser data
- manual GC Data input when the GC/computer link is down
- manual input of process geometry changes

The computing hardware includes the HP-21 MX-E central processor, a 1.7 megabyte, disk, and a 50 megabyte disc. The discs provide enough storage area for programs and files to maintain on line all of the gathered data from the entire experiment. In this way the time history of any process variable can be reviewed immediately over the entire course of the experiment. The 128K cpu provides sufficient memory capability for efficient program execution and data logging tasks. A back-up cpu disc controller and integrating digital voltmeter will also be available in case of equipment failure.

The I/O hardware consisted of 3 high speed (9600 baud) display terminals with hard copy unit and one medium speed (300 baud) TTY. These are used for all TTY-computer communication. Also included is a Versatec printer, alarm box and 3 independent TV interfaces connected to three TV monitors.

The TV monitors are used for various data display purposes throughout the experiment.

Finally, a magnetic tap unit provides backup for all data logged into the computer throughout the experiment, via a file archiving routine.

The data storage, retrieval, manipulation and viewing software is similar to that described for Hoe Creek II. However, enhancements over that system, some which were described above, will be available during Hoe Creek III. To summarize some of these are:

1) Automatic sensing of fluorocarbon tracers
2) Inclusion of the mass spectrometer in the computer operating system
3) Automatic sampling of 1-well gases at regular intervals
4) Dial up capability of remote computer control
5) Increased data storage capability
6) Automatic recording of all liquid injection and production rates
7) Increased reliability with backup CPU and disc controller
8) Automatic resistance measurements for all TC's
9) Increased flexibility in accessing scanner
10) Improved material balance calculations which include estimates of net character formation
11) Real time thermal contouring programs to display burn geometry based on material balances and thermocuple response
12) Real time analysis of HE tracer data

III. Chemical Analysis Systems

W. R. Aiman and J. Clarkson

The primary objective of the Gas Analysis program is to determine the compositions of several process streams and to report these compositions to the field computer. The analyzed process streams will consist of: the product gas stream, four instrument-well sample streams, and the oxygen injection stream. A secondary objective of the program is to identify various freons in samples of the production stream and to maintain capability for general purpose analysis to meet needs which may be identified later.

Analysis of the process streams will be done in an "automatic" mode by a CVC Process Gas Analyzer Mass Spectrometer, a Hewlett-Packard Process Gas Analyzer Gas Chromotograph, two dew point meters (EG&G and General Eastern), a Teledyne Model 326A oxygen analyser, and a special freon analyzer which will be selected later. All of these analyzers will be coupled with the field computer. In addition, several trace species will be determined intermittently with special apparatus.

The specific tasks of this analysis package are: 1) analyze the product gas for the species listed in Table III, 2) analyze for the important species with at least two analyzers, and 3) analyze for the important species in a fast, on-line mode to make control of the process easier. Use of both the mass spectrometer and the gas chromatograph provides extensive redundancy and in addition the mass spectrometer is sufficiently fast to be considered an on-line analyzer. The various species will be determined by the analyzers as shown in Table III.

A clean, reasonably dry gas sample stream from the gasification stream or other sources will be supplied to the analytical laboratory from a series of clean-up systems at a pressure of 5-15 psig. Every effort should be made

Table III. Gas Analysis: Hoe Creek No. 3 Experiment

Component	Possible Concentration Range	Instrumentation				
		CVCMS	PGC	D.P.M.	Special Analyzer	Special Apparatus
N_2	0.1 - 75%	F	S			I
CO_2 *	0.1 - 70%	F	S			I
CO*	0.1 - 35%	F(>2%)	S			I
H_2 *	0.1 - 40%	F	S			I
CH_4 *	0.1 - 10%	F	S			I
C_2H_4	0.01 - 1%		S			I
C_2H_6	0.01 - 1%		S			I
C_3H_6	0.01 - 1%		S			I
C_3H_8	0.01 - 1%		S			I
C_4H_8	0.01 - 1%		S			I
C_4H_{10}	0.01 - 1%		S			I
i-C_4H_{10}	0.01 - 1%		S			I
ΣC_5	0.01 - 1%		S			I
ΣC_6	0.01 - 1%		S			I
H_2O	10 - 50%			F		I
O_2*	0.01 - 100%	F	S		F	
Ar	0.01 - 1%	F				I
He	10 - 1000 ppm	F				
HD	10 - 1000 ppm	F				
H_2S	200 - 5000 ppm	F				I
SO_2	10 - 1000 ppm	F				I
COS	50 - 1000 ppm	F				
NO_X	10 - 100 ppm					I
HCN	10 - 100 ppm					I
NH_3	100 - 1000 ppm					I
Freon		F?			F	I
Tar						I
Particulates						I

F - fast, on line mode; S - slow, off-line mode; I - intermittent mode

* - species of vital importance for control of the process.

to keep the gases to be analyzed as clean and dry as possible. Below is a discussion of the various types of analysis to be utilized.

A. Field Mass Spectrometric Instrumentation and Measurements

Analysis for a wide variety of components will be conducted using a CVC Process Gas Analyzer Mass Spectrometer as shown in Table III. This instrument is to be calibrated periodically in the field using standards as appropriate. The mass spectrometer will be computer controlled and the data is expected to be taken at approximatley ten second intervals for the process gas stream, and from other gas streams at intervals of approximately one hour. Four of these other streams will be sample streams from instrument wells and one will be a sample, stream from the oxygen feed stream.

B. Field Gas Chromatographic Instrumentation and Measurements

The gas components expected to be analyzed by the Hewltt-Packard Model 5840 Refinery Gas Analyzer are shown in Table III. This analyzer will have the primary responsibility for analysis of the hydrocarbon components of the process gas. The instrument will be under computer control and will complete an analysis at intervals of approximately one hour each. This instrument is to be calibrated in the field using LLL mass spectrometrically verified standards, and periodically checked for accuracy during the gasification.

C. Water, Tar, and Ammonia Analysis

The dew point of the product gas will be determined continuously by two similar dew point meters: an EG&G model 660 and a General Eastern model 1200 AP. These dew point meters operate by cooling a mirror, which is exposed to the product gas, until a mist forms on the surface. The temperature at which the mist forms is the dew point.

In a separate apparatus, the water and tar will be condensed out of a sample stream. The gas flow will be measured in a dry gas meter. Comparison

of the amount of water condensed with the gas flow will provide a redundant measure of the water fraction in the product stream. The product tar will be condensed out of the stream with the water. The tar/water ratio will be determined from these samples.

These water and tar samples are to be collected in cannisters attached to the water collection system. The samples shall be stored by the process operator for subsequent analysis at LLL. A balance shall be provided for the determination of the tare and gross weight of the canister and product.

Occasionally, at the request of the project scientist, these samples will be analyzed for tar/water fraction volumetrically of gravimetrically.

Elemental analysis for C, H, N, S, and a simulated distillation will be required on selected tar samples as submitted after the experiment at LLL. The water/tar content of selected samples will also be determined at LLL after the conclusion of the experiment.

Periodically the water from the water/tar collection system will be tested for ammonia and hydrogen cyanide content. This measurement will be done with specific ion electrodes, using appropriate standarization. It is anticipated that this measurement would be done once daily.

D. Freon Analysis

Freon analysis is required for the experiment because bulbs of various freons will be implaced in the coal seam to signal arrival of the burn front. The bulbs will be placed at the 2 m level in wells I1, 3, 4, 5, 9-15, and at the 5 m level in well I5 (See Fig. 2). Two types of analysis are required: 1) sensitive detection of freon (or freon fragments) in the production stream to signal that a bulb has burst, and 2) specific analysis to determine which freon is present in the stream.

The sensitive analysis need not distinguish between the various freons which will be used but this analysis must be sensitive and "on-line." The pattern of evolution should be recorded as concentration vs time. The specific analysis does not need to be as sensitive since a bottle sample will be taken at peak freon concentration.

The sensitive analysis will be done with either a new freon detector or with the mass spectrometer. The specific analysis will be done with a Varian Model 3700 Gas Chromatograph.

E. Spot Sampling

Hydrogen sulfide, sulfur dioxide, and nitrogen oxides will be determined using detector tubes. Although the mass spectrometer is expected to be able to determine hydrogen sulfide, some verification of the values determined seems reasonable. Sampling of the production line for these species will be made at daily intervals.

F. LLL Mass Spectrometric Gas Sample Analysis

It is expected that some samples (not more than one per day) may be taken by the process operator, project scientist, or others, for later analysis at LLL. In order not to flood the LLL mass spectrometer with samples at the end of the experiment, it is suggested that these samples be sent to LLL when 10-12 samples have been taken. These samples should be sent to:

Lawrence Livermore Laboratory
Attention: Carla Wong
Bldg. 222, Rm. 1223
Livermore, California 94550

G. Wobbe Index Recorder

The Wobbe Index Recorder will be installed as a backup heating value indicator. This instrument indicates: (heating value)/(specific gravity)$^{1/2}$.

H. Particulate Sampling

Particulates in the product gas stream will be sampled via an impact tube at an el in the pipe. The sample removed from the main stream will be passed through a cyclone separator and a filter. This separator will remove 99% of the particles larger than 10 μm and the filter will collect smaller particles. The separated samples will be weighed and selected samples will be retained for further analysis.

I. General Purpose Gas Analysis

A capability for general purpose analysis will be maintained based on the Varian 3700 Gas Chromatograph which will be fielded for freon analysis. Use of this capability will be ad hoc at the request of the project scientist.

Included in this general purpose capability will be a third level backup for the process gas analysis (second level backup for argon). This backup capability will consist of the columns, detectors, and carrier gas required to convert the Varian 3700 to analyze the important species (including argon) from Table I. Thus, as a last resort, manual operation of this chromatograph will give analysis of the product stream.

J. Personnel and Facilities

The Analytical Chemistry representative will report to the project scientist and will be in residence at the site during all day shifts and, locally on-call at all other times during which ignition and gasification are being conducted. He will be responsible for checkout, maintenance, calibration, and operation of the analytical instrumentation described above and for the collection of routine bottle samples. He will also advise the project scientist of any analytical procedures or techniques which might be used to enhance the value and reliability of the information obtained.

Due to the magnitude and complexity of equipment expected to be used during this experiment, the use of the entire T-933 trailer or equivalent quarters will be required as the Analytical Laboratory. These quarters should have reasonable temperature controlled facilities, approximately 72°F. We estimate the need for at least four circuits of 20 amps each, as well as other circuits of 15 amps for recorders, and other instrumentation. These circuits should be as free from interruption as possible.

IV. HFEM Burn Front Detection

D. T. Davis and R. J. Lytle

Plans for LLL's Hoe Creek No. 3 UCG Experiment call for a total of 10 HFEM wells, each path to be probed twice daily, with interpreted results to be displayed on the HP 21 MXE computer graphics. We see the need to (1) significantly increase our data acquisition and interpretation rates, (2) increase our transmission distances and (3) improve the timeliness and usefulness of our graphical results as compared to our capabilities during the Hoe Creek No. 2 experiments. Given adequate support during FY'79, we feel that we can meet these requirements. This section outlines the approach we plan to take in achieving these capabilities as well as the financial support required and details concerning the services we will require at the site.

A. Increased Data Acquisition Rate

We anticipate the need for making up to 40 data runs per day in the next experiment as oppossed to about 8 per day for the Hoe Creek No. 2. This five-fold increase could be accomplished by reducing our setup time and improving equipment reliability. We plan to do the following: (1) purchase and install reels of an improved design at each well, thereby reducing the down time and much of the need for moving reels from well to well, (2) permanently placing control, signal and power cables to each reel, thus eliminating that setup time, (3) purchasing better transmit and receive electronics and in adequate numbers to permit rapid setup and recording times and the simultaneous operation between two or more pairs of wells.

Several cable reel improvements are planned. Our new motorized reels will have gear ratio permitting a more rapid raising and lowering of our antennas. Design improvements we are planning will also make them more

reliable resulting in less down time. In addition, through the help of a summer student we had this year, we have worked out most of the details for making the reels semi-automatic. Given some additional engineering and technician support, we should be able to field cable reels, which will stop automatically at the depth we specify and step an incremental distance on command. Our new reels will also be designed to accomodate wheels so that when they need to be moved, it will be much easier than before.

Incidentally, we plan on measuring depth in meters rather than feet as we did at Hoe Creek No. 2.

B. Increased Transmission Path Lengths

Several improvements will permit us to propagate EM waves over the somewhat longer distances planned for Hoe Creek No. 3. We will purchase spectrum analyzers with better signal to noise ratios and design more efficient transmitting antennas and receivers. If need be, we would operate at somewhat lower frequencies.

C. Improved Disimination of Results

We would certainly like to provide results from our HFEM measurements which are more timely and in a format which is more useful to the scientific staff. You have requested that we tie into your HP 21 MXE computer graphics device. We are uncertain at this time as to what is the best approach. Spectrum analyzers could be purchased which permit data recording on cassette tapes. These tapes could then be fed into your computer. We would need to design some interface electronics which would allow us to identify the data run--time, frequency, well pair, etc., -- as well as the depth of each data point. Another approach would be to purchase an x-y plotter and put in ID information and depths by hand. This latter approach would not, however, allow us to use your display hardware. Still another approach would be to

hardwire our spectrum analyzers directly into your computer through an interface which would have to be designed and fabricated. The details of this approach would need to be worked out.

D. HFEM Requirements

We will need the following equipment and services:

Wells - 3" ID, pvc or fibreglass lined between 10m above and below coal seam. No water in wells. Top of casing about 1/2m above ground level.

Power - 110V AC; two circuits from different generators, one for receiver electronics and one for our power amplifiers. (Separate circuits needed for noise suppression).

Surface Piping - Pipes should be low to the ground and out of the field of view as at ARCO's Rocky Hill site to allow visual contact with all wells from our control building.

Shelter - One climate controlled building about 10' x 10' x 8' high with a window for viewing the site. Should be placed near wells. Best location would be near P1. Power plugs in building would be nice.

Office Space - We would like to have a desk in or near the experiment control room.

Hoe Creek III Geotechnical Experiment

H. Ganow

A. Introduction

In-situ gasification of coal forms an underground cavity. Initially, it is desired that the cavity form in the base of the coal seam where subsequent roof collapse exposes fresh coal for gasification. The remaining roof coal acts as a thermal insulator, thereby increasing the efficiency of the gasification process. In this context, roof collapse is a vitally important mechanism that results in increased recovery of the coal resource. Ultimately, a non-coal roof is exposed which detrimentally affects the gasification process in several ways.

First, exposure of the roof rock, and its subsequent collapse into the expanding cavity, results in much heat energy loss, thus reducing process efficiency. Second, rock units permeable to fluid flow are exposed resulting in the loss of injectant or product gases and in the influx of groundwater, if these units are saturated. Again, heat energy is lost in vaporizing water, and the resulting steam dilutes the product gases. The injection of product gases into aquifers containing potable ground water may result in significant contamination. Third, continued roof collapse exacerbates the problems mentioned above and may ultimately lead to disturbance of the ground surface or subsidence.

Following the successful geotechnical experiment associated with Hoe Creek II, we are beginning to appreciate the extent to which roof collapse can affect the gasification process as well as its environmental implications. The acquired data clearly indicate that roof collapse can extend much higher into the overburden than current continuum finite element method (FEM) model codes suggest. This is because these codes treat cavity-induced subsidence

as a prime body force problem that includes only gravity-induced stress, weight and strength of overburden materials, and simplified deformation mechanisms. However, at the present time, FEM codes remain as our only method of calculating roof collapse and surface subsidence. Improvement of these models will come from incorporating other extremely important failure mechanisms such as overburden shrinkage with drying, fissuring, and roof spall. Clearly, both chemical process and environmental concerns demand that the mechanisms controlling the magnitude and rate of gasifier roof collapse and attendant surface subsidence be understood to the fullest possible extent. Such understanding will only come from comprehensive geotechnical instrumentation programs associated with in situ gasification experiments.

B. Purpose

The purpose of this experiment is to basically replicate the first geotechnical experiment done in conjunction with the Hoe Creek II gasification test. We plan to measure both surface and subsurface deformations, in both the horizontal and vertical sense, that result from gasification cavity creation. Knowledge gained from the first experiment is being used to refine the design of many of the instrument systems, their installation, and their plan view locations with respect to the third gasification experiment. Following this experiment, many of the instruments may be sufficiently well developed that they can be applied directly to deeper gasification experiments. The real-time data that are obtained from many of the geotechnical instruments will be of aid to other scientific and engineering groups. First, these data will aid those individuals concerned with operating the gasification facility and assist them in understanding their process-related data. Geotechnical data will also be of benefit to the engineering staff conducting the HFEM (High Frequency Electromagnetic) experiment in their data inter-

pretation. Second, data concerning the height of ultimate roof collapse and the effect of gasification cavity operating pressures on the local ground-water regime are vital to an understanding of the ground-water pollution aspects of in situ coal gasification. Third, the time-history of cavity-induced overburden strains and roof collapse will provide critically important data for verification of the results obtained from highly sophisticated FEM modeling codes.

C. Proposed Subsurface Instrumentation

The various subsurface instruments will be capable of measuring both horizontal and vertical strains, and planar deformations (shearing). Over the center of the cavity, vertical motions are dominant while lateral strain will characteristically occur at the cavity sides. Both deformation modes will be present at locations above and to the side of the cavity. Local shear forces may be concentrated along a "planar" surface termed the "angle of break". This surface rises at an angle of from 30° to 90° (referred to the horizontal) from the cavity margin depending on the overburden strength characteristics and other factors. The locations of the holes used for these measurements are shown as squares in Fig. 2.

1. Borehole Deflectometer. This is a biaxial wire-line probe device that measures the inclination of a near-vertical borehole using servo accelerometer sensing elements. It operates in an internally grooved casing that is anchored full length in a borehole with a neat cement grout. The hermetically sealed transmitter probe is equipped with wheels that travel in the casing grooves and maintain it in the proper orientation.

Following installation, the initial inclination of the borehole is measured by lowering the sensing probe to the bottom, withdrawing it in short incremental distances, and measuring and recording the two inclinations on a digital readout

device. Successive measurements, compared to the first measurement and to each other will yield depth profiles of the casing in two orthogonal dimensions with time. From these data, principal displacement directions, magnitudes, and rates can be calculated using appropriate computer codes.

Six deflectometer boreholes, designated D-1 through D-6 on Fig. 2 will be drilled to a depth of 77.5 meters and completed with 85 mm diameter beaded aluminum casing. They will also have 10-meter long steel surface casings designed to provide a gas-tight seal should the aluminum tubing burn through during the experiment. Boreholes D-1, D-2, and D-3 are arrayed in a line sub-parallel to the experimental axis defined by the main process wells A and B. Boreholes D-4, D-5, and D-6 are oriented perpendicular to the experimental axes. These two arrays should yield data on horizontal displacement rates, magnitudes, and directions near the major and minor experimental axes. Borings D-1 and D-4 will have internally grooved plastic casing sections from about 3 m below the Felix No. 2 Coal to about 3 m above the overlying Felix No. 1 Coal to allow the HFEM apparatus to use these boreholes.

2. Multiple Position Borehole Extensometers (MPBX). This device measures the axial deformation of boreholes. They are insensitive to small transverse deformations, but may be rendered inoperative by a large shear displacement. The downhole portion of this device consists of six expandable mechanical anchors located at various positions along the borehole. These are connected to a gas-tight sensor head, located at the ground surface, by small diameter cables. The sensor head is designed to exert a constant tension on these cables.

The displacements measured at the sensor head are the integrals of vertical strains occurring between the head and the various anchor points, and are measured as an analog electrical output by a rotary resistor/voltage

divider. The plan is to install five six-positions MPBXs designated E-1 through E-5 in Fig. 2. The MPBXs will yield data on roof deflections including the time, magnitude, and approximate vertical location, and the onset and extent of roof collapse. Extensometer borehole E-1 is located over the region of maximum vertical strain and roof collapse. E-2 and E-3 are located in line and symmetrically on either side of E-1, and perpendicular to the major experimental axis. Data from these three units will allow us to address the question of asymmetry of gasifier roof deformation and will yield insight into oblique mode deformation through incorporation of data from the D-4, D-5 and D-6 line previously discussed.

3. Shear Strips. These devices consist of a long thin strip of brittle plastic having two thin parallel metal foils bridged at 0.3-meter intervals by 10 Kohm precision resistors. Two-conductor electrical cables are connected to each end, and the strip, cables, and connections are sealed against water incursion. Shearing displacement along planes inclined at high angles to the borehole axis, or hole elongation, breaks the strip and causes a change in the apparent resistance measured at the ground surface. Knowledge of the strip position, value of the resistors, their spacing, and the measured value of apparent resistance allows calculation of the approximate depth to the break position.

Four borings, each containing a 30 meter long shear strip and designated S-1 through S-4 are planned. They will be placed in small diameter unlined boreholes that extend down to just above the top of the Felix No. 2 Coal and grouted in place using neat cement. Borehole S-4, like E-1, is located in the expected region of maximum roof collapse. It should provide excellent data concerning the rate of collapse and location of the cavity roof. Boreholes S-1, S-2, and S-3 are arrayed in a line radiating from process well A.

Their purpose is to detect an angle-of-break type of shearing deformation rather than roof collapse. Somewhat equivocal data from a single shear strip located in a similar position on Experiment II suggest that this very important mode of deformation may occur.

4. Electrical Piezometers. These devices measure pore-fluid pressure in soils and rocks in an uncased borehole. Their electrical output is proportional to the total pressure head at their respective positions. It is planned that three boreholes, designated U-1 through U-3, each be equipped with five hydraulically isolated transducers. Borehole U-1 will be placed near E-1 and S-4, thus forming a small sub-experiment by interrelating the three types of data. This borehole will extend to just above the top of the Felix No. 2 Coal and thermally armored piezometers equipped with temperature sensors will be installed in selected zones from just over the No. 2 Coal to above the zone of saturation. Boreholes U-2 and U-3 will be located to the side of the expected cavity (Fig. 2), and drilled to a depth of 76 meters. Piezometers will be installed in both the Felix Nos. 1 and 2 Coals, and in selected zones both above and below the No. 2 Coal. These units will yield data regarding the regional effects of in situ gasification on the ground-water pressure regime in many radically different rock units.

D. Proposed Surface Instrumentation

Strains having both vertical and horizontal motion components will occur on the ground surface over and adjacent to the cavity. Preliminary FEM calculations indicate that these strains may occur to nearly 200 feet from the A-B process well line. The instrumentation required to detect these strains consists of isolation bench marks, an optical level and rod, and a tape extensometer.

Approximately 33 isolation bench marks will be installed in a manner similar to the array constructed for Hoe Creek II. One monument line will be parallel to the Experiment III axis defined by process wells A and B, and will extend 76 meters on either side from an origin monument located near E-1. A second monument line will be constructed perpendicular to the first, with its origin at the same location.

Initialization surveys will be made immediately before gasification. Additional surveys will be conducted about midway through the forward gasification phase, and once or twice following the experiment until motions can no longer be detected.

Electrical Remote Monitoring Instrumentation

L. C. Bartel

The electrical remote monitoring (ERM) techniques to be implemented on the Hoe Creek No. 3 experiment are a modified Schlumberger (MS) technique and a direct excitation electrical potential (DEEP) technique. The current electrodes for the MS method are located on either side of the experiment area and separated by approximately five times the depth of the coal seam. The applied current lines for the MS technique are roughly parallel in the coal seam and are distorted by regions of hot conductive coal. One current electrode for the DEEP method is a process well and the other current electrode is an outlying well. In the DEEP configuration, the hot conductive coal in contact with the process well (production well) forms part of the current electrode and the geometry of the current source varies with the shape and extent of the reaction zone. Both the MS and DEEP techniques will utilize the same surface electrical potential electrode array, share a common current electrode, and will use the same measuring hardware.

The surface electrical potentials will be measured by a potential electrode array consisting of 140, 6 in x 6 in, 1/4 in thick, stainless steel plates on nominally a 5 m x 10 m grid as shown in Fig. 4. The potentials of these process wells, A, B, and C, will be measured to give a total of 143 electrical potential measuring points over the 60 m x 100 m grid. The potential electrodes, along with cables, will be buried in 4 ft. deep trenches along lines perpendicular to the Well A-B-C line. These trenches can be adjusted to miss instrumentation wells. One cross trench along the 100 m direction will also be dug to provide protection for the cables running to the instrumentation trailer. The electrodes are buried to provide adequate contact with the earth. All potential measurements will be made with respect to a common electrode.

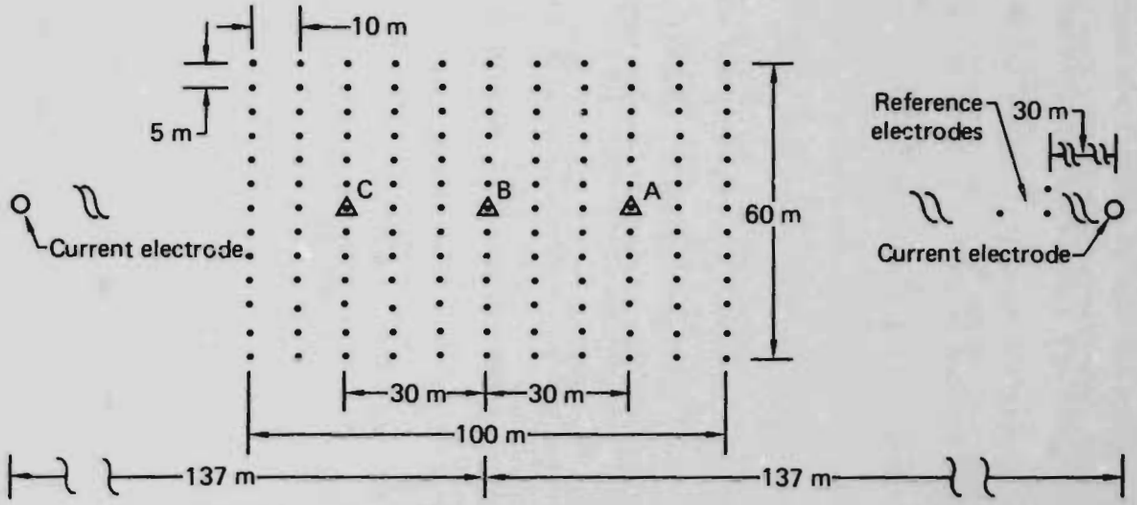

Figure 4. ERT Electrode Array

The location of the two current electrodes for the MS technique are the outlying current electrodes shown in Fig. 4. The DEEP technique utilizes one of the process wells for a current electrode along with one of the outlying current electrodes. The outlying current electrodes can be one 30 ft. section of 6 in casing set into the earth.

To insure good data, some care must be taken to eliminate electrical short circuits. The general rule is that no two points are to be electrically tied together except those tied by the vertical well casings. This will require some care in the installation of the surface plumbing.

Figure 5 is a block diagram of the ERM electrical data acquisition subsystem. The main features of this system are: the mini-computer control of the experiment, data acquisition, data storage and retrieval, and a field plotting capability. For each setting of the group switch, the mini-computer operates the current pulser and scans the 72 channels of data. The first 64 channels are measurements of potentials of the probes; the last 8 channels are: current, battery voltage, potentials of the three process wells, and potentials of the three reference probes shown in Fig. 4. Measurement of all the surface potentials requires three group switch settings. (There are some vacant data channels on the third group switch setting).

The current pulser is controlled by the mini-computer with information provided by the experimenter through a pulse-timing table. Variables to be defined in the table include: number of pulses (up to ten), MS or DEEP-B or DEEP-C current drives, length of time before sampling the positive and negative pulses, and length of time between positive and negative pulses. The positive and negative current pulses are of equal length. (DEEP-B and DEEP-C refer to injecting current into Wells B and C, respectively).

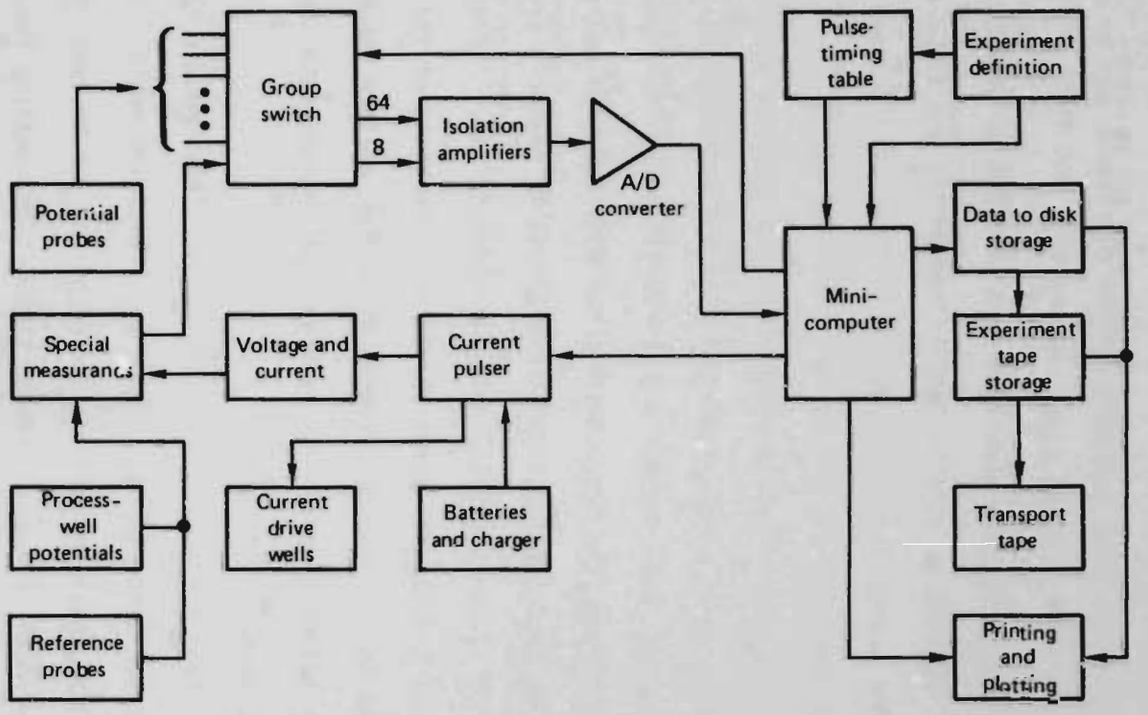

Figure 5. ERN Data Acquisition Subsystem

A schematic of the current pulse, along with the resulting potential, are illustrated in Fig. 6. The 25 millisecond sampling rate was chosen to average the effects of 60 Hz noise. Self potentials and current induced potentials are measured for each group switch setting. Ten samples in 250 milliseconds are taken and averaged for the measurements of the self potentials. These self potentials are stored and used to zero the equipment for potential measurements due to a current pulse. Twenty samples in 500 milliseconds are taken for the current and the resulting potential measurements. (The current and potential measurements are made over the last half second of the positive and negative pulses). For each of the 20 samples of current and potential, the potential (positive value minus negative value) is divided by the current (positive value minus negative value) to give a reduced potential and then these 20 values of reduced potential are averaged and stored.

It is convenient to display the data in the form of equipotential contour plots. A field plotting capability will be available for "real time" plots of the data.

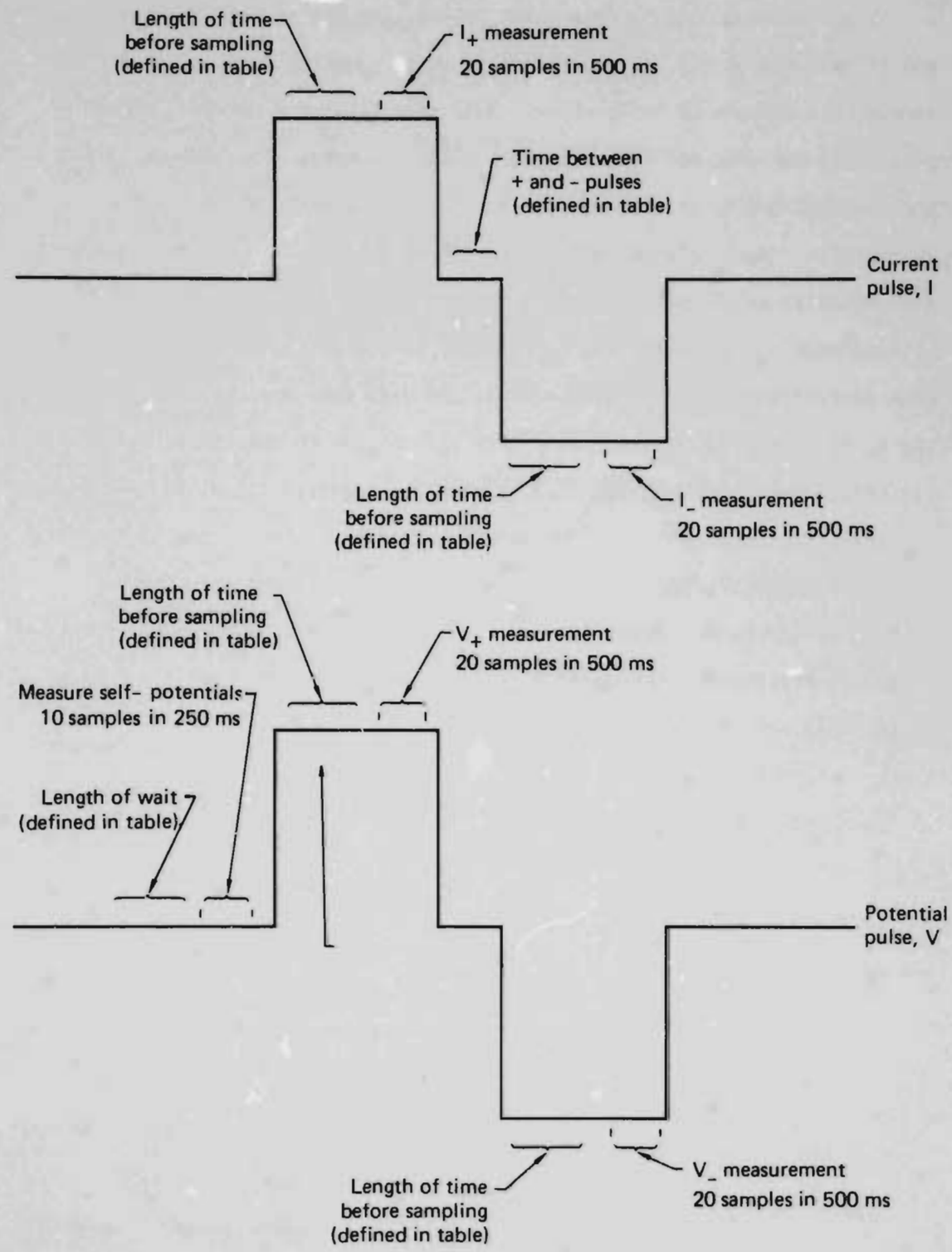

Figure 6. Schematic of Current Pulse and the Resulting Potential Pulse

Inverted Thermocouple String

G. S. Davidson and L. C. Bartel

Thermocouple strings are normally fielded with the extension leads coming from the thermocouple (T/C) junction to the surface. In the event of a high temperature override, the T/C string would experience a failure prior to any significant temperature measured at the lower T/C junctions. A new concept of T/C installation is under investigation to circumvent the high temperature override problem. A T/C string with leads from the T/C junction going downhole rather than uphole could obtain useful data prior to failure in an override situation; this type of installation will be referred to as an "inverted T/C string". For the inverted T/C string to be fielded on the Hoe Creek No. 3 experiment, the data will be transmitted via electromagnetic transmission.

An inverted T/C string, along with a regular T/C string, will be fielded in one well on Hoe Creek No. 3. The data transmission package will be located approximately 10 metres below the coal seam floor. Power to the transmitter will be supplied by a hardwire from the surface until the burn breaks this connection at which time batteries will supply the power. The receiving antenna will be located in a well approximately 15 metres away outside the burn area and at a depth of approximately 10 metres below the coal seam floor. The receiver will be hardwired to the surface. It is anticipated that the transmission frequency will be approximately 10.5 KHz. Thermal data will be transmitted once an hour.

An experimental version of the data transmission system will be tested on the Hanna IV add-on test. To eliminate some hardware problems encountered on the experimental version, a redesign of the electronics for the Hoe Creek version will be necessary.

Hydraulic Testing, Felix No. 2 Coal at Site of Hoe Creek Experiment # 3

R. Stone and T. G. Naymik

Two vertical test wells (HY 1 and HY 2) were constructed and used to measure certain hydraulic and intrinsic properties of the Felix No. 2 coal at the proposed site of Hoe Creek Experiment # 3. The two wells, located 27 m apart and approximately along the proposed process well alignment (see Fig. 2), were drilled, logged (natural gamma radiation log), cased, and cemented to within 0.6 m of the top of the Felix No. 2 coal. Further drilling in each of the wells caused them to be advanced into the Felix No. 2 in three essentially equal increments. Slug-withdrawal tests were performed in the wells at each stage of deepening. The slug-withdrawal tests and their interpretation generally followed the procedure that was used in incremental slug-withdrawal testing of explosion-fractured coal at the Hoe Creek Experiment # 1 site (Stone, 1977). The exception was that water was removed from the wells by bailing rather than by air-ejection. Following the slug testing, a pump was installed in HY 2 and pumping tests were performed with water level drawdown being measured in HY 1.

The results of incremental slug-withdrawal tests in the two wells were treated using the method of Cooper et al. (1967). With one exception (test of Zone I in HY 2) the water level recoveries could be matched with one type of curve. In the exceptional case, the recovery could be equally well matched to either of two types of curves. The permeability estimated in this case is an average of two values corresponding to the two types of curve matches. In all tests, the early recovery appears to have occurred more rapidly than predicted by the model used to analyze the data (early water level recovery data falls below the type curve). This may be a consequence of relatively rapid early inflow

to the wells through a few fractures. The model is based on assumed interstitial flow dominance, but near the wells, at early times, the flow was certainly fracture-dominated. At later times, as the induced negative hydraulic head transient moved further from the wells, the size of the region contributing flow to the wells increased sufficiently, with respect to average fracture spacing in the coal, to cause the flow to conform to the interstitial flow model. Another possible contributor to the departure of early-time recovery data from the type curves is the fact that the slug withdrawals are not really instantaneous as required by the model. Bailing to remove a slug of water from the wells occurred over periods that varied from 30 sec. to 1.5 min. The later recovery data should be more reliable and useful, regardless of the cause of early recovery departure from that predicted theoretically. Therefore, type-curve fits were made using the late-time recovery data.

Analysis of the results of the incremental slug-withdrawal tests in the two wells indicates that the middle third of the Felix No. 2 is more permeable than the upper or lower thirds (see Table IV). The coal in both wells was drilled using the rotary method with normal air circulation. Very little water was lifted during the drilling of the first 2.4 m of the coal in HY 1 and during drilling of its upper 2.1 m in HY 2. It thus appears, based on tests in two wells, that a highly permeable zone in the upper third of the Felix No. 2 at the Hoe Creek # 3 site does not exist.

Upon completion of the incremental slug-withdrawal tests in HY 1 and HY 2, a submersible pump was installed in HY 2 and a 16-hour pump test was performed. Water level drawdown was measured in HY 1. The drawdown data exhibit well-bore storage effects up to about 100 minutes, but are useful for hydraulic analysis threreafter. The data show a certain amount of scatter that is attributed to modest fracture-flow influence. The semi-logarithmic drawndown plot was

TABLE IV

Estimated Horizontal Intrinsic Permeability of Felix No. 2 Coal, Hoe Creek Experiment # 3 Site[a]

Test Well and Interval	Intrinsic Permeability $(\mu m)^2$
HY 1	
Complete seam	0.13
Upper third	0.04
Middle third	0.37
Lower third	b
HY 2	
Complete seam	0.85
Upper third	0.25
Middle third	1.7
Lower third	0.67

[a] Based on single-well, slug withdrawal tests
[b] Permeability too small to measure

used to estimate the overall horizontal intrinsic permeability of the complete Felix No. 2 seam using the modified Theis non-equilibrium method. The permeability estimate from this analysis is 0.97 $(\psi m)^2$, which is in good agreement with that from slug testing the complete seam in HY 2. Surprisingly, the drawdown data from this test indicate no leakage effects. The semi-logarithmic drawdown plot does not exhibit a decrease in slope, from that established in the interval from 100 to 300 minutes, within the 1000 minute test. The logarithmic drawdown plot can be matched nicely to the Theis non-leaky aquifer type curve. Thus, it appears that the Felix No. 2 in the vicinity of HY 1 and HY 2 is not very leaky, and that the overburden i.. the several feet immediately above the top of the Felix No. 2 is of very small vertical permeability.

After the full seam thickness had been tested in the 16-hour pump test, both HY 1 and HY 2 were plugged back with quick-setting cement so that they remained open in only the upper two-thirds of the Felix No. 2. HY 2 was again pumped using the submersible pump. The drawdown in HY 1 occurred in a distinct stepwise manner and does not lend itself to simple quantitative analysis. It seems obvious that the flow involved in this test is fracture-dominated. The three-step semi-logarithmic drawdown response in HY 1 may represent flow largely through three or four separate fractures. These fractures likely have large individual permeabilities, but because of their nature (narrow slits), they store a limited volume of water (giving a small effective storage coefficient to the region that includes them). Hydraulic transients are transmitted through the more permeable fractures with little drawdown. Transmission of the transients through the regions of lower permeability between the more permeable fractures is accompanied by greater drawdown rates. The more permeable fractures are presumed to be located in the middle third of the seam because slug test results of the upper and lower thirds showed permeabilities there to be substantially less, and because sealing off the lower third of the coal in both wells obviously caused a shift in regime from one dominated by interstitial-like flow in the first pump test to the fracture-dominated flow of the second test. Further, in the third pump test, after the middle third of the coal had been sealed off, the regime shifted back towards interstitial-like flow.

The third pump test of HY 2 was performed after both wells had been further plugged back with cement. HY 2 was open to the upper 1.5 m of the Felix No. 2; Hy 1 was open to the upper 0.9 m. The drawdown in HY 1 exhibited a three-step response similar to that seen in the second pump test. The step-wise response was muted, however, and superimposed on an interstitial-like

flow response. Because of the definite fracture-flow influence on the test, its analysis using a porous-flow model can be questioned. Analysis of the semi-logarithmic drawdown plot using the modified Thesis non-equilibrium method yields a 0.33 $(\mu m)^2$ estimate of horizontal intrinisic permeability for the full thickness of the coal seam. The test must be viewed as somehow sensing the permeability of the complete seam because the well spacing is over three times the aquifer (coal) thickness and hence, theoretically, the partial penetration effects must be ignored. The greatest permeability estimated from slug tests for the upper third of the coal is 0.25 $(\mu m)^2$. Because the Theis model is based on a vertically and a really homogeneous aquifer, the permeability estimate resulting from analysis of the third pump test can be viewed as a measure of the upper few feet. Thus, the results of the third pump test are seen to be consistent with other test results.

A fairly crude match of the Theis non-leaky type curve to the logarithmic drawdown curve from the third test provides additional evidence to say that the Felix No. 2 is not very leaky in the vicinity of HY 1 and HY 2. The apparent decrease in drawdown rate near the end of the test is attributed to the influence of fracture flow in the coal rather than to vertical leakage into it.

The experience gained in drilling and testing HY 1 and HY 2 has served to provide positive indications that the site chosen for Hoe Creek Experiment # 3 is at least as good as those of Experiments I and II from two points of view, and probably better. No highly permeable zone in the upper third of the Felix No. 2 coal was identified and the seam is not leaky relative to its nature at the other two gasification sites. A substantial sand bed overlies the Felix No. 1 coal at the Hoe Creek # 3 site, however, and may contribute to significant ground-water intrusion after upward collapse has reached the Felix

No. 1 seam during the gasification process.

We remain convinced of the usefulness of obtaining at least one good complete core of the entire Felix No. 2 seam near HY 1 and HY 2. Examination of the core would provide the opportunity to correlate observed fracture characteristics with the results of hydraulic tests of the coal, and could assist in more complete and positive interpretation of the hydraulic tests. Hoe Creek # 3 may be our last opportunity to obtain such information relatively cheaply. Experimentation in the future at depths three times that to the Felix No. 2 at Hoe Creek may limit the number of boreholes drilled for information gathering purposes.

We must acknowledge the efforts of J. L. Cramer in the conduct of the field work. He supervised the drilling contractor in constructing HY 1 and HY 2, did the borehole gamma-ray logging, made useful suggestions concerning conduct of the hydraulic tests, and helped in their execution.

References

Stone, R., 1977, Measurement of the Spatial Variation of Hydraulic Characteristics of an Explosion-Fractured Coal Seam, Lawrence Livermore Laboratory, Report UCRL-52298.

Cooper, H. H., J. D. Bredehoeft, and I. S. Papadopulos, 1967, Response of a Finite-Diameter Well to an Instantaneous Charge of Water, Water Resource Research, V. 3, 163.

WATER SAMPLING WELLS FOR HOE CREEK III*

S. W. Mead and F. T. Wang

Ground-water and geotechnical measurements, as well as post-burn coring operations, have established that extensive roof collapse occurred at the Hoe Creek # 2 experiment.[1] The enlarged cavity extends roughly 70 ft above the top of the Felix # 2 Coal and constitutes an interconnection between the Felix # 2 Coal aquifer and two overlying aquifers - the Felix # 2 Coal and a channel sand aquifer above it. Since the Hoe Creek site is a recharge area, water from the overlying aquifers is now flowing into the Felix # 2 gasification cavity, thereby changing the local hydraulic heads and flow characteristics of these aquifers and affecting the dispersion of the residual reaction-product contaminants.

Since roof collapse and aquifer interconnection are also likely to occur in conjunction with the Hoe Creek # 3 experiments, we are making special preparations to measure these effects and assess their environmental significance. Fourteen wells (W 1-W 12, Hy 1, Hy 2) primarily intended for water sampling will be provided in the vicinity of the Hoe Creek # 3 experiment (Fig. 1). A majority of these wells (8) will be completed in the Felix # 2 Coal which is to be gasified. The 6 remaining wells will be completed in the overlying aquifers - 5 in the Felix # 2 Coal, and 1 in the channel sand above it. In addition, the process wells A and B, and dewatering wells P 1 - P 3 will also be available for water sampling. All of the water sampling wells will be used for investigating contaminant distribution and transport; some of the wells will also be used for hydrological studies of the effects of aquifer inter-

*Support for these investigations is provided by the Division of Environmental Control Technology (DOE/ASEV), the Office of Research and Development (EPA), and the Division of Fossil Energy Extraction (DOE/ASET).

connection. Well construction will be similar to that of previous Hoe Creek experiments except that PVC casing and screens will be used for wells that are far from the expected burn zone.

As shown in Fig 7, many of the water sampling wells are located along a line extending outward from the gasification zone. This arrangement simplifies the study of contaminant transport, which may be influenced primarily, during the first year or more, by the influx of water from overlying aquifers.

Ground-water sampling before, during, and after gasification will be conducted by LLL personnel with the assistance of the U. S. Geological Survey. Samples will be analyzed in the field and at the laboratories of the USGS, Gulf South Research Institute, and LLL.

References

1. W. R. Aiman and W. T. Fisher, LLL In Situ Coal Gasification Program Quarterly Progress Report, January through March 2978, UCRL-50026-78-1 (1978), p. 37.

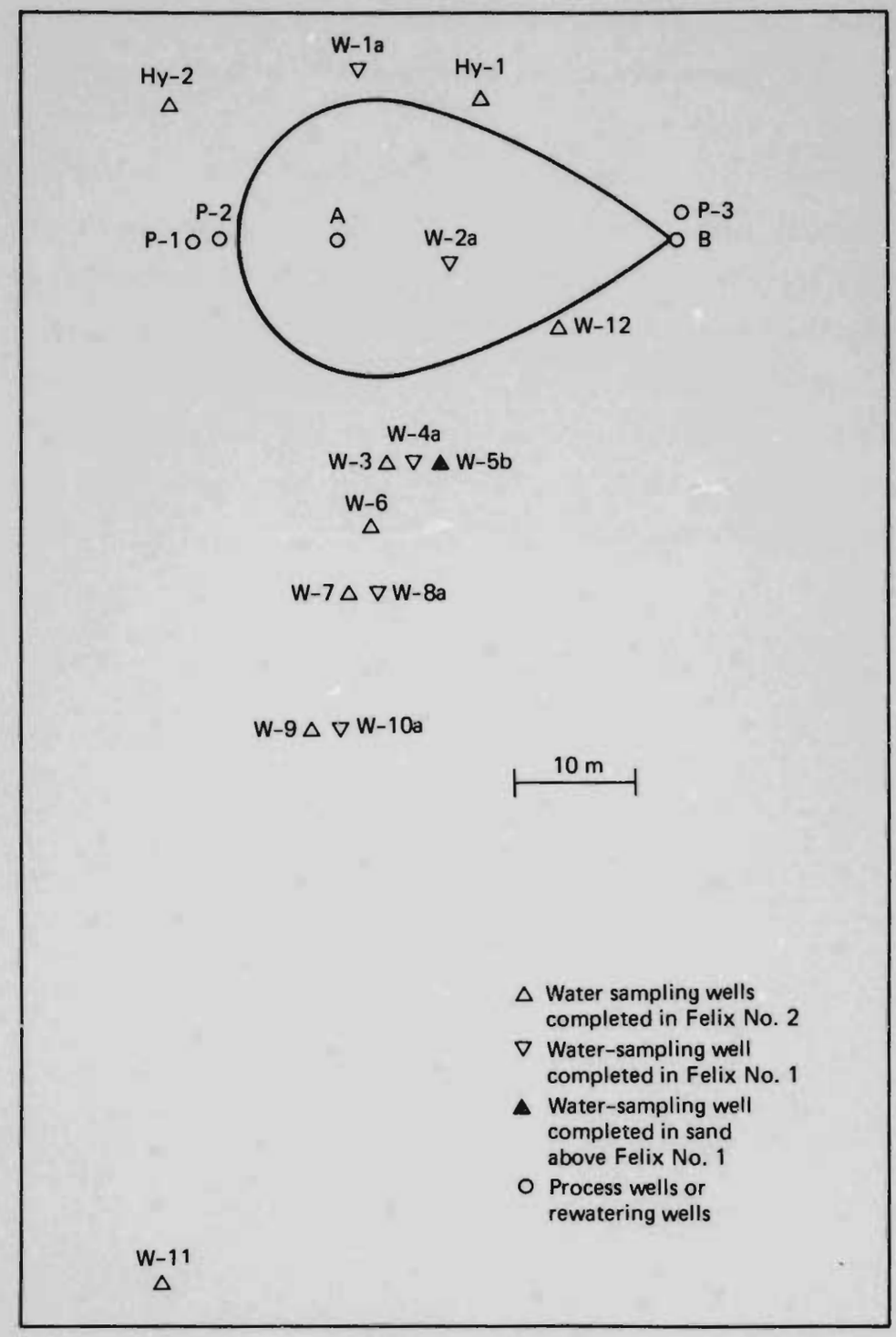

Figure 7. Plan View of Water Sampling Wells

END OF PAPER